High Resolution Spectroscopy of Chirality Recognition and Solvation of Prototype Chiral
Molecular Systems

by

Javix Thomas

A thesis submitted in partial fulfillment of the requirements for the degree of

Doctor of Philosophy

Department of Chemistry
University of Alberta

Abstract

The chirality recognition, chirality induction, chirality amplification, chirality synchronization and solvation of prototypic chiral molecular systems were studied using chirped pulse and cavity based Fourier transform microwave spectroscopy with the aid of high level *ab* initio calculations. The spectroscopic and theoretical results were utilized to derive detailed information about the structures and dynamics of the molecular systems under the conditions of supersonic jet expansion. The various factors contributing to the chirality recognition process in general were explored in the studies.

The chirality recognition study between two permanently chiral molecules glycidol and propylene oxide demonstrates the key roles that the stability and deformation energies of the monomers and their intermolecular interaction energy play in determining the relative stability of the binary conformations. The amplification of chirality in a transient chiral molecule, 2,2,2-trifluoroethanol induced by a permanent chiral molecule propylene oxide was observed. Four out of eight predicted binary conformers were detected, while the other four were shown to relax to these four representative geometries under the jet expansion environment. The study further revealed that the conformational stability in the binary adducts is dominated by intermolecular interaction since the monomeric subunits utilized in each binary adduct are of the same energy. The chirality self-recognition study in the dimer of 2,2,2-trifluoroethanol reports the first experimental detection of the elusive heterochiral dimer. This detection unequivocally establishes that tunneling between the gauche forms of 2,2,2-trifluoroethanol cannot be responsible for the strong chirality synchronization

observed. The result highlights the advantages of using high resolution spectroscopy in comparison to low resolution spectroscopy, in providing detailed and important structural and dynamical information about the molecular recognition process at the microscopic level.

The first step of the solvation process of methyl lactate, a multifunctional chiral molecule, by ammonia was investigated. The nuclear quadrupole hyperfine structures observed provide in-depth information about the charge transfer between a chiral molecule to an achiral molecule due to complex formation. A step wise solvation study of methyl lactate by water showcases the capability of high resolution spectroscopy to differentiate minute conformational variation. It also provides a possible link between the unique orientation of the free hydroxyl groups in these small clusters and the previously observed chirality transfer features of water in aqueous solution of methyl lactate. The solvation study of 2,2,2-trifluoroethanol with water reveals a strong preference for the *insertion* versus *addition* binding topology in the solvation process. Similar preferences were observed in studies of complexes of methyl lactate with water and with ammonia.

Preface

This thesis is based on the research I have done at the University of Alberta between January 2009 and April 2014. The nature and extent of my contribution to the work that has been included in the thesis are briefly summarized below.

Chapter 3 of this thesis has been published as J. Thomas, F. X. Sunahori, N. Borho, and Y. Xu, "Chirality recognition in the glycidol⋯propylene oxide complex: a rotational spectroscopic study," *Chem. Eur. J.* 2011, 17, 4582 – 4587. I was responsible for the data collection and spectral and further data analysis, and wrote the first draft of the manuscript. Dr. F. X. Sunahori assisted in the experiments and manuscript edits. Dr. N. Borho was involved in the planning stage of the project and also contributed to the manuscript edits. Professor Y. Xu was the supervisory author and was involved in the concept formation, data analysis, and manuscript composition.

Chapter 4 of this thesis has been accepted to *Angew. Chem. Int. Ed. as* J. Thomas, W. Jäger and Y. Xu, "Chirality induction and amplification in the 2,2,2-Trifluoroethanol⋯propylene oxide adduct," DOI: 10.1002/anie.201403838 and 10.1002/ ange. 201403838. I was responsible for the data collection, spectral and further data analysis and wrote the first draft of the manuscript. Professor W. Jäger provided assistance in the experiments and was involved in the manuscript composition. Professor Y. Xu was the supervisory author and was involved in the concept formation, data analysis, and manuscript composition.

Chapter 5 of this thesis has been published as J. Thomas and Y. Xu, "Chirality synchronization in trifluoroethanol dimer revisited: the missing heterochiral dimer" *J.*

Phys. Chem. Lett. **2014**, *5*, 1850-1855. I was responsible for the data collection, spectral and further data analysis and I prepared the first draft of the manuscript. Professor Y. Xu was the supervisory author and was involved in the concept formation, data analysis, and manuscript composition.

Chapter 6 of this thesis has been published as J. Thomas, O. Sukhorukov, W. Jäger and Y. Xu, "Chirped pulse and cavity based FTMW spectra of the methyl lactate-ammonia adduct," in *Angew. Chem. Int. Ed.*, 2013, 52, 4402–4405 . I was responsible for the data collection, spectral and additional data analysis. I prepared the first draft of the manuscript. Dr. O. Sukhorukov and Professor W. Jäger assisted in improving the performance of the spectrometer, preliminary experiments, and manuscript edits. This work is one of the first papers written based on the newly built, chirped pulse Fourier transform microwave spectrometer in Professor W. Jäger's laboratory. Professor Y. Xu was the supervisory author and was involved in the concept formation, data analysis, and manuscript composition.

Chapter 7 of this thesis has been published as J. Thomas, O. Sukhorukov, W. Jäger and Y. Xu, "Direct spectroscopic detection of unique free OH orientation in methyl lactate--(water)1,2 clusters: hydration of a chiral hydroxy ester," *Angew. Chem. Int. Ed.* 2014, 53, 1156–1159; *Angew. Chem.* 2014, 126, 1175–1178. I was responsible for the data collection, performance of the experiments and analysis. I prepared the first draft of the manuscript. Dr. O. Sukhorukov and Professor W. Jäger assisted in improving the performance of the spectrometer, preliminary experiments, and manuscript edits. Professor Y. Xu was the supervisory author and was involved in the concept formation, data analysis, and manuscript composition.

Chapter 8 of this thesis has been accepted to *J. Chem. Phys*. as J. Thomas and Y. Xu, "Structure and tunneling dynamics in a model system of peptide co-solvents: rotational spectroscopy of the 2,2,2-trifluoroethanol··water complex". I was responsible for the data collection, spectral and additional data analysis. I prepared the first draft of the manuscript. Professor Y. Xu was the supervisory author and was involved in the concept formation, data analysis and manuscript composition.

Dedicated to:

My late father and loving mother

Acknowledgements

First of all I thank God for being with me all the way and for all his blessings. Also I would like to express my heartfelt thanks to several wonderful people who have helped me throughout my Ph.D program, by their guidance and support.

" The best teachers are those who show you where to look,

but don't tell you what to see." (Alexandra K. Trenfore)

I express my deep and sincere gratitude to Prof. Yunjie Xu, who has been such an inspiring and supportive supervisor. Without her continuous guidance and assistance, it may not have been possible to complete my research works. I thank you for activating the curiosity, knowledge and wisdom in me and showing me 'where to look'. I also want to thank Prof. Wolfgang Jäger, for all his support and also for providing me with many opportunities for detailed discussions and presentations. I also express my sincere gratitude to Professor Mäder for his valuable discussions and suggestions.

I am also grateful to Prof. Charles A. Lucy and Prof. Gabriel Hanna for their support and assistance during my entire Ph.D. program. I wish to express my deep gratitude to my external examiner Prof. Stewart E. Novick from Wesleyan University. I also wish to thank Prof. Arthur Mar and Prof. Michael J. Serpe for agreeing readily to be my exam committee members.

I am also much obliged to those people who are in the Machine and Electronics shops. A special note of thanks to Dr. Norman Gee, my teaching assistant coordinator for his support. I also remember Fumie, Gouchan, Olek, Paul and Jen, as being of much help

and providing me guidance in the initial days of my research works. I express my special thanks to Elijah for his helpful suggestions and discussions. I am also thankful to all my amazing friends- Reza, Zahra, Angelo, Supriya, Chrissy, Amin, Fei, Fahim, Esha, Shawn, Christian, Swaroop, Jerry, Dinesh, Krishna, Paul, Jomon, Anil, Sindhu, Steve and Xing for their friendship and support.

My loving wife Jilsa has always been a great motivation and influence in my life and words are not enough to express my gratitude to her. I also wish to acknowledge my parents and my brothers for their endless love.

Table of Contents

List of Tables (Chapters)

Table   Page

List of Tables (Appendices)

List of Figures (Chapters)

List of Figures (Appendices)

List of Symbols

Symbol	Meaning
ΔD_e	Relative raw dissociation energies
ΔD_0	Corrected dissociation energies
$\mu_{a,b,c}$	Electric dipole moment components
σ	Standard deviation
D_J, D_{JK}, D_K, d_1, d_2	Quartic distortion constants for Watson's S- reduction
E^{dist}	Deformation energies
E^{int}	Interaction energies
ΔE_{rot}	Rotational energy difference
T_{rot}	Rotational temperature
χ	Nuclear quadrupole coupling constant
V_3	Internal rotation barrier
ω_R	Rabi frequency
h	Plank's constant
S	Signal strength
ω	Transition frequency
ΔN_0	Population difference
E_{pulse}	Electric field strength of the chirped pulse
α	Linear sweep range
Δ_J, Δ_{JK}, Δ_K, δ_j, δ_k	Quartic distortion constants for Wartson's A-reduction
I	Signal-to-noise ratio
γ	Line strength
ν	Frequency of the pair of the transitions under consideration

J	Rotational quantum number
K_a (K_c)	K quantum number for prolate (oblate) rotor
ΔE^{conf}	Conformation energy
ΔE^{dist}	Distortion energy
ΔE^{int}	Interaction energy
ρ	Related to the ratio of the molecular rotational constants and the internal rotor rotational constant
F	Effective rotational constant of a top
F_0	Internal rotor rotational constant of a top
β, γ	Euler angles
H	Hamiltonian operator
A,B,C	Rotational Constants
ν_{MW}	Microwave Frequency
K_B	Boltzmann constant

List of Abbreviations

a.u.	Arbitrary units
AWG	Arbitrary waveform generator
BSSE	Basis set superposition energy
CP	Chirped pulse
DC	Direct current
FTIR	Fourier transform infra red spectroscopy
FTMW	Fourier transform microwave spectroscopy
IR	Infrared
ML	Methyl lactate
MW	Microwave
MP2	Moller Plesset second order perturbation theory
NBO	Natural bond-order
PO	Propylene oxide
RG	Rare gas
TFE	2,2,2-Trifluoroethanol
UV	Ultraviolet
VCD	Vibrational circular dichroism
ZPE	Zero point vibrational energy

Chapter 1

Introduction

Alice said to her cat Dinah,

"Perhaps looking glass milk isn't good to drink".

'Through the looking glass' by Lewis **Carroll.**

The term chirality was not coined or known about when these prescient words were written by Lewis Carroll. However, now that the importance of chirality is well known, these words seem surprisingly prophetic.

The concept of reflectional symmetry has long been a fascination for researchers in many different fields of science. The French scientist Jean Baptist Biot made the first significant observation in the field of chirality, while studying polarized light passing through sugar solutions. He discovered that sugar solutions can rotate the polarization plane of linear polarized light. In 1848, Louis Pasteur conducted experiments with tartaric acid and separated two asymmetric forms of tartaric acid crystals, which were mirror images of one another. He also noticed that these crystals, when dissolved in solution, rotated polarized light in opposite directions, i.e. one in clock-wise and the other in anticlockwise.[1] Fischer, in 1894, explained the specificity of enzyme reactions by introducing the 'lock and key' principle,[2] which vividly describes the fundamental mechanism behind all molecular recognition processes. Lord Kelvin coined the term '*chirality*', derived from '*cheir*', the Greek word for hand.[3] He defined chirality, in 1904, as the following:

"I call any geometric figure, or group of points, chiral, and say it has chirality, if its image in a plane mirror, ideally realized, cannot be brought to coincide with itself"

A molecule is chiral if it cannot be superposable on its mirror image. In general, a molecule that lacks an improper rotation axis is called chiral. The physical and chemical properties of bimolecules depend on molecular chirality extensively. The most common example of chiral objects is a pair of human hands. In chemistry the non-superposable mirror images of a chiral molecule are called enantiomers. The enantiomers of chiral molecules have similar physical properties and are indistinguishable in most regards. They interact in the same way with molecules which are achiral. The enantiomers of chiral molecules are distinguishable only in their interactions with other chiral elements such as chiral molecules or chiral light, i.e. circularly polarized light. The ability of a chiral molecule to differentiate between the two enantiomers of a chiral molecule is called chirality recognition.[4]

The chirality of molecules plays a fundamental role in the outcome of biological reactions. It is an important concept, and it finds applications in many areas of research. The most astonishing fact about chirality is the biological homo chirality observed in nature. All of the bimolecules that act as the building blocks of life exhibit the property of chirality. Only L-type amino acids are seen in proteins, and only D-configured sugars can be absorbed by living organisms.

Many aspects and consequences of chirality are not fully understood and are as fascinating to scientists as when chirality was first discovered. Chirality is a central focus in the drug industry and most of the available drugs on the market are also chiral. Different enantiomers of a racemic drug may have different pharmacological activities and metabolic pathways. The receptors in the body are all chiral and, being extremely selective, will interact with the enantiomers of a chiral drug differently to produce

different pharmacological effects. Thus one enantiomer may produce the required therapeutic effects, whereas the other enantiomer may be either inactive or produce detrimental effects. The thalidomide (n-phthalyl-glutamic acid imide) tragedy of the 1960's is an example.[5] Initially thalidomide was prescribed as a sedative and later as an effective antiemetic drug to treat morning sickness in pregnant women, without proper experimental data supporting its safe use in pregnancy. Thousands of babies were born with severe deformities of the limbs and congenital abnormalities of other organs to mothers who had taken thalidomide during pregnancy. This teratogenic effect of thalidomide was ascribed to one of its enantiomers. Its therapeutic activity resided only in the R-(+)-enantiomer, and the S-(+)-enantiomer was teratogenic. The number of enantiopure drugs being introduced in to the market has been increasing annually,[6] and it is estimated that by 2020, almost 95 % of the drugs in the market will be enantiopure. Another field in which chirality plays an important role is agrochemicals. Many of these chemicals are available as racemates of both enantiomers. Only one of the enantiomers in the mixture may be contributing to the desired activity of the chemical, while the other one may have some toxic effects on biological systems. Hence, it is essential to thoroughly test and establish how both enantiomers of these molecules interact with bio-targets.[7]

The intermolecular interaction of chiral molecules at the molecular level, which is called molecular recognition, plays a vital role in biochemistry and biology.[8] In order to understand molecular recognition processes in great detail we need to start from the microscopic level. A thorough understanding of the interaction of chiral molecules with other chiral molecules (i.e. chirality recognition or more generally, molecular

recognition), is very important in understanding and modeling the outcomes of biological events. Biological events in solution are often extremely complex, making it almost impossible to unveil the associated intermolecular interactions in depth to provide a molecular picture of such interactions. The principal goal of my research work is to provide unique and high quality experimental data of some prototype molecular recognition processes and investigate the strong and weak non-covalent interactions that are responsible for such molecular recognitions. Among the non-covalent interactions, my thesis work focuses in particular on the interplay between hydrogen bonding and van der Waals interactions in facilitating the chirality recognition process.

To gain insight into the molecular recognition processes of biomolecules at the molecular level, I investigated rotational spectra of several prototype chiral contact pairs generated under a supersonic jet expansion condition. Since most biological events happen in aqueous solution, I also examined the chiral molecule-water/ammonia clusters as prototype systems in order to investigate intermolecular interactions of chiral molecules with water and other similar small protic molecules. The hydrogen-bonding interactions of chiral molecules with the surrounding solvent molecules, such as water, may also play a key role in the molecular recognition processes. The energy associated with the solvation processes is comparable to the interaction energy between chiral contact pairs in chirality recognition processes.[4] A comprehensive understanding of the solvation process of chiral molecule is therefore very important in understanding the molecular recognition between biomolecules in aqueous solutions.[9] Therefore, water and ammonia were used as the solvent molecules to study the solvation of chiral molecules in my studies.

The study of prototypic molecular systems in the condensed phase is complicated due to the undesired interactions from solvents. Studies of the model prototypic molecular system of interest in the gas phase can eliminate such interactions. A wide range of gas phase spectroscopic techniques such as laser induced fluorescence,[10] resonance enhanced multiphoton ionization,[11] ultra violet (UV)/infrared (IR) double resonance[12], broadband Fourier transform IR spectroscopy,[13,14] IR multiphoton dissociation spectroscopy[15] and UV/IR hole burning [16,17] have been used in the past to explore the short range interactions and conformational landscapes of chiral molecules in the gas phase. In all the above studies, ab initio simulations of the related spectra were critical for the identification of specific conformations because of the low resolution nature of the spectra obtained. In addition, some finer conformational differences cannot be differentiated. Unlike the low-resolution spectroscopic studies, high resolution Fourier transform microwave spectroscopy (FTMW) can provide quantitative information about the structure and relative stability of chiral contact pairs, thus allowing significant insight into molecular recognition processes at the molecular level. One significant advantage of rotational spectroscopy is its extremely high resolution capability, on the order of a few kHz in our experiments. This allows one to differentiate even the most subtle conformational differences in the chiral molecular systems.[18] The presence of a large number of potential structural conformations of targeted chiral systems, such as chiral molecules or complexes of chiral molecules, makes the experimental spectroscopic assignments of these systems highly challenging. So far, there have been only a small number of high resolution spectroscopic studies of chirality recognition reported. Howard and co-workers reported the first high resolution rotational spectroscopic study of

6

chirality recognition in the butan-2-ol dimer, where they assigned one heterochiral dimer. [19] Later, FTMW studies of the chirality self recognition of propylene oxide (PO) with itself,[20] and with transient chiral molecules, namely 2-fluoroethanol[21] and ethanol[22] were published by our research group. Subsequently, Caminati and co-workers reported chirality self-recognition in the glycidol dimers.[23] Later on, a study of chirality self-recognition in the transient chiral molecule 2-fluoroethanol[24] was published. Similarly, in terms of high resolution spectroscopic investigations of chiral molecules with solvent molecules, there has only been a small number of publications. Rotational spectra of alaninamide--water,[25] 3-hydroxy tetrahydrofuran--water,[26] glycidol--water,[27] PO--(water)$_{1,2}$,[28,29] and glycidol--ammonia[30] are some example studies that have been reported.

The goal of my thesis work is to deepen our understanding of chirality recognition and the solvation of chiral molecules by using FTMW spectroscopy and high level ab initio calculations. Several prototype chiral molecules with different numbers of functional groups and conformational flexibility, namely PO (C_3H_6O), glycidol ($C_3H_6O_2$), methyl lactate ($C_4H_8O_3$), and 2,2,2-Trifluoroethanol (TFE,$C_2H_3F_3O$) are utilized in my studies. I also used water (H_2O) and ammonia (NH_3), two protic solvent molecules in my studies. The molecules that I used for chirality recognition and solvation studies are given in figure 1.1. Among the above, PO is chosen for my studies because it is a permanent chiral molecule with a relatively rigid structure. PO is a molecule of considerable theoretical and experimental interest.[31-35] Glycidol is another interesting permanent chiral molecule[36,37] with many possible conformations due to the presence of a hydroxy group and is also an important enantio selective synthetic reagent.[38] Methyl lacate is a

prototype system with multiple functional groups.[39,40] It contains the alpha hydroxy carbonyl function and can be considered as a prototype of amino acids in mimicking their hydrogen bond donor and acceptor properties. TFE is a transient chiral molecule.[41,42] It is commonly used as a co-solvent for studies in protein folding processes.[43] This perfluorinated molecule exhibits some fascinating properties which are vastly different from those of the related ethanol, mono- and trifluoroethanol. In all my research projects, I also apply high level ab initio calculations to aid the spectral assignments and to gain further insight into chirality recognition and solvation processes. Thus, in all my research projects, I applied high resolution FTMW spectroscopy in combination with high level ab initio calculations to study the targeted chiral molecular complexes.

Propylene Oxide   Glycidol   2,2,2,-Trifluoroethanol

Methyl lactate   Ammonia   Water
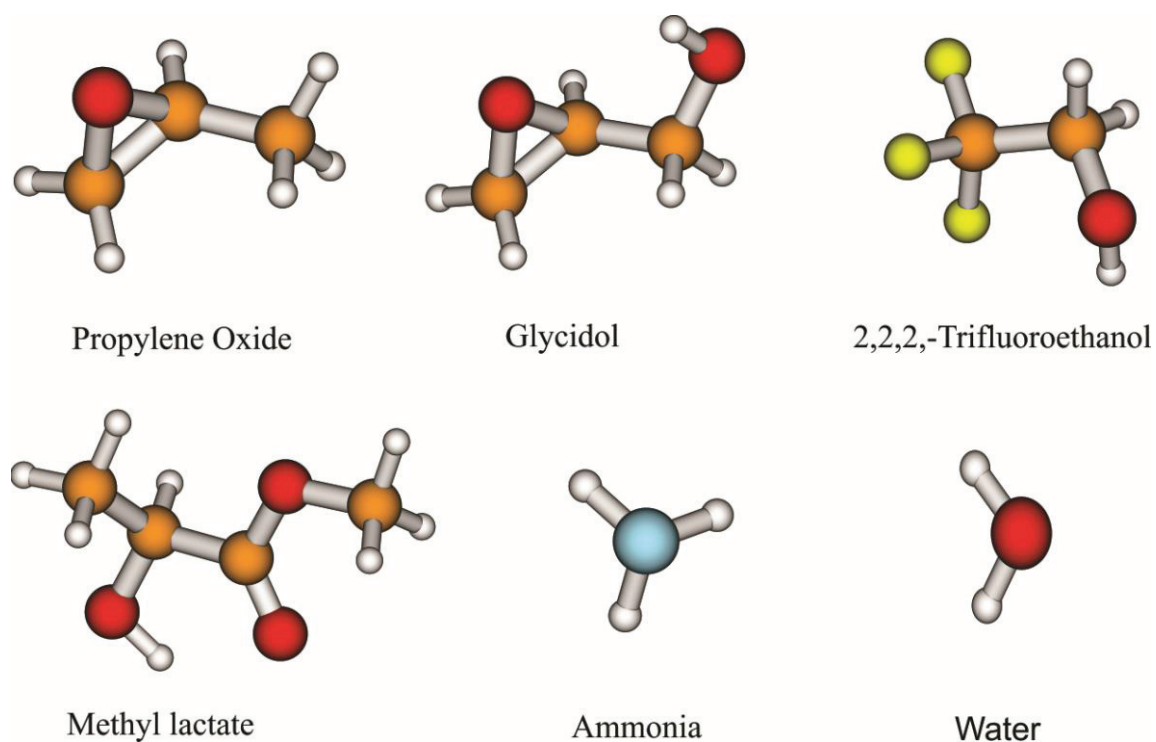
Figure 1.1. The structures of the molecules used for chirality recognition and solvation studies

The remainder of this thesis is divided into eight chapters. Chapter 2 gives details of the experimental set up I used to obtain all my experimental data, along with a short summary of the different theoretical programs that I used to aid in my experimental studies. Chapter 3 reports the first high resolution FTMW study of chirality recognition between two permanently chiral molecules, namely PO and glycidol. Chirality recognition is the ability of a chiral molecule to differentiate between the enantiomers of another chiral molecule. One of the aims of this study is to gain a good understanding of the structural changes in the monomers in the formation of the complex and how that influences the outcome of chirality recognition. Another goal is to evaluate whether the formation of the complexes between PO and glycidol is kinetically controlled or thermodynamically controlled. Chapter 4 is about a prototypical chirality induction model system, the PO-TFE complex. The purpose of this study is to probe whether the permanently chiral molecule PO can preferably induce a specific chirality in the transient chiral molecule (chirality induction) TFE and whether the fast tunneling motion between gauche- and gauche+ forms of TFE is quenched in the hydrogen-bonded complex.[44-46] Chapter 5 reports the chirality self-recognition in the transient chiral molecule TFE. Of particular interest here is the extreme case of chirality synchronization reported before in the TFE dimer.[44-46] In chirality synchronization a molecule preferentially assume only one chirality in the formation of clusters. With the extremely high resolution available in the microwave experiments, we aim to verify the accuracy of the previous reports and to observe the possible tunneling splitting between gauche- and gauche+ forms of TFE in the dimer, if it is not quenched. Chapter 6 is devoted to the solvation study of methyl lactate with ammonia. Chapter 7 describes the step-wise solvation study of methyl lactate

with water. In Chapters 6 and 7, the preferential binding of ammonia and water to methyl lactate is explored. The complex formation of ammonia with methyl lactate provides the opportunity to probe whether there is distortion of the electric field gradient at the ^{14}N nucleus of ammonia. In chapter 7, I mainly investigated the influence of the dangling OH groups in the formation of clusters with subtle structural differences. Chapter 8 reports the interaction of TFE with water. Since TFE is a widely used protein co-solvent with water, one goal of the study is to investigate how TFE interacts with water at the molecular level. The above solvation studies also give detailed insights into the competition between inter- and intra-molecular hydrogen bonds and also on the specificity of the binding of the solvent molecules in the formation of solute-solvent complexes. The final chapter of my thesis gives the general conclusions of this thesis, along with possible future works to further the current research goals. I also included a number of appendices at the end of my thesis which include supporting information associated with Chapters 3to 8.

References

[1] L. Pasteur, *Ann. Chim. Phys*. **1848**, III, *24*, 442–459.

[2] E. Fischer, Ber. *Dtsch. Chem. Ges*. **1894**, *27*, 2985–2993.

[3] Lord Kelvin Baltimore Lectures (1884) on Molecular Dynamics and the Wave
Theory of Light, Clay and Sons: London, 1904, p 449.

[4] A. Zehnacker, M. A. Suhm, *Angew. Chem*. **2008**, *120*, 7076–7100; *Angew. Chem. Int.
Ed*. **2008**, *47*, 6970–6992.

[5] G. Blaschke, H. P. Kraft, K. Fickentscher, F. Kohler, *Drug Res*. **1979**, *29*,   1640–
1642.

[6] S. C. Stinson, Chemical and Engineering News. **1998**, *76*, pp 38–70.

[7] N. Kurihara, J. Miyamot, G. D. Paulson, B. Zeeh, M. W. Skidmore. R. M.
Hollingworth, H. A. Kuiper, *Pure. App. Chem*. **1997**, *69*, pp 2007–2025.

[8] R. A. Sheldon, Chirotechnology: Chirotechnology: Industrial Synthesis of Optically
Active Compounds, Marcel Dekker, Inc.: NewYork, 1993, pp 39–72.

[9] G. A. Jeffrey, W. Saenger, Hydrogen Bonding in Biological Structures, Springer,
Berlin, 1991.

[10] N. Seurre, J. Sepiol, K. Le Barbu-Debus, F. Lahmani, A. Zehnacker- Rentien, *Phys.
Chem. Chem. Phys*. **2004**, *6*, 2867–2877.

[11] A. Giardini Guidoni, S. Piccirillo, D. Scuderi, M. Satta, T. M. Di Palma, M.
Speranza, Phys. Chem. Chem. Phys. **2000**, *2*, 4139–4142.

[12] A. R. Al-Rabaa, K. Le Barbu, F. Lahmani, A. Zehnacker-Rentien, J. *Phys. Chem. A*.
1997, *101*, 3273–3278.

[13] N. Borho, M. Suhm, *Phys. Chem. Chem. Phys*. **2002**, *4*, 2721–2732.

[14] T. B. Adler, N. Borho, M. Reiher, M. A. Suhm, *Angew. Chem*. **2006**, 118, 3518–3523; *Angew. Chem. Int. Ed*. **2006**, *45*, 3440–3445.

[15] F. X. Sunahori, G. Yang, E. N. Kitova, J. S. Klassen, Y. Xu. *Phys. Chem. Chem. Phys*. **2013**, *15*, 1873–1886.

[16] F. O. Talbot, J. P. Simons. *Phys. Chem. Chem. Phys*. **2002**, *4*, 3562–3565.

[17] J. P. Simons, R. A. Jockusch, P. Carcabal, I. Hünig, R. T. Kroemer, N. A. Macleod, L. C. Snoek. *Int. Rev. Phys. Chem*. **2005**, *24*, 489–531.

[18] Y. Xu, W. J. Jäger, *Chem. Phys*. **1997**, *107*, 4788–4796.

[19] A. K. King, B. J. Howard, *Chem. Phys. Lett*. **2001**, *348*, 343–349.

[20] Z. Su, N. Borho, Y. Xu, *J. Am. Chem. Soc*. **2006**, *128*, 17126–17131.

[21] N. Borho, Y. Xu, *J. Am. Chem. Soc*. **2008**, *130*, 5916–5921.

[22] N. Borho, Y. Xu, *Angew. Chem*. **2007**, 119, 2326–2329; *Angew. Chem. Int. Ed*. **2007**, 46, 2276–2279.

[23] A. Maris, B. M. Giuliano, D. Bonazzi, W. Caminati, *J. Am. Chem. Soc*. **2008**, 130, 13860–13861.

[24] X. Liu, N. Borho, Y. Xu, *Chem. Eur. J*. **2009**, *15*, 270–277.

[25] J. Lavrich, M. J. Tubergen, *J. Am. Chem. Soc*. **2000**, *122*, 2938 –2943.

[26] R. J. Lavrich, C. R. Torok, M. J. Tubergen, *J. Phys. Chem. A*. **2001**, *105*, 8317–8322.

[27] A. R. Conrad, N. H. Teumelsan, P. E. Wang, M. J. Tubergen, J. *Phys. Chem. A*. **2010**, *114*, 336–342.

[28] Z. Su, Q. Wen, Y. Xu, *J. Am. Chem. Soc*. **2006**, *128*, 6755–6760.

[29] Z. Su, Y. Xu, *Angew. Chem*. **2007**, *119*, 6275–6278; *Angew. Chem. Int. Ed*. **2007**, *46*, 6163–6166.

[30] B. M. Giuliano, S. Melandri, A. Maris, L. B. Favero, W. Caminati, *Angew. Chem*. **2009**, *121*, 1122–1125; *Angew. Chem. Int. Ed*. **2009**, *48*, 1102–1105.

[31] J. D. Swalen, D. R. Herschbach, *J. Chem. Phys*. **1957**, *27*, 100–108.

[32] D. R. Herschbach, J. D. Swalen, *J. Chem. Phys*. **1958**, *29*, 761–776.

[33] F. Winther, D. O. Hummel, *Spectrochimica Acta*. **1968**, *25a*, 417–423.

[34] M. Imachi, R. L. Kuczkowski, *J. Mol. Struct*. **1982**, *96*, 55–60.

[35] C. Merten, J. Bloino, V. Barone, Y. Xu, *J. Phys. Chem. Lett*. **2013**, *4*, 3424–3428.

[36] W. V. F. Brooks, K. V. L. N. Sastry, *Can. J. Chem*. **1975**, *53*, 2247–2251.

[37] K.-M. Marstokk, H. Møllendal, Y. Stenstrøm, *Acta Chem. Scand*. **1992**, *46*, 432–441.

[38] R. M. Hanson, Chem. Rev. **1991**, *91*, 437–475.

[39] P. Ottaviani, B. Velino, W. Caminati, *Chem. Phys. Lett*. **2006**, *428*, 236–240.

[40] N. Borho, Y. Xu, *Phys. Chem. Chem. Phys*. **2007**, *9*, 1324–1328.

[41] L. H. Xu, G. T. Fraser, F. J. Lovas, R. D. Suenram, C. W. Gillies, H. E. Warner, J. Z. Gillies, *J. Chem. Phys*. **1995**, *103*, 9541–9548.

[42] T. Goldstein, M. S. Snow, B. J. Howard, *J. Mol. Spectrosc*. **2006**, *236*, 1–10.

[43] J. F. Povey, C. M. Smales, S. J Hassard, M. J, Howard, *J. Struct.Biol*. **2007**, *157*, 329–338.

[44] T. Scharge, T. Häber, M. A. Suhm, *Phys. Chem. Chem. Phys*. **2006**, *8*, 4664–4667.

[45] T. Scharge, C. Cézard, P. Zielke, A. Schütz, C. Emmeluth, M. A. Suhm, *Phys. Chem. Chem. Phys*. **2007**, *9*, 4472–4490.

[46] T. Scharge, T. N. Wassermann, M. A. Suhm, *Z. Phys. Chem.* **2008**, *222*, 1407–1452.

Chapter 2

Experimental Details and Analysis of Rotational Spectra

2.1. Introduction

Rotational spectra of all of the molecular systems that I investigated during my thesis work have been recorded using a narrowband cavity-based Fourier transform microwave (FTMW) spectrometer and a broadband chirped pulse FTMW spectrometer. In all of my studies, except the one in Chapter 3 in which I used only the cavity-based FTMW spectrometer, preliminary scans of the rotational spectra were carried out using the chirped-pulse FTMW spectrometer, and the final frequency measurements were done using the cavity-based FTMW spectrometer. This chapter consists of three sections, in which I describe (1) the narrow band cavity-based FTMW spectrometer, (2) the broadband chirped pulse FTMW spectrometer, and (3) the spectral analysis strategy and different computational programs that I used in my studies to aid in the spectral assignment and structural analysis.

2.2. Narrow band cavity-based FTMW spectrometer

2.2.1. Introduction

Microwave spectroscopy is a gas phase technique that is limited to molecules that have a permanent dipole moment. The first commercial microwave spectrometer employed Stark modulation and a wave guide sample cell to study molecular structure.[1,2] The theory of FTMW spectroscopy was established in the 1970s and early 80s by Flygare and McGurk.[3] Flygare later expanded the FTMW experimental instrument by incorporating a Fabry-Perot cavity and a pulsed supersonic expansion. In their spectrometer, Balle and Flygare[4] used a Fabry-Perot cavity that consisted of a pair of spherical mirrors situated inside an evacuated chamber as the sample cell and

introduced the targeted molecular system into the chamber through a pulsed nozzle. This Balle-Flygare FTMW spectrometer provides a much higher frequency resolution and sensitivity than the aforementioned commercial MW spectrometer. Below, I give a brief description of the Balle-Flygare type pulsed molecular beam FTMW spectrometer[4,5] that I used for my studies. Further information regarding the spectrometer can be found in the given references.[6,7]

2.2.2. Theoretical considerations

The basic principles behind FTMW spectroscopy are (1) the excitation of an ensemble of molecular systems in the gas phase by a short coherent pulse of microwave radiation that is in resonance with a rotational transition of interest and (2) the subsequent detection of the coherent spontaneous molecular emission signal as a function of time. The application of the coherent microwave pulse aligns the initially randomly oriented electric dipoles, i.e. molecules with permanent electric dipole, causing them to rotate in phase with each other, thereby creating a macroscopic polarization. In a classical picture, this macroscopic polarization can be viewed as an assembly of aligned dipoles that rotate with the transition frequency. Such oscillating dipoles therefore emit coherent radiation at the transition frequency. The coherent spontaneous emission decays with a polarization relaxation time, T_2, which is typically far greater than the pulse width of the microwave radiation. The emitted signals are collected as free induction decay in the time domain. The time domain signal is then converted into the frequency domain spectrum using Fourier transformation.

The detailed theoretical treatments of the interaction of the molecular ensemble with the coherent pulsed microwave radiation were described before based on Bloch-type

[8,9] equations. Interaction of the molecules with a coherent microwave pulse causes the mixing of the wavefunctions of the two rotational states and generates a superposition state. If one applies a so-called $\pi/2$ pulse of microwave radiation, this results in an equal number of molecules populating both states and imprints the coherence of radiation to the molecules. In other words, the initial population difference is said to convert to a macroscopic polarization.

The strength of the interaction of the molecular ensemble with the applied microwave field determines the magnitude of the macroscopic polarization of the sample and the intensity of the emitted radiation. The macroscopic polarization depends on the Rabi frequency, a measure of the coupling strength between the electric field of the microwave radiation and the electric dipole moment of a transition. Rabi frequency is the frequency of oscillation for a transition between two levels in a given light field. It is a product of the strength of the electric field of the microwave radiation and the electric dipolmoment for a given transition. For a transition between two levels, 1 and 2, the Rabi frequency is given by

$$\omega_{R=}\mu_{12}\,\epsilon/\hbar \quad \text{where } \hbar = h/2\pi. \tag{2.1}$$

where ω_R is the Rabi frequency, μ_{12} is the electric dipole moment of the transition between levels 1 and 2, and ε is the electric field amplitude of the external MW radiation.

2.2.3. Instrument design

The cavity-based FTMW instrument I used for my studies has been described previously in the literature.[10,11] The instrument design is slightly different from that of

18

the original setup of Balle and Flygare. A schematic diagram of the set up of the spectrometer is given below.
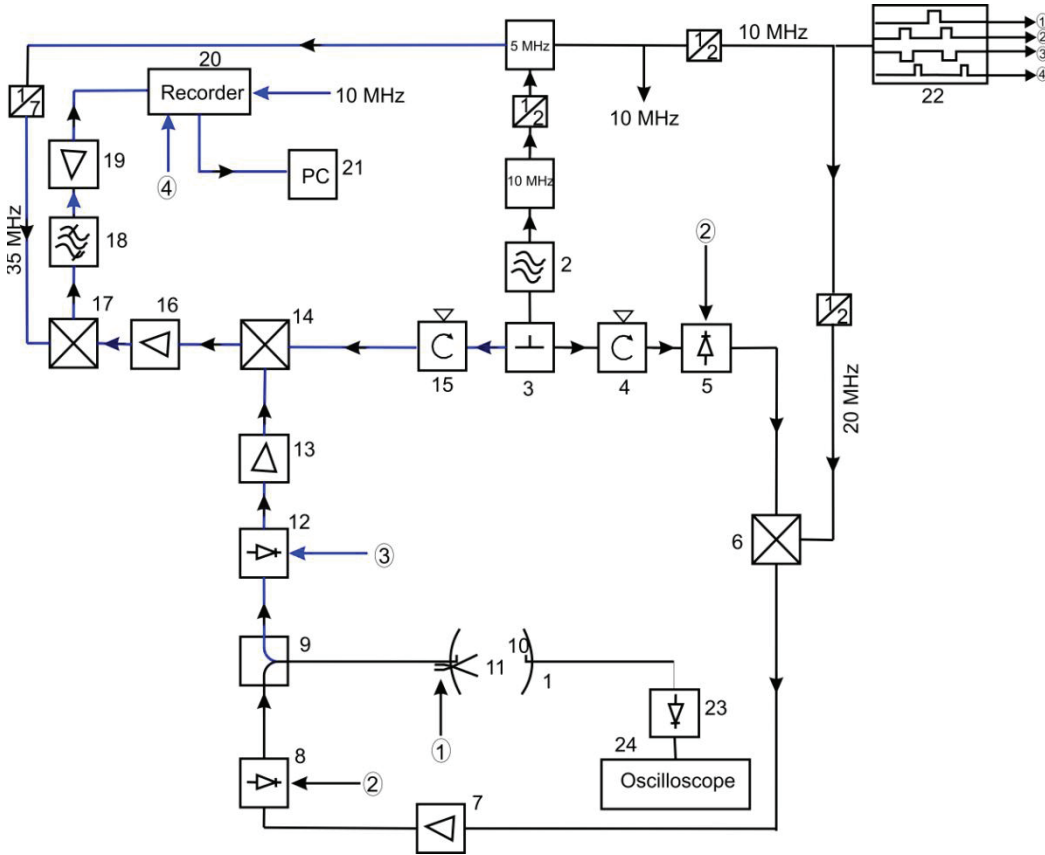
Figure 2.1. A schematic diagram of the Balle-Flygare FTMW spectrometer (adapted from reference 11).

The detection arm of the spectrometer is shown with blue lines and the other part with black lines. The components of the above diagram are the following: (1) nozzle, (2) Hewlett Packard MW synthesizer, (3) power divider, (4) isolator, (5) MW PIN diode switch, (6) 20 MHz double balanced mixer, (7) MW power amplifier, (8) MW PIN switch, (9) circulator, (10) antenna, (11) MW cavity, (12) MW PIN switch, (13) MW power amplifier, (14) image rejection mixer, (15) isolator, (16) radio frequency (RF)

amplifier, (17) RF mixer, (18) 15 MHz band pass filter, (19) RF amplifier, (20) transient recorder, (21) personal computer, (22) pulse generator, and (23) detector.

The heart of the spectrometer is the microwave cavity, formed by two spherical aluminium mirrors, which also serves as the sample cell. The position of one mirror is fixed, while the position of the other one can be adjusted by using a computer controlled motor. The separation between the mirrors is around 30 cm. The microwave cavity is placed inside a vacuum chamber which is pumped by a 12-inch diffusion pump backed by a roughing pump. The microwave excitation pulse is coupled in and out of the cavity using a pair of antennas positioned at the center of the mirrors.

The standing wave patterns (modes) of the cavity are monitored on an oscilloscope. The Fabry-Perot cavity serves as a band pass filter by causing constructive interference for only certain frequencies and causing destructive interference for all others.[11] The bandwidth of the microwave experiment is limited by both the quality factor (Q) of the resonators and the microwave pulse width. Q is the ratio of the energy stored in the resonator to the energy supplied by a generator. At 10 GHz, the bandwidth of the cavity is 1 MHz with a quality factor of 10000. The operating range of the spectrometer is 3-26 GHz. A 10 MHz signal from an internal clock in the MW synthesizer is used to control the timing of the entire experiment.

The molecules or complexes of interest are introduced in a pulsed supersonic jet expansion through the nozzle into the cavity. The nozzle is situated near the center of the stationary mirror just below the antenna. The orientation of the nozzle allows the coaxial propagation of the molecular beam relative to the cavity axis. This arrangement results in

splitting of the rotational transitions into two Doppler components. The coaxial arrangement also allows longer interaction time between the molecular beam and MW radiation compared to the perpendicular arrangement.[12] This reduces the spectral line width to a few KHz which in turn enables observation of very small hyperfine splitting. This is well exploited in the measurement of the hyperfine splittings in the methyl lactate··NH₃ system described in Chapter 6 and the tunneling splitting in the 2,2,2-trifluoroethanol··water complex in Chapter 8.

Each microwave experiment is executed with a train of TTL pulses depicted in Figure 2.2. First, the cavity is tuned into resonance. Then the sample is introduced into the cavity as a pulsed expansion. The excitation frequency from the MW synthesizer is divided into two arms using a power divider. Two MW PIN switches are used to shape the MW pulse after the power divider. After the first MW PIN switch, the frequency is mixed with 20 MHz using a double balanced mixer that generates side bands at 20 MHz from the carrier frequency. The output from the mixer is then passed through the second MW PIN switch to a circulator. From the circulator, the microwave pulse is coupled into the cavity, where it interacts with the gas sample that has already been introduced into the cavity. Due to interaction with the MW radiation, the dipole moments of the molecules align, resulting in a macroscopic polarization. The gas sample, after the microwave pulse, emits radiation, and the molecular emission signal is detected by the antenna and coupled back into the detection arm of the MW circuit through the circulator. The MW PIN switch in the beginning of the detection circuit protects it from the high power MW excitation pulse. The signal is then amplified and down-converted, first to around 20 MHz by mixing with the local oscillator in an image rejection mixer, and then to 15

MHz. The final signal is then fed into a 15 MHz band pass filter. The time domain signal from the band pass filter is then collected in a transient A/D recorder card and then Fourier transformed to obtain the frequency spectrum. A background signal is collected prior to every experiment without the actual sample. The final spectra are obtained after subtraction of the background signals from the experimental signals. The sample conditions used for individual molecular systems are detailed in the respective chapters.
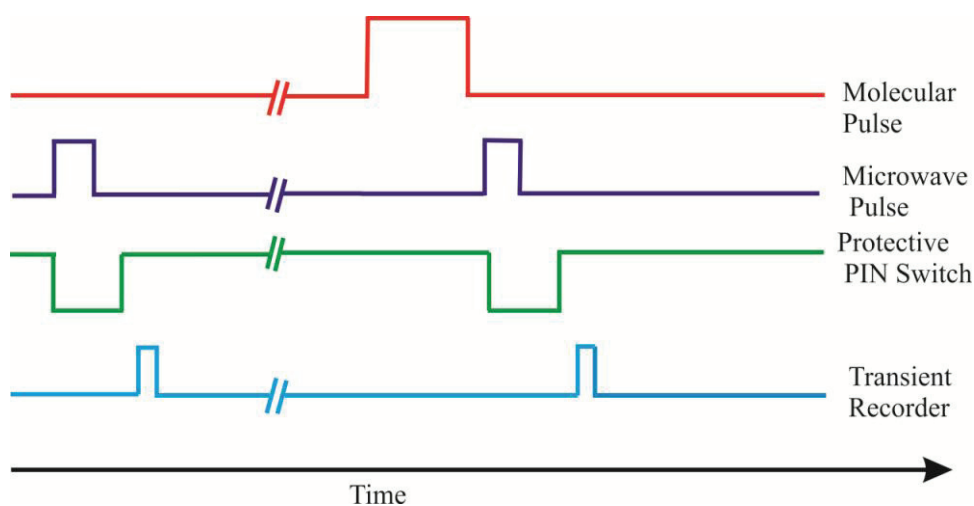
Figure 2.2. A typical timing diagram of pulse sequence used in the Balle-Flygare FTMW spectrometer. In all of them, a crest indicates 'open' and a trough indicates 'closed'.

2.3 Chirped pulse FTMW spectrometer

The usage of a resonator lessens the power requirement of the excitation pulse, amplifies the molecular emission signal, and thereby increases the sensitivity of the cavity-based FTMW spectrometer. The significant drawback is its bandwidth limitation which in our particular case is about 1 MHz. Consequently, it is very tedious to acquire spectra over a wide frequency region with a cavity-based FTMW spectrometer.

22

Typically, acquiring spectra using a cavity-based FTMW spectrometer requires tuning the cavity into resonance at each frequency step, so most of the experiment time is spent to tune the cavity rather than to accumulate the molecular signals. Estimation of the relative abundances of different species, using line intensity is difficult with cavity-based FTMW spectrometer. This is because the experimental intensity often depends sensitively on the cavity mode used, which can differ noticeably in different frequency regions.

There have been significant developments in high speed digital electronics, broadband high power amplifiers and other related electronics in the past ten years. All these advances enabled the development of a new type of FTMW spectrometer. In 2006, Brooks Pate's group at the University of Virginia developed a chirped pulse FTMW spectrometer which is capable of measuring 11 GHz of bandwidth in less than 10 microseconds by exploiting these recent advances in digital electronics.[13]

High speed digitizers, broadband high power amplifiers, and arbitrary waveform generators (AWGs) which are capable of producing frequency chirps across a few GHz in very short time period are utilized in this new type of spectrometer. The chirped pulse FTMW spectrometer [14] that I used for my studies is based on the previously reported designs with some of our modifications.[14,15] A schematic diagram of the chirped pulse instrument is given in Figure 2.3.
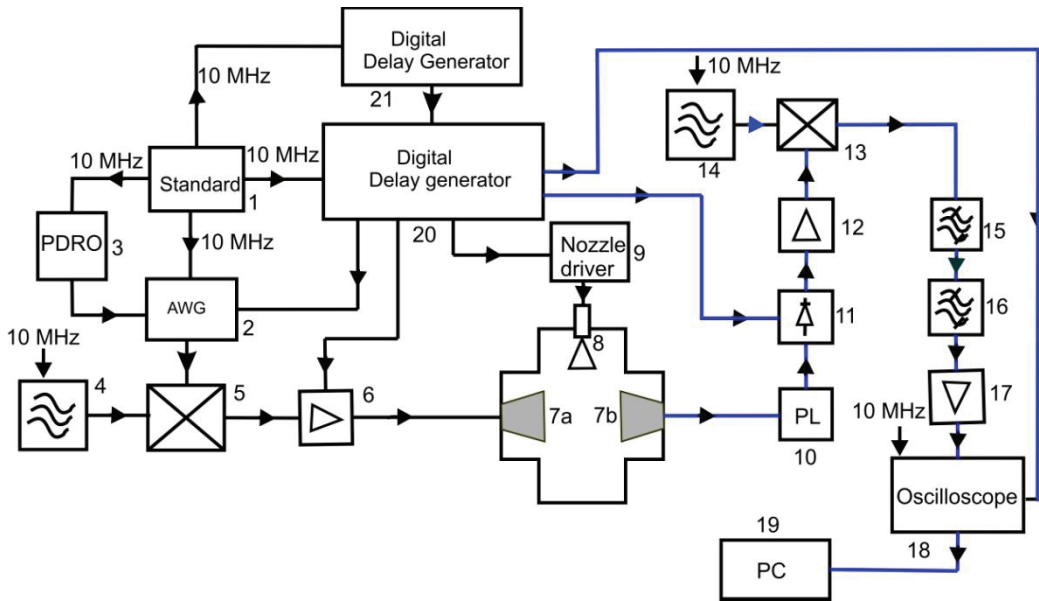
Figure 2.3. A schematic diagram of the broadband chirped-pulse FTMW spectrometer.

The components of the above diagram are the following: (1) Rb- frequency standard, (2) arbitrary waveform generator, (3) 3.96 GHz phase-locked dielectric resonator oscillator (PDRO), (4) synthesizer 1, (5) double balanced mixer, (6) 20 W solid state amplifier, (7) high gain horn antennas, (8) nozzle, (9) nozzle driver, (10) power limiter, (11) PIN diode switch, (12) low noise amplifier, (13) double balanced mixer, (14) synthesizer 2, (15) low pass filter, (16) low pass filter (17) low noise amplifier, (18) oscilloscope, (19) personal computer, (20) digital delay generator, and another (21) digital delay generator. Items 1, 20 and 21 are from Stanford Research Systems; Items 2 and 18 are from Tektronix; Items 4 and 14 are from Agilent Technologies; Item 6 is from MW Power; and item 7 is from RF/MW Instrumentation.

The excitation arm of the experimental setup is shown in black and the detection arm is shown in blue. There are three main processes which are facilitated by the components shown in the schematic. These are (1) generation of a chirped MW pulse, (2)

interaction of the molecular beam with the microwave excitation pulse, and (3) detection of the molecular emission. All of these processes are discussed in detail below.

2.3.1. Generation of the chirped MW pulse

In order to carry out broadband FTMW spectroscopic measurements, one needs a microwave source which is capable of generation of broadband linear frequency sweeps in a short time with a reproducible phase. The chirped pulse is produced by a 4.2 Giga samples/s AWG (Item 2) that is referenced to an external clock, which is operating at 3.96 GHz (Item 3). The AWG produces a chirped pulse of 4 μs duration, ranging from 0 to 1 GHz. The production of a chirped pulse in a short duration is essential because the sample must be polarized faster than the pure dephasing time of the rotational emission. By using a double balanced mixer (Item 5), the chirped pulse from the AWG is then mixed with a fixed MW frequency, ν_{MW}, produced by a microwave synthesizer (Item 4). The main purpose of this mixing is to up convert the output of the AWG to the desired microwave frequency range. This procedure produces a chirped pulse of 2 GHz spectral bandwidth centered at ν_{MW}. The chirped MW pulse is then amplified using a broadband (8-18 GHz) 20 W high power solid sate amplifier (Item 6) and broadcasted into a vacuum chamber through a horn antenna (Item 7). The amplification of the chirped pulse to high power is necessary because there is no build-up of energy in the chirped pulse spectrometer chamber, in contrast to the cavity-based FTMW spectrometer. A high power pulse is essential to adequately excite molecules in a large frequency range.

2.3.2. Interaction of the molecular beam with the microwave excitation pulse

The sample cell of the chirped pulse FTMW spectrometer consists of a six-way cross aluminium chamber. The molecular system of interest is introduced into the sample

chamber as a supersonic jet expansion using a nozzle (Item 8) driven by a nozzle driver (Item 9). The direction of propagation of the molecular jet expansion is perpendicular to that of the chirped excitation pulse. The vacuum in the sample chamber is maintained by a 1300 L/s diffusion pump that is backed by a roughing pump, as is the case for the cavity-based FTMW instrument. Two identical high gain horn antennas (Item 7) are utilized to broadcast the amplified chirped MW pulse and to collect the molecular emission signals. The position of the horn antennas is fixed, and the separation between the two is approximately 30 cm. Because of the perpendicular orientation of the molecular jet with the chirped excitation pulse, the time of interaction between the molecular sample and the excitation pulse is less than that in the cavity-based FTMW spectrometer.

2.3.3. Detection of the molecular emission

It has been shown that the molecular emission signal from a chirped pulse excitation is of the form [16,17]

$$S \propto \omega \mu^2 E_{pulse} \Delta N_0 \left(\frac{\pi}{\alpha} \right)^{1/2} \qquad (2.2)$$

where S is the signal strength, ω is the transition frequency, μ is electric dipole component of interest, E_{pulse} is the electric field strength of the chirped pulse, ΔN_0 is the population difference between two levels at equilibrium, and α is the linear sweep range. From the equation, it is clear that there is an inverse relation between the signal strength and the square root of the sweep range. The signal strength decreases with the square root of the bandwidth for a chirped pulse of finite duration. In the case of a cavity-based FTMW spectrometer, the signal strength decreases linearly with an increase in

26

bandwidth.[15] This indicates that the power required by the chirped pulse spectrometer is less than that required by the cavity-based spectrometer, across the same bandwidth.

The broadband coherent emission signal after the chirped pulse excitation of the molecular sample is measured as follows. The broadband emission signal is collected by one of the high gain horn antenna. The emission signal then goes to a power limiter (Item 10) and a PIN diode switch (Item 11) that protects the low noise signal amplifier from the high power microwave pulse. The PIN diode switch is closed during the excitation of the molecular sample and open only for the detection of the emission pulse. After passing through the PIN diode switch, the signal gets amplified by the low noise amplifier (Item 12) and mixed with a microwave frequency that is 1.5 GHz higher than the center frequency of the chirped pulse. The 1.5 GHz difference is chosen to prevent folding of the rotational spectrum about the center frequency after the FT. The frequency after mixing is then filtered with two 4.4 GHz low pass filters to remove any high frequency artifacts. The signal after the filters is again amplified using another low noise amplifier, and the final signal is digitized, at a rate of 40 Gsample/s with a fast digital oscilloscope (Item 18), transferred to a computer, averaged, and fast Fourier transformed to yield the frequency spectrum. In most of the spectra recorded, 100 000 to 200 000 time domain signals were averaged to achieve good signal-to-noise ratios. An example broadband spectrum recorded for methyl lactate monomer, centered at 9.5 GHz is shown in Figure 2.4.
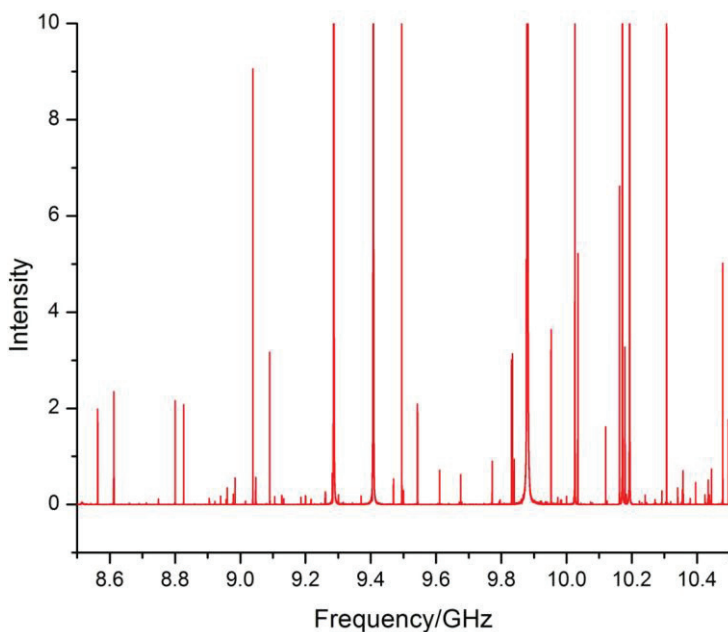
Figue 2.4. A broadband spectrum of methyl lactate monomer centered at 9.5 GHz using the chirped pulse FTMW spectrometer. The sample mixture consisted of 0.06 % methyl lactate in Helium at a stagnation pressure of 6 bars and 200 000 averaging were used for the experiment. The peaks shown in the figure are clipped.

The chirped pulse FTMW spectrometer has a frequency resolution of 25 kHz. The chirped pulse FTMW spectrometer is capable of executing up to 20 microwave experiments during a single molecular pulse. Each experiment includes a chirped pulse excitation, a signal detection and a digitization cycle.[18] Background signal is recorded prior to each molecular pulse in our set up.

Phase stability is essential for averaging of the broadband molecular emission signal in the time domain. If the emission signals are not in phase, they will average out causing decrease in the signal to noise ratio. In order to achieve the phase stability in the experiment, all time sequences in the experiment are referenced to a Rb-frequency standard operating at 10 MHz (Item 1). The TTL signals generated by a pulse generator

(Item 20) control the operation of the pulsed nozzle, AWG, solid state high power MW amplifier, protective switches, and digital oscilloscope. The aforementioned steps constitute one experimental cycle. In order to make sure that every process in one cycle is complete before the next cycle begins, the time allowed for one experimental cycle is optimized manually, and a second pulse generator (Item 21) is used to control the timing between consecutive experimental cycles.

2.4. Analysis of the spectra

To study the molecules or species of interest using MW rotational spectroscopy, we first need to bring the sample into the gas phase. Rotational transition frequencies correspond to energy differences between the rotational energy levels of molecules. Spectroscopic constants, which yield detailed structural information of the molecules of interest, can be obtained from an in depth analysis of the experimental spectral data. Isotopic substitution can give further insights into the structures of molecules or complexes under investigation. This method will be utilized in Chapters 7 and 8 of this thesis.

Since the theories of rotational spectroscopy are described thoroughly in several textbooks,[19,20] I will not repeat these in this thesis. Classification of molecules into different groups based on their moment of inertia and detailed descriptions of their rotational spectroscopic treatments can be found in the textbook of Gordy and Cook[19] which has been invaluable to my study. All the molecular systems investigated in this thesis are asymmetric top rotors which contain either permanently or transiently chiral molecules.

In all of my studies, I have applied a general strategy for assigning and analyzing rotational spectra, as described below. Besides carrying out extensive literature searches [21-27,11] and preparation of the molecular systems of interest, I performed a conformational searches for these systems using *ab inito* calculations. These calculations were carried out using the Gaussian 03[28] and Gaussian 09[29] suite of programs. Typically, Moller Plesset second order perturbation theory (MP2)[30] with different basis sets such as (6-311++G(d,p), 6-311++G(2d,p) and aug-cc-pVTZ) were used for the final calculations. Such combinations were chosen because of their proven performance in similar kinds of systems. These theoretical conformational searches help to narrow down the experimental search range. The rotational constants and electric dipole components from the geometry optimization calculations were used to stimulate the theoretical spectra of all possible conformers.

Broadband scans for the rotational spectra were carried out using the chirped pulse FTMW instrument described above. For example, molecular systems which consist of A and B compounds, rotational spectra were recorded with the sample mixtures of A, B and A+B separately where And B can be any two monomers used in a study. This helps one to disentangle transitions from different molecular species, a large hurdle to overcome to achieve a definite rotational assignment for a specific conformer. The broadband spectra were then compared to the simulated spectra to aid in the spectral assignment. In most cases, the broadband spectrum is saturated due to the presence of many different conformers of the molecule or system of interest. A few empirical approaches I applied in my assignments are to look for the most stable conformer

predicted, to look for those conformers with *a*-type transitions since they have easier to recognize spectral patterns, and to look for transitions with unique hyperfine structures.

Several rotational spectroscopic programs, for example, Pickett's program,[31] Pgopher,[32] XIAM,[33] and ZFAP6 (http://www.uni-ulm.de/~typke /progbe /zfap6.html), have been written over the years to simulate and to fit the experimental rotational spectra. These programs are generously provided by the authors and are freely available to the community of spectroscopists online. An excellent source of information is http://info.ifpan.edu.pl/~kisiel/prospe.htm. It contains a collection of programs for simulating and fitting rotational spectra and for various other application aspects of rotational spectroscopy. The website also contains many supplementary programs to aid the fitting or simulating processes of the rotational spectra. I used Pgopher[32] substantially because of its great graphical interface capability. For fitting of rotational transitions with additional hyperfine structures, I used XIAM[33] to fit hyperfine splitting due to high barrier internal rotation motion and Pgopher for nuclear quadrupole hyperfine structures. The specific programs are mentioned in the respective chapters where they are utilized.

To extract structural information from the obtained rotational constants, two programs STRFIT[34] and PMIFST are utilized. The first one is used for structure fitting and the second one for structural calculations. Kratichman's coordinate analyses[35] were also used to extract detailed information of the structure of the molecules from the isotopic data. For example, the Kratichman's coordinate analyses using the experimental rotational constants of the isotopologues of methyl lactate$\cdot\cdot$(H$_2$O)$_{1,2}$ were used to locate the position of the dangling hydrogen atoms in Chapter 7. The analysis and assignment of

the rotational spectra of the molecules or complexes of interest are also described briefly in the individual chapters.

References

[1] K. B. McAfee, Jr., R. H. Hughes, E. B. Wilson, Jr., *Rev. Sci. Instrum*. **1949**, *20*, 821-826.

[2] R. H. Hughes, E. B. Wilson, Jr., *Phys. Rev*. **1947**, *71* , 562-563.

[3] J. C. McGurk, T. G. Schmalz, W.H. Flygare, Density Matrix, Bloch Equation Description of Infrared and Microwave Transient Phenomena; (eds.; I. Prigogine, S. A. Rice), 1974.

[4] T. J. Balle, W. H. Flygare, *Rev. Sci. Instrum*. **1981**, *52*, 33 – 45.

[5] J.-U. Grabow, W. Stahl, H. Dreizler, *Rev. Sci. Instrum*. **1996**, *67*, 4072-4084.

[6] A.C. Legon, *Ann. Rev. Phys. Chem*. **1983**, *34*, 275-300.

[7] J.-U. Grabow, Fourier Transform Microwave Spectroscopy Measurement and Instrumentation, in: Handbook of High-resolution Spectroscopy, (John Wiley& Sons, Ltd., 2011.)

[8] J. C. McGurk, T. G. Schmalz, W. H. Flygare, *Adv. Chem. Phys*. **1974**, *25*, 1-68.

[9] T. G. Schmalz, W. H. Flygare, in Laser and Coherence Spectroscopy, (ed.; J. I. Steinfeld) Plenum, New York, 1978, pp. 125–196.

[10] Y. Xu, W. Jäger, *J. Chem. Phys*. **1997**, *106*, 7968-7980.

[11] Y. Xu, J. van.Wijngaarden, W. Jäger, *Int. Rev. Phys. Chem*. **2005**, *24*, 301- 338

[12] J-U. Grabow, W .Stahl, *Z. Naturforsch*. **1990**, *45a*, 1043 -1044.

[13] G. G. Brown, B. C. Dian, K. O. Douglass, S. M. Geyer, B. H. Pate, *J. Mol. Spectrosc*. **2006**, *238*, 200-212.

[14] S. Dempster, O. Sukhorukov, Q.-Y. Lei, W. Jäger, *J. Chem. Phys*. **2012**, *137*, 174303/1-8.

[15] G. S. Grubbs II, C. T. Dewberry, K. C. Etchison, K. E. Kerr, S. A. Cooke, *Rev. Sci.Instrum.* **2007**, *78*, 096106/1-3.

[16] Brown, G. G.; Dian, B. C.; Douglass, K. O.; Geyer, S. M.; Shipman, S. T.; Pate, B. H. *Rev. Sci.Instrum*. **2008**, *79*, 053103/1-13.

[17] J. C. McGurk, T. G. Schmalz, W. H. Flygare, *J. Chem. Phys*. **1974**, *60*, 4181-4188.

[18] J. Thomas, J. Yiu, J. Rebling, W. Jäger, Y. Xu, *J. Phys. Chem. A*. **2013**, *117*, 13249–13254.

[19] W. Gordy, R. L. Cook, Microwave Molecular Spectra, 3rd ed. (Wiley, New York, 1984)

[20] C. H. Townes, A. L. Schawlow, Microwave Spectroscopy (Dover, New York, 1975), p. 306

[21] K.R. Leopold, G.T. Fraser, S.E. Novick, W. Klemperer, *Chem. Rev*. **1994**, *94*, 1807-1827

[22] G. S. Grubbs II, P. Groner, Stewart E. Novick, S. A. Cooke, *J. Mol. Spectrosc.* **2012**, *280*, 21-26.

[23] R. Subramanian, J. M. Szarko, W. C. Pringle, S. E. Novick, *J. Mol. Struct*. **2005**, *742*, 165-172.

[24] Y. Xu, W. Jäger, *Chem. Phys. Lett*. **2001**, *350*, 417-422.

[25] A. C. Legon, *Ann. Rev. Phys. Chem*. **1983**, *34*, 275-300.

[26] T.R. Dyke, *Topics Current Chem*. **1984**, *120*, 86-113.

[27] S. E. Novick, K. R. Leopold, W. Klemperer, The Structure of Weakly Bound Complexes as Elucidated by Microwave and Infrared Spectroscopy, in Atomic and Molecular Clusters, (ed.; E.R. Bernstein), Elsevier, 1990, p. 359.

[28] Gaussian 03, Revision B.01, M. J. Frisch, G. W. Trucks, H. B. Schlegel, G. E. Scuseria, M. A. Robb, J. R. Cheeseman, J. A. Montgomery, Jr., T. Vreven, K. N. Kudin, J. C. Burant, J. M. Millam, S. S. Iyengar, J. Tomasi, V. Barone, B. Mennucci, M. Cossi, G. Scalmani, N. Rega, G. A. Petersson, H. Nakatsuji, M. Hada, M. Ehara, K. Toyota, R. Fukuda, J. Hasegawa, M. Ishida, T. Nakajima, Y. Honda, O. Kitao, H. Nakai, M. Klene, X. Li, J. E. Knox, H. P. Hratchian, J. B. Cross, C. Adamo, J. Jaramillo, R. Gomperts, R. E. Stratmann, O. Yazyev, A. J. Austin, R. Cammi, C. Pomelli, J. W. Ochterski, P. Y. Ayala, K. Morokuma, G. A. Voth, P. Salvador, J. J. Dannenberg, V. G. Zakrzewski, S. Dapprich, A. D. Daniels, M. C. Strain, O. Farkas, D. K. Malick, A. D. Rabuck, K. Raghavachari, J. B. Foresman, J. V. Ortiz, Q. Cui, A. G. Baboul, S. Clifford, J. Cioslowski, B. B. Stefanov, G. Liu, A. Liashenko, P. Piskorz, I. Komaromi, R. L. Martin, D. J. Fox, T. Keith, M. A. Al-Laham, C. Y. Peng, A. Nanayakkara, M. Challacombe, P. M. W. Gill, B. Johnson, W. Chen, M. W. Wong, C. Gonzalez, and J. A. Pople, Gaussian, Inc., Pittsburgh PA, 2003.

[29] Gaussian 09, Rev. C.01, M. J. Frisch, G. W. Trucks, H. B. Schlegel, G. E. Scuseria, M. A. Robb, J. R. Cheeseman, G. Scalmani, V. Barone, B. Mennucci, G. A. Petersson, H. Nakatsuji, M. Caricato, X. Li, H. P. Hratchian, A. F. Izmaylov, J. Bloino, G. Zheng, J. L. Sonnenberg, M. Hada, M.Ehara, K. Toyota, R. Fukuda, J. Hasegawa, M. Ishida, T. Nakajima, Y. Honda, O. Kitao, H. Nakai, T. Vreven, J. J. A. Montgomery, J. E. Peralta, F. Ogliaro, M. Bearpark, J. J. Heyd, E. Brothers, K. N. Kudin, V. N. Staroverov, T. Keith, R. Kobayashi, J. Normand, K. Raghavachari, A. Rendell, J.C. Burant, S. S. Iyengar, J. Tomasi, M. Cossi, N. Rega, J. M. Millam, M. Klene, J. E. Knox, J. B. Cross, V. Bakken, C. Adamo, J. Jaramillo, R. Gomperts, R.

E. Stratmann, O. Yazyev, A. J. Austin, R. Cammi, C. Pomelli, J. W. Ochterski, R. L. Martin, K. Morokuma, V. G. Zakrzewski, G. A.Voth, P. Salvador, J. J. Dannenberg, S. Dapprich, A. D. Daniels, O. Farkas, J. B. Foresman, J. V. Ortiz, J. Cioslowski, D. J. Fox, Gaussian, Inc.,Wallingford CT, 2010

[30] J. S. Binkley, J. A. Pople, *Int. J. Quantum Chem*. **1975**, *9*, 229–236.

[31] H. M. Pickett, *J. Mol. Spectrosc*. **1991**, *148*, 371-377 .

[32] Pgopher, a Program for Simulating Rotational Structure, C. M. Western, University of Bristol, http://Pgopher.chm.bris.ac.uk.

[33] H. Hartwig, H. Dreizler, *Z. Naturforsch*. **1996**, *51a*, 923–932.

[34] Z .Kisiel, *J. Mol. Spectrosc*. **2003**, *218*, 58-67.

[35] J. Kraitchmann, *Am. J. Phys*. **1953**, *21*, 17−25.

Chapter 3

Chirality Recognition in the Glycidol···Propylene Oxide

Complex: A Rotational Spectroscopic Study[a]

3.1. Introduction

Molecular chirality often plays a vital role in determining the biological and chemical properties of matter.[1] Chirality recognition, the ability of a chiral molecule to discriminate among the two enantiomers of another chiral molecule, is of paramount importance in stereo-organic synthesis, biochemistry, and drug design.[2] Detailed and quantitative knowledge about the weak non-covalent forces responsible for chirality recognition is of great relevance for computer assisted drug design and screening. How the weak non-covalent intermolecular interactions such as hydrogen (H)-bonding and van der Waals interactions facilitate a chirality recognition process is an area of intense current interest.[3,4] Gas phase spectroscopies, such as laser induced fluorescence,[5] resonance enhanced two or multiphoton ionization,[6] UV/IR double resonance,[5] and broadband FTIR spectroscopy[7] have been used in the last few years to obtain low resolution spectra of chiral molecular complexes and to explore their conformational landscapes with the aid of *ab initio* calculations. More recently, high resolution spectroscopy, specifically Fourier transform microwave (FTMW) spectroscopy, has been successfully applied to the investigation of several chiral molecular systems. For example, Howard and co-workers reported the first high resolution spectroscopic study of a chiral molecular complex, i.e., the butan-2-ol dimer[8] and assigned one heterochiral dimer. Later on, FTMW studies of chirality recognition in the complexes of propylene oxide (PO) with transient chiral 2-fluoroethanol[9] and ethanol,[10] as well as chirality self recognition in the PO dimer have been published.[11] More recently, Caminati and co-workers detected two conformers of the homochiral glycidol dimer.[12]   The low resolution spectroscopic assignment of conformers relies on the comparison of the

observed and calculated vibrational band shifts associated with different conformers which are often minute and difficult to model correctly. One noticeable advantage of high resolution spectroscopic studies is that every conformer has its own distinct set of transitions and the spectral assignments rely on the internal consistency of tens to hundreds of rotational transitions observed, rather than the theoretical modeling. These quantitative data of chiral molecular contact pairs are therefore very valuable for the benchmarking of high level *ab initio* methods.

In this chapter, we report the detailed rotational analysis of six binary, H-bonded conformers of the glycidol (Gly)···PO adduct. This is the first high resolution study of a chiral contact pair with two different permanently chiral molecules. Only three high resolution spectroscopic studies of Gly containing complexes, i.e., Gly···H_2O,[13] Gly···Gly,[12] and Gly···NH_3,[14] have been reported so far, and only one or two conformers were detected in each case. Gly has two major monomeric conformers, with one being about four times more abundant than the other at room temperature.[15] This allows us to see whether the formation of the H-bonded species is a dominantly kinetic process or controlled by thermodynamics. Furthermore, since Gly···PO is relatively small, containing only second row atoms besides H-atoms, it is amenable to high-level *ab initio* calculations. One can therefore gain detailed insights into how conformational structures of Gly are modified to facilitate interactions with PO. In particular, one can investigate if the interactions with PO help to selectively stabilize the less stable Gly conformer. In this sense, Gly···PO can be regarded as a microscopic induced-fit example.

3.2. Results

3.2.1. Preliminary prediction of possible conformers.

One may expect a substantial number of possible conformers to exist for a system like Gly···PO and a systematic analysis of the possible conformers of the 1:1 Gly···PO adduct is desirable. PO is a rigid chiral molecule with a single conformation except for the internal rotation of the methyl group. Gly, on the other hand, can have 3x3, i.e., nine different rotameric conformations based on the two dihedral angles CCOH and OCCO. If the dihedral angle of CCOH is around +60, -60 or 180 degree, it leads to three different conformations, *g+*, *g-* and *t,* respectively. Similarly, we label the three different conformations *G+*, *G-* and *T* if the dihedral angle of OCCO is around +60, -60 or 180 degree, respectively. This consideration gives rise to the following nine rotameric conformations for the Gly monomer: *g+G+*, *g-G+*, *tG+*, *g+G-*, *g-G-*, *tG-*, *g+T*, *g-T* and *tT*. In addition, Gly can bind to the oxygen atom of PO either on the same side (*syn*) of the PO methyl group or on the opposite side (*anti*). This, plus the consideration of homo- and heterochiral contact pairs, leads to a total of 9x2x2=36 binary conformers for the Gly···PO adducts. For simplicity, we use (*S*)-Gly and *R*- or *S*-forms of PO throughout this chapter to build 18 homochiral and 18 heterochiral dimers. To facilitate easy recognition of the binary adduct, a unique naming system was developed. It is of the form *syn/anti* (*S*) *g-G+* Gly···(Hx,Hy) (*R/S*) PO, where x and y take the integer value of 1, 2 or 3 in descending order. H1, H2 and H3 indicate that the corresponding H-atoms involved in the secondary H-bonds belong to the CH, CH_2, and CH_3 groups of PO, respectively.

To further aid the spectral search and assignment, *ab initio* calculations were carried out for the Gly monomer and the binary Gly···PO adduct using the Gaussian 03

program package.[16] Second-order Møller-Plesset perturbation theory (MP2)[17] with the 6-311++G(d,p) basis set[18] was chosen because of its proven performance for the H-bonded chiral contact pairs.[19,20] Eight possible rotameric conformations for the Gly monomer were confirmed to be true minima and the two most stable conformers identified as *g-G+* and *g+G-* are the only ones with an appreciable population at room temperature. The *g-G+* conformer was predicted to be ~2.5 kJ mol^{-1} more stable than *g+G-*. This is consistent with the previous calculations[7a] and the microwave experiments.[15] For the binary Gly···PO adduct, 14 homochiral and 14 heterochiral conformers were identified and their minimum nature was confirmed by the geometric optimization and the subsequent harmonic frequency calculations, respectively. The zero point energies (ZPEs) and the basis set superposition errors (BSSEs) were calculated where counterpoise correction of Boys and Bernadi was used for the latter case.[21] The calculated energies for all 28 binary conformers are summarized in Table 3.S1, Appendix A. The four most stable homochiral and four heterochiral conformers have their relative dissociation energies predicted within 4 kJ mol^{-1} of each other. The rest of the conformers are less stable by more than 8 kJ mol^{-1} and are not expected to be populated in a jet expansion. The geometries of the eight most stable homochiral and heterochiral conformers are depicted in Figure 3.1, together with their unique names and the important intermolecular H-bonds. For easy recognition, simplified names, such as Homo I or Hetero II are also provided, where I, II, III or IV indicate the predicted relative dissociation energy ordering in ascending order.
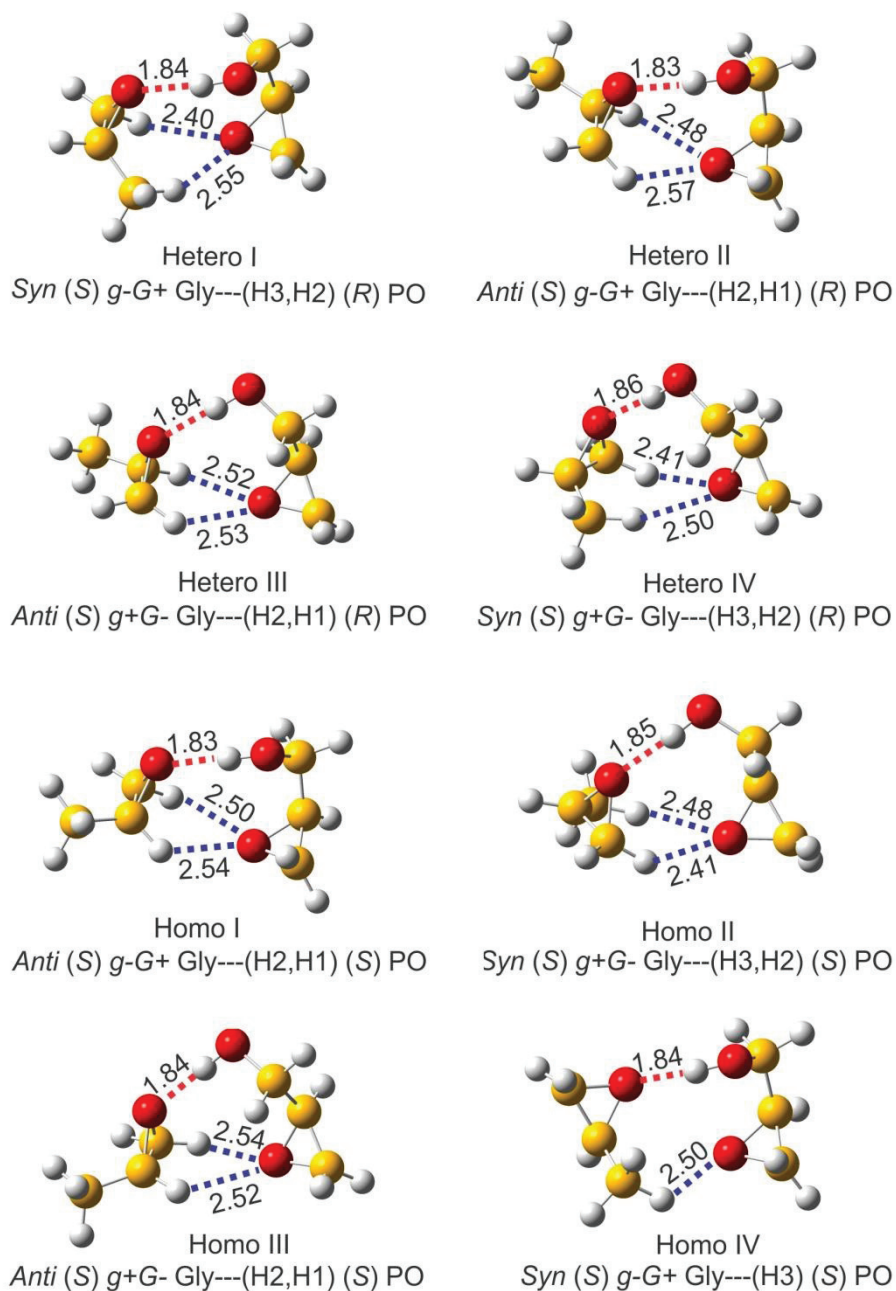
Figure 3.1. Structures of the eight most stable conformers of the Gly...PO complex calculated at the MP2/6-311++G(d,p) level of theory. The primary (in red) and the secondary (in blue) H-bonds are indicated.

The structures of all the other binary and the monomeric conformers are given in Figure 3.S1, Appendix A. The calculated dissociation energies, rotational constants, and electric

dipole moment components of these eight most stable binary conformers are listed in Table 3.1, while the related spectroscopic results for the less stable binary conformers are also given in Table 3.S1, Appendix A.

3.2.2. Rotational assignment of the Gly···PO binary adduct

Spectral searches were carried out first for the four lowest energy binary heterochiral conformers and then for the homochiral conformers. Even with a sample mixture of only PO+Gly+Ne, rotational transitions due to species other than the targeted dimers can show up with fairly strong intensities. For example, those of the PO dimer,[11] the Gly dimers,[12] PO···Ne,[22] and Gly and ^{13}C Gly,[13] were identified and excluded using the previously measured frequencies. Additional tests to reduce the number of candidate transitions were performed using the sample mixtures excluding either PO or Gly. Since water is often an impurity in the sample system, we also checked for transitions due to PO···$(H_2O)_n$ (n = 1, 2),[23] and Gly···H_2O[13] which were found to be extremely weak under the current experimental conditions. It was challenging to assign spectral lines initially since the b-type electric dipole moment component was predicted to be the most prominent one in all eight conformers and the related transition pattern was more difficult to identify than that of the a-type transitions. Since both chiral molecules have permanent chirality, it was possible for us to further test the observed transitions using both homo and heterochiral PO+Gly samples.

After some extensive trials and errors, we were able to unambiguously assign six of the eight low energy conformers predicted. The presence of both strong b- and c-type transitions makes the assignment of Hetero I and II and Homo I easier compared to Homo II and III and Hetero III who have only significant dipole moment along the b-

axis. Although the *a*-dipole moment is fairly small in these six conformers, we were nevertheless able to observe a few *a*-type transitions in the case of Hetero III and Homo II. A total of 29 to 41 rotational transitions were measured for each of these conformers. The transition frequencies are listed in Table 3.S2, Appendix A.

Table 3.1. Calculated relative raw dissociation energies ΔD_e, ZPE and BSSE corrected dissociation energies ΔD_0 (in kJ mol^{-1}), rotational constants *A, B,* and *C* (in MHz) and electric dipole moment components $|\mu_{a,b,c}|$ (in Debye) of the eight most stable H-bonded conformers at the MP2/6-311++G(d,p) level of theory.

	Homochiral pairs			
Const.	Homo I	Homo II	Homo III	Homo IV
ΔD_e	0.23	1.31	1.83	4.20
	(1.31) [a]	(1.79)	(3.12)	(5.42)
ΔD_0	0.46	1.64	1.66	3.86
A	2679	2211	2390	2455
B	842	935	850	960
C	762	815	726	807
$|\mu_a|$	0.03	0.77	0.36	1.06
$|\mu_b|$	2.25	3.07	3.64	1.15
$|\mu_c|$	1.48	0.54	0.79	0.58
	Heterochiral pairs			
	Hetero I	Hetero II	Hetero III	Hetero IV
ΔD_e	0.00[b]	0.26	1.76	2.31
	(0.00)[a]	(1.38)	(2.97)	(2.80)
ΔD_0	0.00[b]	0.51	1.5	2.47
A	2351	2620	2465	2157
B	953	845	840	948
C	858	777	716	818
$|\mu_a|$	0.05	0.20	0.68	0.47
$|\mu_b|$	1.68	2.20	3.50	3.50
$|\mu_c|$	1.51	1.80	0.46	0.79

[a] Values in brackets are the single point energies calculated at the MP2/aug-cc-pVTZ level, using the MP2/6-311++G(d,p) geometries.
[b] D_e and D_0 of Hetero I are -38.51 and -20.97 kJ mol^{-1}, respectively.

We had done extensive spectral searches with more than 200 times the number of experimental cycles than that for the strongest conformer and over much wider frequency coverage than that for the observed conformers in order to locate Hetero IV and Homo

44

IV. However, no candidate lines were detected. Clearly, they have much lower abundance in the jet expansion compared to the other six observed, suggesting these two conformers are much less stable (vide infra).

All of the lines observed were fitted to Watson's A-reduction semirigid rotor Hamiltonian in its I^r representation.[24] The standard deviations of all the spectroscopic fits are a few kHz, similar to the experimental uncertainty in the measured frequencies. In a few transitions, small splittings on the order of a few to twenty kHz were observed. These are possibly due to the internal rotation of the methyl groups. Because such splittings are not resolved in most transitions and the magnitude is small, no attempt was made to analyze them in detail. Rather, the averaged frequencies were used as the centre frequencies in these cases and weighted accordingly in the fit[25] and are identified in Table 3.S2, Appendix A. The experimental rotational constants of all the binary conformers are given in Table 3.2. Since the predicted rotational constants of the targeted conformers are generally quite different, it was straightforward to correlate an experimental set of rotational constants to a particular conformer predicted. The assignment was further confirmed by comparison of the relative magnitudes of the observed and calculated a-, b-, and c-type dipole moment components. A comparison of the experimental and calculated rotational constants shows a maximum deviation of 2.3%, which is comparable to deviations of 1.1-6.3% found in PO···2-fluoroethanol[9] and PO···ethanol.[10] This indicates that the predicted structures are quite close to the ones determined from experiment.

Table 3.2. Experimental spectroscopic constants of the three detected homochiral and three detected heterochiral binary conformers of Gly…PO.

Conformers	Homo I	Homo II	Homo III
A [MHz]	2664.3553(11)[a]	2235.3562(6)	2397.9689(5)
B [MHz]	827.31977(30)	913.53752(48)	834.01761(42)
C [MHz]	751.59776(26)	803.90043(39)	710.78907(37)
Δ_J [kHz]	0.2799(5)	0.313(9)	0.293(6)
Δ_{JK} [kHz]	0.619(17)	1.14(2)	0.0[b]
Δ_K [kHz]	1.63(23)	-0.581(70)	1.65(5)
δ_j [kHz]	0.027(2)	0.055(4)	0.027(3)
δ_k [kHz]	0.0[b]	-1.46(13)	0.0[b]
N^c	34	31	31
σ [kHz]	2.7	3	3.6
Conformers	Hetero I	Hetero II	Hetero III
A [MHz]	2361.0350(2)	2635.5829(16)	2463.7459(7)
B [MHz]	934.6977(3)	824.89066(43)	826.78321(28)
C [MHz]	848.74471(37)	758.76510(37)	707.17163(34)
Δ_J [kHz]	0.343(6)	0.267(7)	0.264(4)
Δ_{JK} [kHz]	1.15(2)	0.739(32)	0.799(20)
Δ_K [kHz]	-.850(37)	1.42(34)	0.842(73)
δ_j [kHz]	0.041(3)	.016(3)	0.036(2)
δ_k [kHz]	1.53(12)	0.0[b]	0.0[b]
$N^{[c]}$	35	29	41
σ [kHz]	2.1	3.7	3.8

[a] Standard errors in parenthesis are expressed in units of last digits. [b] The value was fixed at 0.0 in the fit. [c] Number of transitions included in the fit.

3.3. Discussions

One important goal of the current study was to provide detailed understanding about how the interaction with PO influences the relative stability of the Gly monomeric conformers. Such knowledge is a prerequisite to model induced-fits in larger biomolecular systems quantitatively. An energy diagram that correlates the energies of the conformers of the Gly monomer to those of the Gly··PO binary adducts is shown in Figure 3.2.
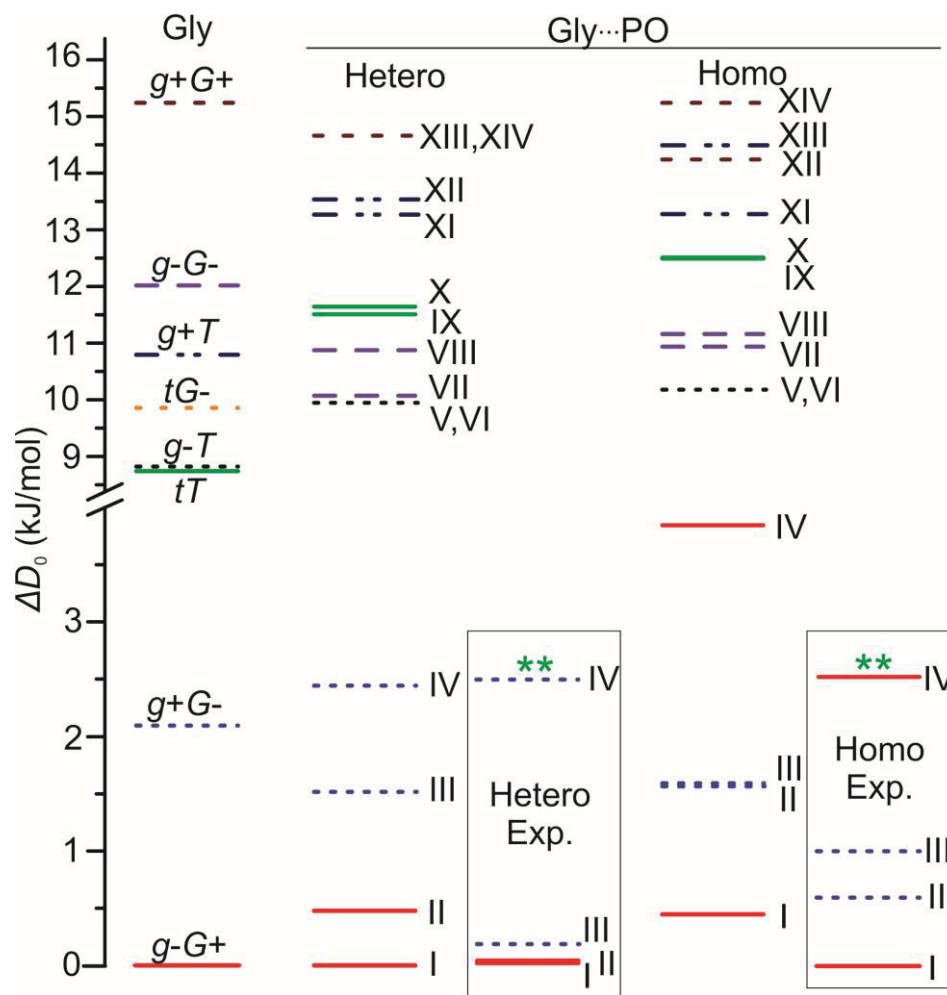
Figure 3.2. Energy correlation diagram for the Gly conformers and the Gly...PO conformers plotted using the MP2/6-311++G(d,p) $\Delta D0$ values. The experimentally estimated values for the all eight conformers observed are also given. ** indicates that the relative energies are higher than 2.5 kJ mol^{-1}. See text for details.

From the figure, it is clear that the eight most stable heterochiral and homochiral binary conformers all consist of the two lowest energy Gly monomeric conformations *g-G+* and *g+G-*, whereas the higher energy binary conformers are all composed of the much less stable Gly monomeric conformers. Overall, the stability of monomers plays a key role in the stability of the associated dimers made of them. Since Gly exists almost exclusively as *g-G+* and *g+G-* at room temperature, we will concentrate on the eight

lowest binary conformers in our discussion. A closer examination of these eight binary conformers indicates that their relative stability is also strongly influenced by interaction between Gly and PO, to the extent that Homo IV. Which contains g-$G+$ Gly, is significantly less stable than those containing $g+G-$ Gly. One may explain this on the basis of the presence of secondary H-bonding interactions, as illustrated in Figure 3.1. For example, Homo IV, the least stable one, has only one secondary H-bond whereas all the other seven dimers have two each.

To gain more quantitative insight, the contribution to the overall dissociation energy, D_e, is decomposed into the following four terms: E_{mon}, E^{dist}_{Gly}, E^{dist}_{PO}, and E^{int}, using similar notation as in Ref. 9. We use D_e for simplicity since the inclusion of BSSE and ZPE corrections do not alter the stability ordering of these eight conformers, as can be seen from Table 3.1. E_{mon} corresponds to the relative monomer energy with respect to the lowest one. This applies only to Gly since PO has just one conformer. E^{dist}_{Gly} is the fragment deformation energy for Gly, corresponding to the energy penalty for distorting the isolated Gly from its equilibrium geometry to the optimal geometry in Gly··PO. E^{dist}_{PO} is similarly defined. E^{int} is the interaction energy of the binary conformer, defined as E_{dimer} - E^{dimer}_{Gly} - E^{dimer}_{PO}, where the first term is the total dimer energy, and the second and third terms are the energies of the two subunits at their optimal geometries in Gly··PO. The values of these terms are provided in Table 3.3

The largest deformation energy difference among these conformers for the fairly rigid PO subunit is only ~0.3 kJ mol^{-1}, whereas the corresponding difference for Gly is ~3.2 kJ mol^{-1}, of similar magnitude as the relative monomer energy E_{mon}, 2.5 kJ mol^{-1}.

E^{int} has an energy span of ~5.4 kJ mol^{-1}. Clearly, the interaction energy is of the greatest importance, while the relative monomer energy and the deformation energy also play significant roles in determining the relative stability of these conformers. The importance of such deformation energy has been discussed in some other previous studies of H-bonded systems.[26]

Table 3.3. The calculated relative monomer, deformation, interaction and raw dissociation energies (in kJmol^{-1}) at the MP2/6-311++G(d,p) level for the eight most stable conformers of Gly...PO. See the text for the definition of these terms.

	E_{mon}	E^{dist}_{Gly}	E^{dist}_{PO}	E^{int}	D_e
Hetero I	0	4.71	0.50	-43.72	-38.51
Hetero II	0	3.35	0.57	-42.17	-38.24
Hetero III	2.51	1.53	0.51	-41.29	-36.75
Hetero IV	2.51	1.84	0.39	-40.92	-36.19
Homo I	0	3.35	0.57	-42.21	-38.28
Homo II	2.51	2.29	0.48	-42.49	-37.20
Homo III	2.51	1.53	0.51	-41.23	-36.68
Homo IV	0	3.72	0.27	-38.31	-34.31

The experimental observation of the six conformers allows one to extract their relative experimental stability ordering and to compare to the calculated one. The intensity measurements were performed with a racemic PO and (*S*) Gly sample mixture. The signal-to-noise ratios of a number of transitions of each conformer were monitored. The relative abundance of all the six dimers was calculated according to the following equation derived specifically for amplitude (also called intensity) spectra obtained with a FTMW spectrometer[27] for example, for conformer I and II:

$$\frac{N_I}{N_{II}} = \frac{I_I}{I_{II}} \cdot \frac{\mu_{II}}{\mu_I} \cdot \frac{\gamma_{II}}{\gamma_I} \cdot \frac{\nu_{II}}{\nu_I} \cdot e^{\left(-\frac{\Delta E_{rot}}{K_B T_{rot}}\right)} \qquad (3.1)$$

Here I, μ, γ and ν are the signal-to-noise ratio, the calculated electric dipole moment component, the line strength and the frequency of the pair of the transitions under consideration, respectively. ΔE_{rot} is the energy difference between the two lower rotational levels of the pair of transitions. T_{rot}, the rotational temperature in the jet, was estimated to be about 1 K using a few pairs of rotational transitions observed. Since only the few lowest energy rotational levels are accessed in our experiment, one single rotational temperature is good enough to describe the population distribution of these levels,[12,28] although for some very light rotors such as H^{3+} with much larger rotational energy spacing, two rotational temperatures had been derived.[29] Although the calculated electric dipole moments have been used in the calculations, the optimized microwave pulse widths for the transitions observed suggest that the calculated electric dipole moment components are consistent with the experimental data. From the equation above, an experimental abundance of the species was obtained: Homo I > Hetero I > Hetero II > Hetero III > Homo II > Homo III = 1 > 0.91 > 0.9 > 0.64 > 0.29 > 0.13.

To convert the relative abundance obtained above to the relative energy difference, one needs to know whether or not a conformational equilibrium for the conformers of interest has been achieved in the free jet expansion and what the conformational temperature is. There have been considerable discussions in the literature about this.[30] For example, it was reported that some of the higher energy forms of Serine conformers were trapped in their local minima because of the associated high

50

interconversion barriers and were detected in a jet expansion.[31] In the present case, the two dominant conformations of the Gly monomer are present with an intensity ratio of 4:1 at room temperature. In the previous jet-cooled FTIR study,[32] it was noted that the intensity ratio of these two monomeric conformers further increases in a helium jet expansion, indicating that the interconversion barrier separating these two monomeric conformers can be overcome. One may therefore expect to overcome such a barrier in a Neon expansion in the present case. For the H-bonded binary Gly··PO conformers, one can expect the complex to experience many repeated formation and dissociation events in a jet expansion prior to reaching conformational equilibrium. Such repeated formation and dissociation events had been proposed before to explain the noticeable preference for a deuterium-bonded over an H-bonded complex.[33] In a few previous studies of H-bonded complexes under similar jet expansion conditions, a conformational temperature of ~60 K was estimated.[34] Assuming the same conformational temperature, the relative energies obtained for the above six conformers in ascending order are 0.00, 0.03, 0.05, 0.20, 0.61 and 1.02 kJ mol^{-1}. The relative energies for Hetero IV and Homo IV could also be derived to be higher than 2.5 kJ mol^{-1} based on the experimental cycles used in the search and the procedure described above. The experimental ordering is also summarized in Figure 3.2 for comparison with predictions. The general stability trend among the three homo and three heterochiral contact pairs was correctly predicted, although the relative energy gaps between homo and heterochiral pairs were not captured accurately at the MP2/6-311++G(d,p) level. We also performed single point MP2/aug-cc-pVTZ energy calculations using the MP2/6-311++G(d,p) optimized geometries for the eight lowest energy conformers. The values obtained are included in Table 3.1 for comparison with

the MP2/6-311++G(d,p) energies. Again, Hetero I was predicted to be more stable than Homo I, contrary to the experimental result. This indicates that it is still quite challenging to capture such subtle energy difference accurately with current *ab initio* methods. We have used dissociation energy rather than free energy calculations in the discussion here. This is a common approach used in the studies of H-bonded complexes generated in a free jet environment.[3,8,12,13] Furthermore, the accuracy of free energy calculations with current *ab initio* methods is not high enough for the discussions of the very subtle energy differences observed here.[35]

3.4. Conclusions

It is interesting to note that in the case of Gly··Gly, only two homochiral conformers were detected, although extensive searches had been carried out for several other Gly··Gly conformers which were predicted to have similar stability.[12] If the formation of the Gly··PO complex is a purely kinetically controlled process, one would expect binary conformers containing *g-G+* to be more than 4 times more abundant than those with *g+G-* in a Neon expansion. This is clearly not the case here since Homo IV of *g-G+* is not observed despite considerable experimental efforts, while Hetero III, Homo II and Homo III of *g+G-* were all detected. This observation suggests a thermodynamically controlled process, i.e., the H-bonded binary adducts experience repeated formation and dissociation processes in the jet expansion and finally reach an equilibrium based on their relative stability.

3.5. Experimental section

The sample mixtures consisted of 0.06 % PO and 0.04% Gly in Neon at a backing pressure of 2.0 to 3.5 bars. PO (99% purity, Fluka, Alfa aesar), Gly (99 % purity, Fluka, Alfa aesar), and Neon (99.9990 %) were used without further purification. The rotational spectrum was recorded in the frequency range from 4 to 9 GHz with a Balle–Flygare type[36] pulsed molecular beam Fourier transform microwave spectrometer, which had been described previously.[37] The experimental uncertainty in the rotational transition frequencies is estimated to be about 2 kHz and the full line width at half height is about 10 kHz for well resolved lines.

References

[1] R. A. Sheldon, Chirotechnology: Chirotechnology: Industrial Synthesis of Optically Active Compounds, Marcel Dekker, Inc.: New York, 1993, pp 39–72.

[2] C. R.Cantor, P. R. Schimmel, Biophysical Chemistry, W. H. Freeman, San Francisco, 1980.

[3] A. Zehnacker, M. A. Suhm, *Angew. Chem*. **2008**, *120*, 7076 − 7100; *Angew. Chem. Int. Ed*. **2008**, *47*, 6970 − 6992.

[4] G. A. Jeffrey, W. Saenger, Hydrogen Bonding in Biological Structures, Springer, Berlin, 1991.

[5] N. Seurre, J. Sepiol, K. Le Barbu-Debus, F. Lahmani, A. Zehnacker-Rentien, P*hys. Chem. Chem. Phys.* **2004**, *6*, 2867-2877.

[6] A. Gardini-Guidoni, S. Piccirillo, D. Scuderi, M. Satta, T. M. Di Palma, M. Speranza, *Phys. Chem. Chem. Phys*. **2000**, *2*, 4139-4142.

[7] N. Borho, M. Suhm, *Phys. Chem. Chem. Phys*. **2002**, *4*, 2721-2732; T. B. Adler, N. Borho, M. Reiher, M. A. Suhm; *Angew. Chem*. **2006**, *118*, 3518-3523; *Angew. Chem. Int. Ed*. **2006**, *45*, 3440-3445.

[8] A. K. King, B. J. Howard, *Chem. Phys. Lett*. **2001**, *348*, 343-349.

[9] X. Liu, N. Borho, Y. Xu, *Chem. Eur. J*. **2009**, *15*, 270-277.

[10] N. Borho, Y. Xu, *Angew. Chem*. 2007, 119, 2326 − 2329; *Angew. Chem. Int. Ed*. **2007**, *46*, 2276-2279.

[11] Z. Su, N. Borho, Y. Xu, *J. Am. Chem. Soc*. **2006**, *128*, 17126-17131.

[12] A. Maris, B. M. Giuliano, D. Bonazzi, W. Caminati, *J. Am. Chem. Soc*. **2008**, *130*, 13860-13861.

[13] A. R. Conard, N. H. Teumelsan, P. E. Wang, M. J. Tubergen, *J. Phys. Chem. A* **2010**, *114*, 336-342.

[14] B. M. Giuliano, S. Melandri, A. Maris, L. B. Favero, W. Caminati, *Angew. Chem.* **2009**, 121, 1122; *Angew. Chem. Int. Ed.* **2009**, *48*, 1102 −1105.

[15] K. M. Marstokk, H. Mollendal, Y. Stenstrom, *Acta. Chem. Scand*. **1992**, *46*, 432-441.

[16] Gaussian 03, Revision B.01, M. J. Frisch, G. W. Trucks, H. B. Schlegel, G. E. Scuseria, M. A. Robb, J. R. Cheeseman, J. A. Montgomery, Jr., T. Vreven, K. N. Kudin, J. C. Burant, J. M. Millam, S. S. Iyengar, J. Tomasi, V. Barone, B. Mennucci, M. Cossi, G. Scalmani, N. Rega, G. A. Petersson, H. Nakatsuji, M. Hada, M. Ehara, K. Toyota, R. Fukuda, J. Hasegawa, M. Ishida, T. Nakajima, Y. Honda, O. Kitao, H. Nakai, M. Klene, X. Li, J. E. Knox, H. P. Hratchian, J. B. Cross, C. Adamo, J. Jaramillo, R. Gomperts, R. E. Stratmann, O. Yazyev, A. J. Austin, R. Cammi, C. Pomelli, J. W. Ochterski, P. Y. Ayala, K. Morokuma, G. A. Voth, P. Salvador, J. J. Dannenberg, V. G. Zakrzewski, S. Dapprich, A. D. Daniels, M. C. Strain, O. Farkas, D. K. Malick, A. D. Rabuck, K. Raghavachari, J. B. Foresman, J. V. Ortiz, Q. Cui, A. G. Baboul, S. Clifford, J. Cioslowski, B. B. Stefanov, G. Liu, A. Liashenko, P. Piskorz, I. Komaromi, R. L. Martin, D. J. Fox, T. Keith, M. A. Al-Laham, C. Y. Peng, A. Nanayakkara, M. Challacombe, P. M. W. Gill, B. Johnson, W. Chen, M. W. Wong, C. Gonzalez, and J. A. Pople, Gaussian, Inc., Wallingford CT, 2004.

[17] J. S. Binkley, J. A. Pople, *Int. Quantum Chem*. **1975**, *9*, 229-236.

[18] R. Krishman, J. S. Binkley, R. Seeger, J. A. Pople, *J. Chem. Phys*. **1980**, *72*, 650-654.

[19] (a) I. Alkorta, J. Elguero, *J. Am. Chem. Soc*. **2002**, *124*, 488-1493; b) I. Alkorta, J. Elguero, *J. Chem. Phys*. **2002**, *117*, 6463- 6468.

[20] Z. Su, Y. Xu, *Phys. Chem. Chem. Phys***. 2005**, *7*, 2554 – 2560.

[21] S. F. Boys, F. Bernardi, *Mol. Phys*. **1970**, *19*, 553-566.

[22] Z. Su, Y. Xu, *J. Mol. Spectrosc*. **2005**, *232*, 112-114.

[23] Z. Su, Y. Xu, *Angew. Chem*. **2007**, *119*, 6275 – 6278; *Angew. Chem. Int. Ed*. **2007**, *46*, 6163-6166.

[24] J. K. G. Watson in Vibrational Spectra and Structure, Vol. 6 (Ed.: J. R. Durig), Elsevier, New York, 1977, pp. 1 – 89.

[25] N. Borho, Y. Xu, *Phys. Chem. Chem. Phys*. **2007**, *9*, 1324-1328; P. Ottaviani, B. Velino and W. Caminati, *Chem. Phys. Lett*. **2006**, *428*, 236-240.

[26] See for example, K. Le Barbu, F. Lahmani, and A. Zehnacker-Rentien, *J. Phys. Chem. A*. **2002**, *106*, 6271–6278.

[27] J.-U. Grabow, W. Caminati, Microwave Spectroscopy: Experimental Techniques. In Frontiers of Molecular Spectroscopy (Ed. J. Laane), Elsevier, Heidelberg, 2008; p 383.

[28] Z. Su, W. S. Tam, Y. Xu, *J. Chem. Phys*. **2006**, *124*, 024311.

[29] M.Fukushima, M.-C. Chan, Y. Xu, A. Taleb-Bendiab, T. Amano, *Chem. Phys. Lett*. **1994**, *230*, 561-566.

[30] P. D. Godfrey, R. D. Brown, F. M. Rodgers, J. *Mol. Struct*. **1996**, *376*, 65-81; P. D. Godfrey, R. D. Brown, *J. Am. Chem. Soc*. **1998**, *120*, 10724-10732; G. M. Florio, R. A. Christie, K. D. Jordan, T. S. Zwier, *J. Am. Chem. Soc*. **2002**, *124*, 10236-10247.

[31] S. Blanco, M. E. Sanz, J. C. López, and J. L. Alonso, *Proc. Natl. Acad. Sci*. **2007**, *104*, 20183-20188.

[32] N. Borho, T. Häber, M. A. Suhm, *Phys. Chem. Chem. Phys*. **2001**, *3*, 1945-1948.

[33] W. Caminati, P. Moreschini, I. Rossi, P. G. Favero, *J. Am. Chem. Soc*. 1998, 120, 11144-11148; Z. Su, Q. Wen, Y. Xu, *J. Am. Chem. Soc*. **2006**, *128*, 6755-6760.

[34] N. Borho, Y. Xu, *Phys. Chem. Chem. Phys*. **2007**, *9*, 4514-4520.

[35] O. Isayev, L. Gorb, J. Leszczynski, *J. Comput. Chem*. **2007**, *28*, 1598-1609.

[36] T. J. Balle, W. H. Flygare, *Rev. Sci. Instrum*. **1981**, *52*, 33-45; U. Andresen, H. Dreizler, J.-U. Grabow, W. Stahl, *Rev. Sci. Instrum*. **1990**, *61*, 3694-3699.

[37] Y. Xu, W. Jäger, *J. Chem. Phys*. **1997**, *106*, 7968-7980.

Chapter 4

Chirality Induction and Amplification in the 2,2,2-Trifluoroethanol··Propylene Oxide Adduct[a]

4.1. Introduction

Chirality induction, a special form of chirality recognition,[1] is at the heart of stereoselective syntheses, such as chiral hydrogenations,[2] chiral bio-organic synthesis,[3] synthesis of inorganic and inorganic-organic chiral porous solids,[4] and the design of chiral polymers.[5] Starting from permanently chiral chemical reactants and/or catalysts, new chirality is induced in the activated complex or reaction intermediate which consist of the chiral species and prochiral or transiently chiral molecules. This process eventually results in one or more new permanent stereogenic centers, or helicity of the product. It is often with significant preference for one specific handedness, and is termed chirality amplification.[5] Some solvents, such as 2,2,2-trifluoroethanol (TFE), are known to promote such chirality induction and amplification processes.[6-8] For example, TFE is widely used as a peptide cosolvent for structural function investigations of protein and peptide folding processes in aqueous solution. The intermolecular interactions of TFE with peptides and proteins can alter their secondary and tertiary structures, thereby facilitating the protein folding process.[7,9-11] In a recent solid-state NMR study, its derivative, phenyl TFE, was used as a chiral solvating agent for enantioselective separation for a number of chiral metal--organic frameworks.[12] Hydrogen bonding and other noncovalent interactions between chiral units and TFE are rationalized to be responsible for the observed chirality induction.[13,14]

Jet-cooled rotational spectroscopy is well known for providing accurate structural and relative stability information for benchmarking theoretical modeling of important intermolecular interactions.[15-19] Because of its high-resolution nature, jet-cooled rotational spectroscopy can distinguish between conformers with only minute structural

differences, free of perturbations by the environment, and allows unambiguous identification of individual conformers independent of theoretical modeling. With the advent of broadband chirped pulse Fourier transform microwave (CP-FTMW) spectroscopy,[20] major progress has been made in rotational spectroscopic studies of systems with a large number of conformers.[15,16] Broadband rotational spectroscopy offers the great advantage of being able to detect all relevant conformers simultaneously and does not require a microwave resonator. The latter helps to overcome the well-known challenges associated with resonator-based FTMW experiments, such as intensity variations for different transitions resulting from resonator-mode adjustments and sample fluctuations.

Herein this chapter we report free-space and cavity-based rotational spectroscopic and *ab initio* studies of the TFE⋯PO (PO=propylene oxide) adduct. TFE can adopt three conformations: *gauche+* (*g+*), *gauche-* (*g-*), and *trans* (*t*), but only the *gauche* forms were observed in gas-phase spectroscopic studies.[21,22] In those studies, evidence for a tunneling motion between the two isoenergetic *gauche* forms was found.[21,22] Of particular interest are the FTIR studies of the TFE dimer in which an extreme case of chirality synchronization, facilitated by an incoherent tunneling motion, was reported: only the homochiral dimer was detected and no evidence for the energetically competitive heterochiral dimer was found in the experiment.[1,14] Equipped with the advantages of broadband CP-FTMW spectroscopy and the ultrahigh resolution of cavity-based FTMW measurements, we aimed to find definite answers for some interesting questions: What hydrogen-bonding topologies will the TFE⋯PO conformers take on? Will chirality induction in TFE⋯PO favor the *g+* or *g-* TFE form exclusively? This

scenario would be similar to the TFE dimer case where one monomer appears to almost quantitatively assume the handedness of the other.[14]

4.2. Results and discussion

We explored the conformational landscape of the TFE···PO adduct with *ab initio* calculations at the MP2/6-311++G(2d,p) level of theory using the Gaussian 09 suite of programs.[23] Eight binary conformers (Figure 4.1) were identified and confirmed to be true minima without imaginary frequencies. While the abundance ratio of the *trans* to the *gauche* configurations in liquid TFE was reported to be 40:60,[24] all binary structures starting with *t* TFE converged to either the *g+* or *g-* TFE···PO conformers, thus strongly suggesting that *t* TFE is still unstable in the hydrogen-bonded binary adduct.[14,21] The calculated dissociation energies, rotational constants, and electric dipole moment components of all eight binary adducts are summarized in Table 4.1. Since the energy differences among the eight conformers are generally small, one expect to observe all of them in a jet. In contrast, given that the TFE subunit in TFE···PO experiences similar hydrogen bonding interactions as in the TFE dimer, one wonders if the permanent chirality of PO will induce a strong chiral preference in the TFE subunit. This preference could be facilitated by a fast interconversion between the *g+* and *g-* TFE, similar to the case of the TFE dimer.[14]
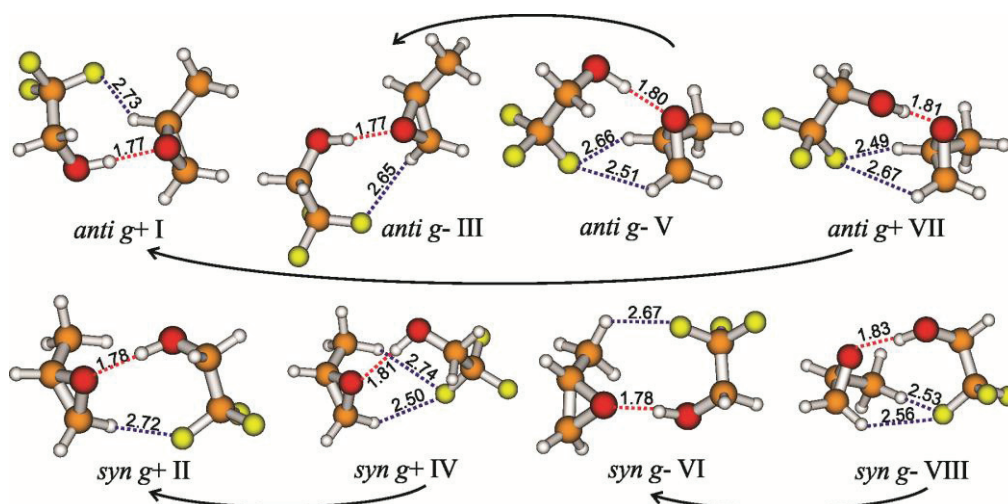
Figure 4.1. Structures of the eight most stable conformers of the TFE··PO adduct. While *syn* and *anti* refer to whether TFE approaches PO from the same or opposite sides of the PO methyl group, respectively. Roman numerals I to VIII label the relative stability starting from the most stable one. The numbers are the intermolecular bond lengths in Å. The arrows indicate the conformational relaxation under the jet expansion conditions. See the text for discussion.

Table 4.1. Calculated relative raw dissociation energies ΔD_e, and the *ZPE* and *BSSE* corrected dissociation energies ΔD_0 (in kJmol^{-1}), rotational constants A, B, and C (in MHz), and electric dipole moment components $|\mu_{a,b,c}|$ (in Debye) of the TFE··PO conformers.

Para.	I	II	III	IV	V	VI	VII	VIII
ΔD_e[a]	0	-0.85	-1.45	-1.25	-1.56	-0.83	-1.82	-3.05
ΔD_0[b]	0	-0.29	-0.49	-0.69	-0.91	-0.94	-1.12	-3.76
A	2161	2471	2954	2180	2360	2326	2306	2078
B	684	609	530	646	593	659	599	666
C	594	570	505	6+40	572	615	560	617
$|\mu_a|$	2.76	2.98	2.91	2.62	2.38	3.19	2.98	3.44
$|\mu_b|$	0.03	0.39	0.10	1.41	1.63	0.2	1.78	2.38
$|\mu_c|$	0.01	0.09	0.09	0.38	1.12	0.06	0.57	0.52

[a]$\Delta D_e(i) = D_e(i) - D_e(I)$ where i = I to VIII and $D_e(I) = 41.92$ kJmol^{-1}. [b]$\Delta D_0(i) = D_0(i) - D_0(I)$ where i = I to VIII and $D_0(I) = 27.70$ kJmol^{-1}.

Broadband spectra of samples containing TFE, PO or both together in helium (or neon) were recorded separately in the frequency range from 7.7 to 10.5 GHz using a CP-FTMW spectrometer.[25] Very dense spectra were obtained. To aid the spectral assignments of TFE···PO, transitions resulting from $(PO)_n$, $(TFE)_n$, $(PO)_n(RG)_m$, or $(TFE)_n(RG)_m$ (with RG=He or Ne; n, m=1, 2, ...) were first removed. Four sets of rotational transitions resulting from TFE···PO were assigned, and the experimental and assignment details are provided in Appendix B, section B4. The final transition frequencies were measured using a resonator-based[26] coaxial pulsed jet FTMW spectrometer[27] and were fitted using Watson's S-reduction Hamiltonian in the I^r representation[28] with the Pgopher program.[29] The standard deviations for all fits are less than 2.5 kHz, similar to the uncertainty of the experimental measurements. Transition frequencies and the corresponding quantum number assignments of all the observed transitions are given in Tables 4.S1 to 4.S5, Appendix B. The experimental spectroscopic constants obtained are listed in Table 4.2.

By comparison of the experimental and theoretical rotational constants and especially the relative intensities of the a-, b-, and c-type transitions, the four observed conformers were clearly identified as I, II, III, and VI. A maximum deviation of 4.6% was observed between the experimental and theoretical rotational constants for a particular assigned conformer, still allowing unambiguous correlation of the observed conformers with the calculated ones. No additional splitting was detected for any of the observed TFE···PO transitions, despite the high resolution capability of the cavity spectrometer. This observation is expected since the $g+$ and g - TFE subunits are locked

into their respective configurations in the binary adducts, along with large structural and thus also energetic differences.

Table 4.2. Experimental spectroscopic constants of the four TFE··PO conformers.

P^a	I	II	III	VI
A	2170.106(11)	2426.6781(19)	2920.124(71)	2336.440(30)
B	652.14861(29)	594.67934(12)	516.98121(23)	632.57360(30)
C	569.66525(28)	560.17041(12)	491.67870(22)	589.52799(23)
D_J	0.42182(64)	0.26478(28)	0.16888(37)	0.42845(70)
D_{JK}	0.4354(25)	0.7830(15)	0.2175(40)	-0.8296(37)
$D_K{}^b$	0.00	5.80(40)	0.00	0.00
d_1	-0.0713(11)	-0.00249(40)	-0.00129(60)	0.02034(85)
$d_2{}^b$	0.00	-0.00232(16)	0.00	0.0
N	50	52	43	45
σ	2.2	1.2	1.9	2.4

[a] Rotational constants in MHz and distortion constants in kHz. N is the number of transitions included in the fit and σ (in kHz) is the standard deviation of the fit. Standard errors in parenthesis are expressed in units of the last digit. [b] D_K and d_1 were kept at 0.0 in the fit because only a-type transitions were observed for conformers I, III, and VI.

The a-type electric dipole moment components are predicted to be similar for all four observed conformers. Using the calculated a-dipole moment components, the relative abundances of the conformers were estimated to be: I/II/III/VI=1:0.75:0.35:0.40 based on the intensities of the a-type transitions in the broadband spectra (see Section B2, Appendix B for details). Among the assigned binary conformers, I and II, formed by S-PO and $g+$ TFE, are favored over III and VI, which consist of S-PO and g-TFE. In addition, no transitions resulting from the conformers IV and V were observed in the broadband spectrum even though they are predicted to be more stable than the assigned conformer VI.

To address the above observations, we examined the subtle balance between the inter- and intramolecular hydrogen bonds in the binary adducts, the factors that contribute to the stability, and possible conformational relaxation in the jet expansion. The dissociation energy, D_e, can be decomposed into $E^{dist}_{PO} + E^{dist}_{TFE} + E^{int}$, as defined in reference [30]. Here, E^{dist}_{PO} and E^{dist}_{TFE} are the monomer deformation energies for PO and TFE, respectively, and correspond to the energy penalty for distorting the isolated monomers from their equilibrium geometries to the ones in the TFE$\cdots$PO complex. E^{int} is the interaction energy of the binary complex and is the difference between the total dimer energy and the energy of the two monomeric PO and TFE units in the TFE$\cdots$PO dimer. The values of these terms are summarized in Table 4.3, together with the values of the basis set superposition error (*BSSE*) and zero-point energy (*ZPE*) corrections.

From Table 4.3, it is clear that the deformation energies of PO are small and contribute little (≤0.15 kJ mol^{-1}) to the conformational preference. This small contribution is reasonable since PO is a fairly rigid molecule. The corresponding TFE deformation energies contribute modestly (≤0.82 kJ mol^{-1}), as do the *BSSE* corrections (≤0.91 kJ mol^{-1}). In comparison, the interaction energies are on the order of 42 kJ mol^{-1} and contribute decisively (≤3.55 kJ mol^{-1}) to the conformational preference among the eight conformers. It is also interesting to note that the *ZPE* corrections make only minor contributions to the relative conformational stability. Concerning the four conformers observed, both the interaction energies and the *BSSE* corrections are the dominant factors in determining the conformational preference.

A detailed comparison of the conformer geometries reveals that one can separate these structures into four groups: *anti g+*, *syn g+*, *anti g-*, and *syn g-*. One may expect that intergroup relaxation is not allowed in a jet expansion. For example, it is difficult for TFE to move from an *anti* position to a *syn* position in a jet expansion. The situation within each group is, however, different. Each group contains two structures, one is *open* with one F⋯H–C secondary hydrogen bond, while the other is *closed* with two F⋯H–C secondary hydrogen bonds (see Figure 4.1). It can be hypothesized that the interconversion barrier between these two conformers in each group is low since it involves only small changes, such as breaking one weak F⋅⋅H–C bond in favor of optimizing the existing primary intermolecular hydrogen bond and the other F⋅⋅H–C bond. Indeed, the four experimentally detected conformers, that is, *anti g+* I, *syn g+* II, *anti g-* III, and *syn g* - VI, correspond to the *open* structure in each group, and are the more stable ones predicted in each group. The proposed conformational relaxations are indicated with arrows in Figure 4.1: IV→II, V→III, VII→I and VIII→VI. This hypothesis explains why IV and V could not be observed even though they were predicted to be more stable than VI.

The predicted Boltzmann ratio for I : II : III : VI is 1 : 0.73 : 0.48 : 0.14, taking into account the conformational relaxation and assuming a conformational temperature of 60 K in the helium expansion.[31] The ratio is in good agreement with the experimental one (see Section B3, Appendix B) with the exception of conformer VI, thus reflecting the challenge in calculating relative dissociation energies to sub-kJmol^{-1} accuracy. Through H-bonding interactions, *S*-PO successfully locks the *gauche* TFE, a transient chiral molecule that is prochiral on average,[1] into a diastereomeric complex and induces a

preference between *g+* and *g-* TFE. Based on the experimental relative abundance of I : II : III : VI = 1 : 0.75 : 0.35 : 0.40, the overall preference for the *g+* TFE··*S*-PO versus *g-* TFE··*S*-PO diastereomers is about 2.8 times at 60 K.

Table 4.3. The calculated deformation, interaction, raw dissociation energies, and *BSSE* and *ZPE* corrections (in kJmol[-1]) at the MP2/6- 311++G(2d,p) level for the eight predicted conformers of TFE··PO.

Conformer	$E^{\text{dist}}_{\text{PO}}$	$E^{\text{dist}}_{\text{TFE}}$	E^{int}	D_e	$BSSE$	ZPE
I	-0.42	-1.28	43.62	41.92	-9.56	-4.66
II	-0.43	-1.38	42.87	41.07	-8.94	-4.72
III	-0.43	-1.34	42.24	40.46	-8.65	-4.61
IV	-0.43	-1.66	42.76	40.66	-9.08	-4.58
V	-0.38	-1.60	42.34	40.36	-8.97	-4.60
VI	-0.47	-1.00	42.56	41.09	-9.55	-4.79
VII	-0.36	-1.74	42.20	40.09	-8.99	-4.53
VIII	-0.32	-1.82	40.07	37.93	-8.85	-4.44
Max. in 8[a]	0.15	0.82	3.55	3.99	0.91	0.35
Max. in 4[a]	0.05	0.38	1.38	1.46	0.91	0.18

[a] Absolute maximum difference (in kJmol[-1]) among the eight predicted and four observed conformers, respectively.

To evaluate the effects of fluorination, we compare the current results with two related model systems, namely ethanol··PO and 2-fluoroethanol··PO. First, fluorination increases the dissociation energies of the most stable group of the binary adducts noticeably from about 16 kJmol[-1] for ethanol, to about 18 kJmol[-1] for 2-fluoroethanol, and finally to about 27 kJ mol^{-1} for TFE, that is by about 70% over its ethanol counterpart. The effect of ethanol fluorination on the first solvating water molecule was reported recently.[32] For comparison, in the binary adducts of water with ethanol, 2-fluoroethanol, and TFE, where water serves as hydrogen bond acceptor, the dissociation energies increase from about 19 kJ mol^{-1} to about 26 kJ mol^{-1}, and finally to about 28 kJ

mol^{-1}, respectively.[32] It therefore appears that the effect of fluorination on dissociation energy switches on more gradually in the complexes with PO than with water. Second, from the experimental abundances it is evident that ethanol···PO subtly favours *syn* diastereofacial interactions, while both 2-fluoroethanol···PO and TFE···PO favour *anti* arrangements. This different preference is not unexpected because the F can participate in F···H–C secondary hydrogen bonds with PO, and this arrangement can be better achieved with the oxirane methyl group out of the way, that is, in the *anti* arrangement. The third interesting difference is that while 2-fluoroethanol···PO strongly favors the *closed* structures with two intermolecular F···H–C bonds, TFE···PO favors the more *open* structures with just one intermolecular F···H–C bond.

One may initially wonder if E^{int}, the interaction energy of the binary complex, is the cause for such differences in the mono- and trifluoroethanol adducts. However, a detailed inspection of the various factors which contribute to the stability of the adducts indicates that E^{int} favors the *open* structures over the *closed* structures on the order of about 4 kJ mol^{-1}, for both the mono-[19] and trifluoroethanol adducts. Rather, the final differences in preference come from the different monomer stabilities and deformation energies. The penalty to fold TFE into the shape needed for the *closed* form of TFE··PO versus that for the *open* form of TFE··PO is about 0.7 kJ mol^{-1}. For 2-fluoroethanol···PO, the *open* form requires the *open gauche* 2-fluoroethanol subunit, while the *closed* form requires the *compact gauche* 2-fluoroethanol subunit. Please note that we adopt the *open gauche* and *compact gauche* labels used for the 2-fluoroethanol monomer in reference (17). The penalty to incorporate the *open gauche* 2-fluoroethanol subunit in the binary

adduct versus the *compact gauche* 2-fluroethanol subunit is about 11 kJ mol^{-1}. Consequently, 2-fluoroethanol···PO favors the *closed* structures over the *open* ones.

4.3. Conclusions

In conclusion, using broadband and narrow-band FTMW spectroscopy in combination with *ab initio* calculations, we investigated the conformational isomerism of an important chirality induction model system, that is, TFE···PO, in great detail. The identities of the four observed conformers were unequivocally established. Furthermore, from the broadband measurements, we were able to deduce reliable conformational abundances and propose possible conformational conversion paths which reduce the observable conformers from eight to four in a jet expansion. A strong preference for the *g+* TFE···*S*-PO diastereomers versus *g-* TFE···*S*-PO was observed, although to a much lesser degree compared to the TFE dimer case where only one homochiral species was detected experimentally.[14] We further show that fluorination has great effects on the overall binding strength of the binary adducts and on the corresponding conformational distribution.

References

[1] A. Zehnacker, M. A. Suhm, *Angew. Chem. Int. Ed*. **2008**, *47*, 6970–6992; *Angew. Chem*. **2008**, *120*, 7076–7100.

[2] J. Halpern, *Science*, **1982**, *217*, 401–407.

[3] R. A. Sheldon, *Chirotechnology: Industrial Synthesis of Optically Active Compounds*; Marcel Dekker, Inc.: New York, 1993; pp 39−72.

[4] R. E. Morris, X. Bu, *Nat. Chem*. **2010**, *2*, 353–361.

[5] A. R. A. Palmans, E. W. Meijer, *Angew. Chem. Int. Ed*. **2007**, *46*, 8948 – 8968; *Angew. Chem*. **2007**, *119*, 9106 –9126.

[6] G. Celebre, G. De Luca, M. Maiorino, F. Iemma, A. Ferrarini, S. Pieraccini, G. P. Spada, *J. Am. Chem. Soc*. **2005**, *127*, 11736–11744.

[7] K. Shiraki, K. Nishikawa, Y. Goto, J. Mol. Biol. **1995**, *245*, 180–194; K. Gast, D. Zirwer, M. M. Frohone, G. Damaschun, *Protein Sci.* **1999**, *8*, 625–634; P. Luo, R. L. Baldwin, *Biochem*. **1997**, *36*, 8413–8421.

[8] V. A. Soloshonok, *Angew. Chem. Int. Ed*. **2006**, *45*, 766–769; *Angew. Chem*. **2006**, *118*, 780–783.

[9] J. F. Povey, C. M. Smales, S. J. Hassard, M. J. Howard, *J. Struct. Biol*. **2007**, *157*, 329–338.

[10] M. Buck, *Q. Rev. Biophys*. **1998**, *31*, 297–355; M. Fioroni, M. D. Diaz, K. Burger, S. Berger, *J. Am. Chem. Soc*. **2002**, *124*, 7737–7744.

[11] R. Carrotta, M. Manno, F. M. Giordano, A. Longo, G. Portale, V. Martorana, P. L. San Biagio. *Phys. Chem. Chem. Phys*. **2009**, *11*, 4007–4018.

[12] H. C. Hoffmann, S. Paasch, P. Müller, I. Senkovska, M. Padmanaban, F.Glorius, S. Kaskel, E. Brunner, *Chem. Commun*. **2012**, *48*, 10484–10486.

[13] D. Hamada, F. Chiti, J. I. Guijarro, M. Kataoka, N. Taddei, C. M. Dobson, *Nat. Struct. Biol*. **2000**, *7*, 58–61.

[14] T. Scharge, T. Häber, M. A. Suhm, *Phys. Chem. Chem. Phys*. **2006**, *8*, 4664–4667; T. Scharge, C. Cézard, P. Zielke, A. Schütz, C. Emmeluth, M. A. Suhm, *Phys. Chem. Chem. Phys*. **2007**, *9*, 4472–4490; T. Scharge, T. N. Wassermann, M. A. Suhm, *Z. Phys. Chem*. **2008**, *222*, 1407–1452.

[15] C. Pérez, M. T. Muckle, D. P. Zaleski, N. A. Seifert, B. Temelso, G. C. Shields, Z. Kisiel, B. H. Pate, *Science*. **2012**, *336*, 897–901.

[16] I. Peña, E. J. Cocinero, C. Cabezas, A. Lesarri, S. Mata, P. Écija, A. M. Daly, Á. Cimas, C. Bermúdez, F. J. Basterretxea, S. Blanco, J. A. Fernández, J. C. López, F. Castaño, J. L. Alonso, *Angew. Chem. Int. Ed*. **2013**, *52*, 11840–11845; *Angew. Chem*. **2013**, *125*, 12056–12061.

[17] J. Thomas, F. X. Sunahori, N. Borho, Y. Xu, *Chem. Eur. J*. **2011**, *17*, 4582–4587.

[18] N. Borho, Y. Xu, *Angew. Chem. Int. Ed*. **2007**, *46*, 2276–2279; *Angew. Chem*. **2007**, *119*, 2326 –2329.

[19] N. Borho, Y. Xu, *J. Am. Chem. Soc*. **2008**, *130*, 5916--5921.

[20] G. G. Brown, B. C. Dian, K. O. Douglass, S. M. Geyer, B. H. Pate, *J. Mol. Spectrosc*. **2006**, *238*, 200–212; G. S. Grubbs II, C. T. Dewberry, K. C. Etchison, K. E. Kerr, S. A. Cooke, *Rev. Sci. Instrum*. **2007**, *78*, 096106/1–3.

[21] L. H. Xu, G. T. Fraser, F. J. Lovas, R. D. Suenram, C. W. Gillies, H. E. Warner, J. Z.

Gillies, *J. Chem. Phys*. **1995**, *103*, 9541– 9548.

[22] T. Goldstein, M. S. Snow, B. J. Howard, *J. Mol. Spectrosc*. **2006**, *236*, 1–10.

[23] Gaussian 09, Rev. C.01, M. J. Frisch, G. W. Trucks, H. B. Schlegel, G. E. Scuseria, M. A. Robb, J. R. Cheeseman, G. Scalmani, V. Barone, B. Mennucci, G. A. Petersson, H. Nakatsuji, M. Caricato, X. Li, H. P. Hratchian, A. F. Izmaylov, J. Bloino, G. Zheng, J. L. Sonnenberg, M. Hada, M.Ehara, K. Toyota, R. Fukuda, J. Hasegawa, M. Ishida, T. Nakajima, Y. Honda, O. Kitao, H. Nakai, T. Vreven, J. J. A. Montgomery, J. E. Peralta, F. Ogliaro, M. Bearpark, J. J. Heyd, E. Brothers, K. N. Kudin, V. N. Staroverov, T. Keith, R. Kobayashi, J. Normand, K. Raghavachari, A. Rendell, J.C. Burant, S. S. Iyengar, J. Tomasi, M. Cossi, N. Rega, J. M. Millam, M. Klene, J. E. Knox, J. B. Cross, V. Bakken, C. Adamo, J. Jaramillo, R. Gomperts, R. E. Stratmann, O. Yazyev, A. J. Austin, R. Cammi, C. Pomelli, J. W. Ochterski, R. L. Martin, K. Morokuma, V. G. Zakrzewski, G. A.Voth, P. Salvador, J. J. Dannenberg, S. Dapprich, A. D. Daniels, O. Farkas, J. B. Foresman, J. V. Ortiz, J. Cioslowski, D. J. Fox, Gaussian, Inc., Wallingford CT, **2010**.

[24] I. Bako, T. Radnai, M. Claire, B. Funel, *J. Chem. Phys*. **2004**, *121*, 12472–12480.

[25] S. Dempster, O. Sukhrukov, Q. Y. Lei, W. Jäger, *J. Chem. Phys*. **2012**, *137*, 174303/1−8; J. Thomas, J. Yiu, J. Rebling, W. Jäger, Y. Xu, *J. Phys. Chem. A*. **2013**, *117*, 13249–13254.

[26] T. J. Balle, W. H. Flygare, *Rev. Sci. Instrum*. **1981**, *52*, 33–45; J.-U. Grabow, W. Stahl, H. Dreizler, *Rev. Sci. Instrum*. **1996**, *67*, 4072–4084.

[27] Y. Xu, W. Jäger, *J. Chem. Phys*. **1997,** *106*, 7968−7980.

[28] J. K. G. Watson, *Aspects of Quartic and Sextic Centrifugal Effects on Rotational Energy Levels. In Vibrational Spectra and Structure*; (Ed.; J. R. Durig), Elsevier: Amsterdam, Netherland, 1977, Vol. 6, p39.

[29] PGOPHER, a Program for Simulating Rotational Structure, C. M. Western, University of Bristol, http://Pgopher.chm.bris.ac.uk.

[30] S. S. Xantheas, *J. Chem. Phys*. **1996**, *104*, 8821–8824; K. Szalewicz, B. Jeziorski, *J. Chem. Phys*. **1998**, *109*, 1198–1200.

[31] N. Borho, Y. Xu, *Phys. Chem. Chem. Phys.* **2007**, *9*, 4514–4520.

[32] M. Heger, T. Scharge, M. A. Suhm, *Phys. Chem. Chem. Phys.* **2013**, *15*, 16065-16073

Chapter 5

Chirality Synchronization in Trifluoroethanol Dimer

Revisited: The Missing Heterochiral Dimer[a]

5.1. Introduction

2,2,2-Trifluoroethanol (TFE) is a fluorinated alcohol with some fascinating properties and capabilities. It is widely used as a peptide co-solvent to mediate peptide and protein folding and unfolding processes and to influence their conformations.[1,2] TFE is known to enhance stability of proteins at low concentration, while at high concentration, it tends to denature proteins.[3] Although it is acknowledged that the intermolecular interactions of TFE with itself, with water, and with peptides and proteins all play some important roles, the detailed mechanisms through which TFE affects protein conformation and stability in solution are still being debated.[4] On the more chemical side, trifluoromethyl alcohol molecules were reported to show remarkable amplification of the self-disproportionation of enantiomers.[5] More recently, Hoffmann et al. used phenyl TFE as a chiral solvating agent to separate a number of chiral metal-organic frameworks enantioselectively.[6] One important aspect related to the interesting properties of TFE is its transient chirality. This transient chirality enables chirality induction, amplification and synchronization events associated with TFE.[7] The TFE monomer has three possible conformations, namely *trans* (*t*), and two isoenergetic *gauche* (+) (*g+*) and *gauche* (-) (*g-*) forms. The two *gauche* forms of TFE are non-superposable mirror images to each other and can interconvert rapidly on the time scale of 170 ps.[8,9] While only the *gauche* forms of TFE were observed in the previous gas phase spectroscopic studies,[8-10] the *t* to *gauche* ratio increases to 40:60 in liquid TFE based on the neutron diffraction measurements.[11] This observation and a few other studies[10,12] suggest that hydrogen (H)-bonding interactions with other binding partners might help to stabilize the *t* form.

To gain detailed understanding of how transient chirality of TFE influences the H-bonding interactions with TFE molecules, a series of studies using Fourier transform infrared (FTIR), Raman, and overtone spectroscopy in conjunction with supersonic molecular pulses were carried out for a family of TFE containing H-bonded clusters.[13-16] Very interestingly, the TFE dimer was shown to exhibit an extreme case of chirality synchronization, i.e. only the homochiral dimer was detected, while the energetically competitive heterochiral dimer was not detected in the experiments.[7,13-15] On the other hand, the other related alcohol molecules, such as ethanol and mono-/di-fluoroethanol, do not demonstrate such behaviour.[17-19] It was suggested that the extreme case of chirality synchronization may be promoted by an incoherent quantum tunneling through a high barrier that separates the most stable homo- and heterochiral TFE dimers which are very close in energy.[7,13,14] Since only moderate differences are predicted for these two conformers in term of their structures and characteristic vibrational bands, Scharge et al., suggested that "it would be interesting to obtain structural evidence for the dominant dimer by microwave spectroscopy".[14] From a more practical point of view, such tunneling assisted chirality synchronization may find important applications in stereoselective synthesis. It is therefore significant to verify the conclusion of the complete preference for the homochiral TFE dimer with high resolution spectroscopy.

FT microwave (MW) spectroscopy coupled with pulse molecular jet expansion can in principle provide detailed structural and dynamical information about conformations of molecules and their clusters[20-23] because of its high resolution and high sensitivity capabilities. Although we initially attempted to identify the possible TFE dimers using cavity based FTMW spectroscopy, a very dense rotational spectrum was

76

obtained with the TFE+Ne sample, making it challenging to achieve a definite assignment. The development of the broadband chirped pulse-FTMW (CP-FTMW) instrument[24,25] provides several major advantages in this regard as one can detect transitions due to all relevant conformers in one molecular pulse in a single frequency chirp. It is therefore easier to recognize spectral patterns and extract relative abundances for molecular systems with a large number of conformers.[26,27] In this chapter, we report a high resolution rotational spectroscopic study of the TFE dimer using both CP-FTMW and cavity-based FTMW spectroscopy with the aid of *ab initio* calculations. We aim to verify the identity of the previously reported homochiral TFE dimer and more importantly to see if there is any sign of the missing heterochiral TFE dimer. Our surprise findings are reported below.

5.2. Results and discussion

Extensive theoretical searches were done in the previous studies to map the conformational landscape of the TFE dimer using both *ab initio* and force field calculations.[13,14] It was reported that the *t* TFE containing binary conformers are much less stable. The related molecular dynamic simulations showed that the conformers of the TFE dimer involving a *t* TFE are very rare.[14] We therefore consider only the TFE dimers with *g+* and *g-* TFE. A total of seven conformers of the TFE dimer are identified to be true minima at the MP2/6-311++G(2d,p) level. Their geometries are summarized in Figure 5.1 and are differentiated from each other based on their H-bonding topologies. First, the conformers are classified as homo- or heterochiral depending on whether the two TFE subunits use the same or different *gauche* configurations, respectively. Second, the OH group of one TFE subunit can be inserted into the existing intramolecular F··H-O

H-bond of the second TFE subunit to form an *insertion* complex with the F··H-O··H-O H-bonded ring. This is denoted as *i*. Or it can be simply H-bonded to the second TFE with an O-H··O bond, leaving the existing intramolecular F··H-O H-bond intact. The latter is identified as an *associated* complex, denoted as *a*. Furthermore, the two TFE subunits can take on a *compact* or an *open* geometry, depending on which O lone pair of the TFE acceptor is utilized in the intermolecular H-bond (See Figure 5.1). These are denoted as *c* and *o* in Figure 5.1. Therefore, the binary adducts are characterized with unique names in the form of *a/i-c/o-hom/het* I (to VII), where the Roman numbers I to VII indicate the descending order of the relative stability of the conformers of the TFE dimer.
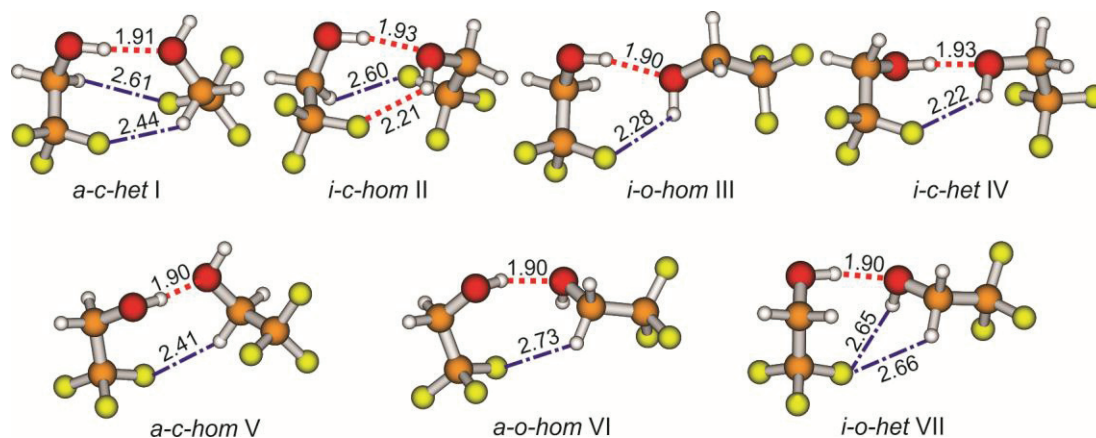
Figure 5.1. Optimized geometries of the seven binary TFE conformers at the MP2/6-311++G(2d,p) level. The primary (red) and the secondary (blue) intermolecular H-bond lengths (in Å) are also indicated. See the text for the naming details.

The calculated relative dissociation energies, as well as the rotational constants and the electric dipole moment components of all seven conformers are given in Table 5.1. One can roughly separate the conformers into three groups based on the D_e values.

While all conformers feature one intermolecular OH··O H-bond, the most stable homo- and heterochiral conformers, i.e. *i-c-hom* II and *a-c-het* I, respectively, also feature two additional inter- and intramolecular CH··F and OH··F contacts below 2.6 Å. The next group of conformers which includes *i-o-hom* III, *i-c-het* IV, *a-c-hom* V, *a-o-hom* VI, all have additionally one intermolecular CH··F contact. Finally, the least stable one, i.e. *i-o-het* VII, has two additional weak intermolecular CH··F and OH··F contacts. It is also noted that the *ZPE* and *BSSE* corrections actually change the relative order for these conformers. For example, while *a-c-het* I and *i-c-hom* II remain the two most stable ones, their relative energy difference becomes much smaller with the *ZPE* and *BSSE* corrections. In fact, *a-c-het* I is predicted to be about 0.03 kJ/mol most stable than *i-c-hom* II, making them essentially isoenergetic. Overall, all seven conformers are of somewhat similar stability, i.e. within 4 kJ/mol, based on the *ZPE* and *BSSE* corrected dissociation energy. Generally speaking, one may expect to observe all of the conformers in a jet expansion,[19-22] perhaps with the exception of *i-o-het* VII.

The spectral searches for the TFE dimer were carried out using a broadband CP-FTMW spectrometer in the frequency range of 7.7-10.5 GHz with a backing pressure of 6~10 atm. All of the dimers except *i-o-het* VII are predicted to have a large *a*-type electric dipole component, showing groups of closely spaced *a*-type transitions. Indeed, a set of *a*-type transitions were identified and assigned to the TFE dimer. Final spectral measurements were carried out with a cavity based FTMW spectrometer. A total of 125 rotations transitions which includes strong *a*- and weak *b*-type were measured, while no *c*-type transitions were found. These transitions were fitted with a Watson's S reduction[28] semi-rigid rotor Hamiltonian in its I^r representation using the Pgopher

program,[29] The resulting spectroscopic constants are given in Table 5.2. Based on the comparison of the experimental and predicted rotational constants and also the relative magnitudes of the a-, b-, and c-type of electric dipole components, we can unequivocally identify the conformer responsible for this set of transitions to be *i-c-hom* II.

Table 5.1. Relative energies (in kJ mol^{-1}), rotational constants (in MHz), and electric dipole components (in Debye) of the seven conformers of the TFE dimer calculated at the MP2/6-311++G(2d,p) level.

Parameter	*a-c-het* I	*i-c-hom* II	*i-o-hom* III	*i-c-het* IV	*a-c-hom* V	*a-o-hom* VI	*i-o-het* VII
ΔD_e [a]	1.11	0.00	3.65	3.52	3.30	3.22	6.33
ΔD_e^{BSSE} [a]	0.32	0.00	0.70	1.65	1.88	1.84	4.14
ΔD_0^{ZPE} [a]	0.76	0.00	3.08	3.23	2.82	2.97	5.86
$\Delta D_0^{ZPE+BSSE}$ [b]	0.00	0.03	0.16	1.38	1.43	1.62	3.71
A	1515	1611	1877	1832	1625	1726	1744
B	444	430	300	352	399	351	327
C	403	411	288	347	380	334	310
$\lvert\mu_a\rvert$	3.12	2.43	1.54	1.28	1.42	1.70	0.02
$\lvert\mu_b\rvert$	1.13	0.13	0.97	0.38	2.34	0.74	0.43
$\lvert\mu_c\rvert$	0.25	1.26	0.22	3.81	3.31	0.88	2.07

[a]$\Delta D_e(i) = D_e(II) - D_e(i)$ where i = I to VIII. ΔD_e^{BSSE} and ΔD_0^{ZPE} are similarly defined. $D_e(II)$, $D_e^{BSSE}(II)$, and $D_0^{ZPE}(II)$ are 35.51, 24.35, and 30.87 kJ/mol, respectively.
[b]$\Delta D_0^{ZPE+BSSE}(i) = D_0^{ZPE+BSSE}(I) - D_0^{ZPE+BSSE}(i)$ where i = I to VIII, and $D_0^{ZPE+BSSE}(I) =$ 19.70 kJ/mol.

It was recognized in the course of this study that the intensity of the observed homochiral TFE dimer could be enhanced noticeably when recorded with a mixture of TFE in helium at a much lower backing pressure of 2 to 4 atm, rather than the 6 to 10 atmosphere used initially. After considerable efforts, we were able to assign another set of transitions due to the TFE dimer. A total of 97 strong a- and weak c-type transitions

were measured using the cavity spectrometer, while no *b*-type transitions were located. Similar spectroscopic fit was carried out and the resulting constants are summarized in Table 5.2. Again, the comparison of the experimental and calculated spectroscopic properties allows unambiguous identification of the carrier to be *a-c-het* I, a heterochiral TFE dimer.

From Table 5.2, one can see that the maximum standard deviations for the fits are ~2 kHz which is similar to the experimental uncertainty in the measured frequencies. A comparison of the experimental and calculated rotational constants shows a maximum deviation of only 5.4% for the observed dimers. This indicates that the predicted structures are close to the actual ones. All of the observed transitions along with the quantum number assignments for *a-c-het* I and *i-c-hom* II are given in Table 5.S1 and 5.S2, Appendix C.

Table 5.2. Experimental spectroscopic parameters of the observed conformers of the TFE dimer

Parameter	*a-c-het* I	*i-c-hom* II
A (MHz)	1524.11367(32)[a]	1623.63820(16)
B (MHz)	386.269645(54)	415.571050(34)
C (MHz)	425.046760(50)	397.875140(39)
D_J (kHz)	0.20484(14)	0.269067(87)
D_{JK} (kHz)	-0.21316(81)	-0.44798(62)
D_K (kHz)	0.475(21)	1.2306(49)
d_1 (kHz)	0.029915(96)	-0.016373(86)
d_2 (kHz)	-0.002095(70)	-0.000850(68)
N[b]	97	125
σ[c] (kHz)	2	1.7

[a] Error in parenthesis in units of the last digit. [b] Number of lines in the fit. [c] RMS error in the fit.

A 0.3 GHz section of the broadband spectrum recorded is shown in Figure 5.2, together with the corresponding simulated spectra of the assigned homo- and heterochiral TFE dimers.
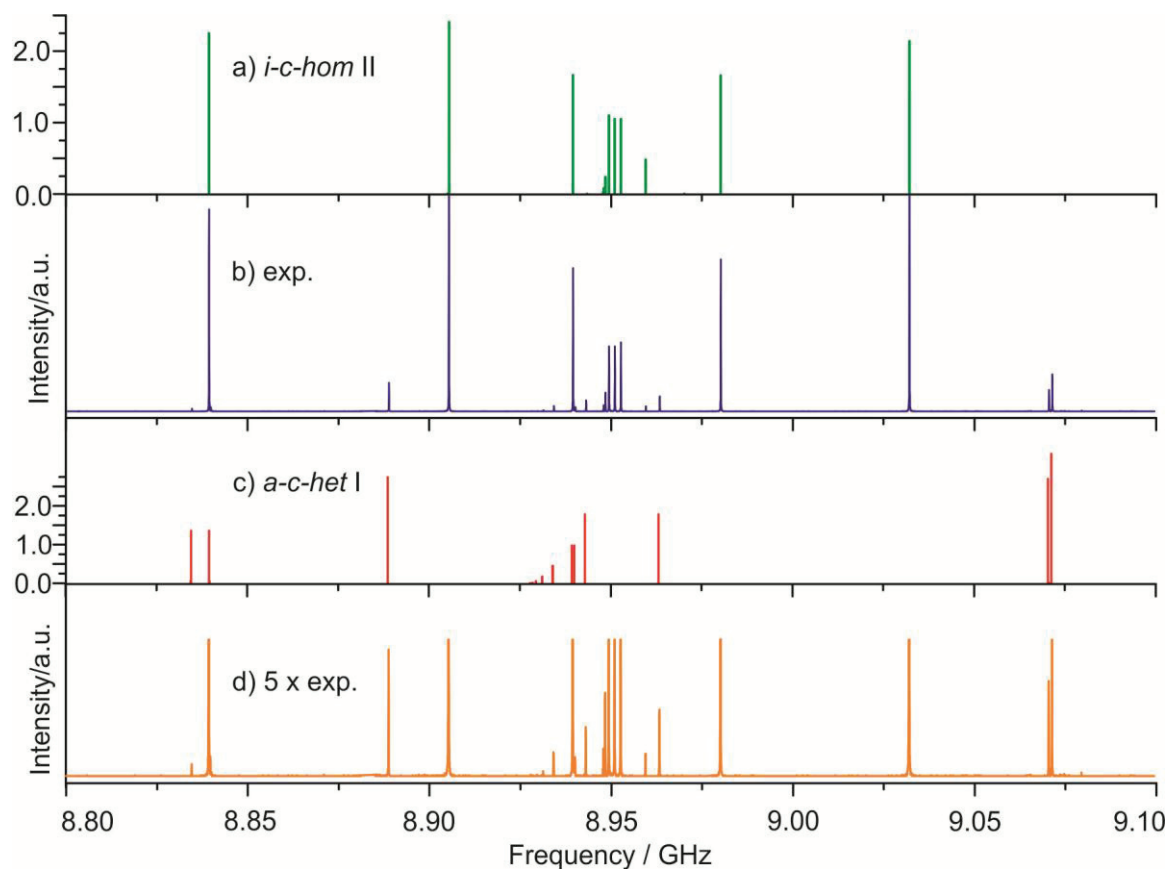
Figure 5.2. Trace a) is the simulated spectra of *i-c-hom* II . Trace b) is a representative 0.3 GHz section of the experimental broadband spectrum recorded with TFE and helium at a low backing pressure of 2 to 4 atm and 200,000 experimental cycles. Trace c) is the simulated spectra of *a-c-het* I. Trace d) is trace b) amplified by a factor of 5 and then truncated at 20% of the maximum intensity in order to show the transitions due to the most stable heterochiral conformer of the TFE dimer.

For the simulation of the spectra, experimental spectroscopic constants in Table 5.2 and the calculated electric dipole components in Table 5.1 were used. Strong lines due to the TFE monomer were removed for clarity. An estimated rotational temperature

of 0.7 K was obtained. The relative abundances of the observed homo- versus heterochiral conformers were estimated to be: *i-c-hom* II : *a-c-het* I = 1 : 0.1 by scaling the simulated spectra with their abundance ratio to reproduce the experimental intensities (see Figure 5.2).

The two conformers observed, i.e. *i-c-hom* II and *a-c-het* I, feature a strong H-bond with a length of 1.9 Å, a moderate H-bond of 2.2 to 2.4 Å, and a weak H-bond of 2.6 Å, while all the other less stable conformers in Figure 5.1 have either one less moderate H-bond or one less weak H-bond. Clearly, the homochiral binary TFE conformer, i.e. *i-c-hom* II, is the most stable conformer of the TFE dimer. Please note that *i-c-hom* II is also the only conformer of the TFE dimer detected and correctly identified in the previous FTIR studies through extensive theoretical and experimental analyses.[13,14] The splittings of the pure rotational transitions of the TFE monomer were reported to be in the order of a few to tens of MHz in the ground vibrational state and the gap between the two tunneling levels is reported to be 5868.6952(16) MHz for TFE.[9] However, despite the very high resolution capability of a few kHz of the cavity based FTMW spectrometer used, no additional splitting was observed for any of the measured TFE dimer transitions. Furthermore, the observed transitions could be fitted well with a semi-rigid rotor model, in contrast to that of the TFE monomer which exhibits a fast tunneling motion between $g+$ and $g-$ TFE.[9] Since *i-c-hom* II and *a-c-het* I were predicted to be accidently very close in energy, we initially speculated that there might be spectral consequences in the observed rotational transitions from, for example, local perturbations or tunneling.[30,31] All the above observations and most importantly the direct observation of the heterochiral binary TFE conformer, i.e. *a-c-het* I, unequivocally prove that these

two conformers are further apart in energy than predicted and it is therefore not surprising that their rotational spectra show no noticeable deviation from a semi-rigid rotor.

If one assumes a Boltzmann distribution of conformers with a conformational temperature of 60 K, a typical conformational temperature obtained for H-bonded complexes with a similar experimental setup.[32] An energy difference of 1.1 kJ mol^{-1} is obtained for the observed homo- and heterochiral TFE dimers. This is in disagreement with the prediction that these two conformers have essentially the same binding energy at the MP2/6-311++G(2d,p) level. On the other hand, this energy difference depends sensitively on the level of theory applied and whether BSSE corrections are applied.[16] For example, *a-c-het* I was predicted to be 0.5 kJ/mol less stable than *i-c-hom* II at the MP2/aug-cc-pVTZ level.[14] An uncertainty of 0.5 kJ/mol was estimated for the relative energies of the conformers of the TFE dimer.[14] The current estimated relative energy between the two observed conformers is roughly within this uncertainty. Generally, it is still challenging to predict relative dissociation energies to sub-kJ/mol accuracy with theoretical calculations.

Based on the *ZPE* and *BSSE* corrected dissociations energies, the predicted Boltzmann ratio for I : II : III : IV : V : VI at 60 K is 1.06 : 1 : 0.77 : 0.07 : 0.06 : 0.04, while VII has essentially no population. Even taking into account of the 0.5 kJ/mol uncertainty in the predicted relative energies,[14] one would still expect to detect *i-o-hom* III with the sensitivity of the broadband instrument employed. However, despite considerable efforts, no transitions due to any other binary TFE conformers could be located. Therefore, a simple explanation that the other conformers are much less stable than the two observed is not likely. Rather we propose that the other less stable homo-

and heterochiral conformers relax *separately* to the observed most stable homo- and heterochiral conformers under the jet expansion conditions. Indeed, it was demonstrated in the study of the H-bonded TFE··propylene oxide adduct[33] that while a cross-relaxation from the homo- to heterochiral conformers was not allowed, conformational relaxation within the group of the homochiral binary conformers or within the group of heterochiral ones does happen. Only the most stable ones in each of the four representative structures, i.e. *anti* or *syn g+* and *anti* or *syn g-*, of the TFE··propylene oxide adduct, were detected experimentally.[33] Here, *syn* and *anti* indicate that the TFE subunit approaches the propylene oxide from the same or opposite side of the oxirane methyl group, respectively and there is no *syn-anti* conformational conversion after formation of the complex. Since these two H-bonded systems employ similar H-bonding topologies, we may expect the same to be true for the TFE dimer. Indeed, this proposed mechanism can explain why only one homo- and one heterochiral representative structures were detected experimentally for the TFE dimer. Taking such conformational relaxation into account, the homo- versus heterochiral TFE dimer abundant ratio is predicted to be 1 : 0.60 at 60 K. This is consistent with the experimental observation that the heterochiral species is less abundant, although the abundance of the heterochiral species is significantly overestimated.

5.3. Conclusions

In summary, we revisited chirality synchronization in the TFE dimer using broadband chirped pulse and cavity based FTMW spectroscopy in combination with *ab initio* calculations. The conformational isomerism of this unique chirality synchronization model system is discussed and the two observed conformers are unequivocally identified

as the most stable homo- and heterochiral conformers of the TFE dimer, i.e. *i-c-hom* II and *a-c-het* I, respectively. A strong preference for the homochiral arrangement over the heterochiral one is observed where the former is about 10 times more abundant than the latter under the current pulsed jet expansion condition. While the present results support the previous FTIR identification of the homochiral TFE dimer,[13,14] they also clearly establish that the heterochiral TFE dimer *does* exist although with considerably lower abundance. The rotational spectroscopic studies show that the *g+* and *g-* TFE subunits are locked into their respective configurations through H-bonding interactions and the observed conformers of the TFE dimer are well described by a semi-rigid rotor Hamiltonian. The current study also highlights the advantages of high resolution spectroscopy in providing decisive and detailed structural and dynamical information about molecular recognition processes in great detail. Compared to the closely related 2-fluoroethanol dimer which shows only very mild preference for the heterochiral arrangement,[17,19] further higher level theoretical investigations will help to fully appreciate why perfluorination at the methyl group brings such drastic preference for the homochiral arrangement in the TFE dimer.

5.4. Experimental section

Survey scans for TFE was recorded using a CP-FTMW spectrometer [34,35] which was designed based on the work of Pate and others.[24,25] In this spectrometer, a radiofrequency (rf) chirp (0.2–1 GHz for 4 μs) generated by an arbitrary waveform generator (Tektronix AWG 710B) was mixed with the output of a MW synthesizer to produce a 2 GHz MW chirp in the 8-18 GHz range. This chirp was then amplified with a 20 W solid state MW amplifier (MW Power Inc., L0818-43) and propagated into free

space and collected using a pair of wide band, high gain, MW horn antennae (rf/MW instrumentation, ATH7G18). The resolution of the broadband spectrometer is 25 kHz. All final frequency measurements were done with a cavity based[36,37] pulsed jet FTMW spectrometer.[38] In this case, the frequency uncertainty is ~2 kHz and the full line width at half height is ~10 kHz. Sample mixtures consisting of 0.5 % TFE in helium at stagnation pressures of 2 to 4 bars were used for the survey scans and for the final cavity based measurements, respectively. TFE (99%, Sigma Aldrich) and helium (99.9990 %) was used without further purification. A General Valve nozzle (series 9) with a diameter of 0.8 mm was used.

All geometry optimization and harmonic frequency calculations were done using the Gaussian 09 program package.[39] Second-order Møller–Plesset perturbation theory (MP2)[40,41] 6-311++G(2d,P) basis set[42] was chosen because of its proven performance for similar kind of hydrogen-bonded systems. The calculated raw dissociation energies were corrected for *ZPE* and *BSSE*s. *BSSE*s were calculated using the counterpoise procedure of Boys and Bernardi.[43]

References

[1] M. Buck, *Quart. Rev. Biophys*. **1998**, *31*, 297–355.

[2] J. F. Povey, C. M. Smales, S. J. Hassard, M. J. Howard, *J. Struct. Biol*. **2007**, *157*, 329–338.

[3] S. Grudzielanek, R. Jansen, R. Winter, *J. Mol. Biol*. **2005**, *351*, 879–894.

[4] R. Carrotta, M. Manno, F. M. Giordano, A. Longo, G. Portale, V. Martorana, P. L. S. Biagio, *Phys. Chem. Chem. Phys*. **2009**, *11*, 4007–4018.

[5] V. A. Soloshonok, *Angew. Chem. Int. Ed.* **2006**, *45*, 766–769; *Angew. Chem.* **2006**, *118*, 780–783.

[6] H. C. Hoffmann, S. Paasch, P. Müller, I. Senkovska, M. Padmanaban, F. Glorius, S. Kaskel, E. Brunner, *Chem.Commun*. **2012**, *48*, 10484–10486.

[7] A. Zehnacker, M. A. Suhm, *Angew. Chem. Int. Ed*. **2008**, 47, 6970–6992; *Angew. Chem.* **2008**, *120*, 7076–7100.

[8] A. J. Barnes, H. E. Hallam, D. Jones, *Proc. R. Soc. London, Ser. A*. **1973**, *335*, 97–111.

[9] L. H. Xu, G. T. Fraser, F. J. Lovas, R. D. Suenram, C. W. Gillies, H. E. Warner, J. Z. Gillies, *J. Chem. Phys*. **1995**, *103*, 9541–9548.

[10] J. Marco, J. M. Orza, *J. Mol. Struct*. **1992**, *267*, 33–38.

[11] I. Bako, T. Radnai, M. Claire, B. Funel, *J. Chem. Phys*. **2004**, *121*, 12472–12480.

[12] M. L. Senent, A. Niño, C. Muñoz-Caro, Y. G. Smeyers, R. Domínguez-Gómez, J. M. Orza, *J. Phys. Chem. A*. **2002**, *106,* 10673–10680.

[13] T. Scharge, T. Häber, M. A. Suhm, *Phys. Chem. Chem. Phys*. **2006**, *8*, 4664–4667.

[14] T. Scharge, C. Cezard, P. Zielke, A. Schutz, C. Emmeluth, M. A. Suhm, *Phys. Chem. Chem.Phys*. **2007**, *9*, 4472-4490.

[15] T. Scharge, D. Luckhaus, M. A. Suhm, *Chem. Phys*. **2008**, *346*, 167–175.

[16] M. Heger, T. Scharge, M. A. Suhm, *Phys. Chem. Chem. Phys.* **2013**, *15*, 16065-16073.

[17] T. Scharge, T. N. Wassermann, M. A. Suhm, *Z. Phys. Chem*. **2008**, *222*, 1407–1452.

[18] M. A. Suhm, *Advances in Chemical Physics*, Vol. 142, S. A. Rice, Ed.; John Wiley & Sons, Inc.

[19] X. Liu, N. Borho, Y. Xu, *Chem. Eur. J.* **2009**, *15*, 270–277.

[20] J. Thomas, F. X. Sunahori, N. Borho, Y. Xu, *Chem. Eur. J.* **2011**, *17*, 4582–4587.

[21] N. Borho, Y. Xu, *Angew. Chem. Int. Ed*. **2007**, *46*, 2276–2279; *Angew. Chem*. **2007**, *119*, 2326 –2329.

[22] N. Borho, Y. Xu, *J. Am. Chem. Soc*. **2008**, *130*, 5916–5921.

[23] Y. Xu, W. Jäger, *Fourier Transform Microwave Spectroscopy of Doped Helium Clusters, in Handbook of High-resolution Spectroscopy*; (Eds.; M. Quack, F. Merkt) John Wiley and Sons, Chichester, **2011**.

[24] G. G. Brown, B. C. Dian, K. O. Douglass, S. M. Geyer, B. H. Pate, *J. Mol. Spec*. **2006**, *238*, 200–212.

[25] G. S. Grubbs II, C. T. Dewberry, K. C. Etchison, K. E. Kerr, S. A. Cooke, *Rev. Sci. Instrum*. **2007**, *78*, 096106/1–3.

[26] C. Pérez, M. T. Muckle, D. P. Zaleski, N. A. Seifert, B. Temelso, G. C. Shields, Z. Kisiel, B. H. Pate, *Science.* **2012**, *336*, 897–901.

[27] I. Peña, E. J. Cocinero, C. Cabezas, A. Lesarri, S. Mata, P. Écija, A. M. Daly, Á. Cimas, C. Bermúdez, F. J. Basterretxea, S. Blanco, J. A. Fernández, J. C. López, F. Castaño, J. L. Alonso, *Angew. Chem. Int. Ed*. **2013**, *52*, 11840–11845; *Angew. Chem*. **2013**, *125*, 12056–12061.

[28] J. K. G. Watson, *Aspects of Quartic and Sextic Centrifugal Effects on Rotational Energy Levels. In Vibrational Spectra and Structure*; (Ed.; J. R. Durig), Elsevier: Amsterdam, Netherland, 1977,Vol. 6, p39.

[29] PGOPHER, a Program for Simulating Rotational Structure, C. M. Western, University of B ristol, http://Pgopher.chm.bris.ac.uk.

[30] S. Albert, P. Lerch, R. Prentner, M. Quack, *Angew. Chem. Int. Ed.* **2013**, *52*, 346 – 349; *Angew. Chem.* **2013**, *125*, 364 –367.

[31] Z. Kisiel, O. Dorosh, A. Maeda, I. R. Medvedev, F. C. De Lucia, E. Herbst, B. J. Drouin, J. C. Pearson, S. T. Shipman, *Phys. Chem. Chem. Phys.* **2010**, *12*, 8329–8339.

[32] N. Borho, Y. Xu, *Phys. Chem. Chem. Phys.* **2007**, *9*, 4514–4520.

[33] J. Thomas, W. Jäger, Y. Xu, *Angew. Chem. Int. Ed.* **2014**, DOI: 10.1002/ anie. 201403838R1 and 10.1002/ange.201403838R1.

[34] S. Dempster, O. Sukhrukov, Q. Y. Lei, W. Jäger, *J. Chem. Phys.* **2012**, *137*, 174303/1−8.

[35] J. Thomas, J. Yiu, J. Rebling, W. Jäger, Y. Xu, *J. Phys. Chem. A*. **2013**, *117*, 13249–13254.

[36] J. Balle, W. H. Flygare, *Rev. Sci. Instrum*. **1981**, *52*, 33–45.

[37] J-U. Grabow, W. Stahl, H. Dreizler, *Rev. Sci. Instrum*. **1996**, *67*, 4072–4084.

[38] Y. Xu, W. Jäger, *J. Chem. Phys*. **1997,** *106*, 7968-7980.

[39] Gaussian 09, Rev. C.01, Frisch, M. J.; Trucks, G. W.; Schlegel, H. B.; Scuseria, G. E.; Robb, M. A.; Cheeseman, J. R.; Scalmani, G.; Barone, V.; Mennucci, B.; Petersson G. A.; Nakatsuji, H.; Caricato, M.; Li, X.; Hratchian, H. P.; . Izmaylov, A. F.; Bloino, J.; Zheng, G.; Sonnenberg, J. L.; Hada, M. ; Ehara, M.; Toyota, K.; Fukuda, R.; Hasegawa, J.; Ishida, M.; Nakajima, T.; Honda, Y.; Kitao, O.; Nakai, H.; Vreven, T.; Montgomery J. J. A.; J. A.; Peralta, J. E.; Ogliaro, F.; Bearpark, M.;

Heyd, J. J.; Brothers, E.; Kudin, K. N.; Staroverov, V. N.; Kobayashi, R.; Normand, J.; Raghavachari, K.; Rendell, A.; Burant, J. C.; Iyengar, S. S.; Tomasi, J.; Cossi, M.; Rega, N.; Millam, J. M.; Klene, M.; Knox, J. E.; Cross, J. B.; Bakken, V.; Adamo, C.; Jaramillo, J.; Gomperts, R.; Stratmann, R. E.; Yazyev, O.; Austin, A. J.; Cammi, R.; Pomelli, C.; Ochterski, J. W.; Martin, R. L.; Morokuma, K.; Zakrzewski, V. G.; Voth, G. A.; Salvador, P.; Dannenberg, J. J.; Dapprich, S.; Daniels, A. D.; Farkas, O.; Foresman, J. B.; Ortiz, J. V.; Cioslowski, J.; Fox, D. J.; Gaussian, Inc.: Wallingford CT, **2010**.

[40] C. Møller, M. S. Plesset, *Phys. Rev.* **1934**, *46*, 618−622.

[41] J. S. Binkley, J. A. Pople, *Int. J. Quantum Chem.* **1975**, *9*, 229−236.

[42] R. Krishnan, J. S. Binkley, R. Seeger, J. A. Pople, *J. Chem. Phys.* **1980**, 72, 650-654.

[43] S. F. Boys, F. Bernardi, *Mol. Phys.* **1970**, *19*, 553−566.

Chapter 6

Chirped-Pulse and Cavity-Based Fourier Transform

Microwave Spectra of the Methyl Lactate···Ammonia Adduct[a]

[a] A version of this chapter has been published. J. Thomas, O. Sukhrukov, W. Jäger, Y. Xu, Chirped-Pulse and Cavity-Based Fourier Transform Microwave Spectra of the Methyl lactate···ammonia adduct, *Angew. Chem. Int. Ed.* 2**013**, *52*, 4402 –4405.

6.1. Introduction

Molecular recognition plays a vital role in biochemistry and biology. The efficiency of a molecular recognition process depends on the selectivity between the lock and the key molecules. Among the intermolecular forces, hydrogen (H)-bonding interactions involving O, H and N atoms are of particular interest because of their prominent roles in driving protein folding, molecular recognition, and other biochemical processes.[1] Studies of molecular recognition between a lock and a key molecule using jet-cooled rotational spectroscopy provide information for detailed understanding of the forces involved in a molecular recognition process. A small number of rotational spectroscopic studies of chiral lock-key systems have been reported before where the molecular subunits typically have only one H-bonding site.[2,3] As a result, the selectivity between lock and key molecules is generally not specific enough, resulting in many number of conformers separated only by very small energy differences.

To better mimic the unique specificity observed in biological systems, we selected methyl lactate (ML), a chiral molecule with multiple functional groups and H-bond binding sites, as our lock, and ammonia as our key. The ML conformer with an intramolecular O-H···O=C H-bond is strongly favoured over all other conformations.[4] It is of great interest to see if ammonia acts exclusively as a proton acceptor or donor, or if it plays a dual role in the ML···NH_3 adduct where there is a competition between intra- and intermolecular H-bonds. Such balance between the intra- and intermolecular H-bonding interactions is commonly encountered in biological systems and has a great influence on the selectivity between lock and key molecules.

Only a few NH_3 containing complexes have been studied so far by high resolution spectroscopy. Ammonia generally acts as a proton acceptor, for example in complexes with cyclopropane, methanol, and ethanol.[5-7] In complexes of ammonia with, for example hydroquinone[8] and 7-hydroxy quinoline,[9] it serves both as a proton donor and acceptor. Only one chiral molecule-NH_3 adduct, namely glycidol··NH_3, was studied before using high resolution spectroscopy.[10] Such studies of chiral-achiral adducts are of considerable relevance in light of the significant current interest in transfer of chirality from a chiral molecule to an achiral subunit through H-bonding interactions in solution and in a cold rare gas matrix.[11-13]

In this chapter, we report a detailed rotational spectroscopic study of the ML··NH_3 adduct, in combination with high-level *ab initio* calculations. The ML··NH_3 adduct is also unique in terms of its spectroscopy. First, this system has three internal rotors: two methyl rotors and one ammonia rotor. This is the first study that probes a molecular recognition process between a lock with two 'spinning' tops and a key which is also a spinning top itself. Second, the ammonia rotor contains a quadrupolar ^{14}N nucleus. It therefore offers the opportunity to probe the distortion of the electric field gradient at the ^{14}N nucleus upon H-bonding with ML. Finally, the coupling of the internal rotations with the overall rotation of the complex may give rise to first order contributions for lines with E internal rotor symmetry. The contributions are from the off diagonal elements of the ^{14}N nuclear quadrupole coupling tensor, allowing their determination experiment-ally.[14,15]

6.2 Results and discussion

The spectral search for the binary adduct was carried out using a broadband chirped pulse Fourier transform microwave (FTMW) spectrometer.[16] Broadband spectra of three different samples, namely ML, NH_3 and ML+NH_3, all in neon, were measured in the 7.7-10.4 GHz region using 10^6 averaging cycles. Transitions that require the presence of both ML and NH_3 could be readily identified. The five most stable binary ML$^{..}NH_3$ adducts identified from *ab initio* calculations are summarised in Table 6.1. A 0.8 GHz section of a chirped pulse MW spectrum is shown in Figure 6.1, together with a portion of a simulated spectrum of conformer I using the *ab initio* spectroscopic constants and the Pgopher[17] program. The simulated intensity pattern does not match with the experimental data completely because of the omission of the ^{14}N nuclear quadrupole and the internal rotor splittings in the simulation.

To confirm the initial assignment and to unravel the complicated hyperfine structures, the final frequency measurements were done with a cavity based FTMW instrument.[18] While splittings because of both the ester methyl internal rotation and ^{14}N nuclear quadrupole coupling were expected, an additional splitting was observed. This splitting is unlikely to be due to the second methyl rotor in ML since no such splitting was detected for the ML monomer.[4] One may hypothesize that the additional splitting arises from the NH_3 internal rotation motion even though one of the H atoms of NH_3 is H-bonded to ML. Indeed, an energy scan for the internal rotation of NH_3 provided an estimated barrier height of about 2.8 kJmol^{-1} (see Figure 6.S1, Appendix D).

Table 6.1. Relative energies and calculated spectroscopic constants of the five most stable ML$\cdots$NH$_3$ conformers.

Conformers	I	II	III	IV	V
$\Delta D_e^{[a]}$ [kJmol^{-1}]	0.0	2.1	16.8	17.5	21.9
$\Delta D_o^{[b]}$ [kJmol^{-1}]	0.0	1.4	9.5	10.3	13.7
A [MHz]	2646	2207	3500	2290	1687
B [MHz]	1208	1389	894	1151	1584
C [MHz]	971	917	834	964	980
μ_a [D]	0.87	0.99	1.32	1.07	3.86
μ_b [D]	0.98	2.28	0.89	1.32	1.20
μ_c[D]	2.39	1.67	0.44	0.17	1.87

[a]Basis set superposition error (BSSE) corrected relative energies at the MP2/6-311++G(d,p) level. [b]Zero point energy (ZPE) corrected.

For simplification, ML$\cdots^{15}$NH$_3$ was considered first. One expects five internal rotation components (j_1,j_2), namely AA=(0,0), EA=(1,0), AE=(0,1), EE=(1,1) and EE'=(1,-1). Here j_1 and j_2 correspond to the internal rotation labels of the ester methyl group and NH$_3$, respectively, and the A/E notation indicates the symmetry species. The subsequent analysis of the ML$\cdots^{14}$NH$_3$ **I** spectrum was aided by using a homemade first-order nuclear quadrupole program. Complex hyperfine patterns of an example transition of the ^{15}NH$_3$ and ^{14}NH$_3$ isotopologues are shown in Figure 6.2.

The final global fits of both isotopologues were performed with the program XIAM,[19] currently the only program which can fit rotational transitions of a C$_1$ symmetry molecular system with multiple internal rotors and with additional nuclear quadrupole splitting. The Hamiltonian used can be written as Equation (6.1).

$$H=H_{rot}+H_{cd}+H_i+H_{ird}+H_{ii}+H_Q. \qquad\qquad (6.1)$$
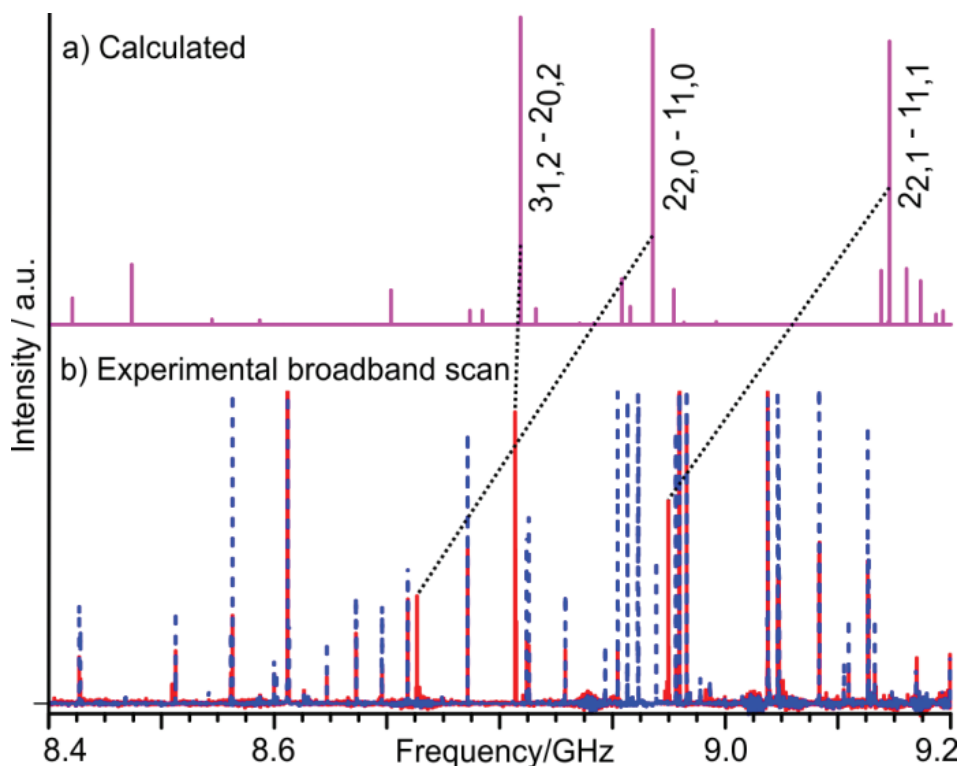
Figure 6.1. a) Simulated 0.8 GHz section of rotational spectrum of ML$\cdots$^{14}NH$_3$ **I** using the spectroscopic constants reported in Table 6.1 with T_{rot} = 1 K. b) 0.8 GHz sections of two broadband chirped pulse microwave scans using ML+NH$_3$+Ne (solid red) and ML+Ne (dashed blue) samples. The scan of NH$_3$+Ne is not shown since the transitions observed are very weak in this frequency region.

Here, H_{rot} is the rigid rotor part, H_{cd} refers the centrifugal distortion part, H_i corresponds to the internal rotation part of the tops, H_{ird} accounts for the torsional state-dependent centrifugal terms such as D_{pi2k}, H_{ii} is the top-top coupling term such as F_{12}, and H_Q corresponds to the nuclear quadrupole coupling terms such as χ_{aa} and χ_{bc}. The measured frequencies and the quantum number assignments of ML$\cdots$^{15}NH$_3$ **I** and ML$\cdots$^{14}NH$_3$ **I** are given in Tables 6.S1 and 6.S2 (Appendix D), respectively. The spectroscopic constants

obtained are summarized in Table 6.2, including the internal rotor parameters for both the ester methyl group and the NH_3 subunit and the diagonal nuclear quadrupole coupling constants of ^{14}N as well as one off-diagonal element.
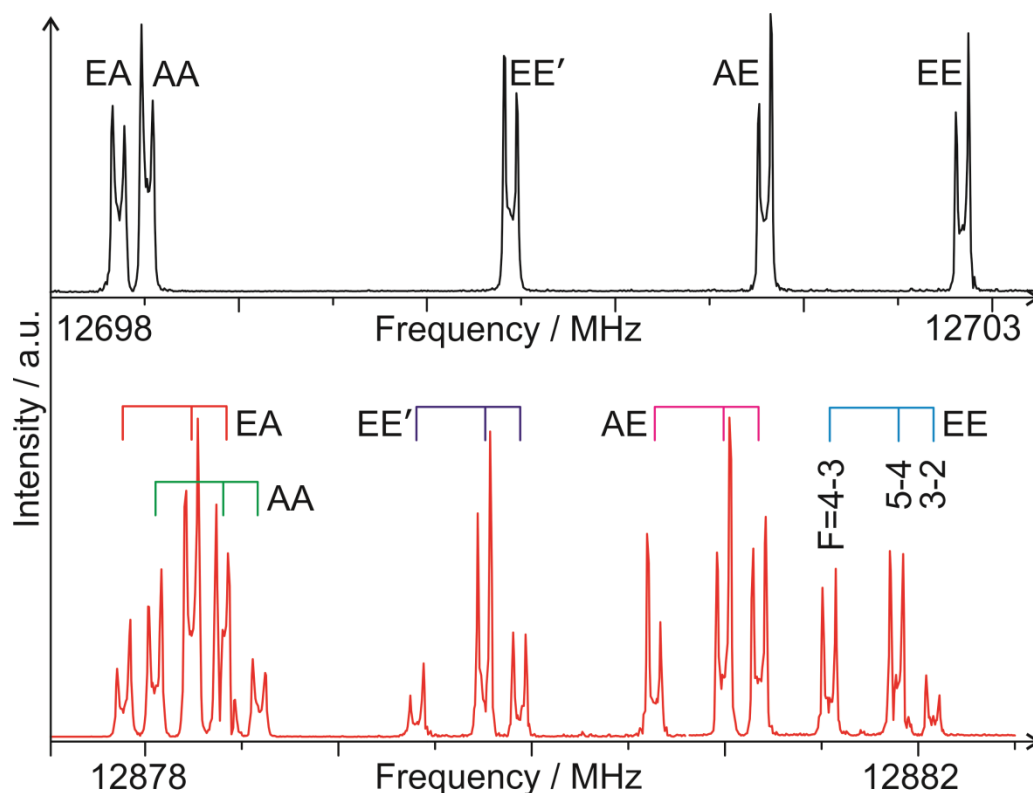
Figure 6.2. Experimental Internal rotation and nuclear quadrupole hyperfine structures of rotational transition $4_{2,2}$-$3_{1,2}$ of ML$^{...15}NH_3$ **I** (top) and ML$^{...14}NH_3$ **I** (bottom). Each spectrum is pieced together with four separate measurements.

The internal rotation barrier heights of the ester methyl group are 4.778(16) and 4.818(18) kJmol^{-1} in ML$^{...15}NH_3$ and ML$^{...14}NH_3$, respectively, comparable to that of the monomer (4.76 kJmol^{-1}).[4] This indicates that the replacement of the intramolecular H-bond by the intermolecular OH$^{...}$NH$^{...}$O=C H-bonds has little effect on the internal rotation of the ester methyl group. The experimental barrier heights for the ammonia

internal rotation in ML$\cdots^{14}$NH$_3$ and ML$\cdots^{15}$NH$_3$ are 2.452(2) and 2.4538(7) kJmol^{-1}, respectively. Since the NH$_3$ internal rotation is mainly hindered by the intermolecular OH$\cdots$NH$\cdots$O=C H-bonds, the magnitude of the barrier height is roughly proportional to the strength of the H-bond. For example, the NH$_3$ internal rotation barrier is 2.438 kJmol^{-1} for the most stable glycidol$\cdots$NH$_3$ conformer.[10] This suggests that the strength of the NH$\cdots$O=C H-bond in ML$\cdots$NH$_3$ is very similar to that in the most stable conformer of glycidol$\cdots$NH$_3$. This similarity is also reflected in the corresponding moment-of-inertia values of the NH$_3$ top, which are related to the extent of the opening of the NH$_3$ "umbrella". For ML$\cdots$NH$_3$ **I**, these are 2.7805 (^{14}N) and 2.7817 uÅ^2 (^{15}N), compared to 2.7849 and 2.7885 uÅ^2 in the most stable glycidol$\cdots$NH$_3$, respectively.

With the available experimental rotational constants, a partially refined r_0-structure was obtained where four H-bonding structural parameters were adjusted to reproduce the experimental rotational constants to about 50 kHz. The resulting values are listed in Table 6.3, together with the corresponding equilibrium values from the *ab initio* calculations.

How much is the electric field gradient at the ^{14}N nucleus perturbed upon H-bonding to ML? There is not enough information to obtain the principal quadrupole coupling tensor components of ^{14}N in ML$\cdots$NH$_3$ using experimental χ constants only. Instead, we utilized the partial experimentally determined r_0-structure and calculated the direction cosine matrix for the principal χ constants at the MP2/6-311++G(d,p) level. The principle quadrupole coupling constants of ^{14}N thus obtained are χ_{xx}= 1.844, χ_{yy}= 1.654, and χ_{zz}= -3.497 MHz, where x, y, and z are the principal quadrupole coupling axes of ^{14}N in the complex. While z is roughly along OH$\cdots$N H-bond direction, y is roughly in the

plane of NH··O H-bond. There is a substantial reduction in the magnitude of these constants in the z and y directions, whereas the change is smaller in the x-direction, compared to the experimental χ_{zz}= -4.0890(1) and $\chi_{xx} = \chi_{yy}$= 2.0450(1) MHz of ^{14}NH$_3$.[20]

Table 6.2. Experimental spectroscopic constants obtained for the ML··NH$_3$ adduct.

Parameter[a]	ML··^{14}NH$_3$		ML··^{15}NH$_3$	
A[MHz]	2576.6761(11)		2550.50192(65)	
B[MHZ]	1219.23607(75)		1196.32952(25)	
C[MHz]	963.39221(55)		945.88376(22)	
D$_J$[kHz]	0.317(15)		0.2690(27)	
D$_{JK}$[kHz]	0.308(20)		0.409(31)	
D$_K$[kHz]	2.480(60)		2.421(53)	
d$_1$[kHz]	-0.025(11)		-0.0567(19)	
d$_2$[kHz]	-0.0220(39)		-0.0153(16)	
top	ester methyl	ammonia	ester methyl	ammonia
D$_{pi2K}$[MHz]	0.0	455.55(5)	0.0 (fixed)	457.0460(60)
D$_{pi2-}$[kHz]	0.0	-58.83(13)	0.0 (fixed)	-56.6210(31)
V[kJ mol^{-1}]	4.778(16)	2.452(2)	4.818(18)	2.4538(7)
ρ	0.01285(4)	-0.006850(6)	0.012526(48)	-0.006793(1)
B[rad]	0.447(1)	1.87784(6)	0.4520(11)	1.91522(2)
Γ[rad]	2.952(5)	2.9055(1)	2.95494(84)	2.90838(2)
F$_0$[GHz][b]	155.33	181.76	156.42	181.67
F[GHz][b]	157.23	182.99	158.28	182.89
F$_{12}$[MHz][b]	-597.6		-562.01	
χ_{aa}[MHz][c]	1.480(1)		-	
χ_- [MHz][c]	-4.214(1)		-	
χ_{bc}[MHz][c]	1.3229(3)		-	
N	216		200	
σ[kHz]	3.6		4.9	

[a]Watsons S reduction[21] in the I^r representation. Physical significance of parameters, that is, which part of the Hamiltonian [Eq.(6.1)] they belong to, is provided in Appendix D. N is the number of transitions included in the fit, and σ is the standard deviation of the fit. [b]Derived from the fitted parameters. [c]The *ab initio* values for χ_{aa}, χ_- and χ_{bc} are 1.6182, -4.6249, and 1.7260 MHz, and for the other two off-diagonal elements, X$_{ab}$ and χ_{ac}, are -0.7536 and 0.2699 MHz, respectively.

This is not too surprising since the x-direction is least affected by the formation of the OH··N and NH··C=O H-bonds. In the H_3N··hydrogen halide series where NH_3 serves only as a proton acceptor, a reduction was observed and attributed to the ZPE averaging of the large amplitude motions and a small electric perturbation at ^{14}N.[22] A similar amount of reduction was reported for glycidol··NH_3.[10] (Please note that there is a typo for the sign of χ_{zz} for glycidol··NH_3 and NH_3 in Ref. (10). In addition, a 14.5% reduction in χ_{zz} upon complexation with ML was predicted theoretically, in good agreement with the experimental observation. Such electric perturbation may be attributed to a small charge transfer facilitated by the cooperative effect of the OH··N and NH··C=O H-bonds. Indeed, a positive charge transfer of +0.026e to the NH_3 subunit was calculated using natural bond-order (NBO) analysis[23] where the positive sign indicates a loss of electrons on NH_3.

Table 6.3. Partial refined r_0 geometry of the ML··NH_3 adduct.

| | ML--NH_3 I | |
	r_e[a]	r_0[b]
Fitted parameters		
N-O_{OH}[Å]	2.858	2.887(5)
NO_{OH}-C[°]	109.26	110.58(1)
NO_{OH}-CC[°]	56.34	52.83(3)
HN--H_{OH}[°]	93.90	97.(4)
Derived H-bond distances		
N--HO[Å]	1.887	1.928
NH--O=C[Å]	2.325	2.359

[a]At the MP2/6-311++G(d,p) level. [b]See the text for details. Values in parentheses are errors in units of the last digit.

Substantial efforts were made to locate the higher energy conformers of ML··NH_3 by analyzing the broadband rotational spectra of ML··$^{15}NH_3$ recorded with 2×10^6 cycles, but without success. While conformers **III** to **V** are predicted to be much less stable and

therefore unlikely to be observed in a jet expansion, **II** is about 1.2 kJ mol^{-1} less stable and would be expected to be observed with the signal-to-noise ratio achieved for **I**. On the other hand, **II** differs only slightly from **I** (Figure 6.S2, Appendix D for details) and the interconversion barrier was estimated to be lower than 7.4 kJ mol^{-1}. [13b] In a neon jet expansion, **II** is likely to relax to **I**, making **II** non-observable.

6.3. Conclusions

In conclusion, complex splitting patterns of the rotational transitions due to the internal rotations of the ester methyl group and the ammonia subunit, as well as the quadrupolar ^{14}N nucleus of ML$^{...14}$NH$_3$ and ML$^{...15}$NH$_3$ **I**, were observed and analyzed. The geometry of the adduct was refined using the experimental rotational constants. A detailed analysis of the nuclear quadrupole coupling tensor shows that the electric field gradient at ^{14}N in the binary adduct deviates noticeably from the cylindrical symmetry in the free NH$_3$ monomer and can be attributed to a small amount of charge transfer facilitated by the cooperative H-bonds.

6.4. Experimental section

Sample mixtures consisting of 0.06 % ML and 0.12% NH$_3$ in Neon at stagnation pressures of 4 to 8 bars were used. ML (99%, Sigma Aldrich), ^{14}NH$_3$ (98 %, Scott Speciality Gases Inc.), ^{15}NH$_3$ (98%, Cambridge Isotope Laboratories Inc.) and Neon (99.9990 %) were used without further purification. The survey scans were carried out using a chirp FTMW spectrometer[16] based on designs reported previously.[24] Briefly, a radiofrequency (rf) chirp (0.2–1 GHz, 4 μs) generated by an arbitrary waveform generator (Tektronix AWG 710B) is mixed with the output of a MW synthesizer to

produce a 2 GHz MW chirp in the 8-18 GHz range. These chirps are amplified with a 20 W solid- state MW amplifier (MW Power Inc., L0818-43) and then propagated into free space using a wide band, high gain, MW horn antenna (rf/MW instrumentation, ATH7G18). The resolution of the broadband spectrometer is 50 kHz. High-resolution measurements were done with a cavity-based[25] pulsed jet FTMW spectrometer.[18] The frequency uncertainty is about 2 kHz and the full line width at half height is about 10 kHz.

All geometry optimization and harmonic frequency calculations were done using G03, while the nuclear quadrupole coupling constants and NBO analysis were done with G09 program package[26] at the MP2/6-311++G(d,p) level. The basis set superposition error corrections were calculated using the counterpoise procedure of Boys and Bernardi.[27]

References

[1] R. E. Hubbard, M. K. Haider, **2010**, *Hydrogen Bonds in Proteins: Role and Strength*, In: Encyclopedia of Life Sciences (ELS), John Wiley & Sons, Ltd: Chichester.

[2] N. Borho, Y. Xu, *Angew. Chem. Int. Ed.*, **2007**, *46*, 2276-2279; N. Borho, Y. Xu, *J. Am. Chem. Soc.*, **2008**, *130*, 5916-5921; J. Thomas, F. X. Sunahori, N. Borho, and Y. Xu, *Chem. Eur. J.*, **2011**, *17*, 4582-4587.

[3] A. Maris, B. M. Giuliano, D. Bonazzi, W. Caminati, *J. Am. Chem. Soc.*, **2008**, *130*, 13860-13861.

[4] P. Ottaviani, B. Velino , W. Caminati, *Chem. Phys. Lett.* **2006**, 428, 236-240; N. Borho, Y. Xu, *Phys. Chem. Chem. Phys.* **2007**, *9*, 1324-1328.

[5] F. E. Susan, K. L. Robert, *Chem. Phys. Lett.* **1994**, *218*, 349-352.

[6] G. T. Fraser, R. D. Suenram, F. J. Lovas, W. J. Stevens, *Chem. Phys.* **1988**, *125*, 31-43.

[7] B. M. Giuliano, L. B Favero, A. Maris, and W. Caminati, *Chem. Eur. J.*, **2012**, *18*, 12759-12763.

[8] S. J. Humphrey, D. W. Pratt, *J. Chem. Phys.* **1997**, *106*, 908-915.

[9] C. Tanner, C. Manca, S. Leutwyler, *Science* **2003**, *302*, 1736-1739.

[10] B. M. Giuliano, S. Melandri, A. Maris, L. B. Favero, W. Caminati, *Angew. Chem. Int. Ed.* **2009**, *48*, 1102-1105.

[11] J. Sadlej, J. C. Dobrowolski, J. E. Rode, *Chem. Soc. Rev.* **2010**, *39*, 1478-1488.

[12] G. Yang, Y. Xu, *J. Chem. Phys.* **2009**, *130*, 164506; M. Losada, P. Nguyen, Y. Xu, *J. Phys. Chem. A* **2008**, *112*, 5621-5627.

[13] C. Merten and Y. Xu, *Chem. Phys. Chem*. **2012**, *14*, 213-219; C. Merten and Y. Xu, *Angew. Chem. Int. Ed.* **2013**, *52*, 2073-2076.

[14] H. Dreizler, H. D. Rudolph, and H. Mäder, *Z. Naturforsch. A, Phys. Sci.* **1970**, *25*, 25.

[15] I. Kleiner, J. T. Hougen, *J. Chem. Phys.* **2003**, *119*, 5505.

[16] S. Dempster, O. Sukhorukov, Q.-Y. Lei, and W. Jäger, *J. Chem. Phys.* **2012**, *137*, 174303.

[17] PGOPHER, C. M. Western, University of Bristol, http://pgopher. chm. bris.ac.uk

[18] Y. Xu, W. Jäger, *J. Chem. Phys.* **1997**, *106*, 7968.

[19] H. Hartwig, H. Dreizler, *Z. Naturforsch.* **1996**, *51*, 923-932.

[20] M. D. Marshall and J. S. Muenter, *J. Mol. Spectrosc.* **1981**, *85*, 322-326.

[21] J. K. G. Watson in Vibrational Spectra and Structure, Vol. 6 (Ed.: J. R. Durig), Elsevier, New York, **1977**, pp. 1 −89.

[22] A. C. Legon, *Chem. Soc. Rev.* **1993**, *22*, 153-163.

[23] A. van der Vaarta, K. M. Merz, Jr, *J. Chem. Phys.* **2009**, *116*, 7380-7388.

[24] G. G. Brown, B. C. Dian, K. O. Douglass, S. M. Geyer and B. H. Pate*, J. Mol. Spectrosc.* 2**006**, *238*, 200-212; G. S. Grubbs II, C. T. Dewberry, K. C. Etchison, K. E. Kerr, and S. A. Cooke, *Rev. Sci. Instrum.* **2007**, *78*, 096106/1-3.

[25] T. J. Balle, W. H. Flygare, *Rev. Sci. Instrum.* **1981**, *52,* 33-45; J.-U. Grabow, W. Stahl, H. Dreizler, *Rev. Sci. Instrum.* **1996**, *67*, 4072-4084.

[26] a) Gaussian 03, Revision B.01, M. J. Frisch, G. W. Trucks, H. B. Schlegel, G. E. Scuseria, M. A. Robb, J. R. Cheeseman, J. A. Montgomery, Jr., T. Vreven, K. N. Kudin, J. C. Burant, J. M. Millam, S. S. Iyengar, J. Tomasi, V. Barone, B. Mennucci, M. Cossi, G. Scalmani, N. Rega, G. A. Petersson, H. Nakatsuji, M. Hada, M. Ehara, K. Toyota, R. Fukuda, J. Hasegawa, M. Ishida, T. Nakajima, Y. Honda, O. Kitao, H. Nakai, M. Klene, X. Li, J. E. Knox, H. P. Hratchian, J. B. Cross, C. Adamo, J. Jaramillo, R. Gomperts, R. E. Stratmann, O. Yazyev, A. J. Austin, R. Cammi, C. Pomelli, J. W. Ochterski, P. Y. Ayala, K. Morokuma, G. A. Voth, P. Salvador, J. J. Dannenberg, V. G. Zakrzewski, S. Dapprich, A. D. Daniels, M. C. Strain, O. Farkas, D. K. Malick, A. D. Rabuck, K. Raghavachari, J. B. Foresman, J. V. Ortiz, Q. Cui, A. G. Baboul, S. Clifford, J. Cioslowski, B. B. Stefanov, G. Liu, A. Liashenko, P. Piskorz, I. Komaromi, R. L. Martin, D. J. Fox, T. Keith, M. A. Al-Laham, C. Y. Peng, A. Nanayakkara, M. Challacombe, P. M. W. Gill, B. Johnson, W. Chen, M. W. Wong, C. Gonzalez, and J. A. Pople, Gaussian, Inc., Pittsburgh PA, **2003**.

b) Gaussian 09, Rev. C.01, M. J. Frisch, G. W. Trucks, H. B. Schlegel, G. E. Scuseria, M. A. Robb, J. R. Cheeseman, G. Scalmani, V. Barone, B. Mennucci, G. A. Petersson, H. Nakatsuji, M. Caricato, X. Li, H. P. Hratchian, A. F. Izmaylov, J. Bloino, G. Zheng, J. L. Sonnenberg, M. Hada, M. Ehara, K. Toyota, R. Fukuda, J. Hasegawa, M. Ishida, T. Nakajima, Y. Honda, O. Kitao, H. Nakai, T. Vreven, J. J. A. Montgomery, J. E. Peralta, F. Ogliaro, M. Bearpark, J. J. Heyd, E. Brothers, K. N. Kudin, V. N. Staroverov, T. Keith, R. Kobayashi, J. Normand, K. Raghavachari, A. Rendell, J. C. Burant, S. S. Iyengar, J. Tomasi, M. Cossi, N. Rega, J. M. Millam, M. Klene, J. E. Knox, J. B. Cross, V. Bakken, C. Adamo, J. Jaramillo, R. Gomperts, R.

E. Stratmann, O. Yazyev, A. J. Austin, R. Cammi, C. Pomelli, J. W. Ochterski, R. L. Martin, K. Morokuma, V. G. Zakrzewski, G. A. Voth, P. Salvador, J. J. Dannenberg, S. Dapprich, A. D. Daniels, O. Farkas, J. B. Foresman, J. V. Ortiz, J. Cioslowski, D. J. Fox, Gaussian, Inc., Wallingford CT, **2010**. In G03, the default value for the nuclear quadrupole moment Q (^{14}N)= 1.56 barn while this value is updated to 2.044 barn in G09.

[27] S. F. Boys, F. Bernardi, *Mol. Phys*. **1970**, *19*, 553-566.

Chapter 7

Direct Spectroscopic Detection of the Orientation of Free OH Groups in Methyl Lactate–(Water)$_{1,2}$ Clusters: Hydration of a Chiral Hydroxy Ester[a]

7.1. Introduction

It is known that a chirality recognition process is greatly influenced by water solvation and desolvation processes.[1-3] This is not surprising since the energy associated with these processes is comparable to the interaction energy between chiral contact pairs in a chirality recognition process. In recent years, distinct vibrational circular dichroism (VCD) signatures at the water bending band have been detected experimentally and attributed to specific chiral molecule--water clusters formed in solution.[4-6] Because of the complexity of the condensed phase and the uncertain reliability of theoretical calculations in capturing the most stable conformations of these chiral solvated clusters, there have been debates about the existence and significance of these specific clusters. Detailed knowledge about the chiral molecule--water interactions at the molecular level is crucial to achieve a comprehensive understanding of the observed phenomena.

Unlike the condensed-phase measurements, jet-cooled high-resolution spectros-copy can differentiate the conformations of isolated chiral-molecule--water clusters with subtly different structures and provide accurate structural and relative stability information about them. Jet-cooled high-resolution spectroscopy has been successfully used to study small (inorganic/organic) molecule--water adducts, such as nitric acid--water,[7] formamide--(water)$_{1,2}$,[8] glycine--(water)$_{1,2}$,[9] and trifluoroacetic acid--(water)$_{1,2,3}$.[10] Only studies of a handful of chiral molecule--water clusters such as alaninamide--water,[11] 3-hydroxytetrahydrofuran--water,[12] glycidol--water,[13] and propylene oxide--(water)$_{1,2}$[14] have been reported.

Herein, this chapter I report rotational spectroscopic and high level *ab initio* computational studies of methyl lactate (ML)--(water)$_{1,2}$ clusters. ML is an α-hydroxy ester with multiple functional groups, offering multiple hydrogen (H)-bonding sites. First, we focus on the delicate competition between intra- and intermolecular H-bonding in the ML--(water)$_{1,2}$ clusters. Second, subtle conformational changes resulting from different orientations of the non-H-bonded, that is, free water –OH groups in these clusters were recently reported to generate drastically different VCD signatures.[4-6] Such dangling –OH groups at interfaces are the subject of intense current interest.[15] We therefore aim to utilize the advantages of high-resolution spectroscopy to identify such subtly different conformations.

7.2. Results and discussion

The dominant ML conformer, also the only one detected in a jet expansion,[16] is stabilized by an intramolecular H-bonded ring formed between the –OH and C=O groups. We identified seven monohydrate conformers based on this dominant ML monomer by *ab initio* calculations and confirmed them to be true minima without imaginary vibrational frequencies. This includes four *insertion* and three *addition* conformations, where water is inserted into the existing intramolecular H-bonded ring of ML or where water serves as an H-donor to one of the oxygen atoms of ML without breaking the existing intramolecular H-bonded ring, respectively. For the dihydrate clusters, a total of 16 ternary conformers were found using the binary conformers as starting points. Among those, seven are *insertion* only conformers and the others are mixed *insertion addition* or *addition* only conformers. All the lowest energy ternary ML--(water)$_2$ conformers exhibit *insertion* only topology. The geometries and the spectroscopic constants of the mono-

and dihydrates are summarized in Table 7.S1 and 7.S2, respectively, Appendix E. Monohydrate conformers are named i-I, i-II, etc, while those of dihydrate are labelled as ii-I, ia-VII, etc. The Roman number indicates the relative stability in their respective class (with I being the most stable), while 'i' or 'a' indicate that water takes on the *insertion* or *addition* topology, respectively. Geometries of some of the most stable conformers are shown in Figure 7.1.
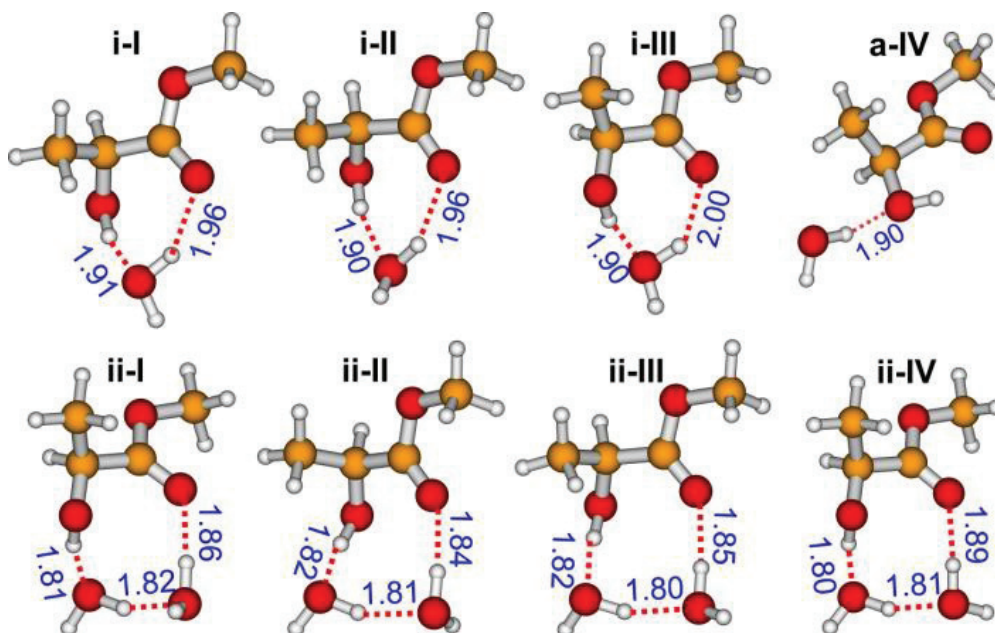
Figure 7.1. Geometries of the most stable conformers of the mono- and dihydrates of ML.

Spectroscopic searches for the mono- and dihydrates of ML were carried out using a broadband chirped pulse FTMW spectrometer.[17] Experimental details and an example broadband spectrum are provided in section E2 and Figure 7.S1 of Appendix E. The final frequency measurements were performed with a cavity based FTMW spectrometer.[18] Transitions of *a*-, *b*-, and *c*-type were observed for the monohydrate

conformer, while only *a*-type transitions could be observed for the dihydrate. Despite considerable efforts, no *b*- and *c*-type transitions were detected in this case.

Extensive isotopic studies were also performed. For the monohydrate, rotational spectra of ML--D$_2$O, ML--DOH, ML--HOD, MLOD (deuterated at the OH of ML)--DOH, and MLOD--HOD were measured and analyzed, in addition to that of ML--H$_2$^{18}O. For the dihydrate, three additional isotopologues were investigated, namely ML--(H$_2$^{18}O)$_2$, ML--H$_2$^{18}O--H$_2$^{16}O and ML--H$_2$^{16}O--H$_2$^{18}O. The measured line frequencies were fitted with the internal rotator program XIAM,[19] using Watson's semi-rigid rotor Hamiltonian in the S-reduction and I^r-representation.[20] A brief summary of the resulting spectroscopic parameters of the mono- and dihydrate isotopologues are given in Table 7.1, while the complete lists are provided in Tables 7.S3 and 7.S4, Appendix E. The measured transition frequencies along with their quantum number assignments for all isotopologues are given in Tables 7.S5 to 7.S15, Appendix E.

While the four *insertion* monohydrate conformers look very similar structurally, their relative dipole moment magnitudes are quite different, depending sensitively on the direction the free hydroxy group is pointing. The experimental rotational constants obtained are similar to the calculated ones for both i-I and i-II. From the optimized microwave pulse widths and transition intensities, it can be estimated that $\mu_a \approx 2\mu_b \approx 2\mu_c$. This trend agrees with what was predicted for i-I and is in contrast to i-II which has essentially zero *b*-dipole moment component. We therefore assign the observed monohydrate to i-I. A potential energy scan as a function of the dihedral angle C=O--OH (of water) was performed at the MP2/6-311++G(d,p) level of theory (see Figure 7. S2,

113

Appendix E) to estimate the conversion barrier from conformer i-II to i-I. This barrier is rather low and can be easily overcome in a jet expansion.

Table 7.1. Experimental spectroscopic constants of the observed isotopologues of i-I and ii-II.[a]

Parameter[a]	A [MHz]	B [MHz]	C [MHz]	V_3 [kJmol^{-1}]	N	σ (kHz)
i-ML--H$_2$O	2566.4940(6)	1278.7597(2)	1011.8730(2)	5.12(2)	106	4.0
i-ML--H$_2^{18}$O	2511.3532(5)	1238.8016(1)	979.5511(1)	5.05(2)	104	3.3
i-ML--DOD	2478.541(1)	1241.9619(7)	975.8648(5)	5.12(1)	49	6.8
i-ML--DOH	2529.399(1)	1271.2273(5)	1001.7533(4)	5.071(9)	62	6.8
i-ML--HOD	2511.849(1)	1249.2938(6)	985.2618(5)	5.11 (1)	62	7.4
i-MLOD--DOH	2529.862(1)	1257.7016(4)	994.9089(4)	5.125(8)	68	7.2
i-MLOD--HOD	2512.3057(8)	1236.4447(2)	978.7656(2)	5.11(3)	85	4.6

Parameter[a]	ii-ML--2H$_2$O	ii-ML--H$_2^{18}$O--H$_2^{18}$O	ii-ML--H$_2^{18}$O--H$_2^{16}$O	ii-ML--H$_2^{16}$O--H$_2^{18}$O
A [MHz]	1703.2142(53)	1647.0764(32)	1694.604(13)	1656.6878(58)
B [MHz]	915.85211(37)	872.66301(30)	887.98776(72)	898.66724(78)
C [MHz]	681.15852(31)	650.40411(23)	666.26735(51)	664.31504(56)
V_3 [kJmol^{-1}]	5.1887(79)	5.1944(83)	5.187(18)	5.223(18)
N	64	61	44	51
σ [kHz]	3.5	3.2	4.8	5.8

[a]Complete lists of the spectroscopic constants of i-I and ii-II are given in Table 7.S3 and 7.S4, respectively in Appendix E. N is the number of transitions included in the fit and σ is the standard deviation of the fit. Errors in parenthesis are expressed in units of the least significant digit.

Kraitchmann's substitution[21] coordinates of the water subunit are compared with the corresponding *ab initio* values of i-I and II in Table 7.S16, Appendix E. Clearly, i-I provides better agreement with the experimental coordinates, thus supporting the above conformer assignment. The experimental rotational constants were used to provide a partially refined effective structure (Table 7.2). The bond lengths, angles and dihedral angles related to the position of the water molecule relative to ML were fitted to the experimental rotational constants of all isotopologues. The remaining structural parameters were kept at their *ab initio* values. The *insertion* nature of the intermolecular

114

H-bonds can be clearly identified from the parameters in Table 7.2. A complete list of the coordinates is provided in Table 7.S17, Appendix E.

Table 7.2. Partially refined geometry of the i-I conformer of ML-H_2O.

Parameter[a]	Exp.[b]	Theo.[c]
O16-H8	1.968(4)	1.9102
O16-H18-O1	162.2(1)	163.1
O16-H8-O1-C2	-55.3(5)	-44.8
H17-O16-H8	78.2(19)	87.4
H17-O16-H8-O1	-2.5(11)	-11.9
H17-O16	1.038(44)	0.968
H18-O16	0.964(33)	0.960
H8-O16	1.968[d]	1.910
H17-O4	1.846[d]	1.958
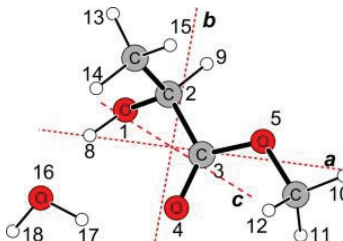
[a]Distances in [Å] and angles in [°]. [b]See the text for details. Values in parentheses are errors in units of the least significant digit. [c]At the MP2/6-311++G(d,p) level. [d]Calculated from the fitted parameters.

For the dihydrate of ML, the situation becomes even more complex. Initially, the set of assigned transitions was tentatively identified as belonging to ii-I, the most stable conformer predicted. However, the failure to observe *c*-type transitions was puzzling since ii-I was predicted to have a sizeable dipole moment component in the *c* direction. Further extensive computational searches for other conformers with subtly different structures revealed a number of other possibilities (cf. Table 7.S2, Appendix E). We note that all the predicted *insertion-* only conformers, except ii-II, have either strong *b*- or *c*-type transitions. Consequently, the observed transitions were identified as belonging to ii-II based on the comparison of the observed and predicted rotational constants and dipole moment components.

115

For the dihydrate conformer, the substitution coordinates of the oxygen atoms of the two water subunits are given in Table 7.3, along with the related *ab initio* values of the dihydrate conformers ii-I and ii-II. Clearly, the experimental coordinates are in good agreement with those of ii-II, whereas they disagree with those of ii-I. This further supports our assignment of the observed ML dihydrate conformer to ii-II.

Table 7.3. Substitution coordinates [Å] of the O atoms of water in ML--(water)$_2$ and the related MP2/6-311++G(d,p) values for ii-I and ii-II.

Atom	Exp.	ii-I	ii-II	
O16				
a	±2.857	-2.370	2.748	
b	±0.455	0.239	0.438	
c	±0.767	1.469	-0.871	
O19				
a	±2.269	-2.632	2.289	
b	±2.091	1.104	-2.065	
c	±0.142	-1.126	0.147	
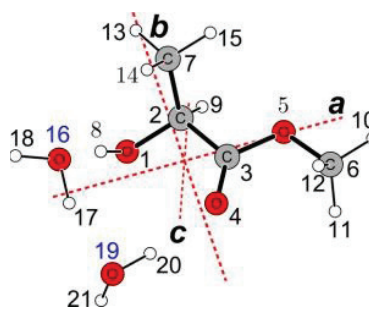
Several attempts to detect other *insertion* ML--(water)$_{1,2}$ conformers were not successful. In retrospect, this is not surprising for the monohydrate because of conformational relaxation in the jet expansion or negligible population to begin with. Furthermore, all unassigned lines observed in the broadband scan were checked using the cavity spectrometer with sample mixtures of ML+H$_2{}^{16}$O and ML+H$_2{}^{18}$O separately. Most of these lines could be ruled out as belonging to hydrated ML clusters since they were observed with both samples. Transitions of ML--H$_2{}^{16}$O or ML--H$_2{}^{18}$O could only be observed with either the ML+H$_2{}^{16}$O or ML+H$_2{}^{18}$O sample, respectively. We therefore conclude that the two conformers observed are the most stable ones for the mono- and dihydrate.

It is interesting to note that in the hydrated chiral clusters studied, a particular orientation of the free OH group(s) of water is strongly favoured over the other possibilities, as suggested by our assignments to specific *ab initio* structures. This is somewhat surprising since in acid--water complexes with "planar symmetry", such as HNO_3--H_2O[7] and CF_3COOH--H_2O[10], large amplitude and tunneling motions associated with the water subunits were commonly reported. For example, the H-tunnelling motion responsible for the observed tunnelling splittings was hypothesized to be a rotation about the H (of acid)--O (of water) intermolecular H-bond, with an estimated barrier of approximately 12 kJ mol^{-1} for the trifluoroacetic acid--water complex (cf. mode II in Ref. 10). In the present cases, similar motions would connect two inequivalent minima such as i-I and i-III or i-II and i-IV. Because of the noticeable energy difference between the two minima, the more stable one is significantly favoured while the less stable one is not observed in the jet expansion.

In the aforementioned acid--water complexes, the H-wagging motion, where the non-bonded H-atom of water flaps from above to below the H-bonded ring plane, was predicted to have a very small barrier and connects two *equivalent* geometries (Figure 3 and 4 of Ref. [10]). This mode is best viewed as associated with a large amplitude motion in these complexes, as suggested by Leopold et al., to account for the absence of the *c*-type transitions.[7] A similar wagging motion in ML--water, on the other hand, connects two inequivalent minima, that is, conformers i-I and i-II, with a very low barrier from i-II to i-I and a more substantial barrier of 3.8 kJmol^{-1} from i-I to i-II (Figure 7.S2, Appendix E). This complex potential energy surface results in the unique and well defined free OH orientation conformations which are detected in the current study.

We further note that while the *ab initio* calculations correctly predicted the most stable monohydrate conformer identified experimentally, it failed in the case of the dihydrate. Clearly, extensive experimental spectroscopic data are crucial for the unambiguous identification of the specific conformations in the gas phase, as demonstrated in the present chapter.

The experimental internal rotation barrier height of the ester methyl group is around 5.1 and 5.2 kJ mol^{-1} for the mono- and dihydrate of ML, respectively, higher than that of the ML monomer at ~4.76 kJ mol^{-1}.[16] This difference is attributed to a decrease in the C=O--H (of the ester methyl group) van der Waals distance(s) when the intramolecular H-bond in ML is replaced with the intermolecular H-bonded ring upon hydration. In ML--water, the van der Waals distances O4--H11 and O4--H12 become slightly shorter, by 0.016 and 0.013 Å, respectively, compared to the monomer distances. In the dihydrate, the corresponding distances are even shorter by 0.019 and 0.029 Å, respectively. The insertion of one or two water molecules offers greater flexibility to optimize both intermolecular H-bonding and the van der Waals interaction between the carbonyl O atom and the H atoms of the ester methyl group, resulting in an increasing internal rotation barrier in going from ML to ML--water to ML--(water)$_2$.

7.3. Conclusions

In summary, ML-(water)$_{1,2}$ strongly favours the compact *insertion* topology over the *addition* one in the delicate competition between intra- and intermolecular H-bonding interactions. The monohydrate conformer identified here is also the dominant one responsible for the induced solvent VCD signatures in water. This result suggests that such tightly bound structure is quite robust, although it must be kept in mind that the bulk

water environment may strongly affect the relative stabilities of the conformers. The unique dihydrate conformer identified is not the most stable one predicted. This finding highlights the significance of high resolution spectroscopic work in providing quantitative data to test theories for identifying specific water binding topologies, thus helping to build a solid foundation for interpreting solution measurements.

References

[1] Y. Levy, J. N. Onuchic, *Annu. Rev. Biophys. Biomol. Struct*. **2006**, *35*, 389–415.

[2] J. A. Jeffrey, W. Saenger, *Hydrogen Bonding in Biological Structures*, Springer, Berlin, 1991.

[3] A. Zehnacker, M. A. Suhm, *Angew. Chem*. **2008**, *120*, 7076 −7100; *Angew. Chem. Int. Ed.* **2008**, *47*, 6970–6992.

[4] J. Sadlej, J. C. Dobrowolski, J. E. Rode, *Chem. Soc. Rev.* **2010**, *39*, 1478–1488; G. Yang, Y. Xu, *Vibrational Circular Dichroism Spectroscopy of Chiral Molecules*, in *Top. Curr. Chem*., Volume: Electronic and Magnetic Properties of Chiral Molecules and Supramolecular Architectures, Eds. R. Naaman, D. N. Beratan, D. H. Waldeck, Springer:Verlag, Berlin, Heidelberg, **2011**, *298*, 189–236.

[5] M. Losada, Y. Xu, *Phys. Chem. Chem. Phys*. **2007**, *9*, 3127–3135.

[6] M. Losada, H. Tran, Y. Xu, *J. Chem. Phys*. **2008**, 128, 014508/1−11; M. Losada, P. Nguyen, Y. Xu, *J. Phys. Chem. A*. **2008,** *112*, 5621−5627 ; G. Yang, Y. Xu, *J. Chem. Phys*. **2009**, *130,* 164506/1−9.

[7] M. Canagaratna, J. A. Phillips, M. E. Ott, K. R. Leopold, *J. Phys. Chem. A* **1998,** *102,* 1489–1497.

[8] S. Blanco, J. C. López, A. Lesarri, J. L. Alonso, *J. Am. Chem. Soc*. **2006**, *128*, 12111–12121.

[9] J. L. Alonso, I. Peña, M. E. Sanz, V. Vaquero, S. Mata, C. Cabezas, J. C. López, *Chem. Commun.,* **2013**, *49*, 3443–3445.

[10] B. Ouyang, T. G. Starkey, B. J. Howard, *J. Phys. Chem. A*. **2007**, *111*, 6165–6175.

[11] J. Lavrich, M. J. Tubergen, *J. Am. Chem. Soc.* **2000**, *122*, 2938–2943.

[12] R. J. Lavrich, C. R. Torok, M. J. Tubergen, *J. Phys. Chem. A*. **2001**, *105*, 8317–8322.

[13] A. R. Conrad, N. H. Teumelsan, P. E. Wang, M. J. Tubergen, *J. Phys. Chem. A.* **2010**, *114*, 336–342.

[14] Z. Su, Q. Wen, Y. Xu, *J. Am. Chem. Soc*. **2006**, *128*, 6755–6760; Z. Su, Y. Xu, *Angew. Chem. Int. Ed.* **2007**, *46*, 6163-6166; *Angew. Chem.* **2007**, *119*, 6275–6278.

[15] J. G. Davis, B. M. Rankin, K. P. Gierszal, D. Ben-Amotz, *Nature Chem.* **2013**, 796–802.

[16] P. Ottaviani, B. Velino, W. Caminati, *Chem. Phys. Lett*. **2006**, *428*, 236–240; N. Borho, Y. Xu, *Phys. Chem. Chem. Phys*. **2007**, *9*, 1324–1328.

[17] S. Dempster, O. Sukhrukov, Q. Y. Lei, W. Jäger, *J. Chem. Phys*. **2012**, *137*, 174303/1−8; J. Thomas, J. Yiu, J. Rebling, W. Jäger, Y. Xu, *J. Phys. Chem. A. **2013, 117,* 13249-13254 .

[18] Y. Xu, W. Jäger, J. *Chem. Phys*. **1997**, *106*, 7968−7980.

[19] H. Hartwig, H. Dreizler, *Z. Naturforsch*. **1996**, *51a*, 923–932.

[20] J. K. G. Watson, In Vibrational Spectra and Structure, Vol. 6 (Ed.: J. R. Durig), Elsevier, New York, 1977, pp. 1−89.

[21] J. Kraitchmann, *Am. J. Phys*. **1953**, *21*, 17−25.

Chapter 8

Structure and Tunneling Dynamics in a Model System of Peptide Co-Solvents: Rotational Spectroscopy of the 2,2,2-Trifluoroethanol··Water Complex[a]

8.1. Introduction

2,2,2-Trifluoroethanol (TFE) is an alcohol based solvent with diverse applications in molecular biology.[1] Nuclear magnetic resonance and circular dichroism studies show that TFE can induce formation of the secondary structure of proteins in aqueous solutions containing a small amount of TFE.[2-4] More recently, Hamada et al., reported that low concentrations of TFE in water favours the folding of proteins into secondary structures, whereas high concentrations destabilize the secondary structure.[5] Several mechanisms have been proposed to explain how TFE stabilizes the secondary structures of peptides and proteins in such co-solvents.[6-9] A few studies proposed that TFE interacts with the carbonyl oxygen atoms and hydrophobic groups within the proteins, and thus penetrates the hydrophobic core of proteins.[4] Another mechanism based on molecular dynamic simulations showed that such stabilization is induced by the preferential aggregation of TFE molecules around the peptides, thus providing a low dielectric environment that favors the formation of intra-peptide hydrogen (H)-bonds.[7] This mechanism suggests that TFE shows strong solvation interactions which are competitive with those of water.[8] To accurately describe the folding and unfolding mechanisms of peptides and proteins in a TFE water mixture, comprehensive knowledge of the hydration of the TFE molecule is critical.[10] Indeed, a detailed understanding of the interaction of TFE with water is a crucial first step.

TFE has three possible forms: *gauche+* (*g+*), *gauche-* (*g-*), and *trans* (*t*). Rot-tunneling spectrum of TFE as a result of the –OH proton tunneling between the two isoenergetic *gauche* conformations were observed previously.[11,12] The stability and

vibrational spectra of the complexes of TFE with water and with ammonia were investigated theoretically before.[13] According to this study, an *insertion* complex with the *gauche* forms of TFE, where the water molecule is inserted into the existing intramolecular H-bonded ring of TFE is the most stable conformer. Heger et al. recently reported a low resolution Fourier transform (FT) infrared study of the complexes containing one water with mono-, di- and trifluoroethanol and explored the effect of fluorination on the first solvating water molecule.[14]

Jet-cooled FT microwave (MW) spectroscopy is well known for providing accurate structural and dynamic information of small H-bonded molecular systems[15-17] and has been applied recently to the studies of a number of hydration clusters.[18-22] Jet-cooled FTMW spectroscopy can distinguish between conformers with only minute differences, such as pointing direction of an –OH bond, and allow unambiguous identification of individual conformers. In this chapter, I report the first rotational spectroscopic study of the TFE··H_2O complex with the aid of high level *ab initio* calculations. In particular, we aim to identify any possible tunneling splitting due either to the tunneling between the *g+* and *g-* configurations of TFE or due to the tunneling of the water subunit in the molecular adduct. We also focus on the binding topologies of water with TFE and on whether TFE acts as a strong H-bond donor or an acceptor in the TFE monohydrate complexes through extensive isotopic studies.

8.2. Experimental and computational details

Sample mixtures consisting of 0.13 % of TFE and 0.13 % of H_2O/D_2O in He/Ne at backing pressures of 4 to 8 bar were used for all measurements. TFE (97%, Sigma

Aldrich), D_2O (98%, Aldrich) and Neon or Helium (99.9990 %) were used without further purification. Preliminary rotational spectral scans were carried out using a broadband chirped pulse FTMW spectrometer[23] based on the design reported previously.[24] Briefly, a radio frequency (rf) chirp (0.2-1 GHz, 4 μs) generated by an arbitrary waveform generator (Tektronix AWG 710B) is mixed with the output of a MW synthesizer to produce a 2 GHz MW chirp in the 8-18 GHz range. These chirps are amplified with a 20 W solid state MW amplifier (MW Power Inc., L0818-43). A pair of wide band, high gain, MW horn antennas (RF/MW Instrumentation, ATH7G18) are used to propagate the MW radiation into free space and to collect the resulting signals. The resolution of the broadband spectrometer is 25 kHz. All final frequency measurements were done with a cavity based[25] pulsed jet FTMW spectrometer.[26] The frequency uncertainty is ~2 kHz and the full line width at half height is approximately 10 kHz.

High level *ab initio* calculations using the Gaussian09 suite of programs [27] were carried out to aid the experimental search and analysis. Second order Moller Plesset perturbation (MP2) theory[28] with the 6-311++G(2d,p) basis set was used to search for the possible TFE··H_2O conformers. Harmonic frequency calculations were also performed to make sure that all the optimized geometries are true minima without any negative frequencies. The calculated raw dissociation energies for all the conformers were corrected for the zero point energy (*ZPE*) effects and the basis set superposition errors (*BSSE*s). *BSSE*s were calculated using the counterpoise procedure of Boys and Bernardi.[29]

8.3. Results and discussion

We considered both *insertion* and *addition* H-bonding topologies in the formation of the TFE··water complex. In addition, all three forms of TFE, i.e. *g+*, *g-* and *t* (Figure 8.1) were taken into consideration. The *gauche* forms of TFE are stabilized by an intramolecular H-bond between the hydroxy hydrogen and one of the fluorine atoms of the CF_3 group. It is not possible to use the usual rotational spectroscopy to distinguish between the binary conformer containing the *g+* TFE subunit with the corresponding one with the *g-* TFE subunit since they are mirror images to each other. On the other hand, since *g+* TFE··H_2O is isoenergetic to *g-* TFE··H_2O, one may be able to observe additional spectral splitting due to the tunneling motion similar to that in the TFE monomer.[11] In the *insertion* conformers, a primary intermolecular H-bond is formed between the hydroxy H atom of TFE and the O of water, while an F atom of the –CF_3 group acts as a proton acceptor to the H atom of the water molecule. Since the hydroxyl H atom of TFE can point to either of the lone pairs of the water oxygen atom, this can lead to two different *insertion* conformations. Only one of the conformers turns out to be a true minimum. In the *addition* complexes, TFE acts only as a proton donor to water. It is noted that *t* TFE only forms *addition* binary conformers.
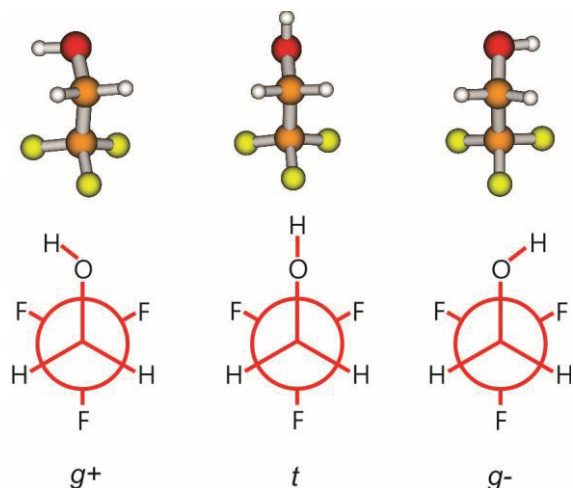
Figure 8.1. Newman projection and geometry of the 3 TFE monomer configurations.

A total of six TFE··water conformers were identified to be true minima. Four of them contain the *g+/g-* TFE subunit while the other two are made with *t* TFE. The optimized geometries of all the TFE··H_2O adducts are shown in Figure 8.2. The related spectroscopic constants and energies of the conformers are given in Table 8.1. The conformations are named as *i/a g/t* TFE··H_2O I to VI where *i* and *a* denote the *insertion* or *addition* binding topology, respectively, and the Roman numerals I to VI indicate the decreasing order of stability. It is interesting to point out that the second and fourth most stable binary adducts are formed from the *t* TFE although only *gauche* TFE monomer was observed experimentally.[11,12] It is further noted that *t* TFE was predicted to be a saddle point or supported by a very shallow potential depending on the level of theory.[30] On the other hand, it was shown that liquid TFE contains about 40% *t* and 60% *gauche* TFE,[31] suggesting that H-bonding interactions can stabilize the *t* TFE form.
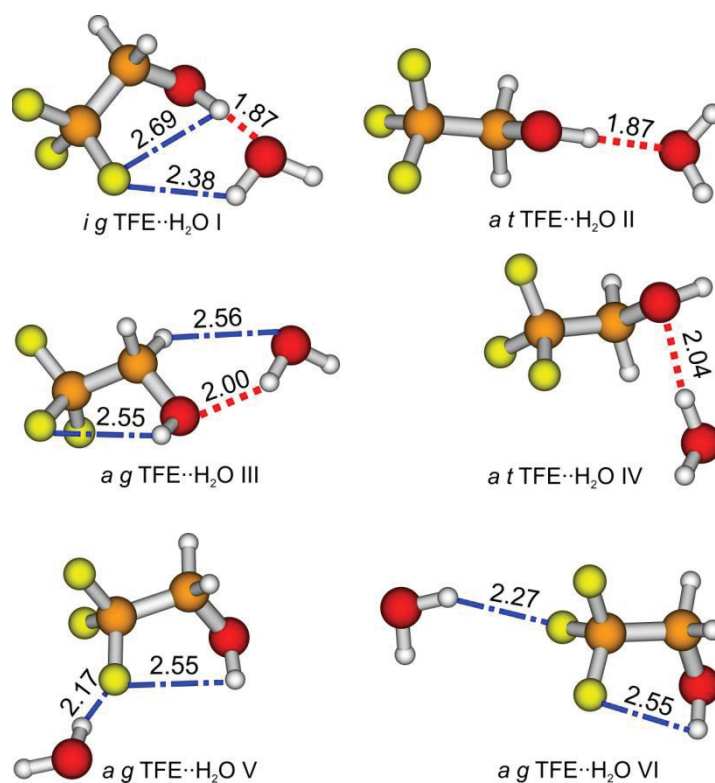
Figure 8.2. Geometries of the six most stable conformers of the TFE··H₂O complex calculated at the MP2/6-311++G(2d,p) level of theory. The primary (red) and the secondary (blue) inter- and intra-molecular H-bond lengths (in Å) are also indicated.

Table 8.1. Calculated relative raw dissociation energies ΔD_e, and the *ZPE* and *BSSE* corrected dissociation energies ΔD_0 (in kJmol⁻¹), rotational constants A, B, and C (in MHz), and electric dipole moment components $|\mu_{a,b,c}|$ (in Debye) of the TFE··H₂O conformers at the MP2/6-311++G (2d,p) level of theory.

Parameters	*i g* TFE·H₂O I	*a t* TFE·H₂O II	*a g* TFE·H₂O III	*a t* TFE·H₂O IV	*a g* TFE·H₂O V	*a g* TFE·H₂O VI
ΔD_e	0	-10.70	-12.10	-18.32	-26.91	-27.42
ΔD_0	0	-7.76	-9.86	-15.67	-17.18	-18.29
A	3533	4918	4168	3593	3137	3519
B	1582	997	1188	1513	1242	1184
C	1383	981	1121	1344	1073	1067
$|\mu_a|$	2.78	5.90	1.00	0.54	1.26	4.25
$|\mu_b|$	1.33	1.43	1.79	1.66	0.43	0.08
$|\mu_c|$	0.67	0.05	0.42	1.07	0.74	0.70

From Table 8.1, it is clear that conformers II to VI are substantially less stable than conformer I. Under the condition of a supersonic expansion, one may expect only to see the most stable conformer. Conformer I is predicted to have all *a*-, *b*-, and *c*-types of transitions. It was recognized earlier on that samples containing TFE gave extremely dense rotational spectra. To identify the spectra due exclusively to the $TFE\cdot\cdot H_2O$ complex, broadband scans with TFE+He/Ne and $TFE+H_2O+He/Ne$ were compared. After careful analyses, rotational spectrum of conformer I was assigned unambiguously. A 0.88 MHz section of the broadband spectrum measured with $TFE+H_2O+He$ is shown in Figure 8.3.
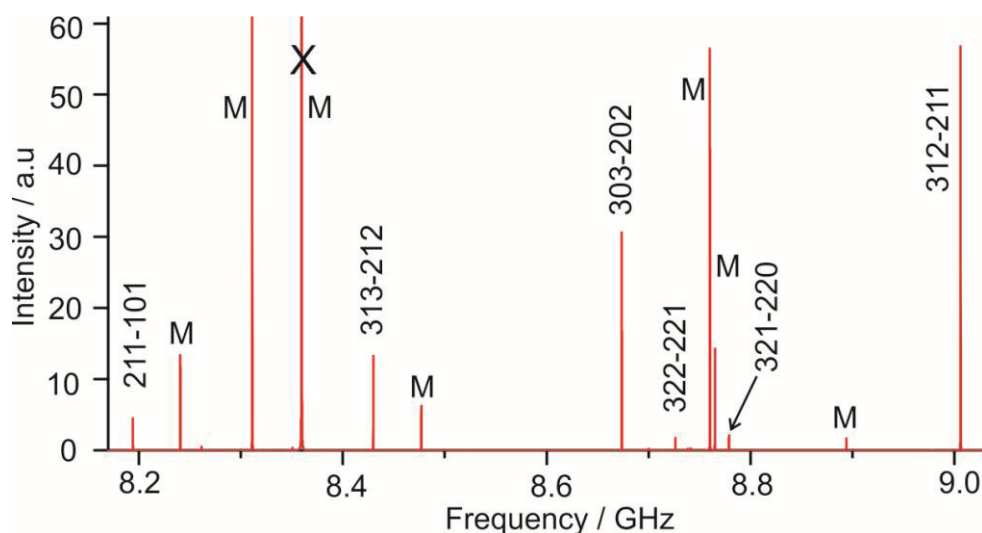
Figure 8.3. A 0.88 GHz section of the broadband chirped pulse spectrum using a sample mixture of $TFE+H_2O+He$. The rotational transitions assigned to the binary adduct *i g* $TFE\cdot\cdot H_2O$ I are indicated. The tunneling splittings are not visible at this frequency scale. The lines marked with M are transitions due to the TFE monomer which were also observed in the broadband spectrum without water. The strongest transition marked with "X" is ~126 times taller than shown.

We detected additional splitting in the order of a few tens of kHz for all of the observed rotational transitions. To confirm the spectral assignment and to unravel the splitting observed, the final frequency measurements were done using the cavity based FTMW instrument. In all of the observed rotational transitions, the two splitting components have an intensity ratio of approximately 3:1. These observed relative intensities of the two components are consistent with the nuclear spin statistical weights of 3:1 for ortho (I=1) versus para (I=0). This strongly suggests that the observed splittings are due to the tunneling motion of the water molecule where it interchanges the bonded and nonbonded H atoms. A total of 45 and 46 transitions which include a-, b- and c-type transitions were observed for the two tunneling states. The transitions due to both states were fitted separately to the Watson's S reduction semi-rigid rotor Hamiltonian in its I^r representation[32] using the Pgopher program.[33] The experimental spectroscopic constants obtained are summarized in Table 8.2. The maximum standard deviation for the fits is less than 3 kHz, similar to the experimental uncertainty. All the observed transitions along with the quantum number assignments for the two states are given in Table 8.S1 and 8.S2 of Appendix F.

Extensive isotopic studies were then carried out to get a deeper insight into the source of the observed splitting in the rotational transitions and the structure of the i g TFE··H_2O I complex. Broadband spectra of TFE+D_2O+He were recorded with more than 200K experimental cycles. A careful analysis of the broadband spectra lead to the assignment of the rotational spectra of TFE··DOH, TFE··D_2O, TFEOD (i.e. deuterated at the OH of TFE)··DOH, TFEOD··HOD and TFEOD··D_2O. It is noted that TFE··HOD, where water is H-bonded to TFE with the H atom rather than the D atom, was not

detected in the broadband spectra. Final frequency measurements for all the isotopologues were performed using the cavity based FTMW instrument.

Table 8.2. Experimental spectroscopic constants of the two tunneling states of $i\ g$ TFE$\cdots$H$_2$O I

Parameter[a]	ortho	Para
A (MHz)	3542.81100(94)	3542.8968(11)
B (MHz)	1550.49684(20)	1550.49258(23)
C (MHz)	1358.30527(21)	1358.28138(24)
D_J (kHz)	1.2998(25)	1.2980(29)
D_{JK} (kHz)	-0.392(16)	-0.372(19)
D_K (kHz)	2.40(19)	2.37(23)
d_1 (kHz)	-0.2435(21)	-0.2412(25)
d_2 (kHz)	0.0364(15)	0.0355(17)
N	45	46
σ (kHz)	2.3	2.7

[a] N is the number of transitions included in the fit and σ is the standard deviation of the fit.

The observed transitions of all the isotopologues of $i\ g$ TFE$\cdots$H$_2$O I were also fitted using the same procedure described above for the normal species. The measured transition frequencies along with their quantum number assignments for all isotopologues of $i\ g$ TFE$\cdots$H$_2$O I are listed in Table 8.S3 to 8.S7, Appendix F. The experimental spectroscopic constants of the observed isotopologues are listed in Table 8.3.

There are several interesting observations. A strong preference for the *insertion* over the *addition* binding topology was observed in the formation of the TFE$\cdots$water binary adduct. This is consistent with the predicted relative dissociation energies and with the rotational spectroscopic studies of other similar hydration clusters such as methyl lactate$\cdots$water,[18] and methyl lactate$\cdots$NH$_3$.[34] Also, the *insertion* of water into the existing intramolecular H-bond of TFE elongates the original F$\cdots$H distance by 0.17 Å in the TFE$\cdots$H$_2$O complex. This preference may influence how water and TFE interact in

solution, although studies of larger hydration clusters of TFE and also clusters of TFE

aggregations with water will be necessary to gain further insights. It is also noted that no

water tunneling splitting was observed for the rotational transitions of the *insertion*

methyl lactate··water complex.[18] The observed water tunnelling splitting in the present

case may be the result of a weaker Ow-Hw··F(F_2)C intermolecular H-bond in TFE··water

in comparison with a stronger Ow-Hw··O=C H-bond in methyl lactate··water. Here Ow

and Hw indicate the O and the H-bonded H atom of water, respectively.

Table 8.3. Experimental spectroscopic constants of the observed isotopologues of *i g*
TFE··H_2O I.

Parameter[a]	TFE··DOH	TFE··D_2O	TFEOD··DOH	TFEOD··HOD	TFEOD··D_2O
A (MHz)	3489.3022(33)	3476.3923(58)	3470.8801(24)	3508.5786(61)	3457.10824(89)
B (MHz)	1529.38122(69)	1469.3626(12)	1516.22574(63)	1476.6863(18)	1457.79934(85)
C (MHz)	1334.99184(63)	1287.6854(10)	1322.33345(66)	1297.0543(15)	1276.21855(73)
D_J (kHz)	1.2946(64)	1.1589(92)	1.2032(90)	1.112(13)	1.122(11)
D_{JK} (kHz)	-0.320(27)	0.00[b]	-0.358(45)	0.00[b]	0.00[b]
D_K (kHz)	3.07(64)	3.9(11)	1.08(19)	2.40[c]	2.40[c]
d_1 (kHz)	-0.2409(79)	-0.221(14)	-0.2196(84)	-0.135(20)	-0.166(10)
d_2 (kHz)	0.0347(42)	0.0378(58)	0.0315(48)	0.0413(85)	0.0241(71)
N	30	26	30	26	28
σ (kHz)	2.7	3.7	3.6	5.6	4.9

[a] N is the number of transitions included in the fit and σ (in kHz) is the standard deviation
of the fit.[b] Fixed to zero.[c] Fixed to that of the parent species *i g* TFE··H_2O I.

In the cavity measurements for the isotopologues, no splittings similar to those

observed for *i g* TFE··H_2O I were detected. First of all, with the HOD species, the

tunneling between the two water hydrogens is quenched by asymmetric isotopic

substitution. Rather the H-bonded and the D-bonded binding arrangements result in two

distinct structures with their own set of rotational constants. This is exemplified in the

case of TFEOD··HOD and TFEOD··DOH whose rotational constants differ vastly from

each other, in contrast to the very similar rotational constants obtained for the two

tunnelling states of TFE··H$_2$O (See Table 8.2). Both the nuclear spin statistical analysis and the absence of splitting in the above isotopologues clearly indicates that the splitting we observed in TFE··H$_2$O is due to the exchange of the two identical water hydrogens, rather than the tunneling between *g*+ and *g*- TFE. Since no other tunneling splittings were detected, we conclude that the tunneling between the *g*+ and *g*- TFE subunits is quenched upon H-bonding interactions with water, consistent with the previous studies of the other H-bonded TFE containing complexes.[35,36] No tunneling splittings of the lines were resolved for the TFE··D$_2$O and TFEOD··D$_2$O isotopologues. This is not surprising as D is much heavier than H. The deuterium nuclear hyperfine structures result only in very small splittings and are not well resolved experimentally. Therefore the averages of the line frequencies are taken as the center frequencies for the transitions. This explains an increase in the standard deviation of the fits of the TFE··H$_2$O isotopologues in Table 8.3.

The intensity of the rotational transitions of TFEOD··HOD was approximately a quarter of that of the TFEOD··DOH species. This may be a result of the lower *ZPE* of the D-bonded species compared to the H-bonded species. The same explanation can explain the absence of TFE··HOD in the broadband spectrum where TFE··DOH is present. Similar observations were reported previously, for example in the studies of the fluorobenzene··H$_2$O[37] and C$_2$H$_4$··H$_2$O[38] complexes.

A Kratichman's coordinate analysis[39] was carried out using TFEOD··D$_2$O as the parent species and the relevant isotopologues. The resulting coordinate values are listed in Table 8.4, along with the atom numbering of TFEOD··D$_2$O and the corresponding *ab initio* values. From Table 8.4, one can see that the experimental coordinates of the three H atoms are close to the corresponding *ab initio* values in general. This indicates that the

133

actual structure of the molecule is fairly close to the prediction. In fact, in the process of assigning rotational spectra of the deuterium isotopologues, it was essential turn to the ab initio structure in order to predict the systematic shifts in the corresponding rotational constants to facilitate the identification of a specific isotopologue.

Table 8.4. Experimental substitution coordinates (in Å) of the two deuterium atoms of D_2O and the D of TFEOD in the principal inertial axis system of $TFEOD \cdot \cdot D_2O$ and the corresponding *ab initio* values.

	Exp.	Theory
D7		
a	±1.642	1.674
b	±0.885	0.914
c	±0.077	0.081
D11		
a	±2.076	2.311
b	±1.404	-1.313
c	±0.321	0.315
D12		
a	±3.626	3.687
b	±0.689	-0.633
c	±0.244	0.233
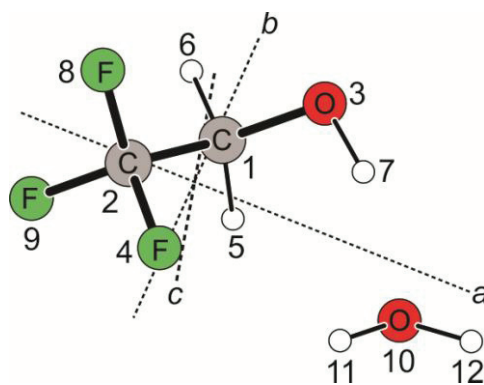
8.4. Conclusion and remarks

Rotational spectra of the simplest model system of peptide co-solvents, i.e. the TFE··water complex, and five of its isotopologues were studied using chirped pulse and cavity based FTMW spectroscopy with the aid of high level *ab initio* calculations. Tunneling splittings were detected in the rotational transitions of $TFE \cdot \cdot H_2O$. Based on the relative intensity of the two tunneling components, the associated nuclear spin statistical analysis, and the further isotopic evidence, the cause of the splitting can be conclusively attributed to the interchange of the bonded and nonbonded H atoms of

water. It further appears that the tunneling between $g+$ and $g-$ TFE is quenched in the H-bonded TFE$\cdot\cdot$H$_2$O complex. This study also shows that TFE preferentially forms an *insertion* rather than *addition* complex with water.

References

[1] M. Buck, *Q. Rev. Biophys*. **1998**, *31*, 297-355.

[2] A. Jasanoff, A. Fersht, *Biochemistry*. **1994**, *33*, 2129-2135.

[3] D. -P. Hong, M. Hoshino, R. Kuboi, Y. Goto, *J. Am. Chem. Soc*. **1999**, *121*, 8427-8433.

[4] J. F. Povey, C. M. Smales, S. J. Hassard, M. J. Howard, *J. Struct. Biol*. **2007**, *157*, 329-338.

[5] D. Hamada, F. Chiti, J. I. Guijarro, M. Kataoka, N. Taddei, C. M. Dobson, *Nat. Struct. Biol*. **2000**, 7, 58-61.

[6] P. Luo, R. L. Baldwin, *Biochemistry.* **1997**, 36, 8413-8421; M. Buck, S. E. Radford, C.M. Dobson, *Biochemistry.* **1993**, *32*, 669–678.

[7] D. Roccatano, G. Colombo, M. Fioroni, A. E. Mark, *Proc. Natl. Acad. Sci*. **2002**, *99* 12179–12184.

[8] A. Kundu, N. Kishore, *Biophys. Chem*. **2004**, *109*, 427–442.

[9] M. Guo, Y. Mei, *J. Mol. Model*. **2013**, *19*, 3931–3939.

[10] A. Burakowski, J. Gliński, B. Czarnik-Matusewicz, P. Kwoka, A. Baranowski, K. Jerie, H. Pfeiffer, N. Chatziathanasiou, *J. Phys. Chem. B*. **2012**, *116*, 705–710

[11] L. H. Xu, G. T. Fraser, F. J. Lovas, R. D. Suenram, C. W. Gillies, H. E. Warner, J. Z. Gillies, *J. Chem. Phys*. **1995**, *103*, 9541-9548.

[12] T. Goldstein, M. S. Snow, B. J. Howard, J. *Mol. Spectrosc*. **2006**, *236*, 1–10.

[13] M. L. Senent, A. Niño and C. Muñoz-Caro, Y. G. Smeyers, R. Domínguez-Gómez, J. M. Orza, *J. Phys. Chem. A*. **2002**, *106*, 10673-10680.

[14] M. Heger, T. Scharge, M. A. Suhm, *Phys. Chem. Chem. Phys*. **2013**, *15*, 16065-16073.

[15] J. Thomas, F. X. Sunahori, N. Borho, Y. Xu, *Chem. Eur. J.* **2011**, 17, 4582–4587.

[16] N. Borho, Y. Xu, *Angew. Chem. Int. Ed*. **2007**, *46*, 2276-2279.; *Angew. Chem*. **2007**, *119*, 2326-2329.

[17] N. Borho, Y. Xu, *J. Am. Chem. Soc*. **2008**, *130*, 5916-5921.

[18] J. Thomas, O. Sukhrukov, W. Jäger, Y. Xu, *Angew. Chem. Int. Ed.* **2014***, 53,* 1156 – 1159; Angew. Chem. 2014, **126**, 1175-1178.

[19] R. J. Lavrich, M. J. Tubergen, *J. Am. Chem. Soc.* **2000**, *122*, 2938–2943.

[20] R. J. Lavrich, C. R. Torok, M. J. Tubergen, *J. Phys. Chem. A*. **2001**, *105*, 8317– 8322.

[21] A. R. Conrad, N. H. Teumelsan, P. E. Wang, M. J. Tubergen, *J. Phys. Chem. A.* **2010**, *114*, 336–342.

[22] Z. Su, Q. Wen, Y. Xu, *J. Am. Chem. Soc*. **2006**, *128*, 6755–6760; Z. Su, Y. Xu, *Angew. Chem. Int. Ed.* **2007**, *46*, 6163-6166; *Angew. Chem.* **2007**, *119*, 6275–6278.

[23] S. Dempster, O. Sukhrukov, Q. Y. Lei, W. Jäger, *J. Chem. Phys*. **2012**, *137*, 174303/1-8; J. Thomas, J. Yiu, J. Rebling, W. Jäger, Y. Xu, *J. Phys. Chem. A.* **2013,** *117*, 13249-13254.

[24] G. G. Brown, B. C. Dian, K. O. Douglass, S. M. Geyer, B. H. Pate, *J. Mol. Spectrosc*. **2006**, *238*, 200–212; G. S. Grubbs II, C. T. Dewberry, K. C. Etchison, K. E. Kerr, S. A. Cooke, *Rev. Sci. Instrum*. **2007**, *78*, 096106/1–3.

[25] T. J. Balle, W. H. Flygare, *Rev. Sci. Instrum*. **1981**, *52*, 33–45; J.-U. Grabow, W. Stahl, H. Dreizler, *Rev. Sci. Instrum*. **1996**, *67*, 4072–4084.

[26] Y. Xu, W. Jäger, *J. Chem. Phys*. **1997,** *106*, 7968−7980.

[27] Gaussian 09, Rev. C.01, M. J. Frisch, G. W. Trucks, H. B. Schlegel, G. E. Scuseria, M. A. Robb, J. R. Cheeseman, G. Scalmani, V. Barone, B. Mennucci, G. A. Petersson, H. Nakatsuji, M. Caricato, X. Li, H. P. Hratchian, A. F. Izmaylov, J. Bloino, G. Zheng, J. L. Sonnenberg, M. Hada, M. Ehara, K. Toyota, R. Fukuda, J. Hasegawa, M. Ishida, T. Nakajima, Y. Honda, O. Kitao, H. Nakai, T. Vreven, J. J. A. Montgomery, J. E. Peralta, F. Ogliaro, M. Bearpark, J. J. Heyd, E. Brothers, K. N. Kudin, V. N. Staroverov, T. Keith, R. Kobayashi, J. Normand, K. Raghavachari, A. Rendell, J. C. Burant, S. S. Iyengar, J. Tomasi, M. Cossi, N. Rega, J. M. Millam, M. Klene, J. E. Knox, J. B. Cross, V. Bakken, C. Adamo, J. Jaramillo, R. Gomperts, R. E. Stratmann, O. Yazyev, A. J. Austin, R. Cammi, C. Pomelli, J. W. Ochterski, R. L. Martin, K. Morokuma, V. G. Zakrzewski, G. A.Voth, P. Salvador, J. J. Dannenberg, S. Dapprich, A. D. Daniels, O. Farkas, J. B. Foresman, J. V. Ortiz, J. Cioslowski and D. J. Fox, Gaussian, Inc.,Wallingford CT, **2010**.

[28] J. S. Binkley, J. A. Pople, *Int. J. Quantum Chem*. **1975**, *9*, 229-236

[29] S. F. Boys, F. Bernardi, *Mol. Phys*. **1970**, *19*,553-566.

[30] T. Scharge, C. Cezard, P. Zielke, A. Schutz, C. Emmeluth, M. A. Suhm, *Phys. Chem. Chem.Phys*. **2007**, *9*, 4472-4490

[31] I. Bako, T. Radnai, M. Claire, B. Funel, *J. Chem. Phys*. **2004**, *121*, 12472–12480.

[32] J. K. G. Watson, *Aspects of Quartic and Sextic Centrifugal Effects on Rotational Energy Levels. In Vibrational Spectra and Structure*; (Ed.; J. R. Durig), Elsevier: Amsterdam, Netherland, 1977,Vol. 6, p39.

[33] PGOPHER, A Program for Simulating Rotational Structure, C. M. Western, University of Bristol, http://Pgopher.chm.bris.ac.uk

[34] J. Thomas, O. Sukhrukov, W. Jäger and Y. Xu, *Angew. Chem. Int. Ed* **2013**, *52,* 4402-4405; *Angew. Chem*. **2013**, *125*, 4498-4501.

[35] J. Thomas, W. Jäger and Y. Xu, *Angew. Chem. Int. Ed.* DOI: 10.1002/anie.201403838R2 and 10.1002/ange.201403838R2 (**2014**).

[36] J. Thomas, Y. Xu, *J. Phys. Chem. Lett*. **2014**, *5*, 1850-1855.

[37] K. Brendel, H. Mäder, Y. Xu, W. jäger, *J. Mol. Spectrosc*. **2011**, *268*, 47-52.

[38] A. M. Andrews, R. L. Kuczkowski, *J. Chem. Phys*. **1993**, *98*, 791-795

[39] J. Kraitchmann, *Am. J. Phys*. **1953**, *21*, 17−25.

Chapter 9

Conclusions and Future Work

During my PhD studies, I have investigated several prototype hydrogen-bonded chiral molecular systems using chirped pulse and cavity-based Fourier transform microwave spectroscopy to deepen our understanding of chirality recognition and solvation of chiral molecules. *Ab initio* calculations and several spectroscopic programs have been used to aid the spectral data analysis. The significant results of my thesis, which provide insights into the processes of chirality recognition and solvation of chiral species at the molecular level, are summarized in the following.

In Chapters 3 to 5, I explored chirality recognition, chirality induction and amplification, and chirality synchronization in three model chiral contact pair systems. I examined how various factors, such as the relative stability of the monomer and the intermolecular interactions, contribute to chirality recognition processes in general. In Chapter 3, chirality recognition between two permanently chiral molecules, namely propylene oxide and glycidol was investigated. In this study, rotational spectra of six out of the eight hydrogen-bonded conformers were observed experimentally and assigned unambiguously. The binary interaction energy, relative monomer stability, and deformation energy of the monomers all play a significant role in determining the relative stability of the binary conformers under the conditions of a supersonic expansion. Overall, this chiral contact pair exhibits little preference for the homo- or hetero-chiral combinations.

Chirality amplification in a transient chiral molecule, 2,2,2-trifluoroethanol (TFE), as a result of chirality induction by the permanently chiral molecule, propylene oxide, was observed in the TFE··propylene oxide complex. It was shown experimentally that the fast tunneling motion between the $g+$ and $g-$ forms of TFE is quenched in this

hydrogen-bonded complex. This study also revealed that the interaction energy is the dominant factor that determines the conformational stability of the binary TFE··propylene oxide conformers, in which the monomers taking part in the complex formation are isoenergetic. Of particular interest is a noticeable preference for the *g+* TFE··*S*-propylene oxide diastereomers versus *g-* TFE··*S*-propylene oxide. Furthermore, new insights into the possible conformer conversion pathways in a supersonic jet expansion were provided, as four out of eight predicted stable conformers were observed experimentally while the other four were shown to relax into the four representative geometries observed.

Chirality synchronization in the dimer of the transient chirality molecule TFE was revisited in Chapter 5. This study highlighted the advantages of using high resolution spectroscopy, in comparison to low resolution spectroscopy, in providing comprehensive and crucial structural and dynamical information about the molecular recognition processes at the molecular level. One particularly significant result was the experimental observation of the missing heterochiral TFE dimer. In addition, a strong preference for the homochiral arrangement over the heterochiral one is observed where the former is about 10 times more abundant than the latter under the current pulsed jet condition. This is in contrast to the closely related 2-fluoroehtanol dimer which shows only very mild preference for the heterochiral arrangement.

In Chapters 6 to 8, the solvation process of prototype chiral molecular systems was explored. In Chapter 6, the observed ^{14}N nuclear quadrupole hyperfine structures of the complex of methyl lactate (ML) with ammonia provided a good understanding of the charge transfer between the chiral lock and the achiral key which is facilitated by

cooperative hydrogen-bonds. The stepwise solvation study of ML with water was described in Chapter 7. This study highlighted the significance of high resolution spectroscopic studies in judging the quality of theoretical predictions for identifying specific water binding topologies in a solvation process in general. This study also provided a potential link between the specific orientation of the dangling OH groups and the observed chirality transfer vibrational circular dichroism features of water in aqueous solutions of ML. The solvation study of TFE with water in Chapter 8 revealed a strong preference for the *insertion* binding topology over the *addition* one. The study also clearly established the additional splitting observed can be attributed to the interchange of the bonded and nonbonded hydrogen atoms of water. Again, the tunneling between $g+$ and $g-$ TFE was quenched in the monohydrate of TFE. All of the above solvation studies demonstrate preferences for the *insertion* binding topology over the *addition* one in these solvation clusters and allow a detailed understanding of the competition between inter- and intra-molecular hydrogen-bonds.

In summary, prototype molecular recognition processes involving chiral molecules have been studied in considerable detail in this thesis. The results show that even weak interactions between the monomers can be decisive in determining the stability of the resulting binary complexes under jet expansion conditions. The step wise solvation of chiral molecules and the preferential binding topology of the solvent molecules in the corresponding complexes were also explored in this thesis. Also, my work demonstrates the great potential of using chirped pulse and cavity-based Fourier transform microwave spectroscopy to probe structural and dynamic information of hydrogen-bonded chiral clusters.

It would be of significant interest to extend the studies to larger chiral clusters beyond two binding partners, such as ternary and quaternary molecular systems. In particular, stepwise solvation of chiral molecules with the addition of one water molecule at a time is highly desirable to trace solvation processes at the microscopic level and to bridge the gap to the condensed phase. Such studies will also provide the opportunity to examine how conformational preferences change as the cluster size grows. Another direction is to implement a laser ablation system in the sample system to allow easy introduction of amino acids and other biological samples into the gas phase and to probe their chirality recognition and solvation processes in great detail. However, larger hydration clusters and the aforementioned biological molecules will have in general larger principle moments of inertia and thus smaller rotational constants. Consequently, more rotational levels will be populated, leading to much lower population at each level. Furthermore transition frequencies with the same J and K quantum numbers will occur at lower frequencies which may fall below the operating range of the chirped-pulse or cavity-based microwave spectrometers. As a result, one may need to start searching for conformers using higher J and K rotational transitions which are expected to be much weaker. Nevertheless, with the sensitivity achieved with the two microwave spectrometers available, I expect that such studies will be feasible. On the theoretical front, studying larger molecular systems will be computationally challenging as the number of possible conformers and the flexibility of the molecules will increase noticeably with size. To ensure a systematic search for all possible conformers, one may utilize some molecular dynamics software packages, such as Amber[1], rather than the *ab initio* method, to carry out the initial conformational searches.

Reference

[1] D. A. Case, T. A. Darden, T. E. Cheatham, III, C. L. Simmerling, J. Wang, R. E. Duke, R. Luo, R. C. Walker, W. Zhang, K. M. Merz, B. Roberts, S. Hayik, A. Roitberg, G. Seabra, J. Swails, A. W. Goetz, I. Kolossváry, K. F. Wong, F. Paesani, J. Vanicek, R. M. Wolf, J. Liu, X. Wu, S. R. Brozell, T. Steinbrecher, H. Gohlke, Q. Cai, X. Ye, J. Wang, M. -J. Hsieh, G. Cui, D. R. Roe, D. H. Mathews, M. G. Seetin, R. Salomon-Ferrer, C. Sagui, V. Babin, T. Luchko, S. Gusarov, A. Kovalenko, and P. A. Kollman (2012), AMBER 12, University of California, San Francisco.

Bibliography

[1] L. Pasteur, *Ann. Chim. Phys*. **1848**, III, *24*, 442–459.

[2] E. Fischer, *Ber. Dtsch. Chem. Ges*. **1894**, *27*, 2985–2993.

[3] Lord Kelvin B*altimore Lectures (1884) on Molecular Dynamics and the Wave Theory of Light*, Clay and Sons: London, **1904**, p 449.

[4] A. Zehnacker, M. A. Suhm, *Angew. Chem*. **2008**, *120*, 7076–7100; *Angew. Chem. Int. Ed*. **2008**, *47*, 6970–6992.

[5] G. Blaschke, H. P. Kraft, K. Fickentscher, F. Kohler, *Drug Res*. **1979**, *29*, 1640–1642.

[6] S. C. Stinson, *Chemical and Engineering News*. **1998**, *76*, pp 38–70.

[7] N. Kurihara, J. Miyamot, G. D. Paulson, B. Zeeh, M. W. Skidmore. R. M. Hollingworth, H. A. Kuiper, *Pure. App. Chem.* **1997**, *69*, pp 2007–2025.

[8] R. A. Sheldon, *Chirotechnology: Chirotechnology: Industrial Synthesis of Optically Active Compounds,* Marcel Dekker, Inc.: New York, **1993,** pp 39–72.

[9] G. A. Jeffrey, W. Saenger, *Hydrogen Bonding in Biological Structures*, Springer, Berlin, **1991**.

[10] N. Seurre, J. Sepiol, K. Le Barbu-Debus, F. Lahmani, A. Zehnacker- Rentien, *Phys. Chem. Chem. Phys*. **2004**, *6*, 2867–2877.

[11] A. Giardini Guidoni, S. Piccirillo, D. Scuderi, M. Satta, T. M. Di Palma, M. Speranza, *Phys. Chem. Chem. Phys*. **2000**, *2*, 4139–4142.

[12] A. R. Al-Rabaa, K. Le Barbu, F. Lahmani, A. Zehnacker-Rentien, *J. Phys. Chem. A.* **1997**, *101*, 3273–3278.

[13] N. Borho, M. Suhm, *Phys. Chem. Chem. Phys*. **2002**, *4*, 2721–2732.

[14] T. B. Adler, N. Borho, M. Reiher, M. A. Suhm, *Angew. Chem*. **2006**, *118*, 3518–3523; *Angew. Chem. Int. Ed*. **2006**, *45*, 3440–3445.

[15] F. X. Sunahori, G. Yang, E. N. Kitova, J. S. Klassen, Y. Xu. *Phys. Chem. Chem. Phys*. **2013**, *15*, 1873–1886.

[16] F. O. Talbot, J. P. Simons. *Phys. Chem. Chem. Phys*. **2002**, *4*, 3562–3565.

[17] J. P. Simons, R. A. Jockusch, P. Carcabal, I. Hünig, R. T. Kroemer, N. A. Macleod, L. C. Snoek. *Int. Rev. Phys. Chem*. **2005**, *24*, 489–531.

[18] Y. Xu, W. J. Jäger, *Chem. Phys*. **1997**, *107*, 4788–4796.

[19] A. K. King, B. J. Howard, *Chem. Phys. Lett*. **2001**, *348*, 343–349.

[20] Z. Su, N. Borho, Y. Xu, *J. Am. Chem. Soc*. **2006**, *128*, 17126–17131.

[21] N. Borho, Y. Xu, *J. Am. Chem. Soc*. **2008**, *130*, 5916–5921.

[22] N. Borho, Y. Xu, *Angew. Chem*. **2007**, *119*, 2326–2329; *Angew. Chem. Int. Ed*. **2007**, *46*, 2276–2279; *Angew. Chem*. **2007**, *119*, 2326–2329.

[23] A. Maris, B. M. Giuliano, D. Bonazzi, W. Caminati, *J. Am. Chem. Soc*. **2008**, *130*, 13860–13861.

[24] X. Liu, N. Borho, Y. Xu, *Chem. Eur. J*. **2009**, *15*, 270–277.

[25] R. J. Lavrich, M. J. Tubergen, *J. Am. Chem. Soc*. **2000**, *122*, 2938 –2943.

[26] R. J. Lavrich, C. R. Torok, M. J. Tubergen, *J. Phys. Chem. A*. **2001**, *105*, 8317–8322.

[27] A. R. Conrad, N. H. Teumelsan, P. E. Wang, M. J. Tubergen, J. *Phys. Chem. A*. **2010**, *114*, 336–342.

[28] Z. Su, Q. Wen, Y. Xu, *J. Am. Chem. Soc*. **2006**, *128*, 6755–6760.

[29] Z. Su, Y. Xu, *Angew. Chem*. **2007**, *119*, 6275–6278; *Angew. Chem. Int. Ed*. **2007**, *46*, 6163–6166.

[30] B. M. Giuliano, S. Melandri, A. Maris, L. B. Favero, W. Caminati, *Angew. Chem*. **2009**, *121*, 1122–1125; *Angew. Chem. Int. Ed*. **2009**, 48, 1102–1105.

[31] J. D. Swalen, D. R. Herschbach, *J. Chem. Phys*. **1957**, *27*, 100–108.

[32] D. R. Herschbach, J. D. Swalen, *J. Chem. Phys*. **1958**, *29*, 761–776.

[33] F. Winther, D. O. Hummel, *Spectrochimica Acta*. **1968**, *25A*, 417–423.

[34] M. Imachi, R. L. Kuczkowski, *J. Mol. Struct*. **1982**, *96*, 55–60.

[35] C. Merten, J. Bloino, V. Barone, Y. Xu, *J. Phys. Chem. Lett.* **2013**, *4*, 3424–3428.

[35] W. V. F. Brooks, K. V. L. N. Sastry, *Can. J. Chem.* **1975**, *53*, 2247–2251.

 [36] R. M. Hanson, *Chem. Rev.* **1991**, *91*, 437–475.

[37] P. Ottaviani, B. Velino, W. Caminati, *Chem. Phys. Lett*. **2006**, *428*, 236–240.

[37] N. Borho, Y. Xu, *Phys. Chem. Chem. Phys*. **2007**, *9*, 1324–1328.

[38] L. H. Xu, G. T. Fraser, F. J. Lovas, R. D. Suenram, C. W. Gillies, H. E. Warner, J. Z. Gillies, *J. Chem. Phys*. **1995**, *103*, 9541–9548.

[39] T. Goldstein, M. S. Snow, B. J. Howard, *J. Mol. Spectrosc*. **2006**, *236*, 1–10.

[40] J. F. Povey, C. M. Smales, S. J Hassard, M. J, Howard, *J. Struct.Biol*. **2007**, *157*, 329–338.

[41] T. Scharge, T. Häber, M. A. Suhm, *Phys. Chem. Chem. Phys*. **2006**, *8*, 4664–4667.

[42] T. Scharge, C. Cézard, P. Zielke, A. Schütz, C. Emmeluth, M. A. Suhm, *Phys. Chem. Chem. Phys*. **2007**, *9*, 4472–4490.

[43] T. Scharge, T. N. Wassermann, M. A. Suhm, *Z. Phys. Chem*. **2008**, *222*, 1407–1452.

[44] K. B. McAfee, Jr., R. H. Hughes, E. B. Wilson, Jr., *Rev. Sci. Instrum*. **1949**, *20*, 821-826.

[45] R. H. Hughes, E. B. Wilson, Jr., *Phys. Rev*. 1**947**, *71* , 562-563.

[46] J. C. McGurk, T. G. Schmalz, W.H. Flygare, *Density Matrix, Bloch Equation Description of Infrared and Microwave Transient Phenomena*; (eds.; I. Prigogine, S.A. Rice), 1974.

[47] T. J. Balle, W. H. Flygare, *Rev. Sci. Instrum*. **1981**, *52*, 33 – 45.

[48] J.-U. Grabow, W. Stahl, H. Dreizler, *Rev. Sci. Instrum*. **1996**, *67*, 4072-4084.

[49] A.C. Legon, *Ann. Rev. Phys. Chem*. **1983,** *34,* 275-300.

[50] J.-U. Grabow, *Fourier Transform Microwave Spectroscopy Measurement and Instrumentation*, in: Handbook of High-resolution Spectroscopy, (John Wiley& Sons, Ltd., 2011.)

[51] J. C. McGurk, T. G. Schmalz, W. H. Flygare, *Adv. Chem. Phys*. **1974**, *25*, 1-68.

[52] T. G. Schmalz, W. H. Flygare, in Laser and Coherence Spectroscopy, (ed.; J. I. Steinfeld), Plenum, New York, 1978, pp. 125–196.

[53] Y. Xu, W. Jäger, *J. Chem. Phys*. **1997**, *106*, 7968-7980.

[54] Y. Xu, J. van.Wijngaarden, W. Jäger, *Int. Rev. Phys. Chem*. **2005**, *24*, 301- 338

[55] J.-U. Grabow, W .Stahl, *Z. Naturforsch*. **1990**, *45a*, 1043 -1044.

[56] G. G. Brown, B. C. Dian, K. O. Douglass, S. M. Geyer, B. H. Pate, *J. Mol. Spectrosc*. **2006**, *238*, 200-212.

[57] S. Dempster, O. Sukhorukov, Q.-Y. Lei, W. Jäger, *J. Chem. Phys*. **2012**, *137*, 174303/1-8.

[58] G. S. Grubbs II, C. T. Dewberry, K. C. Etchison, K. E. Kerr, S. A. Cooke, *Rev. Sci. Instrum*. **2007**, *78*, 096106/1-3.

[59] Brown, G. G.; Dian, B. C.; Douglass, K. O.; Geyer, S. M.; Shipman, S. T.; Pate, B. H. *Rev. Sci. Instrum*. **2008**, *79*, 053103/1-13.

[60] J. C. McGurk, T. G. Schmalz, W. H. Flygare, *J. Chem. Phys*. **1974**, *60*, 4181-4188.

[61] J. Thomas, J. Yiu, J. Rebling, W. Jäger, Y. Xu, *J. Phys. Chem. A*. **2013**, *117*, 13249–13254.

[62] W. Gordy, R. L. Cook, Microwave Molecular Spectra, 3rd ed. (Wiley, New York, 1984)

[63] C. H. Townes, A. L. Schawlow, Microwave Spectroscopy (Dover, New York, 1975), p. 306

[64] K.R. Leopold, G.T. Fraser, S.E. Novick, W. Klemperer, *Chem. Rev*. **1994**, *94*, 1807-1827

[65] G. S. Grubbs II, P. Groner, Stewart E. Novick, S. A. Cooke, *J. Mol. Spectrosc*. **2012**, *280*, 21-26.

[66] R. Subramanian, J. M. Szarko, W. C. Pringle, S. E. Novick, *J. Mol. Struct*. **2005**, *742*, 165-172.

[67] Y. Xu, W. Jäger, *Chem. Phys. Lett*. **2001**, *350*, 417-422.

[68] T.R. Dyke, *Topics Current Chem*. **1984**, *120*, 86-113.

[69] S. E. Novick, K. R. Leopold, W. Klemperer, *The Structure of Weakly Bound Complexes as Elucidated by Microwave and Infrared Spectroscopy*, in Atomic and

Molecular Clusters, (ed.; E.R. Bernstein), Elsevier, 1990, p. 359.

[70] Gaussian 03, Revision B.01, M. J. Frisch, G. W. Trucks, H. B. Schlegel, G. E. Scuseria, M. A. Robb, J. R. Cheeseman, J. A. Montgomery, Jr., T. Vreven, K. N. Kudin, J. C. Burant, J. M. Millam, S. S. Iyengar, J. Tomasi, V. Barone, B. Mennucci, M. Cossi, G. Scalmani, N. Rega, G. A. Petersson, H. Nakatsuji, M. Hada, M. Ehara, K. Toyota, R. Fukuda, J. Hasegawa, M. Ishida, T. Nakajima, Y. Honda, O. Kitao, H. Nakai, M. Klene, X. Li, J. E. Knox, H. P. Hratchian, J. B. Cross, C. Adamo, J. Jaramillo, R. Gomperts, R. E. Stratmann, O. Yazyev, A. J. Austin, R. Cammi, C. Pomelli, J. W. Ochterski, P. Y. Ayala, K. Morokuma, G. A. Voth, P. Salvador, J. J. Dannenberg, V. G. Zakrzewski, S. Dapprich, A. D. Daniels, M. C. Strain, O. Farkas, D. K. Malick, A. D. Rabuck, K. Raghavachari, J. B. Foresman, J. V. Ortiz, Q. Cui, A. G. Baboul, S. Clifford, J. Cioslowski, B. B. Stefanov, G. Liu, A. Liashenko, P. Piskorz, I. Komaromi, R. L. Martin, D. J. Fox, T. Keith, M. A. Al-Laham, C. Y. Peng, A. Nanayakkara, M. Challacombe, P. M. W. Gill, B. Johnson, W. Chen, M. W. Wong, C. Gonzalez, J. A. Pople, Gaussian, Inc., Pittsburgh PA, **2003**.

[71] Gaussian 09, Rev. C.01, M. J. Frisch, G. W. Trucks, H. B. Schlegel, G. E. Scuseria, M. A. Robb, J. R. Cheeseman, G. Scalmani, V. Barone, B. Mennucci, G. A. Petersson, H. Nakatsuji, M. Caricato, X. Li, H. P. Hratchian, A. F. Izmaylov, J. Bloino, G. Zheng, J. L. Sonnenberg, M. Hada, M.Ehara, K. Toyota, R. Fukuda, J. Hasegawa, M. Ishida, T. Nakajima, Y. Honda, O. Kitao, H. Nakai, T. Vreven, J. J. A. Montgomery, J. E. Peralta, F. Ogliaro, M. Bearpark, J. J. Heyd, E. Brothers, K. N. Kudin, V. N. Staroverov, T. Keith, R. Kobayashi, J. Normand, K. Raghavachari,

A. Rendell, J.C. Burant, S. S. Iyengar, J. Tomasi, M. Cossi, N. Rega, J. M. Millam, M. Klene, J. E. Knox, J. B. Cross, V. Bakken, C. Adamo, J. Jaramillo, R. Gomperts, R. E. Stratmann, O. Yazyev, A. J. Austin, R. Cammi, C. Pomelli, J. W. Ochterski, R. L. Martin, K. Morokuma, V. G. Zakrzewski, G. A.Voth, P. Salvador, J. J. Dannenberg, S. Dapprich, A. D. Daniels, O. Farkas, J. B. Foresman, J. V. Ortiz, J. Cioslowski, D. J. Fox, Gaussian, Inc.,Wallingford CT, **2010**

[72] J. S. Binkley, J. A. Pople, *Int. J. Quantum. Chem*. **1975**, *9*, 229–236.

[73] H. M. Pickett*, J. Molec. Spectrosc*. **1991***, 148***,** 371-377 .

[74] Pgopher, a Program for Simulating Rotational Structure, C. M. Western, University of Bristol, http://Pgopher.chm.bris.ac.uk.

[75] H. Hartwig, H. Dreizler, *Z. Naturforsch*. **1996**, *51a*, 923–932.

[76] Z .Kisiel, *J. Mol. Spectrosc*. **2003**, *218*, 58-67.

[77] J. Kraitchmann, *Am. J. Phys*. **1953**, *21*, 17−25.

[78]C. R. Cantor, P. R. Schimmel, *Biophysical Chemistry*, W. H. Freeman, San Francisco, **1980**.

[79] Gaussian 03, Revision B.01, M. J. Frisch, G. W. Trucks, H. B. Schlegel, G. E. Scuseria, M. A. Robb, J. R. Cheeseman, J. A. Montgomery, Jr., T. Vreven, K. N. Kudin, J. C. Burant, J. M. Millam, S. S. Iyengar, J. Tomasi, V. Barone, B. Mennucci, M. Cossi, G. Scalmani, N. Rega, G. A. Petersson, H. Nakatsuji, M. Hada, M. Ehara, K. Toyota, R. Fukuda, J. Hasegawa, M. Ishida, T. Nakajima, Y. Honda, O. Kitao, H. Nakai, M. Klene, X. Li, J. E. Knox, H. P. Hratchian, J. B. Cross, C. Adamo, J. Jaramillo, R. Gomperts, R. E. Stratmann, O. Yazyev, A. J. Austin, R. Cammi, C. Pomelli, J. W. Ochterski, P. Y. Ayala, K. Morokuma, G. A. Voth, P. Salvador, J. J.

Dannenberg, V. G. Zakrzewski, S. Dapprich, A. D. Daniels, M. C. Strain, O. Farkas, D. K. Malick, A. D. Rabuck, K. Raghavachari, J. B. Foresman, J. V. Ortiz, Q. Cui, A. G. Baboul, S. Clifford, J. Cioslowski, B. B. Stefanov, G. Liu, A. Liashenko, P. Piskorz, I. Komaromi, R. L. Martin, D. J. Fox, T. Keith, M. A. Al-Laham, C. Y. Peng, A. Nanayakkara, M. Challacombe, P. M. W. Gill, B. Johnson, W. Chen, M. W. Wong, C. Gonzalez, J. A. Pople, Gaussian, Inc., Wallingford CT, **2004**.

[80] J. S. Binkley, J. A. Pople, *Int. Quantum Chem*. **1975**, *9*, 229-236.

[81] R. Krishman, J. S. Binkley, R. Seeger, J. A. Pople, *J. Chem. Phys*. **1980**, *72*, 650-654.

[82] I. Alkorta, J. Elguero, *J. Am. Chem. Soc*. **2002**, *124*, 488-1493; I. Alkorta, J. Elguero, *J. Chem. Phys*. **2002**, *117*, 6463- 6468.

[83] Z. Su, Y. Xu, *Phys. Chem. Chem. Phys*. **2005**, *7*, 2554 – 2560.

[84] S. F. Boys, F. Bernardi, *Mol. Phys*. **1970**, *19*, 553-566.

[86] Z. Su, Y. Xu, *J. Mol. Spectrosc*. **2005**, *232*, 112-114.

[87] J. K. G. Watson in Vibrational Spectra and Structure, Vol. 6 (Ed.: J. R. Durig), Elsevier, New York, **1977**, pp. 1 – 89.

[88] K. Le Barbu, F. Lahmani, A. Zehnacker-Rentien, *J. Phys. Chem. A* **2002**, *106*, 6271–6278.

[89] J.-U. Grabow, W. Caminati, *Microwave Spectroscopy: Experimental Techniques. In Frontiers of Molecular Spectroscopy* (Ed. J. Laane), Elsevier, Heidelberg, **2008**, p 383.

[90] Z. Su, W. S. Tam, Y. Xu, *J. Chem. Phys.* **2006**, *124*, 024311.

[91] M. Fukushima, M.-C. Chan, Y. Xu, A. Taleb-Bendiab, T. Amano, *Chem. Phys. Lett.* **1994**, 230, 561-566.

[91] P. D. Godfrey, R. D. Brown, F. M. Rodgers, *J. Mol. Struct.* **1996**, *376*, 65-81.

[92] P. D. Godfrey, R. D. Brown, J. Am. Chem. Soc. **1998**, *120*, 10724-10732.

[93] G. M. Florio, R. A. Christie, K. D. Jordan, T. S. Zwier, *J. Am. Chem. Soc.* **2002**, *124*, 10236-10247.

[94] S. Blanco, M. E. Sanz, J. C. López, J. L. Alonso, *Proc. Natl. Acad. Sci.* **2007**, *104*, 20183-20188.

[95] N. Borho, T. Häber, M. A. Suhm, *Phys. Chem. Chem. Phys.* **2001**, *3*, 1945-1948.

[96] W. Caminati, P. Moreschini, I. Rossi, P. G. Favero, *J. Am. Chem. Soc.* **1998**, *120*, 11144-11148

[97] N. Borho, Y. Xu, *Phys. Chem. Chem. Phys.* **2007**, *9*, 4514-4520.

[98] O. Isayev, L. Gorb, J. Leszczynski, *J. Comput. Chem.* **2007**, *28*, 1598-1609.

[99] U. Andresen, H. Dreizler, J.-U. Grabow, W. Stahl, *Rev. Sci. Instrum.* **1990**, *61,* 3694-3699.

[100] J. Halpern, *Science*, **1982**, *217*, 401–407.

[101] R. E. Morris, X. Bu, *Nat. Chem.* **2010**, *2*, 353–361.

[102] A. R. A. Palmans, E. W. Meijer, *Angew. Chem. Int. Ed.* **2007**, *46*, 8948 – 8968; *Angew. Chem.* **2007**, *119*, 9106 –9126.

[103]   G. Celebre, G. De Luca, M. Maiorino, F. Iemma, A. Ferrarini, S. Pieraccini, G. P. Spada, *J. Am. Chem. Soc*. **2005**, *127*, 11736–11744.

[104] K. Shiraki, K. Nishikawa, Y. Goto, *J. Mol. Biol*. **1995**, *245*, 180–194.

[105] K. Gast, D. Zirwer, M. M. Frohone, G. Damaschun, *Protein Sci*. **1999**, *8*, 625–634.

[106] P. Luo, R. L. Baldwin, *Biochem*. **1997**, *36*, 8413–8421.

[107] V. A. Soloshonok, *Angew. Chem. Int. Ed*. **2006**, *45*, 766–769; *Angew. Chem*. **2006**, *118*, 780–783.

[108] M. Buck, *Q. Rev. Biophys*. **1998**, *31*, 297–355.

[109] M. Fioroni, M. D. Diaz, K. Burger, S. Berger, *J. Am. Chem. Soc*. **2002**, *124*, 7737–7744.

[110] R. Carrotta, M. Manno, F. M. Giordano, A. Longo, G. Portale, V. Martorana, P. L. San Biagio. *Phys. Chem. Chem. Phys*. **2009**, *11*, 4007–4018.

[111] H. C. Hoffmann, S. Paasch, P. Müller, I. Senkovska, M. Padmanaban, F.Glorius, S. Kaskel, E. Brunner, *Chem. Commun*. **2012**, *48*, 10484–10486.

[112] D. Hamada, F. Chiti, J. I. Guijarro, M. Kataoka, N. Taddei, C. M. Dobson, *Nat. Struct. Biol*. **2000**, *7*, 58–61.

[113] J. Thomas, F. X. Sunahori, N. Borho, Y. Xu, *Chem. Eur. J.* **2011**, *17*, 4582–4587.

[114] C. Pérez, M. T. Muckle, D. P. Zaleski, N. A. Seifert, B. Temelso, G. C. Shields, Z. Kisiel, B. H. Pate, *Science.* **2012**, *336*, 897–901.

[115] I. Peña, E. J. Cocinero, C. Cabezas, A. Lesarri, S. Mata, P. Écija, A. M. Daly, Á. Cimas, C. Bermúdez, F. J. Basterretxea, S. Blanco, J. A. Fernández, J. C. López, F.

Castaño, J. L. Alonso, *Angew. Chem. Int. Ed.* **2013**, *52*, 11840–11845; *Angew. Chem.* **2013**, *125*, 12056–12061.

[116] I. Bako, T. Radnai, M. Claire, B. Funel, *J. Chem. Phys.* **2004**, *121*, 12472–12480.

[117] J. K. G. Watson, *Aspects of Quartic and Sextic Centrifugal Effects on Rotational Energy Levels. In Vibrational Spectra and Structure*; (Ed.; J. R. Durig), Elsevier: Amsterdam, Netherland, 1977, Vol. 6, p39.

[118] S. S. Xantheas, *J. Chem. Phys.* **1996**, *104*, 8821–8824; K. Szalewicz, B. Jeziorski, *J. Chem. Phys.* **1998**, *109*, 1198–1200.

[119] S. Albert, P. Lerch, R. Prentner, M. Quack, *Angew. Chem. Int. Ed.* **2013**, *52*, 346 – 349; *Angew. Chem.* **2013**, *125*, 364 –367.

[120] S. Grudzielanek, R. Jansen, R. Winter, *J. Mol. Biol.* **2005**, *351*, 879–894.

[121] A. J. Barnes, H. E. Hallam, D. Jones, *Proc. R. Soc. London, Ser. A.* **1973**, *335*, 97–111.

[122] J. Marco, J. M. Orza, *J. Mol. Struct.* **1992**, *267*, 33–38.

[123] M. L. Senent, A. Niño, C. Muñoz-Caro, Y. G. Smeyers, R. Domínguez-Gómez, J. M. Orza, *J. Phys. Chem. A.* **2002**, *106,* 10673–10680.

[124] T. Scharge, D. Luckhaus, M. A. Suhm, *Chemical Physics.* **2008**, *346*, 167–175.

[125] M. Heger, T. Scharge, M. A. Suhm, *Phys. Chem. Chem. Phys.* **2013**, *15*, 16065-1607.

[126] M. A. Suhm, *Advances in Chemical Physics*, Vol. 142, (Ed.; S. A. Rice), John Wiley & Sons, Inc.

[127] Y. Xu, W. Jäger, Fourier Transform Microwave Spectroscopy of Doped Helium Clusters, in *Handbook of High-resolution Spectroscopy*; (Eds.; M. Quack, F. Merkt), John Wiley and Sons, Chichester, **2011**.

[128] J. Thomas, W. Jäger, Y. Xu, *Angew. Chem. Int. Ed. DOI*: 10.1002/ange.201403838 and 10.1002/ ange. 201403838.

[129] C. Møller, M. S. Plesset, *Phys. Rev.* **1934**, *46*, 618−6222.

[130] R. E. Hubbard, M. K. Haider, **2010**, *Hydrogen Bonds in Proteins: Role and Strength*, In: Encyclopedia of Life Sciences (ELS), John Wiley & Sons, Ltd: Chichester.

[131] F. E. Susan, K. L. Robert, *Chem. Phys. Lett.* **1994**, *218*, 349.

[132] G. T. Fraser, R. D. Suenram, F. J. Lovas, W. J. Stevens, *Chem. Phys.* **1988**, *125*, 31.

[133] B. M. Giuliano, L. B Favero, A. Maris, W. Caminati, *Chem. Eur. J.*, **2012**, *18*, 12759.

[134] S. J. Humphrey, D. W. Pratt, *J. Chem. Phys.* **1997**, *106*, 908.

[135] C. Tanner, C. Manca, S. Leutwyler, *Science* **2003**, *302*, 1736.

[136] J. Sadlej, J. C. Dobrowolski, J. E. Rode, *Chem. Soc. Rev.* **2010**, *39*, 1478.

[137] G. Yang, Y. Xu, *J. Chem. Phys.* **2009**, *130*, 164506.

[138] M. Losada, P. Nguyen, Y. Xu, *J. Phys. Chem. A.* **2008**, *112*, 5621.

[139] C. Merten, Y. Xu, *Chem. Phys. Chem*. **2012**, *14*, 213.

[140] C. Merten. Y. Xu, *Angew. Chem. Int. Ed.* **2013**, *52*, 2073.

[141] H. Dreizler, H. D. Rudolph, H. Mäder, *Z. Naturforsch. A, Phys. Sci.* **1970**, *25*, 25.

[142] I. Kleiner, J. T. Hougen, *J. Chem. Phys.* **2003**, *119*, 5505.

[143] M. D. Marshall, J. S. Muenter, *J. Mol. Spectrosc.* **1981**, *85*, 322.

[144] A. C. Legon, *Chem. Soc. Rev.* **1993**, *22*, 153.

[145] A. van der Vaarta, K. M. Merz, Jr., *J. Chem. Phys.* **2009**, *116*, 7380.

[146] Y. Levy, J. N. Onuchic, *Annu. Rev. Biophys. Biomol. Struct*. **2006**, *35*, 389–415.

[147] G. Yang, Y. Xu, Vibrational Circular Dichroism Spectroscopy of Chiral Molecules, in *Top. Curr. Chem*., Volume: Electronic and Magnetic Properties of Chiral Molecules and Supramolecular Architectures, (Eds.; R. Naaman, D. N. Beratan, D. H. Waldeck), Springer:Verlag, Berlin, Heidelberg, **2011**, *298*, 189–236.

[148] M. Losada, Y. Xu, *Phys. Chem. Chem. Phys*. **2007**, *9*, 3127–3135.

[149] M. Losada, H. Tran, Y. Xu, *J. Chem. Phys.* **2008**, *128*, 014508/1–11;

[150] M. Canagaratna, J. A. Phillips, M. E. Ott, K. R. Leopold, *J. Phys. Chem. A.* **1998,** *102,* 1489–1497.

[151] S. Blanco, J. C. López, A. Lesarri, J. L. Alonso, *J. Am. Chem. Soc*. **2006**, *128*, 12111–12121.

[152] J. L. Alonso, I. Peña, M. E. Sanz, V. Vaquero, S. Mata, C. Cabezas, J. C. López, *Chem. Commun.,* **2013**, *49*, 3443–3445.

[153] B. Ouyang, T. G. Starkey, B. J. Howard, *J. Phys. Chem. A.* **2007**, *111*, 6165–6175.

[154] J. G. Davis, B. M. Rankin, K. P. Gierszal, D. Ben-Amotz, *Nature Chem.* **2013**, 796–802.

[155] J. Thomas, J.Yiu, J. Rebling, W. Jäger, Y. Xu, *J. Phys. Chem. A.* **2013**, 117, 13249-13254.

[156] A. Jasanoff, A. Fersht, *Biochemistry.* **1994**, *33*, 2129-2135.

[157] D. -P. Hong, M. Hoshino, R. Kuboi, Y. Goto, *J. Am. Chem. Soc.* **1999**, *121*, 8427-8433.

[158] M. Buck, S. E. Radford, C.M. Dobson, *Biochemistry.* **1993**, *32*, 669–678.

[159] D. Roccatano, G. Colombo, M. Fioroni, A. E. Mark, *Proc. Natl. Acad. Sci.* **2002**, *99* ,12179–12184.

[160]A. Kundu, N. Kishore, *Biophys. Chem.* **2004**, *109*, 427–442.

[161] M. Guo, Y. Mei, *J. Mol. Model.* **2013**, *19*, 3931–3939.

[162] A. Burakowski, J. Gliński, B. Czarnik-Matusewicz, P. Kwoka, A. Baranowski, K. Jerie, H. Pfeiffer, N. Chatziathanasiou, *J. Phys. Chem. B.* **2012**, *116*, 705–710.

[162] J. Thomas, O. Sukhrukov, W. Jäger, Y. Xu, *Angew. Chem. Int. Ed.* **2014***, 53,* 1156 – 1159; Angew. Chem. 2014, **126**, 1175-1178.

[163] J. Thomas, Y. Xu, J. *Phys. Chem. Let.* **2014**, *5*, 1850-1855.

[164] A. M. Andrews, R. L. Kuczkowski, *J. Chem. Phys.* **1993**, *98*, 791-795.

[165] K. Brendel, H. Mäder, Y. Xu, W.jäger, *J. Mol. Spectrosc.* **2011**, *268*, 47-52.

[166] K. M. Marstokk, H. Mollendal, Y. Stenstrom, *Acta. Chem. Scand.* **1992**, *46*, 432-441.

[167] M. Heger, T. Scharge, M. A. Suhm, *Phys. Chem. Chem. Phys.* **2013**, *15*, 16065-16073.

[168] D. A. Case, T. A. Darden, T. E. Cheatham, III, C. L. Simmerling, J. Wang, R. E. Duke, R. Luo, R. C. Walker, W. Zhang, K. M. Merz, B. Roberts, S. Hayik, A. Roitberg, G. Seabra, J. Swails, A. W. Goetz, I. Kolossváry, K. F. Wong, F. Paesani, J. Vanicek, R. M. Wolf, J. Liu, X. Wu, S. R. Brozell, T. Steinbrecher, H. Gohlke, Q. Cai, X. Ye, J. Wang, M. -J. Hsieh, G. Cui, D. R. Roe, D. H. Mathews, M. G. Seetin, R. Salomon-Ferrer, C. Sagui, V. Babin, T. Luchko, S. Gusarov, A. Kovalenko, P. A. Kollman (2012), AMBER 12, University of California, San Francisco.

Appendix A

Supporting Information for Chapter 3

Chirality Recognition in the Glycidol···Propylene Oxide Complex: A Rotational Spectroscopic Study

Contents:

A.1. Calculated spectroscopic constants of the homo and hetero dimers of glycidol···propylene oxide complex.

A.2. Lists of measured rotational transitions of the six glycidol··· propylene oxide H-bonded conformers.

A.3. Geometries of the (a) eight conformers of glycidol and (b) geometries of the 20 next higher energy glycidol···propylene oxide conformers.

A.**1.** Calculated spectroscopic constants of the homo and hetero dimers of

glycidol···propylene oxide complex.

Table 3. S1. Calculated relative raw dissociation energies ΔD_e and ZPE and BSSE corrected dissociation energies ΔD_0 (in kJ mol^{-1}), rotational constants A, B, C (in MHz) and electric dipole moment components $|\mu_{a,b,c}|$ (in Debye) of all the 28 predicted H-bonded glycidol··propylene oxide conformers at the MP2/6-311++G(d,p) level of theory.

	ΔD_e	ΔD_0	A	B	C	$|\mu_a|$	$|\mu_b|$	$|\mu_c|$
Homo dimers								
Homo I	0.00	0.00	2679	841	762	0.03	2.25	1.48
Homo II	1.08	1.18	2211	935	815	0.77	3.07	0.54
Homo III	1.60	1.20	2390	850	726	0.36	3.64	0.79
Homo IV	3.97	3.40	2455	960	807	1.06	1.15	0.58
Homo V	9.98	9.70	2385	850	763	5.00	1.70	0.30
Homo VI	9.98	9.70	2386	850	763	4.99	1.76	0.30
Homo VII	11.2	10.5	3178	725	635	0.00	1.52	1.19
Homo VIII	10.0	10.8	2445	877	771	1.31	1.13	2.42
Homo IX	15.5	12.0	4321	485	457	4.54	1.03	1.13
Homo X	16.2	12.1	5494	427	418	4.35	1.16	1.65
Homo XI	14.98	12.7	3064	670	609	4.04	2.01	1.63
Homo XII	13.6	13.8	2426	969	772	0.32	0.54	0.97
Homo XIII	16	14.0	2959	570	522	5.15	0.75	0.71
Homo XIV	15.45	14.7	2680	888	745	0.53	0.61	1.11
Hetero dimers								
	ΔD_e	ΔD_0	A	B	C	$|\mu_a|$	$|\mu_b|$	$|\mu_c|$
Hetero I	0.00	0.00	2351	953	858	0.05	1.68	1.51
Hetero II	0.26	0.51	2620	845	777	0.20	2.20	1.80
Hetero III	1.76	1.50	2465	840	716	0.68	3.50	0.46
Hetero IV	2.31	2.47	2157	948	818	0.47	3.50	0.79
Hetero V	11.0	9.96	2304	880	684	4.82	1.05	0.88
Hetero VI	11.0	9.96	2304	880	684	4.82	1.05	0.87
Hetero VII	8.90	10	2234	1034	770	398	1.65	1.21
Hetero VIII	10.8	10.8	2706	833	724	0.02	1.80	1.06
Hetero IX	15.8	12.5	4303	478	460	4.62	740	1.61
Hetero X	16.4	12.6	5470	427	418	4.38	0.46	1.82
Hetero XI	15.1	13.3	3120	582	571	4.87	1.04	0.57
Hetero XII	16.2	13.5	3267	537	524	4.88	0.64	1.22
Hetero XIII	15.5	14.6	2495	901	782	1.67	0.15	1.64
Hetero XIV	15.0	14.6	3155	772	681	0.43	0.38	1.01

A.2. Lists of measured rotational transitions of the six glycidol⋯propylene oxide H-bonded

conformers.

Table 3. S2. Observed rotational transition frequencies of the six glycidol⋯propylene

oxide H-bonded conformers.

						Syn (*S*) *g-G+* Gly⋯(H3,H2) (*R*) PO (Hetero I)	
J'	K_a'	K_c'	J"	$K_a"$	$K_c"$	ν_{EXP} / MHz	$\Delta\nu^{[a]}$ / KHz
2	1	2	1	0	1	4907.2627	0.1
2	2	1	1	1	0	7931.8301	-0.7
2	2	0	1	1	1	8021.5434	0.1
2	1	1	1	0	1	5165.1003	0.2
2	2	0	1	1	0	7935.5962	0.7
2	2	1	1	1	1	8017.7757	0.2
2	2	1	2	1	2	4536.8533	-1.1
2	2	0	2	1	2	4540.6179	1.8
2	2	0	2	1	1	4282.7860[b]	-3.9
2	2	1	2	1	1	4279.0150	-0.4
3	1	3	2	0	2	6563.2192	0.6
3	1	2	2	0	2	7078.7854	0.3
3	2	1	3	1	3	4686.8395	1.2
3	2	1	3	1	2	4171.2715	3.3
3	2	2	3	1	3	4668.0526	-1.2
3	2	2	3	1	2	4152.4830[b]	2.4
3	3	1	3	2	2	7348.8590	0.2
3	3	1	3	2	1	7330.0649[b]	4.9
4	1	4	3	0	3	8182.5086	1.4
4	0	4	3	1	3	5868.4873	-0.9
4	0	4	3	1	2	5352.9234	-2.9
4	3	1	4	2	2	7303.6646	-1.3
4	3	2	4	2	3	7358.9743	-2.2
4	3	1	4	2	3	7359.6986	-4.1
4	2	2	4	1	3	4041.5308	-3.2
4	2	3	4	1	4	4844.2107	-1.2
4	2	2	4	1	4	4900.2419	-1.3
5	0	5	4	1	4	7757.7203	1.4
5	3	3	5	2	4	7379.1717	0.4
5	2	4	5	1	5	5066.0843	0.6
5	3	2	5	2	4	7382.0539	1.5
5	3	2	5	2	3	7252.7966	-0.1
6	1	5	5	2	3	7015.9667	-0.3
6	3	4	6	2	5	7413.9533	1.1

6	3	3	6	2	5	7422.5720	0.1

<table>
<tr><td colspan="8" align="center">Anti (S) g-G+ Gly···(H2,H1) (R) PO (Hetero II)</td></tr>
</table>

2	1	2	1	0	1	4910.0648	-0.4
2	2	1	1	1	0	8664.8606	7.2
2	2	0	1	1	1	8733.4082	-4.6
2	1	1	1	0	1	5110.2382	1.7
2	2	0	1	1	0	8666.6822	-4
2	2	1	1	1	1	8731.5995	-6.3
2	2	0	2	1	1	5433.8620	-8.9
2	2	1	2	1	1	5432.0411	1.7
3	1	3	2	0	2	6393.7031	-0.5
3	1	2	2	0	2	6794.0213	-0.7
3	2	1	3	1	2	5342.1360	-3.1
3	2	2	3	1	2	5333.0856	4.5
3	2	2	3	1	3	5733.4045	3.6
3	2	1	3	1	3	5742.4523	-1.4
4	0	4	3	1	3	4662.3349	-0.2
4	0	4	3	1	2	4262.0155	1.2
4	1	4	3	0	3	7846.9675	0.6
4	2	2	4	1	3	5229.0008	-3.9
4	2	3	4	1	3	5201.9294	2.1
4	2	3	4	1	4	5868.9578	1.4
5	0	5	4	1	4	6346.4994	0.6
5	0	5	4	1	3	5679.4756	-3.3
5	2	3	5	1	4	5102.2042	-5.4
5	2	4	5	1	4	5039.3231	5.4
5	2	4	5	1	5	6039.3231	0.6
6	0	6	5	1	4	7041.9432[b]	2.5
6	0	6	5	1	5	8041.9417	-0.7
6	2	4	6	1	6	6369.7491	-0.2
6	2	4	6	1	5	4971.1487[b]	-6.1

<table>
<tr><td colspan="8" align="center">Anti (S) g+G- Gly···(H2,H1) (R) PO   (Hetero III)</td></tr>
</table>

2	2	1	1	1	0	8098.3718	-1.1
2	1	2	1	0	1	4585.2487	-0.7
2	2	0	1	1	1	8224.3006	-0.6
2	2	0	1	1	0	8104.6904	-1.7
2	1	1	1	0	1	4944.0913	-11.2
2	2	1	1	1	1	8217.9772	4.8
2	2	0	2	1	1	4917.1771[b]	3.1
2	2	1	2	1	2	5269.6963	-1.9
3	1	3	2	0	2	5942.2345	-1.5
3	0	3	2	0	2	4576.6814	-0.3
3	1	3	2	1	2	4418.5697	-1.4
3	1	2	2	1	1	4777.1900	-3.8
3	1	2	2	0	2	6659.6879	-4.8
3	2	1	3	1	2	4766.9678	-2.1

3	2	2	3	1	3	5452.9416	1.3
4	1	4	3	0	3	7250.0518	-0.3
4	0	4	3	1	3	4708.0587	-0.4
4	2	2	3	2	1	6192.9416	3.2
4	1	3	3	1	2	6361.6766	-0.5
4	1	4	3	1	3	5884.4977	2
4	1	3	3	0	3	8444.6817	-3.6
4	2	3	3	2	2	6130.8025	6.4
4	0	4	3	0	3	6073.6105	-0.3
4	2	2	4	1	3	4598.2336	0.8
4	2	3	4	1	4	5699.2506	1.6
4	3	1	4	2	2	8412.3646	-7
4	2	3	4	1	3	4504.6215[b]	4.2
5	0	5	4	1	4	6371.8523	0.4
5	0	5	4	0	4	7548.2941	-0.1
5	2	3	4	2	2	7776.8765	0.2
5	2	4	4	2	3	7655.5698	4.5
5	1	4	4	1	3	7938.7498	0.5
5	1	5	4	1	4	7345.0910	0.3
5	1	5	4	0	4	8521.5291	3.5
5	2	3	5	1	4	4436.3608	0
5	3	3	5	2	4	8538.0974	6.5
6	0	6	5	1	5	8026.2835	1.4
6	2	4	6	1	5	4309.4680[b]	-3.6
6	2	5	6	1	6	6385.1153	5.3
7	1	6	6	2	5	7168.7883[b]	-4
7	2	5	7	1	6	4245.1787	-11.1
Anti (*S*) *g-G*+ Gly··(H2,H1) (*S*) PO (Homo I)							
2	1	2	1	0	1	4919.1351	0.2
2	1	1	1	0	1	5146.2984	0.9
2	2	1	1	1	0	8744.6123	4.3
2	2	0	1	1	0	8746.9137	-4.1
2	2	1	1	1	1	8820.3345	3.9
2	2	0	1	1	1	8822.6363	-5
2	2	0	2	1	1	5513.3709	-6.1
2	2	1	2	1	2	5738.2299	6
2	2	0	2	1	2	5740.5270[b]	1.8
2	2	1	2	1	1	5511.0614[b]	10.5
3	1	2	2	0	2	6839.6106	-1.2
3	1	3	2	0	2	6385.3273	1.4
3	2	2	3	1	2	5398.9388	-2.7
3	2	1	3	1	2	5410.3883	-1.7
3	2	2	3	1	3	5853.2164	0.4
3	2	1	3	1	3	5864.6697	-2.4
4	1	4	3	0	3	7817.4632	-0.8
4	0	4	3	1	3	4635.0329	-0.7

4	1	3	3	0	3	8574.3554	1.1
4	0	4	3	1	2	4180.7494	2.1
4	2	2	4	1	3	5284.6735	-2.3
4	2	3	4	1	4	6007.3156	-2.4
4	2	2	4	1	4	6041.5656	-0.2
4	2	3	4	1	3	5250.4182	0.9
5	0	5	4	1	4	6324.5488	1.3
5	0	5	4	1	3	5567.6562	-0.2
5	2	3	5	1	4	5145.9882	-0.8
5	2	4	5	1	4	5066.5082	1.2
5	2	4	5	1	5	6201.0762	-0.4
5	2	3	5	1	5	6280.5571	-3.3
6	0	6	5	1	5	8024.2318	-0.5
6	0	6	5	1	4	6889.6695	-4.6
6	2	4	6	1	5	5006.0828	1.2
6	2	5	6	1	6	6435.0423	1
Syn (*S*) *g+G*- Gly¨(H3,H2) (*S*) PO (Homo II)							
2	1	2	1	0	1	4647.0356	-1.2
2	2	1	1	1	0	7509.9405	-0.7
2	2	0	1	1	1	7626.1238	0.7
2	2	0	1	1	0	7516.4843	-2.3
2	2	1	1	1	1	7619.5831	-0.8
2	2	1	2	1	2	4294.3567	5.5
2	2	0	2	1	2	4300.9064	-2
3	1	3	2	0	2	6202.5502	0.4
3	1	3	2	1	2	4983.8396	0.3
3	0	3	2	0	2	5126.2663	-0.9
3	1	2	2	1	1	5312.5142	-2
3	2	2	2	2	1	5152.2569[b]	-4.4
3	1	2	2	0	2	6860.1506	-2.9
3	3	0	3	2	1	6854.8182	-0.4
3	3	1	3	2	2	6887.1252	4.9
4	1	4	3	0	3	7714.2879	3
4	0	4	3	0	3	6805.6095	1.9
4	1	4	3	1	3	6638.0055	0.2
4	2	2	3	2	1	6928.5827	7.7
4	2	3	3	2	2	6864.5532	-15.3
4	0	4	3	1	3	5729.3245	1.7
4	3	2	4	2	3	6904.5645	1.7
4	2	3	4	1	4	4689.3133	-6.3
4	3	1	4	2	2	6809.6659	-0.7
5	0	5	4	1	4	7554.0147	3.8
5	3	2	5	2	3	6724.9983	2.3
5	2	4	5	1	5	4974.9795	4.4
5	3	3	5	2	4	6939.0794	-1.6
6	1	5	5	2	4	7236.6100	-3.1

6	3	3	6	2	4	6590.5181	-4.2
6	3	4	6	2	5	6997.8860	0.4

Anti (*S*) *g+G-* Gly···(H2,H1) (*S*) PO   (Homo III)

2	1	2	1	0	1	4530.3268	-0.8
2	2	0	1	1	1	8034.8884	0.1
2	2	1	1	1	0	7904.6597	1.9
2	1	1	1	0	1	4900.0110	-1.3
2	2	0	1	1	0	7911.6605	-0.4
2	2	1	1	1	1	8027.8873	2.6
2	2	0	2	1	1	4698.8273	1.2
2	2	1	2	1	2	5061.5141	-0.5
2	2	0	2	1	2	5068.5200	-7.8
3	1	3	2	0	2	5893.0122	0.5
3	1	2	2	0	2	6632.1292	-2.1
3	2	2	3	1	3	5250.6074	2.4
3	2	1	3	1	3	5285.4509	2.4
3	2	2	3	1	2	4511.4911	4.3
3	2	1	3	1	2	4546.3363	2.5
4	1	4	3	0	3	7205.8902	0.6
4	0	4	3	1	3	4824.0197	-0.1
4	3	1	4	2	2	8048.9480	-3.7
4	2	2	4	1	3	4377.8685	-2
4	2	3	4	1	4	5504.8938	-1.7
5	0	5	4	1	4	6494.8661	-0.9
5	1	5	4	0	4	8483.1156	0
5	3	3	5	2	4	8187.7947	1.4
5	3	2	5	2	3	7957.6644	4.3
5	2	3	5	1	4	4221.1377	-7.8
5	2	4	5	1	5	5825.5185	-1.1
6	0	6	5	1	5	8152.3404	0.4
6	3	3	6	2	4	7811.5588	5.9
6	2	4	6	1	5	4106.3288[b]	-14.8
6	3	4	6	2	5	8251.0993	-8.1
6	2	5	6	1	6	6213.1521	3.2

[a]Δν= ν$_{CALC}$ - ν$_{EXP}$ [b] Small splitting up to about 20 kHz were observed for theses lines and the frequencies given are the average. The splitting may be due to the methyl internal rotor. The average was used because the A-A and E-E transitions have the same intensity and there is no simple *frequency* relationship to obtain the hypothetical unsplit central frequencies from them (Ref. 25).

A.3. Geometries of the (a) eight conformers of glycidol and (b) geometries of the 20 next higher energy glycidol···propylene oxide conformers.

Figure 3. S1. (a) Geometries of the eight conformers of glycidol and (b) geometries of the 20 next higher energy glycidol···propylene oxide conformers

(a)

(b)

Hetero IX
Syn (S) tT Gly---(*R*)PO

Hetero XIV
*Syn (S) α+G+*Gly---(*R*) PO

Homo IX
Syn (S) tT Gly---(*S*) PO

Homo XIV
Syn (S) g+G+ Gly---(*H2*) (*S*) PO

Hetero VIII
Syn (S) g-G- Gly---(*H2*) (*R*) PO

Hetero XIII
*Anti (S) g+G+*Gly---(*H2*) (*R*) PO

Hetero VIII
Syn (S) g-G- Gly---(*H3*) (*S*) PO

Homo XIII
Anti (S) g+T Gly---(*S*) PO

Hetero VII
Anti (S) g-G- Gly...(*H3,H1*) (*R*) PO

Hetero XII
Anti (S) g+T Gly---(*R*) PO

Homo VII
*Anti (S) g-G-*Gly---(*H2*) (*S*) PO

Homo XII
Anti (S) g+G+ Gly---(*H1*) (*S*) PO

Hetero VI
Anti (S) g-T Gly---(*R*) PO

Hetero XI
Syn (S) g+T Gly---(*R*) PO

Homo VI
*Anti (S)g-T*Gly---(*S*) PO

Homo XI
Syn (S) g+T Gly---(*S*) PO

Hetero V
Syn (S) g-T Gly---(*R*) PO

Hetero X
Anti (S) tT Gly---(*R*) PO

Homo V
Syn (S) g-T Gly---(*S*) PO

Homo X
Anti (S) tT Gly---(*S*) PO

169

Appendix B

Supporting Information for Chapter 4

Chirality Induction and Amplification in the 2,2,2-Trifluoroethanol··Propylene Oxide Adduct

Contents:

B.1. Details of spectral assignments and conformational identification.

B.2. Table 4.S1-4.S4: Transition frequencies and their quantum number assignments of the four observed 2,2,2-trifluoroethanol··propylene oxide (TFE··PO) conformers.

B.3. Estimation of relative abundance of the observed conformers.

B.4. Experimental and theoretical details.

B.5. Comparison of the factors which contribute to the relative stability of the most stable binary TFE··PO conformers (Table 4.S5) and binary 2-fluoroethanol··PO conformers (Table 4.S6).

B.1. Details of spectral assignments and conformational identification

All the most stable TFE··PO conformers were predicted to have strong *a*-type rotational transitions (See Table 4.1). Broadband spectra of samples containing TFE or PO or both together in helium (or neon) were recorded separately in the frequency range from 7.7 to 10.5 GHz. Very dense spectra were obtained. To aid the assignments of TFE··PO, transitions due to to $(PO)_n$, $(TFE)_n$, $(PO)_n(RG)_m$, or $(TFE)_n(RG)_m$ (with RG = He or Ne; n, m = 1, 2…), as well as any known impurities in the sample system, were first removed. After careful analysis of the resulting broadband spectra, we were able to assign four sets of rotational transitions due to TFE··PO.

To identify the conformers responsible for the observed transitions, we compared the experimental and theoretical rotational constants and also the observed relative intensities of the *a*-, *b*-, and *c*-type of transitions with the predictions. First, only *a*-type transitions were observed for complexes I, III and VI, whereas both *a*-type and a few *b*-type transitions were detected for conformer II. The identities of II and III can be confidently stated to be due to the similarity between the experimental and calculated rotational constants. The last observed set of rotational constants does not allow us to discriminate between V, VI and VIII. However, since no *b*- or *c*-type transitions could be detected, one can rule out the possibility of V and VII as both are predicted to have substantial *b*- and *c*-type electric dipole moment components. While the first set of experimental rotational constants is in better agreement with those predicted for conformer I than IV, a similar argument based on the electric dipole moment components provides the decisive support for the assignment to I.

B.2. Transition frequencies and their quantum number assignments of the four observed TFE··PO conformers

Table 4. S1. Measured rotational transition frequencies of the *anti g+* I conformer.

J'	Ka'	Kc'	J"	Ka"	Kc"	ν_{EXP} / MHz	$\Delta\nu^a$ / MHz
5	1	4	4	1	3	6299.8497	0.0004
5	2	3	4	2	2	6165.4618	0.0001
5	3	2	4	3	1	6120.9293	0.0006
5	3	3	4	3	2	6119.2305	-0.0001
5	4	1	4	4	0	6116.0655	-0.0026
5	2	4	4	2	3	6101.5742	-0.0008
5	0	5	4	0	4	6044.9586	0.0003
5	1	5	4	1	4	5889.2016	-0.0003
6	1	5	5	1	4	7549.4226	-0.0002
6	2	4	5	2	3	7424.9044	0.0012
6	3	3	5	3	2	7350.7712	0.0011
6	3	4	5	3	3	7346.2596	-0.0006
6	4	2	5	4	1	7341.5956	0.0022
6	4	3	5	4	2	7341.5308	-0.0026
6	2	5	5	2	4	7315.8014	0.0013
6	0	6	5	0	5	7221.3569	0.0013
6	1	6	5	1	5	7059.1550	-0.0010
7	3	5	6	3	4	8574.3637	-0.0007
7	2	6	6	2	5	8526.7335	-0.0012
7	4	3	6	4	2	8568.4207	0.0025
7	2	5	6	2	4	8694.8600	0.0025
7	1	6	6	1	5	8792.5773	-0.0003
7	0	7	6	0	6	8383.7969	0.0009
7	1	7	6	1	6	8225.4711	-0.0002
7	3	4	6	3	3	8584.4448	0.0004
7	5	2	6	5	1	8563.5768	-0.0014
7	5	3	6	5	2	8563.5768	0.0003
8	1	8	7	1	7	9388.0368	0.0005
8	0	8	7	0	7	9533.8095	0.0001
8	2	7	7	2	6	9733.8712	-0.0026
8	2	6	7	2	5	9973.1546	-0.0101
8	1	7	7	1	6	10027.6519	0.0008
8	2	6	7	2	5	9973.1675	0.0028
8	3	5	7	3	4	9823.1831	0.0013
8	3	6	7	3	5	9803.2277	-0.0008
8	4	4	7	4	3	9796.8180	0.0023
8	4	5	7	4	4	9796.2720	0.0030
8	5	3	7	5	2	9789.4698	-0.0040
8	5	4	7	5	3	9789.4698	0.0028
8	6	2	7	6	1	9785.7340	-0.0004

J'	Ka'	Kc'	J"	Ka"	Kc"	ν_{EXP} / MHz	$\Delta\nu^a$ / MHz
8	6	3	7	6	2	9785.7340	-0.0004
9	1	9	8	1	8	10546.9024	0.0005
9	0	9	8	0	8	10674.2598	0.0011
9	2	8	8	2	7	10936.7457	-0.0042
9	4	6	8	4	5	11025.8062	0.0011
9	4	5	8	4	4	11027.1114	0.0002
9	3	7	8	3	6	11032.3743	-0.0015
9	3	6	8	3	5	11068.4045	0.0012
9	1	8	8	1	7	11252.7866	-0.0002
9	2	7	8	2	6	11256.2832	0.0035

^{a} $\Delta\nu = \nu_{CALC} - \nu_{EXP}$.

Table 4. S2. Measured rotational transition frequencies of the *syn g+* II conformer.

J'	Ka'	Kc'	J"	Ka"	Kc"	ν_{EXP} / MHz	$\Delta\nu^a$ / MHz
2	2	1	1	1	0	7840.0935	-0.0015
2	2	0	1	1	1	7875.0838	0.0000
3	2	1	2	1	2	9066.3366	0.0009
3	2	2	2	1	1	8960.3968	0.0005
4	1	4	3	0	3	6297.1800	0.0003
5	1	5	4	0	4	7368.4416	-0.0004
6	1	6	5	1	5	6821.5895	-0.0007
6	0	6	5	0	5	6912.0708	-0.0005
6	2	5	5	2	4	6926.6610	0.0000
6	3	4	5	3	3	6931.3254	-0.0010
6	3	3	5	3	2	6931.5606	-0.0001
6	2	4	5	2	3	6943.4568	-0.0014
6	1	5	5	1	4	7028.4017	0.0003
7	1	6	6	1	5	8197.7434	0.0006
7	1	7	6	1	6	7956.7192	0.0001
7	0	7	6	0	6	8056.8446	0.0008
7	2	6	6	2	5	8079.7891	-0.0001
7	2	5	6	2	4	8106.5187	0.0000
7	4	4	6	4	3	8085.8141	-0.0020
7	4	3	6	4	2	8085.8141	0.0017
7	3	5	6	3	4	8087.2398	-0.0013
7	3	4	6	3	3	8087.7698	-0.0004
7	1	7	6	0	6	9470.1936	-0.0004
8	3	5	7	3	4	9244.4785	-0.0018
8	3	6	7	3	5	9243.4159	0.0001
8	4	4	7	4	3	9241.4475	0.0050
8	2	7	7	2	6	9232.3111	0.0000
8	0	8	7	0	7	9198.4590	0.0011
8	2	6	7	2	5	9272.0879	-0.0007
8	1	7	7	1	6	9366.0749	0.0008
8	1	8	7	1	7	9091.0754	-0.0003
8	5	3	7	5	2	9240.3027	0.0012
8	5	4	7	5	3	9240.3027	0.0012
8	1	8	7	0	7	10504.4226	0.0003
9	1	9	8	1	8	10224.5838	0.0005

9	0	9	8	0	8	10336.6559	0.0005
9	2	8	8	2	7	10384.1425	-0.0004
9	5	4	8	5	3	10395.6931	0.0000
9	5	5	8	5	4	10395.6931	-0.0001
9	4	6	8	4	5	10397.2771	-0.0009
9	4	5	8	4	4	10397.3018	-0.0015
9	3	7	8	3	6	10399.8572	-0.0013
9	3	6	8	3	5	10401.7979	-0.0009
9	2	7	8	2	6	10440.3237	0.0000
9	1	8	8	1	7	10533.2076	0.0013
10	1	10	9	1	9	11357.1890	0.0002
10	0	10	9	0	9	11471.2966	0.0014
10	2	9	9	2	8	11535.1985	-0.0007
10	3	8	9	3	7	11556.5437	-0.0010
10	3	7	9	3	6	11559.8635	-0.0015
10	2	8	9	2	7	11611.2675	-0.0001

[a] $\Delta \nu = \nu_{CALC} - \nu_{EXP}$.

Table 4. S3. Measured rotational transition frequencies of the *anti g*- III conformer.

J'	Ka'	Kc'	J"	Ka"	Kc"	ν_{EXP} / MHz	$\Delta\nu^{a}$ / MHz
6	1	6	5	1	5	5974.3451	-0.0070
6	0	6	5	0	5	6044.8735	0.0013
6	2	5	5	2	4	6050.9092	0.0002
6	4	2	5	4	1	6052.4465	-0.0011
6	4	3	5	4	2	6052.4465	-0.0010
6	2	4	5	2	3	6057.8495	-0.0008
6	1	5	5	1	4	6126.0869	-0.0033
7	1	6	6	1	5	7146.2547	-0.0013
7	2	5	6	2	4	7069.9154	-0.0014
7	3	4	6	3	3	7062.0740	0.0001
7	4	3	6	4	2	7061.3293	0.0009
7	4	4	6	4	3	7061.3293	0.0014
7	2	6	6	2	5	7058.8297	-0.0006
7	0	7	6	0	6	7049.3019	0.0011
7	1	7	6	1	6	6969.2995	0.0028
8	1	8	7	1	7	7963.8959	0.0014
8	0	8	7	0	7	8052.3468	0.0002
8	2	7	7	2	6	8066.4911	-0.0007
8	1	7	7	1	6	8166.0219	0.0058
8	4	4	7	4	3	8070.2740	0.0002
8	4	5	7	4	4	8070.2740	0.0015
8	3	6	7	3	5	8071.1656	0.0010
8	3	5	7	3	4	8071.4116	0.0014
8	2	6	7	2	5	8083.0782	0.0008
9	1	9	8	1	8	8958.1077	0.0023
9	0	9	8	0	8	9053.8411	0.0011
9	2	8	8	2	7	9073.8548	-0.0017
9	4	5	8	4	4	9079.2912	-0.0020
9	4	6	8	4	5	9079.2912	0.0012

9	3	7	8	3	6	9080.5053	0.0010
9	3	6	8	3	5	9080.9518	-0.0024
9	2	7	8	2	6	9097.4604	0.0001
9	1	8	8	1	7	9185.3010	-0.0017
10	1	9	9	1	8	10204.0441	0.0001
10	2	8	9	2	7	10113.1742	0.0004
10	2	9	9	2	8	10080.8863	-0.0016
10	0	10	9	0	9	10053.6310	-0.0001
10	1	10	9	1	9	9951.8930	0.0002
11	1	11	10	1	10	10945.2238	-0.0006
11	0	11	10	0	10	11051.5969	0.0005
11	2	10	10	2	9	11087.5467	-0.0028
11	2	9	10	2	8	11130.3007	0.0012
11	1	1 0	10	1	9	11222.1639	0.0001

[a] $\Delta\nu = \nu_{CALC} - \nu_{EXP}$.

Table 4. S4. Measured rotational transition frequencies of the *syn g*- VI conformer.

J'	Ka'	Kc'	J"	Ka"	Kc"	ν_{EXP} / MHz	$\Delta\nu^a$ / MHz
5	1	5	4	1	4	5999.2717	-0.0013
5	0	5	4	0	4	6094.2743	0.0001
5	2	4	4	2	3	6108.5390	0.0014
5	3	2	4	3	1	6113.2351	-0.0011
5	3	3	4	3	2	6113.0416	0.0030
5	2	3	4	2	2	6124.5566	0.0002
5	1	4	4	1	3	6214.2835	0.0005
6	1	6	5	1	5	7196.9475	-0.0008
6	0	6	5	0	5	7304.3638	-0.0019
6	2	5	5	2	4	7328.6591	0.0023
6	4	2	5	4	1	7335.1358	-0.0027
6	4	3	5	4	2	7335.1358	0.0006
6	3	3	5	3	2	7337.0244	0.0004
6	3	4	5	3	3	7336.4975	0.0000
6	2	4	5	2	3	7356.5262	-0.0011
6	1	5	5	1	4	7454.6602	-0.0001
7	0	7	6	0	6	8509.9337	-0.0019
7	2	6	6	2	5	8547.9157	0.0040
7	4	3	6	4	2	8558.3182	-0.0053
7	3	5	6	3	4	8560.3394	0.0010
7	3	4	6	3	3	8561.5207	-0.0005
7	2	5	6	2	4	8592.0867	-0.0018
7	1	6	6	1	5	8693.5977	-0.0003
7	5	2	6	5	1	8557.2716	0.0003
7	5	3	6	5	2	8557.2716	0.0004
7	1	7	6	1	6	8393.5172	-0.0002
8	0	8	7	0	7	9710.5602	0.0002
8	2	7	7	2	6	9766.1663	0.0057
8	2	6	7	2	5	9831.5031	-0.0027
8	3	5	7	3	4	9786.9191	-0.0001
8	4	4	7	4	3	9781.8210	0.0025

8	4	5	7	4	4	9781.7893	0.0008
8	5	3	7	5	2	9780.2026	-0.0012
8	5	4	7	5	3	9780.2026	-0.0010
8	1	8	7	1	7	9588.8621	0.0002
8	1	7	7	1	6	9930.7830	-0.0002
9	1	9	8	1	8	10782.8903	-0.0005
9	0	9	8	0	8	10906.0502	-0.0038
9	2	8	8	2	7	10983.2729	0.0084
9	2	7	8	2	6	11074.7991	-0.0043
9	3	6	8	3	5	11013.4418	-0.0007
9	3	7	8	3	6	11009.1333	0.0031
9	1	8	8	1	7	11165.8692	-0.0005
11	1	11	10	1	10	13166.7815	0.0010
11	0	11	10	0	10	13282.3314	-0.0022

[a] $\Delta \nu = \nu_{CALC} - \nu_{EXP}$.

B.3. Estimation of the relative abundances of the observed conformers

We used the chirped pulse measurements to derive the relative abundances of the four observed conformers in the jet expansion. Comparison of the experimental and simulated spectral patterns using the Pgopher program (Ref. 29) indicates that the rotational temperature is about 0.45 K. An example section is shown in Figure 4. S1. Using the calculated a-type electric dipole moment components, which are predicted to be similar for all four observed conformers, the relative abundances of the four observed conformers were estimated to be: I : II : III : VI = 1 : 0.75 : 0.35 : 0.40.
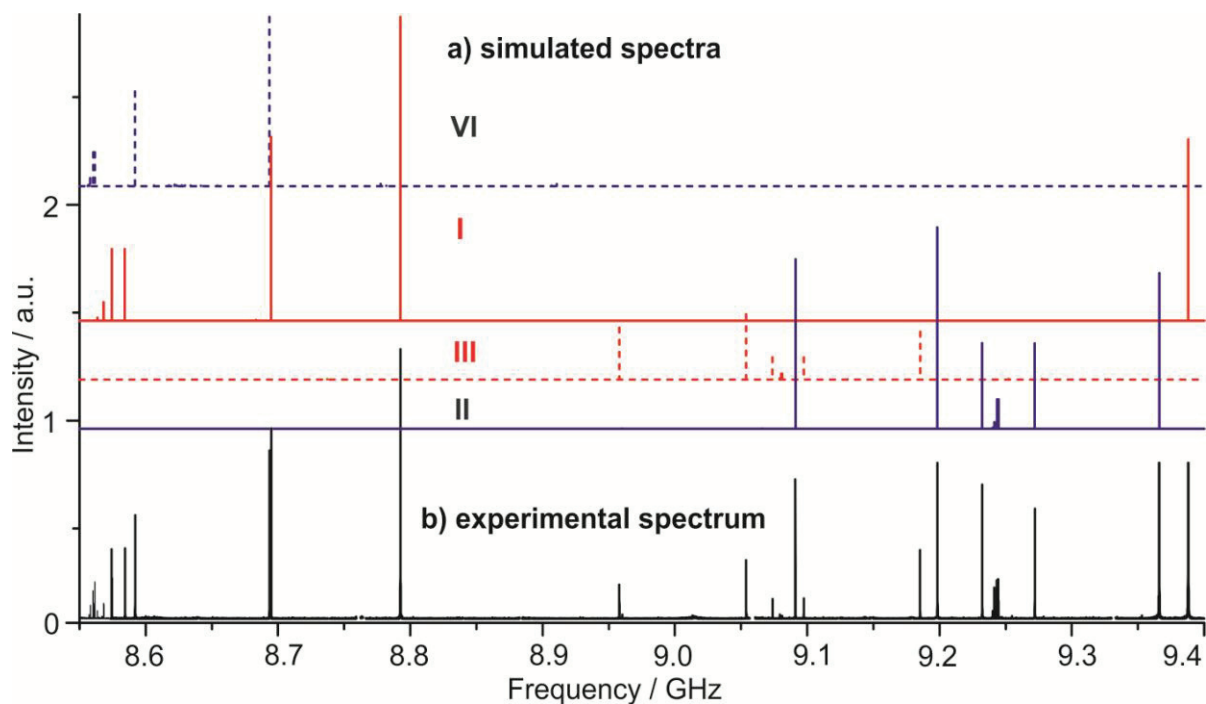
Figure 4. S1. A 0.85 GHz broadband spectrum of TFE··PO (bottom) and the simulated spectra of the four observed conformers using the spectroscopic constants given in Table 4.2. The intensity of each conformer was scaled to best reproduce the corresponding experimental intensity.

B.4. Experimental and theoretical details

Preliminary searches for the TFE··PO adducts were carried out using a CP-FTMW spectrometer built in Edmonton based on previously reported designs (Ref. 20). Briefly, a radiofrequency (rf) chirp (0.01-1 GHz, 4 μs) generated by an arbitrary waveform generator (Tektronix AWG 710B) is mixed with the output of a MW synthesizer to produce a 2 GHz MW chirp in the 8-18 GHz range. Each chirp is amplified with a 20 W solid state MW amplifier (MW Power Inc., L0818-43) and then propagated into free space using a wide band, high gain, MW horn antenna (rf/MW Instrumentation, ATH7G18). It was recognized earlier that samples containing TFE gave extremely dense rotational spectra. To identify the spectra due exclusively to the TFE··PO adduct, broadband scans with TFE or PO+Helium (or Neon) and TFE+PO+Helium

(or Neon) were compared. The resolution of the broadband spectrometer is 25 kHz. All final frequency measurements were done with a cavity-based coaxial pulsed jet FTMW spectrometer. The frequency uncertainty is ~2 kHz and the full line width at half maximum is ~10 kHz.

Sample mixtures consisting of 0.2 % each of TFE and PO in neon or helium at stagnation pressures of 4 to 8 bars were used. *S*-PO (99%, Sigma Aldrich), TFE (97%, Sigma Aldrich) and neon or helium (99.9990 %) were used without further purification.

High level *ab initio* calculations were carried out using the Gaussian 09 suite of programs. Second order Moller Plesset perturbation theory (MP2) (J. S. Binkley, J. A. Pople, *Int. J. Quantum Chem*. **1975**, *9*, 229–236.) with the 6-311++G(2d,p) basis set was used to explore the conformational landscape of the TFE⋯PO adduct. Harmonic frequency calculations were also performed to make sure that all the optimized geometries were true minima without negative frequencies. The calculated raw dissociation energies for all the conformers were corrected for the zero point energy (*ZPE*) effects and basis set superposition errors (*BSSE*s). *BSSE*s were calculated using the counterpoise procedure of Boys and Bernardi. (S. F. Boys, F. Bernardi *Mol. Phys.* **1970**, *19*, 553–566.)

B.5. Comparison of the factors which contribute to the relative stability of the most stable binary TFE⋯PO and binary 2-fluoroethanol⋯PO conformers

Table 4. S5. The relative values of different energy terms that contribute to the stability of TFE··PO calculated at the MP2/6-311++G(2d,p) level of theory. The relative values in kJmol^{-1} are referred to the most stable conformer *anti g+* I.[a] The conformers observed experimentally are highlighted in red.

Diasteromers		ΔE_{TFE}^{conf}	ΔE_{TFE}^{dist}	ΔE_{PO}^{dist}	$\Delta E_{TFE...PO}^{int}$	ΔD_e	$\Delta E_{TFE...PO}^{BSSE}$	$\Delta E_{TFE...PO}^{ZPE}$
Open	*anti g+* I	0.00	0.00	0.00	0.00	0.00	0.00	0.00
	anti g- III	0.00	-0.06	-0.01	-1.22	-1.46	0.91	0.05
Closed	*anti g-* V	0.00	-0.32	0.04	-1.28	-1.56	0.59	0.06
	anti g+ VII	0.00	-0.46	0.06	-1.42	-1.83	0.57	0.13
Open	*syn g+* II	0.00	-0.10	-0.01	-0.75	-0.85	0.62	-0.06
	syn g- VI	0.00	0.28	-0.05	-0.86	-0.83	0.01	-0.13
Closed	*syn g+* IV	0.00	-0.38	-0.01	-1.06	-1.26	0.48	0.08
	syn g- VII	0.00	-0.54	0.10	-3.55	-3.05	0.71	0.22

Table 4. S6. The relative values of different energy terms that contribute to the stability of 2-fluoroethanol (FE)··PO calculated at the MP2/6-311++G(d,p) level of theory. The relative values in kJmol^{-1} are referred to the most stable conformer *anti G-g+*.[a] The conformers observed experimentally are highlighted in red. All data are taken from Ref. 17.

Diasteromers		ΔE_{FE}^{conf}	ΔE_{FE}^{dist}	ΔE_{PO}^{dist}	$\Delta E_{PO...FE}^{int}$	$\Box D_e$	$\Delta E_{PO...FE}^{BSSE}$	$\Delta E_{PO...FE}^{ZPE}$
Open	*anti G+g+*	-11.01	1.31	-0.15	3.15	-6.70	-1.16	-0.19
	anti G-g-	-11.01	1.04	-0.18	4.84	-5.31	0.15	-0.19
Closed	*anti G-g+*	0.00	0.00	0.00	0.00	0.00	0.00	0.00
	anti G+g-	0.00	0.00	0.01	-0.16	-0.16	0.03	0.03
Open	*syn G+g+*	-11.01	1.47	-0.05	3.41	-6.19	-0.02	-0.25
	syn G-g-	-11.01	1.33	-0.09	3.79	-5.98	-0.75	-0.37
Closed	*syn G-g+*	0.00	0.10	0.08	-1.60	-1.42	0.15	-0.18
	syn G+g-	0.00	-0.85	0.03	0.77	-0.05	-0.08	-0.04

[a] The absolute energy values of E_{TFE}^{conf}, E_{TFE}^{dist}, E_{PO}^{dist}, $E_{TFE...PO}^{int}$, $E_{TFE...PO}^{BSSE}$, $E_{TFE...PO}^{ZPE}$, and D_e for *anti g+* I of TFE··PO are 0.00, -1.28, -0.42, 43.62, -9.56, 383.80 and 41.92 kJmol^{-1}, respectively. The corresponding values for *anti G-g+* FE··PO are 0.00, -2.94, -0.35, 38.19, 11.55, 428.35, and 34.95 kJmol^{-1}, respectively (Ref. 17).

Experimentally, only *open* TFE··PO conformers were detected, in contrast to that only *closed* FE··PO conformers were observed. One may initially wonder if E^{int}, the interaction energy of the binary complex, is the cause for such differences in mono- and trifluoroethanol adducts. However, a detailed inspection of the various factors which contribute to the stability of the adducts, indicates that E^{int} favors the *open* structures over the *closed* structures on the order of about 4 kJmol^{-1}, for both mono (Ref. 17) and trifluoroethanol adducts. Rather, the final differences in preference come from the different monomeric stabilities and deformation energies. The penalty to fold TFE into the shape needed for the *closed* form of TFE··PO versus that for the *open* form of TFE··PO is about 0.7 kJmol^{-1}. For 2-fluoroethanol··PO, the *open* form requires the *open gauche* 2-fluoroethanol subunit, while the *closed* form requires the *compact gauche* 2-fluoroethanol subunit. The penalty to incorporate the *open gauche* 2-fluoroethanol subunit in the binary adduct versus the *compact gauche* 2-fluroethanol subunit is about 11 kJmol^{-1}. Consequently, 2-fluoroethanol··PO favors the *closed* structures over the *open* ones.

Appendix C

Supporting Information for Chapter 5

Chirality Synchronization in Trifluoroethanol Dimers Revisited: The Missing Heterochiral Dimer.

Contents:

C.1. Table 5.S1-5.S2: Transition frequencies and their quantum number assignments of the observed homo- and hetero-chiral TFE dimers.

C.1. Transition frequencies and their quantum number assignments of the observed

homo- and heterochiral TFE dimers.

Table 5. S1. Observed rotational transition frequencies of the *a-c-het* I conformer

J'	Ka'	Kc'	J"	Ka"	Kc"	ν_{EXP} / MHz	$\Delta\nu^{a}$ / MHz
3	3	0	2	2	1	8026.8279	0.0145
4	4	0	3	3	1	11074.5093	-0.0001
5	3	3	4	2	2	9640.8189	-0.0018
5	3	2	4	2	3	9655.4316	-0.0033
6	1	6	5	0	5	6412.5035	-0.0003
6	2	5	5	1	4	8513.1933	0.0045
6	3	4	5	2	3	10440.3721	-0.0013
6	3	3	5	2	4	10474.0191	-0.0044
7	2	5	6	1	6	8751.5031	0.0002
7	2	6	6	1	5	9440.5042	-0.0005
7	3	5	6	2	4	11231.0243	-0.0031
8	1	7	7	1	6	6316.9005	0.0004
8	0	8	7	0	7	6410.6593	-0.0002
8	2	7	7	2	6	6477.8430	-0.0003
8	6	2	7	6	1	6494.0351	-0.0005
8	6	3	7	6	2	6494.0351	-0.0005
8	5	3	7	5	2	6495.1278	0.0035
8	4	4	7	4	3	6497.2852	0.0011
8	4	5	7	4	4	6497.2123	0.0008
8	3	5	7	3	4	6500.2465	-0.0007
8	3	6	7	3	5	6504.3344	0.0041
8	2	6	7	2	5	6557.2147	0.0001
8	1	8	7	1	7	6622.9107	0.0000
8	1	8	7	0	7	8377.9600	-0.0013
8	2	6	7	1	7	9508.3751	-0.0018
8	2	7	7	1	6	10387.3121	-0.0022
9	1	8	8	1	7	7101.3457	-0.0002
9	0	9	8	0	8	7191.5728	0.0002
9	2	8	8	2	7	7283.2080	-0.0006
9	6	3	8	6	2	7306.3981	-0.0002
9	6	4	8	6	3	7306.3981	-0.0001
9	5	5	8	5	4	7307.9606	-0.0009
9	5	4	8	5	3	7307.9606	0.0010
9	4	5	8	4	4	7311.0827	-0.0008
9	4	6	8	4	5	7310.9092	-0.0005
9	3	6	8	3	5	7314.5012	-0.0001
9	3	7	8	3	6	7321.9390	0.0001
9	2	7	8	2	6	7392.7001	-0.0003

9	1	9	8	1	8	7442.7265	0.0006
9	1	9	8	0	8	9410.0288	0.0011
9	2	7	8	1	8	10278.1665	-0.0001
10	1	10	9	1	9	8259.2469	0.0003
10	1	9	9	1	8	7884.3558	0.0005
10	0	10	9	0	9	7968.0135	0.0010
10	2	9	9	2	8	8087.0640	0.0006
10	6	4	9	6	3	8118.9752	-0.0004
10	6	5	9	6	4	8118.9752	-0.0003
10	5	6	9	5	5	8121.1325	-0.0009
10	4	7	9	4	6	8125.1245	0.0001
10	4	6	9	4	5	8125.4995	-0.0003
10	3	7	9	3	6	8128.9773	-0.0003
10	3	8	9	3	7	8141.6123	-0.0004
10	2	8	9	2	7	8231.0031	-0.0005
10	2	8	9	1	9	11066.4439	-0.0004
11	3	9	10	3	8	8943.5181	-0.0004
11	3	8	10	3	7	8963.7975	0.0001
11	4	7	10	4	6	8940.6352	-0.0004
11	1	11	10	1	10	9071.8892	0.0000
11	2	10	10	2	9	8889.2659	0.0003
11	1	10	10	1	9	8665.9525	0.0008
11	0	11	10	0	10	8740.9269	0.0005
11	5	7	10	5	6	8934.6821	0.0025
11	5	6	10	5	5	8934.6637	-0.0026
11	6	5	10	6	4	8931.7914	-0.0001
11	6	6	10	6	5	8931.7914	0.0001
11	2	9	10	2	8	9070.9579	-0.0009
12	0	12	11	0	11	9511.3712	0.0004
12	1	11	11	1	10	9446.1920	-0.0011
12	2	11	11	2	10	9689.6857	-0.0008
12	7	6	11	7	5	9742.6900	0.0009
12	7	5	11	7	4	9742.6900	0.0009
12	6	6	11	6	5	9744.8697	-0.0003
12	6	7	11	6	6	9744.8697	0.0000
12	5	8	11	5	7	9748.6382	-0.0026
12	5	7	11	5	6	9748.6149	0.0046
12	4	9	11	4	8	9755.2180	-0.0001
12	4	8	11	4	7	9756.6133	0.0000
12	3	9	11	3	8	9757.9320	-0.0006
12	3	10	11	3	9	9788.9591	0.0008
12	1	12	11	1	11	9880.0481	-0.0007
12	2	10	11	2	9	9911.2732	0.0009
13	1	12	12	1	11	10225.1648	-0.0004
13	0	13	12	0	12	10280.3327	0.0004
13	2	12	12	2	11	10488.2153	-0.0003

13	6	7	12	6	6	10558.2352	-0.0004
13	6	8	12	6	7	10558.2352	0.0006
13	3	10	12	3	9	10572.0014	-0.0003
13	4	10	12	4	9	10571.1157	-0.0004
13	4	9	12	4	8	10573.5802	-0.0004
13	3	11	12	3	10	10617.5374	-0.0004
13	1	13	12	1	12	10683.1410	-0.0002
13	2	11	12	2	10	10750.6943	-0.0001
14	1	13	13	1	12	11002.9733	-0.0005
14	0	14	13	0	13	11048.6069	0.0000
14	2	13	13	2	12	11284.7626	-0.0005
14	3	11	13	3	10	11385.4908	0.0016
14	3	12	13	3	11	11449.8915	0.0001

[a] $\Delta v = v_{CALC} - v_{EXP}$.

Table 5. S2. Observed rotational transition frequencies of the *i-c-hom* II conformer

J'	Ka'	Kc'	J"	Ka"	Kc"	v_{EXP} / MHz	Δv^{a} / MHz
2	2	0	1	1	0	5268.9630	0.0026
2	2	1	1	1	1	5286.4630	0.0054
3	3	0	2	2	0	8524.7769	-0.0059
3	3	1	2	2	1	8524.9682	-0.0056
4	2	2	3	1	2	6854.2495	0.0020
4	2	3	3	1	3	6957.5249	0.0039
5	1	5	4	1	4	4022.0380	0.0009
5	0	5	4	0	4	4063.2445	0.0002
5	2	4	4	2	3	4066.6865	-0.0005
5	3	3	4	3	2	4067.7862	0.0000
5	3	2	4	3	1	4067.8142	-0.0004
5	2	3	4	2	2	4070.5375	-0.0007
5	1	4	4	1	3	4110.4748	-0.0003
5	2	3	4	1	3	7636.0706	0.0005
5	2	4	4	1	4	7806.2637	0.0013
5	3	2	4	2	2	10150.1217	0.0012
5	3	3	4	2	3	10152.9766	0.0017
5	4	1	4	3	1	12585.4917	-0.0027
5	5	0	4	4	0	15019.1011	0.0006
5	5	1	4	4	1	15019.1011	0.0006
6	1	6	5	1	5	4825.8681	0.0015
6	0	6	5	0	5	4873.7184	-0.0002
6	2	5	5	2	4	4879.6003	-0.0015
6	4	3	5	4	2	4881.1846	0.0019
6	4	2	5	4	1	4881.1846	0.0022
6	3	4	5	3	3	4881.5172	0.0004
6	3	3	5	3	2	4881.5929	-0.0018

6	2	4	5	2	3	4886.3219	0.0018
6	1	5	5	1	4	4931.9438	-0.0005
6	4	2	5	3	2	13398.8672	-0.0053
6	4	3	5	3	3	13398.8944	0.0040
6	5	1	5	4	1	15832.5664	-0.0002
6	5	2	5	4	2	15832.5664	-0.0001
7	0	7	6	0	6	5683.0284	-0.0008
7	1	7	6	1	6	5629.3988	-0.0013
7	1	6	6	1	5	5753.0583	0.0003
7	2	5	6	2	4	5703.0029	0.0010
7	2	6	6	2	5	5692.2812	-0.0007
7	3	5	6	3	4	5695.3332	-0.0012
7	3	4	6	3	3	5695.4977	-0.0003
7	1	6	6	0	6	7166.2923	-0.0012
7	5	2	6	4	2	16645.9742	0.0008
7	5	3	6	4	3	16645.9742	0.0011
8	1	8	7	1	7	6432.5825	-0.0009
8	0	8	7	0	7	6491.0100	-0.0011
8	2	7	7	2	6	6504.6923	0.0004
8	4	5	7	4	4	6508.4873	-0.0009
8	4	4	7	4	3	6508.4873	0.0015
8	3	6	7	3	5	6509.2352	-0.0013
8	3	5	7	3	4	6509.5632	0.0010
8	2	6	7	2	5	6520.6956	0.0009
8	1	7	7	1	6	6573.7519	-0.0004
8	1	7	7	0	7	8057.0142	0.0009
9	1	9	8	1	8	7235.3854	0.0001
9	0	9	8	0	8	7297.5225	-0.0001
9	2	8	8	2	7	7316.7985	-0.0010
9	4	6	8	4	5	7322.2112	-0.0026
9	4	5	8	4	4	7322.2112	0.0033
9	3	7	8	3	6	7323.2230	0.0003
9	3	6	8	3	5	7323.8279	0.0002
9	2	7	8	2	6	7339.4949	0.0005
9	1	8	8	1	7	7393.9490	-0.0005
9	1	8	8	0	8	8959.9546	0.0001
10	6	4	9	6	3	8134.9476	-0.0001
10	6	5	9	6	4	8134.9476	-0.0001
10	5	5	9	5	4	8135.2707	-0.0009
10	5	6	9	5	5	8135.2707	-0.0010
10	1	10	9	1	9	8037.7769	0.0004
10	0	10	9	0	9	8102.4631	-0.0007
10	2	9	9	2	8	8128.5584	-0.0012
10	4	7	9	4	6	8135.9841	0.0026
10	4	6	9	4	5	8136.0027	-0.0033
10	3	8	9	3	7	8137.2955	0.0000

10	3	7	9	3	6	8138.3302	0.0002
10	2	8	9	2	7	8159.4601	0.0009
10	1	9	9	1	8	8213.5703	0.0002
10	1	9	9	0	9	9876.0034	-0.0007
11	1	11	10	1	10	8839.7309	-0.0008
11	0	11	10	0	10	8905.7654	0.0001
11	2	10	10	2	9	8939.9344	0.0000
11	6	5	10	6	4	8948.4042	0.0011
11	6	6	10	6	5	8948.4042	0.0011
11	5	6	10	5	5	8948.8571	-0.0001
11	5	7	10	5	6	8948.8571	-0.0003
11	4	8	10	4	7	8949.8297	-0.0039
11	4	7	10	4	6	8949.8486	0.0026
11	3	9	10	3	8	8951.4414	-0.0002
11	3	8	10	3	7	8953.1191	-0.0002
11	2	9	10	2	8	8980.6099	0.0003
11	1	10	10	1	9	9032.5333	-0.0004
12	1	12	11	1	11	9641.2227	-0.0006
12	0	12	11	0	11	9707.4169	0.0016
12	2	11	11	2	10	9750.8932	-0.0005
12	6	6	11	6	5	9761.8529	-0.0005
12	6	7	11	6	6	9761.8529	-0.0005
12	5	7	11	5	6	9762.4605	0.0009
12	5	8	11	5	7	9762.4605	0.0005
12	4	9	11	4	8	9763.7307	0.0000
12	4	8	11	4	7	9763.7778	0.0004
12	3	10	11	3	9	9765.6460	-0.0005
12	3	9	11	3	8	9768.2477	-0.0002
12	2	10	11	2	9	9802.9098	-0.0003
12	1	11	11	1	10	9850.7447	-0.0004
13	1	13	12	1	12	10442.2366	0.0003
13	0	13	12	0	12	10507.4619	0.0003
13	2	12	12	2	11	10561.3914	0.0045
13	7	6	12	7	5	10574.8939	-0.0005
13	7	7	12	7	5	10574.8939	-0.0005
13	6	7	12	6	6	10575.2870	0.0009
13	6	8	12	6	7	10575.2870	0.0009
13	5	9	12	5	8	10576.0853	-0.0016
13	5	8	12	5	7	10576.0853	-0.0007
13	4	10	12	4	9	10577.7068	-0.0014
13	4	9	12	4	8	10577.7893	0.0005
13	3	11	12	3	10	10579.8892	-0.0004
13	3	10	12	3	9	10583.7776	-0.0009
13	2	11	12	2	10	10626.2692	0.0013
13	1	12	12	1	11	10668.1072	-0.0001
14	0	14	13	0	13	11305.9908	-0.0007

14	1	14	13	1	13	11242.7632	0.0001
14	2	13	13	2	12	11371.4096	-0.0004
14	3	12	13	3	11	11394.1460	-0.0003
14	3	11	13	3	10	11399.7738	0.0000
14	2	12	13	2	11	11450.5505	0.0004
14	1	13	13	1	12	11484.5166	0.0002

[a] $\Delta \nu = \nu_{CALC} - \nu_{EXP}$.

Appendix D

Supporting Information for Chapter 6

**Chirped-pulse and cavity-based Fourier transform microwave spectra
of the methyl lactate···ammonia adduct**

Contents:

D.1. Internal rotation barrier.

D.2. Geometries of conformer I and II of the methyl lactate-ammonia complex.

D.3. Lists of rotational transitions and hyperfine splittings of methyl lactate-^{14}NH$_3$ and -^{15}NH$_3$.

D.4. Explanation of the spectroscopic constants in Table 6.1.

D.1. Internal rotation barrier.
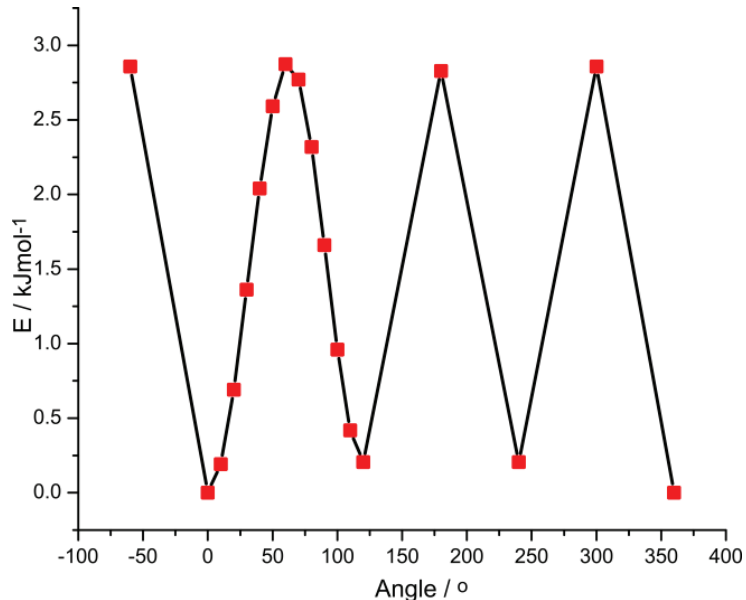
Figure 6. S1. Potential energy scan for the ammonia internal rotor. The barrier height is estimated to be about 2.8 kJ/mol.

D.2. Geometries of conformer I and II of the methyl lactate-ammonia complex.
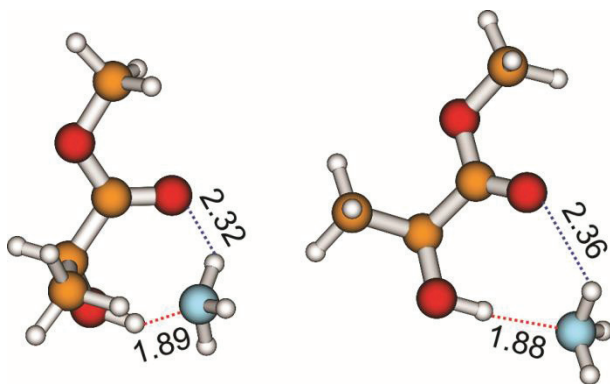
Figure 6. S2. Optimized geometries of conformer **I** and **II**. The interconversion barrier was estimated to be ~1.4 kcal/mol at B3LYP/6-311++G(2d,p) without considering the zero-point-energy (Ref. 13b). One expects this to be even lower with the inclusion of the zero-point-energy.

D.3. Lists of rotational transitions and hyperfine splittings of methyl lactate-^{15}NH$_3$ and -^{14}NH$_3$.

Table 6. S1. Experimental transition frequencies (v) and discrepancies between observed and calculated frequencies (Δv) of ML--^{15}NH$_3$

J"	Ka"	Kc"	Ka'	Kc'	Components	v/MHz	Δv/kHz
2	2	0	1	1	0	AA	8629.4380	-4.6
						EA	8630.8040	-0.4
						AE	8658.3789	4.8
						EiE	8664.5635	-1.9
						EEj	8651.7523	-2.2
2	1	2	1	0	1	AA	5388.3390	-0.3
						EA	5388.2414	-3.4
						AE	5389.9794	2.7
						EiE	5389.5352	-0.3
						EEj	5390.2290	0.4
2	2	1	1	1	1	AA	8848.5843	1.8
						EA	8846.7388	-5
						AE	8818.7014	2.7
						EiE	8812.0562	-1
						EEj	8824.8131	-1.1
2	1	1	1	0	1	AA	6140.9819	3.6
						EA	6140.8745	0.2
						AE	6146.4459	3.3
						EiE	6146.1727	0.3
						EEj	6146.5129	7.7
2	0	2	1	0	1	AA	4253.6630	2.6
						EA	4253.6233	-1.1
						AE	4248.8048	-2.2
						EiE	4248.9753	4.4
						EEj	4248.5690	-2.2
2	1	1	1	1	0	AA	4536.2750	-4.5
						EA	4536.1986	6.9
						AE	4534.7298	-0.8
						EiE	4534.0994	1.5
						EEj	4535.1970	5.1
2	2	1	1	1	0	AA	8597.7035	1.6
						EA	8595.7639	-3.7
						AE	8562.2307	0.6
						EiE	8554.3068	0.5
						EEj	8569.4401	-4.5
2	2	0	1	1	1	AA	8880.3254	2.2

						EA	8881.7777	-2.8
						AE	8914.8468	4.1
						EiE	8922.3220	5.7
						EEj	8907.1280	3.9
3	2	1	2	2	0	AA	6551.7995	-6.5
						EA	6550.4417	2
3	0	3	2	0	2	AA	6304.3472	-8.7
						EA	6304.3137	3.5
						AE	6299.6256	-4.4
						EiE	6299.7573	3.3
						EEj	6299.4140	-0.5
3	1	2	2	1	1	AA	6783.1383	-2.5
						EA	6783.0589	4.5
						AE	6779.3831	-5.4
						EiE	6779.2134	2.1
						EEj	6779.4019	8.8
3	1	3	2	1	2	AA	6033.0461	1.7
						EA	6033.0281	1.9
						AE	6032.5343	-4.0
						EiE	6032.6398	6.2
						EEj	6032.4061	-0.8
3	2	2	2	2	1	AA	6428.0727	-5.6
						EA	6429.3298	2.1
3	3	1	2	2	0	AA	13811.1909	4
						EA	13799.1980	-4.7
3	3	0	2	2	0	AA	13813.7258	4.8
						EA	13821.6263	-4.4
						AE	13848.2369	-1.4
						EiE	13851.9413	-8.2
						EEj	13843.6244	-2.3
3	3	0	2	2	1	AA	13845.4654	3.7
						EA	13856.6620	-5.4
3	3	1	2	2	1	AA	13842.9314	3.8
						EA	13834.2335	-5.9
						AE	13808.1092	9.1
						EiE	13803.6272	3.2
						EEj	13811.9166	-2.6
3	2	2	2	1	1	AA	10489.5090	8.3
						EA	10488.9076	3.9
						AE	10473.7113	1.8
						EiE	10469.5415	-1.2
						EEj	10476.9073	-5.7
3	1	3	2	0	2	AA	7167.7190	-4.2
						EA	7167.6517	5.1
						AE	7173.7085	0.5
						EiE	7173.1937	-4.6

						EEj	7174.0678	3.6
3	1	2	2	0	2	AA	8670.4579	-0.7
						EA	8670.3079	3.7
						AE	8677.0188	-5.2
						EiE	8676.4047	-8.2
						EEj	8677.3442	17.2
3	2	1	2	1	1	AA	10644.9676	-1.5
						EA	10645.0465	-5.9
						AE	10653.9277	-0.5
						EiE	10657.4170	-4.7
						EEj	10650.3639	-6.1
3	2	2	2	1	2	AA	11242.1331	-6.6
						EA	11241.5330	-0.2
						AE	11230.1768	1.3
						EiE	11226.1790	-0.6
						EEj	11233.1938	4.3
4	2	2	3	2	1	AA	8836.6750	-5.1
						EA	8836.3622	4.2
						AE	8827.2490	-4.7
						EEj	8829.4618	5.2
4	0	4	3	0	3	AA	8279.8509	-2.2
						EA	8279.8091	5.4
						AE	8275.1841	-3.6
						EiE	8275.2885	2.6
						EEj	8274.9925	2.1
4	1	3	3	1	2	AA	9000.8657	-5.4
						EA	9000.7709	5.1
						AE	8993.2549	-7
						EiE	8993.3272	6.1
						EEj	8992.9908	-1.6
4	1	4	3	1	3	AA	8012.4132	-6
						EA	8012.3963	6.2
4	2	3	3	1	3	AA	13755.0545	2.6
						EA	13754.6232	-1.3
						AE	13748.4583	
						EiE	13746.6979	-0.1
						EEj	13749.3799	6.7
4	1	4	3	0	3	AA	8875.7900	3.4
						EA	8875.7294	3
						AE	8887.4114	-3
						EiE	8886.7136	-3.4
						EEj	8887.9970	5.1
4	1	3	3	0	3	AA	11366.9717	-2.2
						EA	11366.7703	10.5
						AE	11370.6527	-3.2
						EiE	11369.9730	-7

4	2	2	3	1	2	AA	12698.5083	-0.2
						EA	12698.3548	-1.2
						AE	12701.7901	-3.4
						EiE	12702.8329	-6
						EEj	12700.4324	-1.1
4	2	3	3	2	2	AA	8545.9520	-4.6
						EA	8546.1206	3.1
						AE	8550.8167	-4.4
						EiE	8553.1566	4.6
						EEj	8548.5937	3.2
4	3	2	3	2	1	AA	15886.6884	3.2
						EA	15880.5696	-0.3
4	3	1	3	2	1	AA	15904.2642	2.5
						EA	15908.8800	-1.2
4	3	1	3	2	2	AA	16059.7316	1.4
4	3	2	3	2	2	AA	16042.1553	1.7
5	2	3	4	2	2	AA	11164.5834	-6.9
						EA	11164.4086	7.2
						AE	11159.3346	-7.6
						EiE	11158.2230	1
						EEj	11160.0979	3.2
5	1	4	4	1	3	AA	11174.0505	-5.2
						EA	11173.9380	5.3
						AE	11163.7685	-6.9
						AE	11163.7685	-6.9
						EiE	11163.9688	1.9
						EEj	11163.3351	-3.4
5	0	5	4	0	4	AA	10190.3932	-5.2
						EA	10190.3546	7.2
						AE	10182.9129	-7.7
						EiE	10183.1299	1.7
						EEj	10182.6184	6.4
5	1	5	4	1	4	AA	9971.1580	-7.1
						EA	9971.1376	5.7
						EEj	9976.4716	1.2
5	2	4	4	2	3	AA	10642.9399	-4.3
						EA	10642.9280	1.6
						AE	10641.8294	-8.3
						EiE	10642.6210	3.8
						EEj	10641.0141	0.8
5	1	5	4	0	4	AA	10567.0940	-4.6
						EA	10567.0598	5.1
5	0	5	4	1	4	AA	9594.4560	-8.9
						EA	9594.4336	9
6	2	4	5	2	3	AA	13499.3807	-8.1
						EA	13499.2142	4.6

						AE	13492.7605	-0.9
						EiE	13492.2279	2.7
						EEj	13492.9470	6.6
6	0	6	5	0	5	AA	12065.4013	-6.5
						EA	12065.3590	6.8
						AE	12049.9312	-5.9
						EiE	12050.4228	1.7
						EEj	12049.3565	2.7
6	1	5	5	1	4	AA	13284.3670	-8.2
						EA	13284.2472	5.8
						AE	13274.0542	1.7
						EiE	13274.2472	10.4
						EEj	13273.5971	-3.5
6	1	6	5	1	5	AA	11910.6002	-1.3
						EA	11910.5722	2.1
						AE	11924.2607	-6.1
						EiE	11923.6783	4.1
						EEj	11924.7883	3.6
6	2	5	5	2	4	AA	12714.7379	-4.3
						EA	12714.6750	3.7
						AE	12711.8695	10.2
						EiE	12712.1355	4.7
						EEj	12711.4883	1.5
6	1	6	5	0	5	AA	12287.3010	-0.7
						EA	12287.2758	-1.6

Table 6. S2. The observed reference frequency $\nu_{ref}(Obs.)$ of one of the hyperfine component and the difference $\Delta_\nu(Obs.) = \nu(Obs.) - \nu_{ref}(Obs.)$ (in MHz) of ML--^{14}NH$_3$. The residuals from the fit of nuclear quadrupole coupling constants are $\delta\Delta = \Delta_\nu(Obs.) - \Delta_\nu(Cal.)$.

Transitions								Components									
								AA		EA		AE		EiE		EEj	
J''	K_{a}''	K_{c}''	J'	K_{a}'	K_{c}'	F'	F''	$\nu_{ref}(Obs.)$ / $\Delta_\nu(Obs.)$	$\delta\nu$/ kHz	$\nu_{ref}(Obs.)$ / $\Delta_\nu(Obs.)$	$\delta\nu$/ kHz	$\nu_{ref}(Obs.)$ / $\Delta_\nu(Obs.)$	$\delta\nu$/ kHz	$\nu_{ref}(Obs.)$ / $\Delta_\nu(Obs.)$	$\delta\nu$/ kHz	$\nu_{ref}(Obs.)$ / $\Delta_\nu(Obs.)$	$\delta\nu$/ kHz
2	1	1	1	0	1	3	2	6235.7934	-3.5	6235.6877	0.2	6241.3138	-4	6241.0074	-3.3	6241.4153	8.6
						2	2	0.9172	1.3	0.9165	0.7	0.9116	-0.5			0.9091	-3.2
						2	1	0.4753	3.6	0.4775	5.9	0.4700	2.3			0.4642	-3.7
						1	0	0.1578	0.1	0.1487	-9						
						1	1	-0.9506	2.2	-0.9549	-2.1	-0.9513	-0.4	-0.9513	-0.6	-0.9569	-5.9
2	0	2	1	0	1	1	1	4333.2836	0.9								
2	2	1	1	1	0	3	2	8693.8869	2.7	8691.8960	-1.7						
						2	2	-0.4736	2.4								
						2	1	-0.8900	-3.2	-0.8844	-3.5						
						1	0	0.8791	0.7	0.8726	-2.3						
						1	1	-0.1432	3.3								
2	2	0	1	1	1	3	2	8982.9326	1.1	8984.4110	-2.3						
						2	1	0.4959	-4.3	0.4852	-9						
						1	0	-1.0807	2.3								
						1	1	1.0507	-1.8								
2	2	0	1	0	1	3	2	8726.8490	4.4	8728.2286	1.5						
						2	1	-0.7682	-2.4	-0.7762	-5						
						1	0	0.8108	-0.6	0.8136	-0.5						
						1	1	-0.2099	3.7								
2	2	1	1	1	1	3	2	8949.9722	1.1	8948.0827	-1.3	8924.1272	0.6	8917.2962	-9.2	8930.3384	0.9
						2	2	-0.4718	4.2	-0.4686	1.7	-0.4363	1.3	0.4148	3.7	0.4084	-1.1

J'	Ka'	Kc'	J''	Ka''	Kc''	F'	F''	obs₁	o−c	obs₂	o−c	obs₃	o−c	obs₄	o−c	obs₅	o−c
2	1	2	1	0	1	2	1	0.3746	-4.6	0.3798	-4.7						
						1	0	-1.0125	3.4	-1.0210	-2.4						
						1	1	1.1185	-1								
3	2	1	2	2	0	3	2	5467.2044	-1.8	5467.1064	-0.1						
						2	2	-0.4399	0	-0.4394	0.5						
						2	1	-0.8816	2.6	-0.8868	-2.7						
						1	0	0.9123	1.8	0.9097	-0.8						
						1	1	-0.1964	3.6	-0.1954	4.6						
3	0	3	2	0	2	4	3	6677.7059	-5.2	6676.3172	3.6						
						3	2	0.6539	-1.5	0.6606	0.3						
						2	1	-0.2988	3.6	-0.3154	-10.1						
3	1	2	2	1	1	4	3	6420.9446	-0.6	6420.9047	6.7						
						3	2	-0.1595	2.3	-0.1617	0.1						
						2	1	0.1337	4.1	0.1290	-0.6						
3	1	3	2	0	2	4	3	6911.6554	-4.9	6911.5760	5.1						
3	2	1	2	1	1	4	3	7279.4193	-5	7279.3486	5.6						
						3	2	-0.7167	7	-0.7246	-1						
						2	1	0.3303	4	0.3290	2.7						
3	2	2	2	1	2	4	3	10782.1153	-3.7	10782.1968	1.8	10788.8344	1.3	10792.0857	0.4	10785.5388	-1
						3	2	-0.6165	-1	-0.6156	0.5	-0.6261	1.3	-0.6286	4	-0.6230	-0.5
						2	1	0.4068	3.2	0.4069	3.1	0.4073	0.3	0.4059	-2.8	0.4071	1.8
3	3	1	2	2	0	4	3	11389.3215	-0.3	11388.6940	0.4	11379.5647	-1.8	11375.7790	-2	11382.2891	0.6
						3	2	0.4399	0	0.4388	-1.8	0.4604	3.6	0.4653	3.7	0.4539	1.7
						2	1	-0.2440	0.2	-0.2472	-2.8	-0.2505	-0.2	-0.2495	2.4	-0.2502	-1.4
3	3	0	2	2	1	4	3	13961.7744	1.8								
						3	2	-0.2262	-0.1								
3	3	0	2	2	1	4	3	13997.4136	2.5			13996.9426	4.9	14000.8413	-6.6	13992.0182	-3.9
3	3	0	2	2	0	4	3	13964.4530	2.3	13972.5607	-7.5						
						3	2	-0.2168	1.5	-0.2188	-2.7	-0.1859	-1.6	-0.1827	-1.6	-0.1899	-1.2

N'	Ka'	Kc'	N''	Ka''	Kc''	F'	F''	ν (series A)	o−c	res %	ν (series B)	o−c	res %	ν (series C)	o−c	res %	ν (series D)	o−c	res %	ν (series E)	o−c	res %
3	3	1	2	2	1	4	3	13994.7340	−0.1014	1; 3.7	13985.7883	−0.1014	−3.2; 5.8	13962.0616	−0.1377	6.7; 1.8	13957.3354	−0.1382	0.4; 4.5	13966.1316	−0.1339	−0.2; 1.3
3	1	2	2	0	2	3	2	8814.1776	0.6708 / −0.1649	3.2; −3.6; −2												
3	2	2	2	1	1	4	3	13950.4944	0.5432 / −0.1750	−3.3; 2.8; −1.9	13950.0539	0.5426 / −0.1745	2.3; 2; −1.3	13944.5584	0.5455 / −0.1746	−1.9; 0.1; 0	13942.9088	0.5468 / −0.1747	1.3; 0.1; 0.2	13945.3326	0.5465 / −0.1716	4.4; 2.2; 2.7
4	2	3	3	1	3	5	4	12878.3828	−0.3503 / 0.1893	−2; 1.5; 3.3	12878.2241	−0.3514 / 0.1922	3.8; 0.5; 6.1	12880.9730	−0.3510 / 0.1841	0.2; −2; −0.7	12881.8682	−0.3486 / 0.1870	−1.5; 2.2; 1.8	12879.7409	−0.3481 / 0.1885	1.2; −0.8; 4.2
4	1	3	3	1	2	5	4	9170.4590	0.0940	−4.9; −1.8				10607.3626	−0.8940 / 0.5056	0.6; 2.2; 4.7	10603.4542	−0.8942 / 0.4998	3.2; −3.7; 0.9	10610.2278	−0.9024 / 0.4992	−0.4; −1.1; −3.6
4	1	4	3	1	3	5	4	8161.2146		0.3				11567.2619		−10.6	11566.5786		3.5	11567.5335	0.8215	8.8; 1.3
4	1	4	3	0	3	5	4	9019.6910	−0.5683 / 0.1672	−2.4; 1.2; 2.8					−0.1925	−0.2		−0.1982	−5.6			
4	0	4	3	1	3	5	4	7572.5629	0.3660 / −0.1305	3.2; −1.2; −1.9												
4	2	3	3	2	2	5	4	8706.6732		−3.5												
4	3	1	3	2	1	5	4	16093.6770	−0.3600 / 0.1162	1.5; −2.3; −3.6												
4	2	2	3	2	1	5	4	9007.9195	0.3793 / −0.0706	−6.6; 2.1; −1.5	9007.6046	0.3794 / −0.0726	8.4; 1.7; −3.3	8999.8711	0.3867 / −0.0735	−8.8; −2.8; 0.3				9001.9321	0.3834 / −0.0787	5.1; −2.4; −6.3

D.4. Explanation of the spectroscopic constants in Table 6.1.

The Hamiltonian used is

$$H=H_{rot}+H_{cd}+H_i+H_{ird}+H_{ii}+H_Q. \qquad (6.1)$$

Here, H_{rot} is the rigid rotor part, H_{cd} refers the centrifugal distortion part, H_i corresponds to the internal rotation part of the tops, H_{ird} accounts for the torsional state-dependent centrifugal terms, H_{ii} is the top-top coupling term, and H_Q corresponds to the nuclear quadrupole coupling terms.

A, B, and C are the rotational constants of the complex. They correspond to H_{rot} in eq. 6.1.

D_J, D_{JK}, D_K, d_1, and d_2 are the quartic centrifugal distortion constants, corresponding to H_{cd} in eq. 6.1

D_{pi2K} and D_{pi2-} are torsional state-dependent centrifugal terms, related to H_{ird}.

V (barrier height), F(effective rotational constant of a top), F_0 (internal rotor rotational constant of a top), ρ(dimensionless, related to the ratio of the molecular rotational constants and the internal rotor rotational constant F_0), and finally β and γ (two Euler angles to transform each top from its own internal axes system to the principal axes system), are related to H_i in eq. 6.1.

$F_{12,}$ the top-top coupling term, is related to H_{ii}.

χ_{aa}, $\chi_-(=\chi_{bb}-\chi_{cc})$ and χ_{bc} are the diagonal and off-diagonal nuclear quadrupole coupling constants, respectively. They correspond to H_Q.

Appendix E

Supporting Information for Chapter 7

Direct Spectroscopic Detection of the Orientation of Free OH Groups in Methyl Lactate–(Water)$_{1,2}$ Clusters: Hydration of a Chiral Hydroxy Ester.

Contents:

E.1. Calculated spectroscopic constants and geometries of the mono- and dihydrate conformers.

E.2. Experimental and theoretical details.

E.3. An example section of a broadband spectrum.

E.4. Complete lists of the experimental spectroscopic constants for the mono- and dihydrate conformers observed.

E.5. Conversion barrier between the monohydrate conformer I and II.

E.6. Lists of measured rotational transitions of the mono- and dihydrate conformers and their isotopologues.

E.7. Experimental substitution coordinates and partially refined principal axis coordinates of ML--water.

E.1. Calculated spectroscopic constants and geometries of the mono- and dihydrate conformers.
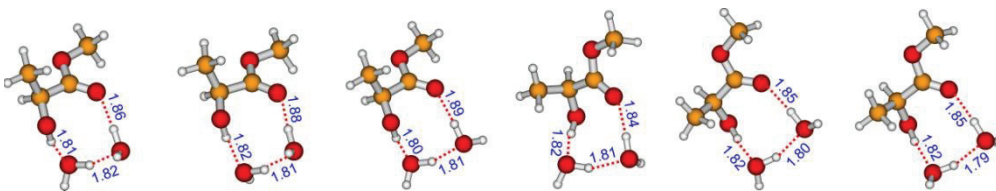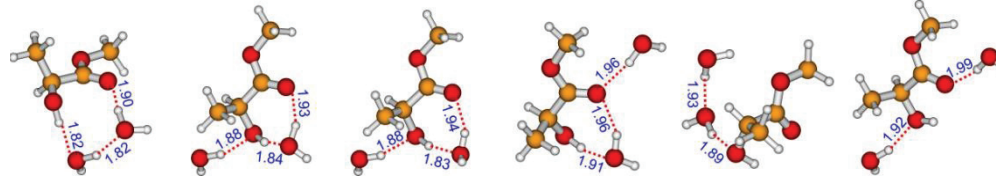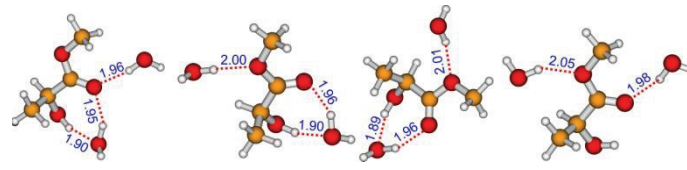
Table 7. S1. Calculated relative raw dissociation energies ΔD_e, *ZPE* and *BSSE* corrected dissociation energies ΔD_0 (in kJ/mol), rotational constants *A*, *B*, and *C* (in MHz), and electric dipole moment components $|\mu_{a,b,c}|$ (in Debye) of the seven most stable ML--water conformers[a] at the MP2/6-311++G (d,p) level of theory.

Const.	i-I	i-II	i-III	a-IV	a-V	i-VI	a-VII
ΔD_e[b]	0.00	3.40	3.90	8.90	12.10	6.90	18.80
ΔD_0[b]	0.00	2.10	2.60	2.80	3.40	4.70	10.00
A	2622	2569	2180	4799	2908	2211	1855
B	1275	1272	1471	835	1043	1437	1604
C	1022	1003	934	757	848	917	986
$|\mu_a|$	2.17	2.64	2.02	3.25	0.57	3.16	3.64
$|\mu_b|$	0.90	0.01	1.50	0.52	1.27	1.85	0.85
$|\mu_c|$	1.27	3.30	0.33	1.17	0.77	2.43	0.33
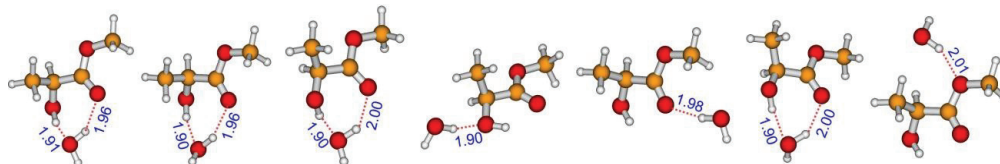
[a]The prefixes i or a indicate that water takes on the *insertion* or *addition* topology respectively, when it interacts with methyl lactate. The Roman number indicates the relative stability of a particular monohydrate conformer based on ΔD_0. [b]The differences in dissociation energies are defined as ΔD (conformer) = D(most stable conformer) – D(conformer) so that this value is more positive for a less stable conformer.

Table 7. S2. Calculated relative raw dissociation energies ΔD_e, *ZPE* and *BSSE* corrected dissociation energies ΔD_0 (in kJ/mol), rotational constants *A, B,* and *C* (in MHz), and electric dipole moment components $|\mu_{a,b,c}|$ (in Debye) of the sixteen ML--(water)$_2$ conformers[a] at the MP2/6-311++G (2d,p) level of theory.

Const.	ii-I	ii-III	ii-IV	ii-II	ii-V	ii-VI
ΔD_e[b]	0.00	2.40	1.74	0.50	0.89	3.18
ΔD_0[b]	0.00	0.93	1.13	0.77	1.25	1.89
A	1558	1597	1569	1717	1718	1715
B	965	914	936	931	917	908
C	753	717	711	697	676	670
$|\mu_a|$	1.37	3.02	1.68	1.34	1.91	2.54
$|\mu_b|$	0.25	0.89	1.89	0.48	0.84	0.24
$|\mu_c|$	0.97	1.06	1.28	0.15	2.17	1.67

Const.	ii-VII	ia-VIII	ia-IX	ia-X	aa-XI	aa-XII
ΔD_e[b]	6.74	10.44	12.92	17.67	15.25	25.02
ΔD_0[b]	4.38	6.78	8.58	11.77	12.22	12.52
A	1588	1660	1646	1583	1286	2612
B	913	858	853	935	1110	580
C	706	647	638	668	864	502
$|\mu_a|$	3.33	2.75	2.99	0.11	2.11	1.05
$|\mu_b|$	3.32	0.86	0.16	0.05	1.10	0.43
$|\mu_c|$	1.83	0.85	1.43	0.66	0.57	1.06

Const.	ia-XIII	ia--XIV	ia-XV	aa-XVI
ΔD_e[b]	20.30	24.94	26.06	33.79
ΔD_0[b]	13.46	17.4	18.41	20.73
A	1529	1788	1820	1635
B	955	880	866	844
C	658	666	670	607
$|\mu_a|$	0.02	0.52	2.53	0.51
$|\mu_b|$	1.25	2.61	1.19	2.12
$|\mu_c|$	0.44	2.84	1.16	0.21

[a]The prefixes i or a indicate that water takes on the *insertion* or *addition* topology respectively, when it interacts with methyl lactate. The Roman number indicates the relative stability of a particular dihydrate conformer. [b]The differences in dissociation energies are defined as ΔD (conformer) = D(most stable conformer) $- D$(conformer) so that this value is more positive for a less stable conformer.

E.2. Experimental and theoretical details.

Sample mixtures consisting of 0.06 % *R*-ML (99%, Sigma Aldrich) and 0.12% H_2O in neon or helium at stagnation pressures of 4 to 8 bars were used. Isotopically enriched D_2O and $H_2^{18}O$ (99.8% Cambridge Laboratories) were used for the isotopic studies. Please note that the *R*-enantiomer of ML was used. This bears no direct significance for the hydration clusters studied. The main reason is to minimize the number of different ML self-aggregates in the sample system. If one uses the racemic sample, one will have also the heterochiral aggregates, i.e. *RS* and *SR* complexes or even larger mixed clusters, in addition to all possible homochiral aggregates (*RR* and *SS* and so on). This may potentially complicate the spectral assignment.

The survey scans were carried out using a broadband chirped pulse FTMW spectrometer which is based on designs reported previously (Refs: G. G. Brown, B. C. Dian, K. O. Douglass, S. M. Geyer and B. H. Pate*, J. Mol. Spectrosc.* **2006**, *238*, 200−212; G. S. Grubbs II, C. T. Dewberry, K. C. Etchison, K. E. Kerr, and S. A. Cooke, *Rev. Sci. Instrum.* **2007**, *78*, 096106). Briefly, a radio frequency (rf) chirp (0.2–1 GHz 4 µs) generated by an arbitrary waveform generator (Tektronix AWG 710B) is mixed with the output of a MW synthesizer to produce a 2 GHz MW chirp in the 8-18 GHz range. This chirp is amplified with a 20 W solid state MW amplifier (MW Power Inc., L0818-43) and then propagated into free space using a wide band, high gain, MW horn antenna

(rf/MW instrumentation, ATH7G18). The resolution of the broadband spectrometer is 25 kHz. Final measurements were done with a cavity based (Refs: T. J. Balle, W. H. Flygare, *Rev. Sci. Instrum.* **1981**, *52,* 33−45; J.-U. Grabow, W. Stahl, H. Dreizler, *Rev. Sci. Instrum.* **1996**, *67,* 4072) pulsed jet FTMW spectrometer. The frequency uncertainty is ~2 kHz and the full line width at half height is ~10 kHz.

All geometry optimization and harmonic frequency calculations were done using with the Gaussian G09 program package (Ref: Gaussian 09, Rev. C.01, M. J. Frisch, G. W. Trucks, H. B. Schlegel, G. E. Scuseria, M. A. Robb, J. R. Cheeseman, G. Scalmani, V. Barone, B. Mennucci, G. A. Petersson, H. Nakatsuji, M. Caricato, X. Li, H. P. Hratchian, A. F. Izmaylov, J. Bloino, G. Zheng, J. L. Sonnenberg, M. Hada, M. Ehara, K. Toyota, R. Fukuda, J. Hasegawa, M. Ishida, T. Nakajima, Y. Honda, O. Kitao, H. Nakai, T. Vreven, J. J. A. Montgomery, J. E. Peralta, F. Ogliaro, M. Bearpark, J. J. Heyd, E. Brothers, K. N. Kudin, V. N. Staroverov, T. Keith, R. Kobayashi, J. Normand, K. Raghavachari, A. Rendell, J. C. Burant, S. S. Iyengar, J. Tomasi, M. Cossi, N. Rega, J. M. Millam, M. Klene, J. E. Knox, J. B. Cross, V. Bakken, C. Adamo, J. Jaramillo, R. Gomperts, R. E. Stratmann, O. Yazyev, A. J. Austin, R. Cammi, C. Pomelli, J. W. Ochterski, R. L. Martin, K. Morokuma, V. G. Zakrzewski, G. A. Voth, P. Salvador, J. J. Dannenberg, S. Dapprich, A. D. Daniels, O. Farkas, J. B. Foresman, J. V. Ortiz, J. Cioslowski, D. J. Fox, Gaussian, Inc., Wallingford CT, **2010**.) at the MP2/6-311++G(d,p) level. The BSSE corrections were calculated using the counterpoise procedure of Boys and Bernardi (Ref: S. F. Boys, F. Bernardi, *Mol. Phys.* **1970**, *19,* 553-566.)

Spectral Assignment: In the broadband spectra obtained, transitions originating from ML, its self-aggregates, and its complexes with rare gases were excluded by

comparing the spectra obtained with and without water in the sample mixtures. All the new strong lines observed with water included were tentatively identified as belonging to an *insertion* binary conformer, while a set of much weaker lines were assigned to an *insertion* only ternary conformer. A 0.6 GHz section of a broadband spectrum recorded with ML+water in helium is shown in Figure 7.S1 below.

The Hamiltonian used for the fits can be written as $H=H_{rot}+H_i+H_{CD}$, where H_{rot} is the rigid rotor part, H_i corresponds to the internal rotation part, and H_{CD} refers to the centrifugal distortion part. The fitting process resulted in a set of rotational constants, centrifugal distortion constants and parameters that describe the internal rotation of the ester methyl group. (For detailed description of internal rotator constants see L. Kang, A. R. Keimowitz, M. R. Munrow, S. E. Novick, *J. Mol. Spectrosc.* **2002**, *213*, 122–129; I. Kleiner *J. Mol. Spectrosc.* **2010**, *260*, 1–18).

E.3. An example section of a broadband spectrum.
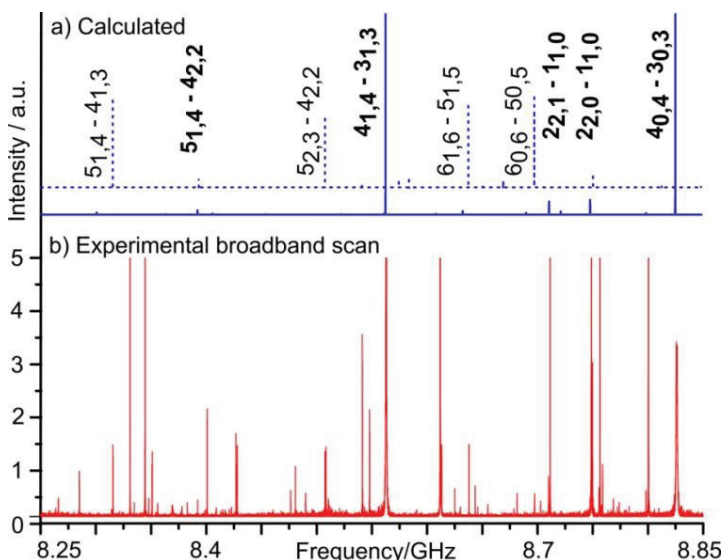
Figure 7. S1. (a) Simulated rotational spectra of the monohydrate i-I conformer (solid) and dihydrate ii-II conformer (dotted) using the spectroscopic constants reported in Table 1 and 2 with T_{rot} = 1 K. (b) A 0.6 GHz broadband chirped pulse microwave spectrum.

The vertical axis is truncated with the intensity of the strongest transition $4_{1,4}$-$3_{1,3}$ of i-I at 500. Strong unmarked lines are due to ML itself.

E.4. Complete lists of the experimental spectroscopic constants for the mono- and dihydrate conformers observed.

Table 7. S3. Experimental spectroscopic constants of the observed isotopologues of i-I.

Parameter[a]	i-ML--H_2O	i-ML--$H_2^{18}O$	i-ML--DOD	i-ML--DOH	i-ML--HOD	i-MLOD--DOH	i-MLOD--HOD
A (MHz)	2566.4940(6)	2511.3532(5)	2478.541(1)	2529.399(1)	2511.849(1)	2529.862(1)	2512.3057(8)
B (MHz)	1278.7597(2)	1238.8016(1)	1241.9619(7)	1271.2273(5)	1249.2938(6)	1257.7016 (4)	1236.4447(2)
C (MHz)	1011.8730(2)	979.5511(1)	975.8648(5)	1001.7533(4)	985.2618(5)	994.9089(4)	978.7656(2)
D_J (kHz)	0.235(2)	0.235(1)	0.220(6)	0.219(6)	0.21696)	0.212(4)	0.212(2)
D_{JK} (kHz)	0.82(1)	0.86(1)	0.63(8)	1.09(9)	0.78(8)	0.87(6)	0.78(3)
D_K (kHz)	1.85(4)	1.94(4)	1.85^c	2.2(1)	1.9(1)	1.6(1)	1.9(1)
d_1 (kHz)	-0.028(1)	-0.026(1)	-0.026(5)	-0.040(4)	-0.035(4)	-0.029(3)	-0.032(1)
d_2 (kHz)	-0.011(1)	-0.0116(9)	-0.010(3)	-0.011(3)	-0.011(4)	-0.015(2)	-0.0116(1)
V_3 (kJmol^{-1})	5.12(2)	5.05(2)	5.12(1)	5.071(9)	5.11 (1)	5.125(8)	5.11(3)
ρ	0.01301(6)	0.01263(5)	0.01230[b]	0.01292[b]	0.0125[b]	0.0128[b]	0.01263(9)
β (rad)	0.415(2)	0.436(2)	0.448(10)	0.410(7)	0.435(9)	0.419(6)	0.425(3)
γ (rad)	2.98(1)	3.00(1)	3.03(4)	2.99(4)	2.91(2)	3.05(5)	3.06(3)
F_0 (GHz)	160.951[b]	158.944[b]	160.951[c]	160.951[c]	160.951[c]	160.951[c]	160.577[b]
N	106	104	49	62	62	68	85
σ (kHz)	4.0	3.3	6.8	6.8	7.4	7.2	4.6

[a]N is the number of transitions included in the fit and σ is the standard deviation of the fit. Standard errors in parenthesis are expressed in units of the least significant digit. [b]Derived from the fitted parameters. [c]Fixed at the value of the parent species.

Table 7. S4. Experimental spectroscopic constants of the observed isotopologues of ii-II.

Parameter[a]	ii-ML--2H$_2$O	ii-ML--H$_2^{18}$O--H$_2^{18}$O	ii-ML--H$_2^{18}$O--H$_2^{16}$O	ii-ML--H$_2^{16}$O--H$_2^{18}$O
A (MHz)	1703.2142(53)	1647.0764(32)	1694.604(13)	1656.6878(58)
B (MHz)	915.85211(37)	872.66301(30)	887.98776(72)	898.66724(78)
C (MHz)	681.15852(31)	650.40411(23)	666.26735(51)	664.31504(56)
D_J (kHz)	0.2665(25)	0.2754(17)	0.2870(61)	0.2857(45)
D_K (kHz)	8.93(42)	0.00[c]	5.0(22)	0.00[c]
d_1 (kHz)	-0.0702921)	-0.0637(16)	-0.0730(45)	-0.0743(49)
d_2 (kHz)	-0.0251(15)	-0.0063(14)	-0.0227(50)	-0.0026(25)
V_3 (kJmol^{-1})	5.1887(79)	5.1944(83)	5.187(18)	5.223(18)
$\rho^{[b]}$	0.007537	0.007120	0.007120	0.007256
β (rad)	2.4928 (59)	2.4736(61)	2.438(15)	2.471(13)
γ (rad)	2.8691(41)	2.8633(38)	2.8740(80)	2.8568(97)
N	64	61	44	51
σ (kHz)	3.5	3.2	4.8	5.8

[a]N is the number of transitions included in the fit and σ is the standard deviation of the fit. Standard errors in parenthesis are expressed in units of the least significant digit. D_{JK} is fixed at 0.0 kHz and F_0 at the normal isotopologues of i-I value of 160.951 GHz. [b]Derived from the fitted parameters. [c]Fixed.

E.5. Conversion barrier between the monohydrate conformer I and II.
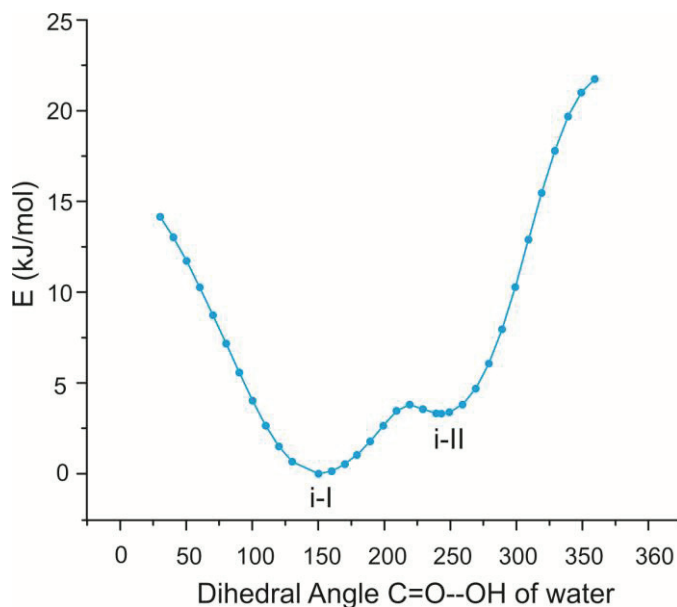
Figure 7. S2. A potential energy scan as a function of the dihedral angle C=O--OH(of water) at the MP2/6-311++G(d,p) level. At each point, all structural parameters except

the dihedral angle were re-optimized and a dissociation energy value was calculated. The estimated conversion barrier from i-II to i-I is less than 1 kJ/mol.

E.6. Lists of measured rotational transitions of the mono- and dihydrate conformers and their isotopologues.

Table 7. S5. Observed transition frequencies of the i-ML--H_2O-I conformer.

J'	Ka'	Kc'	J"	Ka"	Kc"	Symmetry	ν_{EXP} / MHz	$\Delta\nu^{[a]}$ / MHz
2	0	2	1	0	1	A	4543.9338	0.0012
2	0	2	1	0	1	E	4543.9041	0.0004
2	1	1	1	1	0	A	4848.1674	0.0022
2	1	2	1	1	1	A	4314.3794	-0.0033
2	2	1	1	1	0	A	8711.4547	0.0017
2	2	1	1	1	0	E	8709.9553	-0.0031
2	2	0	1	1	0	A	8748.8001	0.0029
2	2	0	1	1	0	E	8749.7414	-0.0102
2	2	0	1	1	1	A	9015.6877	-0.0014
2	2	0	1	1	1	E	9016.7110	-0.0094
2	2	1	1	1	1	A	8978.3491	0.0041
2	2	1	1	1	1	E	8976.9214	-0.0058
3	2	1	2	2	0	A	7016.6516	-0.0001
3	2	1	2	2	0	E	7015.6276	-0.0012
3	0	3	2	0	2	A	6727.1292	-0.0016
3	0	3	2	0	2	E	6727.0967	0.0028
3	1	2	2	1	1	A	7247.0184	-0.0001
3	1	2	2	1	1	E	7246.9488	0.0007
3	1	3	2	1	2	A	6449.6593	0.0066
3	1	3	2	1	2	E	6449.6346	-0.0038
3	2	2	2	2	1	A	6871.8828	-0.0001
3	2	2	2	2	1	E	6872.8182	0.0058
3	2	2	3	1	3	A	5086.2011	0.0086
3	1	3	2	0	2	A	7507.8754	-0.0005
3	1	3	2	0	2	E	7507.8075	0.0063
3	2	2	2	1	1	A	10735.1724	0.0016
3	2	2	2	1	1	E	10734.6744	-0.0025
3	0	3	2	1	2	A	5668.9007	-0.0070
3	0	3	2	1	2	E	5668.9348	0.0037
3	3	0	2	2	0	A	13965.6912	-0.0021
3	3	0	2	2	0	E	13972.8928	-0.0011
3	1	2	2	0	2	A	9105.9209	0.0048

3	1	2	2	0	2	E	9105.7802	0.0036
3	2	1	2	1	1	A	10917.2850	0.0013
3	3	1	2	2	1	A	13999.7292	-0.0037
3	3	1	2	2	1	E	13991.7762	0.0033
3	2	2	2	1	2	A	11535.8453	0.0001
3	2	2	2	1	2	E	11535.3394	-0.0032
4	2	2	3	2	1	A	9469.4444	-0.0013
4	2	2	3	2	1	E	9469.2049	0.0002
4	0	4	3	0	3	A	8826.1165	0.0020
4	0	4	3	0	3	E	8826.0741	0.0003
4	3	1	3	3	0	A	9247.8121	-0.0006
4	3	1	3	3	0	E	9242.8852	0.0007
4	1	3	3	1	2	A	9610.9174	0.0008
4	1	3	3	1	2	E	9610.8318	0.0010
4	3	2	3	3	1	A	9228.2491	0.0041
4	3	2	3	3	1	E	9233.0531	0.0030
4	1	4	3	1	3	A	8562.9277	-0.0025
4	1	4	3	1	3	E	8562.8961	-0.0107
4	2	3	3	2	2	A	9133.2967	-0.0015
4	2	3	3	2	2	E	9133.4124	0.0021
4	3	2	3	2	1	A	16173.9795	-0.0025
4	1	4	3	0	3	A	9343.6717	-0.0035
4	1	4	3	0	3	E	9343.6175	0.0034
4	2	3	3	1	2	A	12621.4515	0.0010
4	2	3	3	1	2	E	12621.1398	0.0007
4	0	4	3	1	3	A	8045.3656	-0.0038
4	2	3	3	1	3	A	14219.4949	0.0042
4	2	3	3	1	3	E	14219.1104	-0.0042
4	3	1	3	2	2	A	16378.9641	-0.0031
4	3	1	3	2	2	E	16382.7699	0.0107
4	3	1	3	2	1	A	16196.8514	-0.0028
4	3	1	3	2	1	E	16200.1512	0.0017
4	3	2	3	2	2	A	16356.0920	-0.0030
4	3	2	3	2	2	E	16352.0161	0.0055
5	0	5	4	0	4	A	10858.2345	0.0072
5	0	5	4	0	4	E	10858.1894	0.0046
5	3	2	4	3	1	A	11617.0276	-0.0006
5	3	2	4	3	1	E	11614.1540	0.0015
5	1	4	4	1	3	A	11920.9593	-0.0027
5	1	4	4	1	3	E	11920.8618	0.0001
5	3	3	4	3	2	A	11550.4681	-0.0019
5	3	3	4	3	2	E	11553.1820	-0.0060
5	1	5	4	1	4	A	10653.1049	0.0010
5	1	5	4	1	4	E	10653.0752	-0.0015
5	0	5	4	1	4	A	10340.6691	0.0026
5	0	5	4	1	4	E	10340.6416	-0.0028

5	2	3	4	1	3	A	15491.9508	0.0027
5	2	3	4	1	3	E	15491.7167	-0.0036
6	2	4	5	2	3	A	14453.5855	0.0019
6	2	4	5	2	3	E	14453.4447	0.0029
6	0	6	5	0	5	A	12859.3667	-0.0058
6	0	6	5	0	5	E	12859.3305	0.0039
6	3	3	5	3	2	A	14038.1024	-0.0007
6	3	3	5	3	2	E	14037.2386	-0.0069
6	1	5	5	1	4	A	14155.4395	-0.0001
6	1	5	5	1	4	E	14155.3307	0.0010
6	1	6	5	1	5	A	12722.3808	0.0012
6	1	6	5	1	5	E	12722.3549	0.0017
6	0	6	5	1	5	A	12546.9299	-0.0052
6	0	6	5	1	5	E	12546.8943	0.0000
6	4	2	5	4	1	A	13876.3379	-0.0046
6	4	2	5	4	1	E	13872.8904	-0.001
6	3	4	5	3	3	A	13870.0180	-0.0006
6	3	4	5	3	3	E	13870.6814	0.0001
6	4	3	5	4	2	A	13867.8329	0.0006
6	4	3	5	4	2	E	13871.1012	0.0041
6	2	5	5	2	4	A	13577.8325	-0.0025
6	2	5	5	2	4	E	13577.7767	0.0015
6	1	6	5	0	5	A	13034.8174	0.0005
6	1	6	5	0	5	E	13034.7929	0.0074
7	2	5	6	2	4	A	16902.5472	0.0026
7	2	5	6	2	4	E	16902.3879	-0.0004
7	0	7	6	0	6	A	14856.9614	-0.0027
7	0	7	6	0	6	E	14856.9083	0.0000

[a] $\Delta\nu = \nu_{CALC} - \nu_{EXP}$.

Table 7. S6. Observed transition frequencies of the i-ML--D$_2$O-I.

J'	Ka'	Kc'	J"	Ka"	Kc"	Symmetry	ν_{EXP} /MHz	$\Delta\nu$[a] / MHz
2	2	0	1	1	0	A	8450.0758	0.0019
2	2	1	1	1	1	A	8677.6876	0.0143
2	2	1	1	1	0	A	8411.5662	-0.0041
2	2	0	1	1	1	A	8716.1898	0.0129
2	1	1	1	0	1	A	6204.4773	-0.0029
3	1	2	2	1	1	A	7026.5612	-0.0014
3	1	2	2	1	1	E	7026.4889	-0.0029
3	1	3	2	1	2	A	6231.7805	-0.0042
3	1	3	2	1	1	E	6231.7588	-0.0106
3	1	2	2	0	2	A	8833.8777	-0.003
3	1	2	2	0	2	E	8833.7376	-0.0106
3	2	1	2	1	1	A	10550.7262	-0.0062
3	2	1	2	1	1	E	10550.7084	-0.0136

3	2	2	2	2	1	A	6653.4643	-0.0074
3	0	3	2	0	2	A	6504.5240	-0.0071
3	0	3	2	0	2	E	6504.4958	0.0005
4	2	2	3	2	1	A	9185.5314	0.0078
4	2	2	3	2	1	E	9185.3137	0.0048
4	0	4	3	0	3	A	8526.6600	-0.0027
4	0	4	3	0	3	E	8526.6263	0.0012
4	1	3	3	1	2	A	9315.0689	0.0018
4	1	3	3	1	2	E	9314.9838	0.0034
4	1	4	3	1	3	A	8271.5315	0.0036
4	1	4	3	1	3	E	8271.4955	-0.009
4	2	3	3	2	2	A	8841.1785	0.0099
4	2	3	3	2	2	E	8841.2603	0.0111
4	3	2	3	3	1	A	8938.8030	0.0018
5	0	5	4	0	4	A	10483.1896	-0.005
5	0	5	4	0	4	E	10483.1652	0.0078
5	2	3	4	2	2	A	11607.3875	-0.0032
5	2	3	4	2	2	E	11607.2447	-0.0033
5	1	4	4	1	3	A	11547.5375	0.0027
5	1	4	4	1	3	E	11547.4372	0.0026
5	1	5	4	1	4	A	10287.8744	0.0061
5	1	5	4	1	4	E	10287.8443	0.0028
5	2	4	4	2	3	A	11003.6458	0.004
5	2	4	4	2	3	E	11003.6100	-0.0029
6	0	6	5	0	5	A	12411.2468	-0.004
6	0	6	5	0	5	E	12411.2170	0.0043
6	1	5	5	1	4	A	13701.6188	0.0023
6	1	5	5	1	4	E	13701.5070	-0.0023
6	1	6	5	1	5	A	12283.3027	0.0033
6	1	6	5	1	5	E	12283.2794	0.0070
6	2	5	5	2	4	A	13136.0286	-0.0045
6	2	5	5	2	4	E	13135.9653	-0.0050
6	2	4	5	2	3	A	14022.2129	0.0013
6	2	4	5	2	3	E	14022.0668	-0.0005
7	0	7	6	0	6	A	14337.4333	-0.0036
7	0	7	6	0	6	E	14337.3902	-0.0034

[a] $\Delta v = v_{CALC} - v_{EXP}$.

Table 7. S7. Observed transition frequencies of the i-ML--DOH-I.

J'	Ka'	Kc'	J"	Ka"	Kc"	Symmetry	v_{EXP} / MHz	$\Delta v^{[a]}$ / MHz
2	2	1	1	1	0	A	8590.0350	-0.0093
2	2	0	1	1	0	A	8628.8623	-0.0109
2	2	0	1	1	1	A	8898.3443	-0.0081

2	2	1	1	1	1	A	8859.5132	-0.0103
2	2	1	1	1	1	E	8858.0355	-0.0028
2	1	1	1	0	1	A	6343.1457	0.0068
2	1	1	1	0	1	E	6343.0420	0.0031
3	1	2	2	1	1	A	7196.8637	-0.0098
3	1	2	2	1	1	E	7196.7956	-0.0060
3	1	3	2	1	2	A	6391.9907	0.0061
3	1	3	2	1	2	E	6391.9666	-0.0040
3	2	2	2	2	1	A	6818.9131	-0.0092
3	2	1	2	2	0	A	6969.1748	0.0011
3	3	0	2	2	0	A	13770.9478	0.0079
3	3	1	2	2	1	A	13806.2279	-0.0001
3	2	1	2	1	1	A	10782.5934	-0.0058
3	2	1	2	1	1	E	10782.6130	0.0084
3	0	3	2	0	2	A	6668.6906	-0.0034
3	0	3	2	0	2	E	6668.6593	0.0028
3	1	3	2	0	2	A	7419.5465	0.0031
3	1	3	2	0	2	E	7419.4800	0.0145
3	1	2	2	0	2	A	9032.8670	-0.0010
3	1	2	2	0	2	E	9032.7358	0.0105
4	2	2	3	2	1	A	9409.0633	-0.0033
4	0	4	3	0	3	A	8744.0837	0.0011
4	0	4	3	0	3	E	8744.0469	0.0057
4	1	3	3	1	2	A	9541.7260	-0.0065
4	1	3	3	1	2	E	9541.6405	-0.0044
4	1	4	3	1	3	A	8484.7850	0.0008
4	1	4	3	1	3	E	8484.7622	0.0014
4	2	3	3	2	2	A	9061.5151	-0.0013
4	2	3	3	2	2	E	9061.6294	-0.0069
4	1	3	3	0	3	A	11905.9165	0.0101
4	1	3	3	0	3	E	11905.7273	0.0136
4	0	4	3	1	3	A	7993.2279	-0.0053
4	0	4	3	1	3	E	7993.2279	-0.0042
4	1	4	3	0	3	A	9235.6306	-0.0030
4	1	4	3	0	3	E	9235.5827	0.0128
5	0	5	4	0	4	A	10752.8931	-0.0026
5	0	5	4	0	4	E	10752.8607	0.0083
5	2	3	4	2	2	A	11888.4816	-0.0051
5	2	3	4	2	2	E	11888.3378	0.0003
5	1	4	4	1	3	A	11830.1449	-0.0005
5	1	4	4	1	3	E	11830.0426	-0.0006
5	1	5	4	1	4	A	10553.9367	0.0045
5	1	5	4	1	4	E	10553.9071	0.0021
5	2	4	4	2	3	A	11278.6721	0.0019
5	2	4	4	2	3	E	11278.6430	-0.0090
5	1	5	4	0	4	A	11045.4825	-0.0007

5	1	5	4	0	4	E	11045.4340	0.0003
5	0	5	4	1	4	A	10261.3496	0.0049
5	0	5	4	1	4	E	10261.3190	-0.0047
6	0	6	5	0	5	A	12732.5597	-0.0085
6	0	6	5	0	5	E	12732.5260	0.0048
6	1	5	5	1	4	A	14039.5642	-0.0024
6	1	5	5	1	4	E	14039.4592	0.0045
6	1	6	5	1	5	A	12601.9130	-0.0033
6	1	6	5	1	5	E	12601.8885	-0.0015
6	2	5	5	2	4	A	13465.4708	-0.0011
6	2	5	5	2	4	E	13465.4155	0.0036
6	2	4	5	2	3	A	14361.2517	-0.0027
6	2	4	5	2	3	E	14361.1134	0.0032

[a] $\Delta\nu = \nu_{CALC} - \nu_{EXP}$.

Table **7. S8.** Observed transition frequencies of the i-MLOD--DOH-I conformer.

J'	Ka'	Kc'	J"	Ka"	Kc"	Symmetry	ν_{EXP} / MHz	$\Delta\nu^{[a]}$ / MHz
2	2	1	1	1	0	A	8584.5846	-0.0058
2	2	1	1	1	0	E	8583.1578	0.0122
2	2	0	1	1	0	A	8621.2554	0.0019
2	2	0	1	1	0	E	8622.1604	-0.0198
2	2	0	1	1	1	A	8884.0575	0.0057
2	2	1	1	1	1	A	8847.3952	0.0066
2	2	1	1	1	1	E	8846.0119	-0.0054
2	1	1	1	0	1	A	6303.0228	-0.0003
2	1	1	1	0	1	E	6302.9243	-0.0035
3	1	3	2	0	2	A	7388.1759	-0.0086
3	1	3	2	0	2	E	7388.1177	0.0037
3	2	2	2	2	1	A	6757.8210	0.0032
3	2	2	2	2	1	E	6758.7320	0.0147
3	0	3	2	0	2	A	6615.6782	-0.0024
3	3	1	2	2	0	A	13760.5060	0.0000
3	3	0	2	2	0	A	13763.7332	-0.0073
3	1	2	2	0	2	A	8961.7359	0.0033
3	1	2	2	0	2	E	8961.5922	-0.0036
3	2	1	2	2	0	A	6899.9632	-0.0084
3	2	1	2	2	0	E	6898.9838	0.0043
3	1	2	2	1	1	A	7127.2757	-0.0034
3	1	2	2	1	1	E	7127.2074	-0.0020
3	3	1	2	2	1	A	13797.1724	0.0032
3	3	0	2	2	1	A	13800.4076	0.0039
3	2	2	2	1	1	A	10574.3720	-0.0087
4	1	4	3	1	3	A	8420.2188	0.0086

4	1	4	3	1	3	E	8420.1830	-0.0048
4	1	4	3	0	3	A	9192.7055	-0.0087
4	1	4	3	0	3	E	9192.6629	0.0062
4	0	4	3	0	3	A	8679.9894	0.0057
4	2	2	3	2	1	A	9311.9552	0.0091
4	2	2	3	2	1	E	9311.7171	0.0066
4	2	3	3	2	2	A	8981.7502	0.0029
4	2	2	3	2	2	E	8981.8562	0.0011
4	1	3	3	1	2	A	9452.2303	-0.0048
4	1	3	3	1	2	E	9452.1480	-0.0022
4	3	1	3	3	0	A	9094.1372	0.0010
4	3	1	3	3	0	E	9089.3121	-0.0128
4	0	4	3	1	3	A	7907.4724	-0.0074
4	1	3	3	0	3	A	11798.2974	0.0102
4	1	3	3	0	3	E	11798.0960	-0.0049
4	2	2	3	1	2	A	12937.8672	0.0025
4	2	2	3	1	2	E	12937.7151	0.0118
5	0	5	4	0	4	A	10678.3570	-0.0013
5	0	5	4	0	4	E	10678.3310	0.0105
5	2	3	4	2	2	A	11764.3678	-0.0071
5	2	3	4	2	2	E	11764.2202	-0.0103
5	1	4	4	1	3	A	11724.3610	-0.0039
5	1	4	4	1	3	E	11724.2690	0.0028
5	1	5	4	1	4	A	10475.5738	-0.0069
5	2	4	4	2	3	A	11181.6239	-0.0038
6	2	4	5	2	3	A	14213.9028	0.0028
6	2	4	5	2	3	E	14213.7596	0.0006
6	0	6	5	0	5	A	12646.0366	-0.0002
6	1	5	5	1	4	A	13922.3450	-0.0043
6	1	5	5	1	4	E	13922.2444	0.0024
6	1	6	5	1	5	A	12510.3918	0.0086
6	1	6	5	1	5	E	12510.3628	0.0077
6	2	5	5	2	4	A	13352.7300	-0.0022
6	2	5	5	2	4	E	13352.6782	0.0045
6	3	3	5	3	2	A	13804.4032	-0.0006
7	2	5	6	2	4	A	16622.9179	0.0011
7	2	5	6	2	4	E	16622.7618	0.0003
7	0	7	6	0	6	A	14610.0676	-0.0017
7	0	7	6	0	6	E	14610.0246	-0.0046
7	1	6	6	1	5	A	16030.0123	-0.0065
7	1	6	6	1	5	E	16029.9164	0.0074
7	1	7	6	1	6	A	14528.7902	-0.0037

[a] $\Delta\nu = \nu_{CALC} - \nu_{EXP}$.

Table 7. S9. Observed transition frequencies of the i-ML--HOD-I conformer.

J'	Ka'	Kc'	J"	Ka"	Kc"	Symmetry	ν_{EXP} / MHz	$\Delta\nu^{[a]}$ / MHz
2	2	1	1	1	0	A	8520.9019	0.0066
2	2	0	1	1	0	A	8558.1306	-0.0076
2	2	0	1	1	1	A	8822.1906	0.0153
2	1	1	1	0	1	A	6259.7680	-0.0161
2	1	1	1	0	1	E	6259.7070	0.0148
2	2	1	1	1	1	A	8784.9400	0.0076
3	2	1	2	2	0	A	6847.9537	-0.0070
3	2	1	2	2	0	E	6847.0295	0.0038
3	1	2	2	1	1	A	7074.5577	-0.0004
3	1	2	2	1	1	E	7074.4868	-0.0017
3	1	3	2	1	2	A	6285.7753	-0.0011
3	2	2	2	2	1	A	6703.6604	0.0053
3	3	0	2	2	0	A	13664.4630	0.0035
3	1	2	2	0	2	A	8902.4621	0.0003
3	1	2	2	0	2	E	8902.3397	0.0101
3	2	2	2	1	2	A	11283.4865	-0.0165
3	2	2	2	1	2	E	11283.0305	-0.0130
3	2	1	2	1	1	A	10672.9422	0.0003
3	0	3	2	0	2	A	6559.3563	-0.0087
3	1	3	2	0	2	A	7321.5690	-0.0015
3	1	3	2	0	2	E	7321.5080	0.0062
3	3	1	2	2	0	A	13661.1362	-0.0004
3	3	1	2	2	1	A	13698.3780	-0.0015
4	2	2	3	2	1	A	9243.8012	0.0008
4	2	2	3	2	1	E	9243.5747	0.0003
4	0	4	3	0	3	A	8603.2332	0.0047
4	0	4	3	0	3	E	8603.1847	-0.0014
4	3	1	3	3	0	A	9023.3724	-0.0011
4	1	3	3	1	2	A	9381.0454	0.0034
4	1	3	3	1	2	E	9380.9548	-0.0019
4	1	4	3	1	3	A	8344.5875	0.0056
4	1	4	3	1	3	E	8344.5543	-0.0032
4	2	3	3	2	2	A	8909.0762	0.0025
4	2	3	3	2	2	E	8909.1676	-0.0016
4	1	4	3	0	3	A	9106.7806	-0.0067
4	1	4	3	0	3	E	9106.7354	0.0034
4	0	4	3	1	3	A	7841.0184	-0.0046
5	0	5	4	0	4	A	10581.1872	0.0081
5	0	5	4	0	4	E	10581.1300	-0.0029
5	2	3	4	2	2	A	11679.6556	0.0017
5	2	3	4	2	2	E	11679.5088	-0.0029
5	1	4	4	1	3	A	11633.7030	0.0007
5	1	4	4	1	3	E	11633.6026	-0.0001

5	1	5	4	1	4	A	10380.4497	0.0049
5	1	5	4	1	4	E	10380.4194	0.0014
5	2	4	4	2	3	A	11090.0848	0.0128
5	2	4	4	2	3	E	11090.0544	0.0074
5	1	5	4	0	4	A	10883.9882	-0.0155
5	1	5	4	0	4	E	10883.9697	0.0058
5	0	5	4	1	4	A	10077.6097	-0.0106
6	2	4	5	2	3	A	14111.3786	0.0020
6	2	4	5	2	3	E	14111.2350	-0.0011
6	0	6	5	0	5	A	12529.0747	0.0114
6	0	6	5	0	5	E	12529.0051	-0.0036
6	1	5	5	1	4	A	13810.8845	-0.0044
6	1	5	5	1	4	E	13810.7804	0.0005
6	1	6	5	1	5	A	12395.6182	0.0012
6	1	6	5	1	5	E	12395.5885	-0.0064
6	2	5	5	2	4	A	13241.8770	-0.0022
6	2	5	5	2	4	E	13241.8132	-0.0037
7	0	7	6	0	6	A	14473.8414	-0.0010
7	0	7	6	0	6	E	14473.7679	0.0022

[a] $\Delta v = v_{CALC} - v_{EXP}$.

Table 7. S10. Observed transition frequencies of the i-MLOD--HOD-I conformer.

J'	Ka'	Kc'	J"	Ka"	Kc"	Symmetry	v_{EXP} / MHz	$\Delta v^{[a]}$ / MHz
2	2	1	1	1	0	A	8515.7689	0.0000
2	2	1	1	1	0	E	8514.3416	-0.0007
2	2	0	1	1	0	A	8551.0020	0.0022
2	2	0	1	1	0	E	8551.9188	-0.0086
2	2	0	1	1	1	A	8808.6850	0.0005
2	1	1	1	0	1	A	6221.7028	0.0090
2	1	1	1	0	1	E	6221.6080	0.0067
2	2	1	1	1	1	A	8773.4580	0.0043
2	2	1	1	1	1	E	8772.1004	0.0021
3	2	1	2	2	0	A	6782.3807	-0.0001
3	2	1	2	2	0	E	6781.3953	-0.0008
3	1	2	2	1	1	A	7008.4098	-0.0049
3	1	2	2	1	1	E	7008.3454	-0.0005
3	1	3	2	1	2	A	6238.4192	0.0079
3	1	3	2	1	2	E	6238.3941	-0.0037
3	2	2	2	2	1	A	6645.6140	-0.0043
3	2	2	2	1	1	A	10473.2798	0.0060
3	2	2	2	1	1	E	10472.8119	0.0029
3	3	0	2	2	0	A	13657.6620	0.0003
3	3	0	2	2	0	E	13664.5714	0.0056
3	3	0	2	2	1	A	13692.8922	-0.0003
3	3	1	2	2	0	A	13654.6155	-0.0016

3	0	3	2	0	2	A	6508.8704	-0.0009
3	1	3	2	0	2	A	7291.8456	-0.0057
3	1	3	2	0	2	E	7291.7787	-0.0052
3	1	2	2	0	2	A	8834.9063	-0.0010
3	1	2	2	0	2	E	8834.7743	0.0006
3	2	1	2	1	1	A	10645.2645	-0.0027
3	2	1	2	1	1	E	10645.2804	0.0014
3	3	1	2	2	1	A	13689.8422	-0.0057
3	3	1	2	2	1	E	13682.2471	0.0031
3	2	2	2	1	2	A	11246.3277	0.0012
3	2	2	2	1	2	E	11245.8422	-0.0086
4	2	3	3	2	2	A	8833.2687	-0.0037
4	2	3	3	2	2	E	8833.3783	-0.0015
4	2	2	3	2	1	A	9151.7465	-0.0027
4	2	2	3	2	1	E	9151.5135	-0.0014
4	1	3	3	1	2	A	9295.8931	-0.0018
4	1	3	3	1	2	E	9295.8104	-0.0007
4	0	4	3	0	3	A	8542.1176	-0.0065
4	3	1	3	3	0	A	8941.0504	-0.0019
4	1	4	3	1	3	A	8283.2190	0.0082
4	1	4	3	1	3	E	8283.1886	-0.0002
4	1	4	3	0	3	A	9066.1929	0.0021
4	1	4	3	0	3	E	9066.1378	0.0017
4	3	2	3	2	1	A	15795.2516	0.0023
4	3	1	3	2	1	A	15816.3334	0.0002
4	3	2	3	2	2	A	15967.2414	-0.0012
4	3	1	3	2	2	A	15988.3261	-0.0004
4	2	2	3	1	2	A	12788.5988	-0.0029
4	2	2	3	1	2	E	12788.4403	-0.0077
4	1	3	3	0	3	A	11621.9354	0.0045
4	1	3	3	0	3	E	11621.7524	0.0041
4	0	4	3	1	3	A	7759.1448	0.0007
5	0	5	4	0	4	A	10510.1878	-0.0060
5	0	5	4	0	4	E	10510.1664	0.0090
5	2	3	4	2	2	A	11561.8589	0.0002
5	2	3	4	2	2	E	11561.7132	-0.0019
5	1	4	4	1	3	A	11532.8902	-0.0017
5	1	4	4	1	3	E	11532.7930	-0.0014
5	3	2	4	3	1	A	11229.8916	-0.0001
5	3	3	4	3	2	A	11168.4538	0.0058
5	2	4	4	2	3	A	10997.8059	0.0056
5	2	4	4	2	3	E	10997.7772	-0.0038
5	1	5	4	1	4	A	10305.9660	0.0090
5	1	5	4	1	4	E	10305.9324	0.0016
5	0	5	4	1	4	A	9986.1176	-0.0095
6	2	4	5	2	3	A	13971.2618	-0.0009

6	2	4	5	2	3	E	13971.1206	-0.0021
6	0	6	5	0	5	A	12446.7892	-0.0049
6	0	6	5	0	5	E	12446.7615	0.0030
6	1	5	5	1	4	A	13698.9208	-0.0024
6	1	5	5	1	4	E	13698.8174	-0.0002
6	1	6	5	1	5	A	12308.6022	0.0106
6	1	6	5	1	5	E	12308.5686	0.0050
6	2	5	5	2	4	A	13134.6116	0.0025
6	2	5	5	2	4	E	13134.5537	0.0021
7	2	5	6	2	4	A	16343.1066	0.0027
7	2	5	6	2	4	E	16342.9548	0.0047
7	0	7	6	0	6	A	14378.7925	-0.0045
7	0	7	6	0	6	E	14378.7586	-0.0018
7	1	6	6	1	5	A	15777.8228	-0.0062
7	1	7	6	1	6	A	14295.0534	-0.0022
7	2	6	6	2	5	A	15240.6290	0.0010
7	2	6	6	2	5	E	15240.5522	-0.0015

[a] $\Delta v = v_{CALC} - v_{EXP}$.

Table 7. S11. Observed transition frequencies of the i-ML--$H_2{}^{18}$O-I conformer.

J'	Ka'	Kc'	J"	Ka"	Kc"	Symmetry	v_{EXP} / MHz	$\Delta v^{[a]}$ / MHz
2	2	0	1	1	0	A	8549.4196	0.0044
2	2	0	1	1	0	E	8550.3130	0.0019
2	2	0	1	1	1	A	8808.6730	0.0016
2	2	0	1	1	1	E	8809.6345	-0.0019
2	2	1	1	1	0	A	8513.6944	0.0018
2	2	1	1	1	0	E	8512.3046	-0.0002
2	2	1	1	1	1	A	8772.9480	-0.0008
2	2	1	1	1	1	E	8771.6294	-0.0007
3	2	1	2	2	0	A	6793.6521	0.0002
3	2	1	2	2	0	E	6792.6938	0.0013
3	2	2	2	2	1	A	6655.0414	-0.0014
3	2	2	2	2	1	E	6655.9078	0.0016
3	0	3	2	0	2	A	6516.4476	-0.0034
3	0	3	2	0	2	E	6516.4157	0.0013
3	1	2	2	1	1	A	7019.8510	-0.0004
3	1	2	2	1	1	E	7019.7806	0.0001
3	1	3	2	1	2	A	6245.2051	0.0056
3	1	1	2	1	2	E	6245.1804	-0.0041
3	1	3	2	0	2	A	7294.2485	-0.0003
3	1	3	2	0	2	E	7294.1869	0.0050
3	2	2	2	1	1	A	10472.7651	-0.0004
3	2	2	2	1	1	E	10472.3115	0.0007
3	3	0	2	2	0	A	13654.3164	0.0034

3	3	0	2	2	0	E	13661.1409	-0.0011
3	1	2	2	0	2	A	8846.6719	0.0037
3	1	2	2	0	2	E	8846.5348	0.0016
3	2	1	2	1	1	A	10647.0951	-0.0021
3	2	1	2	1	1	E	10647.0951	-0.0084
3	3	1	2	2	1	A	13686.9153	-0.0085
3	3	1	2	2	1	E	13679.4043	0.0007
3	2	2	2	1	2	A	11250.5285	-0.0046
3	2	2	2	1	2	E	11250.0637	-0.0024
3	3	1	2	2	0	A	13651.2049	0.0037
3	3	1	2	2	0	E	13641.3980	0.0007
3	3	0	2	2	1	A	13690.0351	-0.0005
3	3	0	2	2	1	E	13699.1479	-0.0004
4	2	2	3	2	1	A	9167.9163	-0.0005
4	2	2	3	2	1	E	9167.6842	0.0000
4	0	4	3	0	3	A	8550.6935	0.0007
4	0	4	3	0	3	E	8550.6552	0.0017
4	1	3	3	1	2	A	9310.3970	-0.0030
4	1	3	3	1	2	E	9310.3117	-0.0015
4	1	4	3	1	3	A	8291.8284	0.0071
4	1	4	3	1	3	E	8291.7896	-0.0081
4	3	1	3	3	0	A	8954.8217	0.0042
4	3	1	3	3	0	E	8950.1641	0.0010
4	3	2	3	3	1	A	8936.3833	-0.0006
4	3	2	3	3	1	E	8940.9173	0.0054
4	2	3	3	2	2	A	8845.4484	-0.0011
4	2	3	3	2	2	E	8845.5495	0.0002
4	1	4	3	0	3	A	9069.6135	-0.0055
4	1	4	3	0	3	E	9069.5679	0.0027
4	0	4	3	1	3	A	7772.8895	-0.0055
4	0	4	3	1	3	E	7772.8895	0.0035
4	1	3	3	0	3	A	11640.6218	0.0046
4	1	3	3	0	3	E	11640.4325	0.0005
4	3	2	3	2	2	A	15968.2666	0.0017
4	3	2	3	2	2	E	15964.4114	0.0021
4	2	3	3	1	3	A	13850.7858	0.0028
4	2	3	3	1	3	E	13850.4284	-0.0025
4	2	2	3	1	2	A	12795.1612	-0.0014
4	2	2	3	1	2	E	12795.0078	0.0006
4	3	2	3	2	1	A	15793.9332	0.0000
4	3	2	3	2	1	E	15789.6155	-0.0012
5	2	3	4	2	2	A	11582.7627	0.0006
5	2	3	4	2	2	E	11582.6138	-0.0019
5	0	5	4	0	4	A	10519.5459	-0.0062
5	0	5	4	0	4	E	10519.5159	0.0036
5	1	4	4	1	3	A	11549.6473	-0.0021

5	1	4	4	1	3	E	11549.5488	0.0002
5	3	3	4	3	2	A	11185.2340	-0.0023
5	3	3	4	3	2	E	11187.8027	0.0017
5	1	5	4	1	4	A	10316.1680	0.0013
5	1	5	4	1	4	E	10316.1393	-0.0001
5	1	5	4	0	4	A	10835.0864	-0.0065
5	1	5	4	0	4	E	10835.0592	0.0081
5	0	5	4	1	4	A	10000.6258	0.0000
5	0	5	4	1	4	E	10000.5997	-0.0010
5	2	3	4	1	3	A	15067.5260	0.0012
5	2	3	4	1	3	E	15067.3110	0.0013
5	3	2	4	3	1	A	11247.9936	-0.0012
5	3	2	4	3	1	E	11245.2634	-0.0044
6	2	4	5	2	3	A	13996.0717	0.0010
6	2	4	5	2	3	E	13995.9258	-0.0003
6	0	6	5	0	5	A	12457.2706	-0.0042
6	0	6	5	0	5	E	12457.2362	0.0029
6	3	3	5	3	2	A	13590.5712	-0.0015
6	3	3	5	3	2	E	13589.7514	0.0001
6	1	5	5	1	4	A	13716.8254	-0.0014
6	1	5	5	1	4	E	13716.7187	0.0012
6	1	6	5	1	5	A	12320.2518	0.0002
6	1	6	5	1	5	E	12320.2271	0.0026
6	1	6	5	0	5	A	12635.7917	-0.0008
6	1	6	5	0	5	E	12635.7697	0.0065
6	3	4	5	3	3	A	13431.7972	-0.0030
6	3	4	5	3	3	E	13432.4191	-0.0013
7	2	6	6	2	5	A	15259.0088	0.0002
7	2	6	6	2	5	E	15258.9312	0.0007
7	0	7	6	0	6	A	14390.7631	-0.0045
7	0	7	6	0	6	E	14390.7198	0.0007
7	2	5	6	2	4	A	16370.7507	0.0020
7	2	5	6	2	4	E	16370.5894	0.0000
7	1	6	6	1	5	A	15795.7796	-0.0023
7	1	6	6	1	5	E	15795.6741	0.0035

[a] $\Delta v = v_{CALC} - v_{EXP}$.

Table 7. S12. Observed transition frequencies of the ii-ML--2H$_2$O-II conformer.

J'	Ka'	Kc'	J"	Ka"	Kc"	Symmetry	v_{EXP} / MHz	$\Delta v^{[a]}$ / MHz
3	0	3	2	0	2	A	4620.6379	0.0003
3	0	3	2	0	2	E	4620.6104	-0.0052
3	1	3	2	1	2	A	4413.0581	0.0015
3	1	3	2	1	2	E	4413.0455	0.0016
3	1	2	2	1	1	A	5111.5963	-0.0003

3	1	2	2	1	1	E	5111.5551	0.0018
3	2	2	2	2	1	A	4791.0213	-0.0039
3	2	2	2	2	1	E	4791.1741	0.0061
3	2	1	2	2	0	A	4961.4023	-0.0032
3	2	1	2	2	0	E	4961.2000	0.0046
4	0	4	3	0	3	A	6011.2682	-0.0036
4	0	4	3	0	3	E	6011.2507	0.0034
4	1	4	3	1	3	A	5842.6358	0.0010
4	1	4	3	1	3	E	5842.6151	-0.0061
4	1	3	3	1	2	A	6749.0023	0.0010
4	1	3	3	1	2	E	6748.9440	-0.0042
4	2	3	3	2	2	A	6352.6048	0.0040
4	2	3	3	2	2	E	6352.5898	-0.0024
4	2	2	3	2	1	A	6728.7563	0.0011
4	2	2	3	2	1	E	6728.6746	0.0033
5	0	5	4	0	4	A	7357.8842	-0.0014
5	0	5	4	0	4	E	7357.8539	0.0021
5	1	5	4	1	4	A	7249.2999	0.0006
5	1	5	4	1	4	E	7249.2999	0.0067
5	1	4	4	1	3	A	8315.5565	-0.0004
5	1	4	4	1	3	E	8315.4971	-0.0022
5	2	4	4	2	3	A	7885.0490	-0.0011
5	2	4	4	2	3	E	7885.0137	-0.0012
5	2	3	4	2	2	A	8507.6663	-0.0013
5	2	3	4	2	2	E	8507.5894	0.0020
5	3	3	4	3	2	A	8090.9132	0.0025
5	3	3	4	3	2	E	8091.2791	0.0022
5	3	2	4	3	1	A	8198.0191	-0.0028
5	3	2	4	3	1	E	8197.5371	-0.0026
5	4	2	4	4	1	A	8084.8730	0.0056
5	4	2	4	4	1	E	8086.5885	0.0046
5	4	1	4	4	0	A	8089.2955	0.0028
5	4	1	4	4	0	E	8087.4658	-0.0004
6	0	6	5	0	5	A	8697.3605	-0.0013
6	0	6	5	0	5	E	8697.2988	0.0013
6	1	6	5	1	5	A	8637.8819	-0.0014
6	1	6	5	1	5	E	8637.9063	0.0010
6	1	5	5	1	4	A	9789.1626	-0.0030
6	1	5	5	1	4	E	9789.1046	-0.0045
6	2	5	5	2	4	A	9383.9788	-0.0031
6	2	5	5	2	4	E	9383.9317	-0.0063
6	2	4	5	2	3	A	10249.1219	-0.0018
6	2	4	5	2	3	E	10249.0356	0.0012
6	3	4	5	3	3	A	9707.3097	0.0033
6	3	4	5	3	3	E	9707.3375	-0.0001
6	3	3	5	3	2	A	9963.5773	-0.0050

6	3	3	5	3	2	E	9963.3979	-0.0079
6	4	3	5	4	2	A	9729.3200	0.0025
6	4	3	5	4	2	E	9731.9965	-0.0004
6	4	2	5	4	1	A	9748.6379	-0.0021
6	4	2	5	4	1	E	9745.8270	0.0023
7	0	7	6	0	6	A	10043.6708	-0.0026
7	0	7	6	0	6	E	10043.5209	0.0015
7	1	7	6	1	6	A	10014.2713	-0.0008
7	1	7	6	1	6	E	10014.3828	0.0018
7	1	6	6	1	5	A	11172.0920	0.0014
7	1	6	6	1	5	E	11172.0376	0.0012
7	2	5	6	2	4	A	11922.0979	0.0040
7	2	5	6	2	4	E	11922.0009	0.0037

[a] $\Delta v = v_{CALC} - v_{EXP}$.

Table 7. S13. Observed transition frequencies of the ii-ML--2H$_2$^{18}O-II conformer.

J'	Ka'	Kc'	J"	Ka"	Kc"	Symmetry	v_{EXP} / MHz	$\Delta v^{[a]}$ / MHz
3	2	1	2	2	0	A	4725.9380	-0.0058
3	2	1	2	2	0	E	4725.7451	-0.0032
3	0	3	2	0	2	A	4412.4369	0.0014
3	0	3	2	0	2	E	4412.4131	-0.0018
3	1	2	2	1	1	A	4873.8369	-0.0041
3	1	2	2	1	1	E	4873.8032	0.0023
3	1	3	2	1	2	A	4211.9816	0.0057
3	1	3	2	1	2	E	4211.9629	-0.0010
4	1	3	3	1	2	A	6437.9419	0.0044
4	1	3	3	1	2	E	6437.8885	0.0003
4	2	2	3	2	1	A	6407.9732	0.0018
4	2	2	3	2	1	E	6407.8965	0.0032
4	0	4	3	0	3	A	5743.5460	-0.0029
4	0	4	3	0	3	E	5743.5248	-0.0013
4	1	4	3	1	3	A	5577.6873	0.0058
4	1	4	3	1	3	E	5577.6646	-0.0041
5	2	4	4	2	3	A	7523.6130	0.0012
5	2	4	4	2	3	E	7523.5789	-0.0001
5	0	5	4	0	4	A	7031.0215	0.0010
5	0	5	4	0	4	E	7030.9918	0.0024
5	1	5	4	1	4	A	6921.8741	-0.0042
5	1	5	4	1	4	E	6921.8741	0.0020
5	1	4	4	1	3	A	7937.6001	0.0024
5	1	4	4	1	3	E	7937.5432	-0.0008
5	3	2	4	3	1	A	7809.0789	-0.0003
5	3	2	4	3	1	E	7808.6181	-0.0001

5	2	3	4	2	2	A	8104.0160	-0.0002
5	2	3	4	2	2	E	8103.9423	0.0007
5	3	3	4	3	2	A	7713.5876	-0.0016
5	3	3	4	3	2	E	7713.9424	-0.0001
6	2	4	5	2	3	A	9768.1342	-0.0009
6	2	4	5	2	3	E	9768.0514	-0.0005
6	0	6	5	0	5	A	8309.9213	0.0005
6	0	6	5	0	5	E	8309.8639	0.0011
6	1	6	5	1	5	A	8248.8174	-0.0093
6	1	6	5	1	5	E	8248.8479	0.0026
6	3	3	5	3	2	A	9486.1046	0.0041
6	3	3	5	3	2	E	9485.9357	0.0022
6	1	5	5	1	4	A	9351.7306	-0.0002
6	1	5	5	1	4	E	9351.6806	0.0026
6	2	5	5	2	4	A	8956.4847	0.0012
6	2	5	5	2	4	E	8956.4440	0.0016
6	4	2	5	4	1	A	9290.3339	-0.0009
6	4	3	5	4	2	A	9273.7145	-0.0055
6	4	3	5	4	2	E	9276.2063	-0.0011
6	3	4	5	3	3	A	9255.9571	-0.0007
6	3	4	5	3	3	E	9255.9859	-0.0039
7	2	5	6	2	4	A	11370.6342	-0.0038
7	0	7	6	0	6	A	9594.7428	-0.0002
7	0	7	6	0	6	E	9594.6073	0.0007
7	1	6	6	1	5	A	10679.6377	-0.0009
7	1	6	6	1	5	E	10679.5886	0.0002
7	1	7	6	1	6	A	9563.9144	-0.0005
7	1	7	6	1	6	E	9564.0126	0.0035
7	4	3	6	4	2	A	10900.3367	0.0002
7	4	3	6	4	2	E	10899.2215	-0.0016
7	4	4	6	4	3	A	10847.5796	0.0064
8	0	8	7	0	7	A	10886.3947	-0.0009
8	0	8	7	0	7	E	10886.0483	0.0010
8	1	8	7	1	7	A	10871.8345	-0.0011
8	1	8	7	1	7	E	10872.1455	0.0065

[a] $\Delta v = v_{CALC} - v_{EXP}$.

Table 7. S14. Observed transition frequencies of the ii-ML--$H_2^{18}O$--$H_2^{16}O$-II conformer.

J'	Ka'	Kc'	J"	Ka"	Kc"	Symmetry	v_{EXP} / MHz	$\Delta v^{[a]}$ / MHz
3	1	2	2	1	1	A	4967.8188	-0.0081
3	1	2	2	1	1	E	4967.7874	0.0044
3	0	3	2	0	2	A	4511.5162	0.0011
3	0	3	2	0	2	E	4511.4892	-0.0037
3	1	3	2	1	2	A	4307.2158	0.0064

3	1	3	2	1	2	E	4307.1937	-0.0023
4	1	3	3	1	2	A	6566.0371	0.0005
4	1	3	3	1	2	E	6565.9832	0.0007
4	2	2	3	2	1	A	6524.0003	-0.0008
4	2	2	3	2	1	E	6523.9173	-0.0002
4	2	3	3	2	2	A	6185.8080	-0.0005
4	2	3	3	2	2	E	6185.7828	-0.0143
4	0	4	3	0	3	A	5878.3363	-0.0048
4	0	4	3	0	3	E	5878.3208	0.0033
4	1	4	3	1	3	A	5705.8332	0.0042
4	1	4	3	1	3	E	5705.8096	-0.0049
5	2	4	4	2	3	A	7683.0727	0.0005
5	2	4	4	2	3	E	7683.0421	0.0066
5	0	5	4	0	4	A	7199.5242	-0.0041
5	0	5	4	0	4	E	7199.5029	0.0052
5	1	5	4	1	4	A	7083.2222	-0.0073
5	1	5	4	1	4	E	7083.2222	0.0015
5	1	4	4	1	3	A	8102.8919	0.0002
5	1	4	4	1	3	E	8102.8335	0.0007
5	2	3	4	2	2	A	8251.3018	-0.0007
5	2	3	4	2	2	E	8251.2228	0.0020
6	0	6	5	0	5	A	8510.0221	0.0003
6	0	6	5	0	5	E	8509.9667	-0.0008
6	1	6	5	1	5	A	8443.3002	-0.0074
6	1	6	5	1	5	E	8443.3303	0.0099
6	1	5	5	1	4	A	9557.3551	0.0024
6	1	5	5	1	4	E	9557.2967	0.0014
6	2	5	5	2	4	A	9150.3426	0.0000
6	2	5	5	2	4	E	9150.2993	0.0020
6	3	4	5	3	3	A	9441.4781	-0.0005
6	3	4	5	3	3	E	9441.5031	-0.0048
6	3	3	5	3	2	A	9657.3031	0.0065
6	3	3	5	3	2	E	9657.1124	-0.0060
7	1	7	6	1	6	A	9791.2152	-0.0016
7	1	7	6	1	6	E	9791.2963	0.0015
7	0	7	6	0	6	A	9825.6730	-0.0021
7	0	7	6	0	6	E	9825.5559	0.0029
7	1	6	6	1	5	A	10925.8588	-0.0073
7	1	6	6	1	5	E	10925.8167	0.0040

[a] $\Delta v = v_{CALC} - v_{EXP}$.

Table 7. S15. Observed transition frequencies of the ii-ML--$H_2{}^{16}O$--$H_2{}^{18}O$-II conformer.

J'	Ka'	Kc'	J"	Ka"	Kc"	Symmetry	ν_{EXP} / MHz	$\Delta\nu^{[a]}$ / MHz
3	1	2	2	1	1	A	5007.9254	-0.0052
3	1	2	2	1	1	E	5007.8897	-0.0004
3	0	3	2	0	2	A	4514.0532	-0.0011
3	0	3	2	0	2	E	4514.0277	-0.0059
3	1	3	2	1	2	A	4310.7759	0.0069
3	1	3	2	1	2	E	4310.7599	0.0031
4	1	3	3	1	2	A	6608.3316	0.0031
4	1	3	3	1	2	E	6608.2760	-0.0029
4	2	2	3	2	1	A	6599.1658	0.0038
4	2	2	3	2	1	E	6599.0884	0.0021
4	2	3	3	2	2	A	6215.4101	0.0069
4	2	3	3	2	2	E	6215.3858	-0.0055
4	0	4	3	0	3	A	5867.4996	-0.0038
4	0	4	3	0	3	E	5867.4820	0.0020
4	1	4	3	1	3	A	5705.3353	0.0039
4	1	4	3	1	3	E	5705.3126	-0.0064
5	2	4	4	2	3	A	7711.9491	0.0082
5	2	4	4	2	3	E	7711.9054	-0.0013
5	0	5	4	0	4	A	7179.0627	-0.0035
5	0	5	4	0	4	E	7179.0326	0.0006
5	1	5	4	1	4	A	7076.8368	-0.0017
5	1	5	4	1	4	E	7076.8368	0.0020
5	1	4	4	1	3	A	8135.2128	0.0012
5	1	4	4	1	3	E	8135.1627	0.0045
5	2	3	4	2	2	A	8342.8219	0.0044
5	2	3	4	2	2	E	8342.7425	-0.0003
5	3	3	4	3	2	A	7922.6007	-0.0055
5	3	3	4	3	2	E	7922.8776	-0.0082
6	2	4	5	2	3	A	10045.4832	0.0108
6	2	4	5	2	3	E	10045.3902	0.0014
6	0	6	5	0	5	A	8485.2592	-0.0063
6	0	6	5	0	5	E	8485.1956	-0.0010
6	1	6	5	1	5	A	8430.4511	0.0089
6	1	6	5	1	5	E	8430.4761	0.0054
6	1	5	5	1	4	A	9566.8526	0.0023
6	1	5	5	1	4	E	9566.7979	-0.0004
6	2	5	5	2	4	A	9174.2086	-0.0058
6	2	5	5	2	4	E	9174.1799	0.0069
6	3	4	5	3	3	A	9503.8977	-0.0091
6	3	4	5	3	3	E	9503.9192	-0.0017
6	4	3	5	4	2	A	9529.1389	-0.0121
6	4	3	5	4	2	E	9531.5283	0.0021
6	4	2	5	4	1	A	9550.2882	-0.0137

6	3	3	5	3	2	A	9772.9432	0.0111
6	3	3	5	3	2	E	9772.7808	0.0009
7	2	6	6	2	5	A	10601.3949	0.0043
7	2	6	6	2	5	E	10601.3519	0.0041
7	0	7	6	0	6	A	9798.7556	-0.0035
7	0	7	6	0	6	E	9798.5889	0.0020
7	1	6	6	1	5	A	10908.6747	-0.0027
7	1	6	6	1	5	E	10908.6236	-0.0035

[a] $\Delta v = v_{CALC} - v_{EXP}$.

E.7. Experimental substitution coordinates and partially refined principal axis coordinates of

ML--water.

Table 7. S16. Experimental substitution coordinates (in Å) of the H and O atoms of water in the principal axis system of ML--H_2O and the corresponding ab initio values for the two most stable conformers predicted.

	Exp.	i-I	i-II
H17			
a	±1.491	-1.556	-1.607
b	±1.683	-1.771	-1.759
c	±0.309	0.247	0.291
H18			
a	±3.014	-3.025	-2.927
b	±2.105	-2.181	-1.830
c	±0.249	0.099	1.069
O16			
a	±2.486	-2.461	-2.539
b	±1.428	-1.459	-1.499
c	± 0.387	0.388	0.256
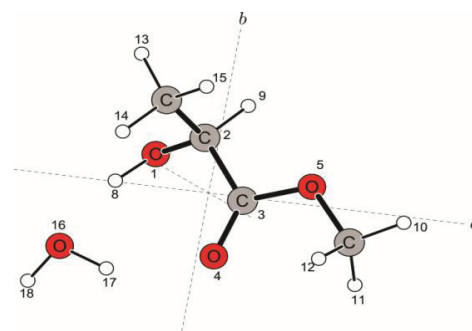
Table 7. S17. Partially refined principal axis coordinates of i-I conformer in the principal axis system of ML--H_2O.[a]

ATOM NO.	a	b	c
1	-1.47852	-0.81559	-1.05184
2	-0.34448	-1.13517	-0.28332
3	0.602914	0.051546	-0.15691
4	0.266035	1.218613	-0.06849
5	1.881538	-0.35244	-0.09811
6	2.836272	0.702059	0.120561
7	-0.70472	-1.62271	1.122788
8	-1.99054	-0.14764	-0.56742
9	0.186324	-1.92247	-0.82383
10	3.805773	0.209276	0.149686
11	2.793433	1.424654	-0.69552
12	2.630405	1.208945	1.064752
13	-1.35022	-2.50019	1.03908
14	-1.2479	-0.8407	1.662505
15	0.194237	-1.89159	1.685691
16	-2.49339	1.494582	0.393958
17	-1.50611	1.692104	0.13908
18	-3.01895	2.109238	-0.13154
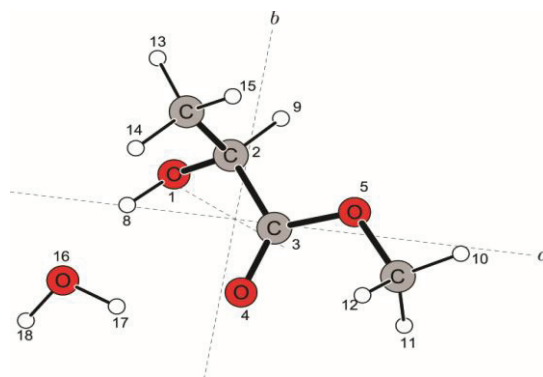
[a]All important bond lengths, angles and dihedral angles related to the position of the water molecule relative to the ML subunit were obtained from the structure fit, while the rest of the structural parameters were kept at their *ab initio* values. See text for details.

Appendix F

Supporting Information for Chapter 8

Structure and Tunneling Dynamics in a Model System of Peptide Co-Solvents: Rotational Spectroscopy of the 2,2,2-Trifluoroethanol··Water Complex.

Contents:

F.1. Lists of measured rotational transitions of the *i g* TFE··H2O I and its isotopologues.

Table 8. S1. Observed transition frequencies of the *i g* TFE··H$_2$O I (ortho) conformer.

J'	Ka'	Kc'	J"	Ka"	Kc"	ν_{EXP} / MHz	$\Delta\nu^a$ / MHz
1	1	1	0	0	0	4901.1128	-0.0024
1	1	0	0	0	0	5093.2979	0.0022
2	1	1	1	1	0	6009.7371	0.0108
2	1	2	1	0	1	7617.6932	0.0007
2	1	1	1	0	1	8194.2522	-0.0011
2	2	1	1	1	0	11986.6695	-0.0002
2	2	0	1	1	0	11999.9136	0.0009
2	2	1	1	1	1	12178.8598	-0.0009
2	2	0	1	1	1	12192.1051	-0.0010
2	0	2	1	0	1	5804.3203	-0.0012
2	1	2	1	1	1	5625.3826	-0.0023
3	0	3	2	0	2	8673.7080	0.0015
3	2	2	2	2	1	8726.2751	-0.0033
3	2	1	2	2	0	8778.8379	-0.0027
3	1	2	2	1	1	9005.9479	-0.0003
3	1	3	2	1	2	8429.9964	0.0013
3	1	3	2	0	2	10243.3730	-0.0005
3	1	2	2	0	2	11395.8807	-0.0011
3	2	2	2	1	1	14703.1936	-0.0005
3	2	2	2	1	2	15279.7490	0.0013
3	2	1	2	1	2	15345.5595	-0.0006
4	0	4	3	1	3	9936.4288	-0.0006
4	1	4	3	1	3	11225.7085	0.0000
4	0	4	3	0	3	11506.0910	0.0001
4	2	3	3	2	2	11624.5668	0.0014
4	3	2	3	3	1	11659.7557	-0.0024
4	3	1	3	3	0	11663.1786	-0.0028
4	2	2	3	2	1	11753.3492	0.0004
4	1	4	3	0	3	12795.3701	0.0014
4	1	3	3	0	3	14713.0988	-0.0011
4	1	3	3	1	2	11990.9263	0.0013
5	2	4	5	1	5	7751.7856	0.0010
5	0	5	4	1	4	13006.3835	-0.0003
5	1	5	4	1	4	14010.7752	-0.0007
5	0	5	4	0	4	14295.6632	0.0003
5	2	4	4	2	3	14513.9489	-0.0001
5	3	3	4	3	2	14583.1887	0.0007
5	3	2	4	3	1	14595.0851	0.0025
5	2	3	4	2	2	14761.5168	0.0004
5	1	4	4	1	3	14959.5902	-0.0002

J'	Ka'	Kc'	J"	Ka"	Kc"	ν_{EXP} / MHz	$\Delta\nu^a$ / MHz
5	1	5	4	0	4	15300.0535	0.0013
6	1	6	5	1	5	16784.3517	0.0001
6	0	6	5	0	5	17044.7485	-0.0007
6	2	5	5	2	4	17392.3070	-0.0001
6	2	4	5	2	3	17798.5755	0.0007
6	1	5	5	1	4	17905.7350	-0.0013

[a] $\Delta\nu = \nu_{CALC.} - \nu_{EXP}.$

Table 8. S2. Observed transition frequencies of the *i g* TFE··H_2O I (para) conformer.

J'	Ka'	Kc'	J"	Ka"	Kc"	ν_{EXP} / MHz	$\Delta\nu^a$ / MHz
1	1	1	0	0	0	4901.1752	-0.0029
1	1	0	0	0	0	5093.3882	-0.0066
2	1	1	1	1	0	6009.7130	-0.0016
2	1	2	1	0	1	7617.7138	-0.0059
2	1	1	1	0	1	8194.3256	-0.0014
2	2	1	1	1	0	11986.9015	0.0014
2	2	0	1	1	0	12000.1490	0.0011
2	2	1	1	1	1	12179.1135	-0.0013
2	2	0	1	1	1	12192.3610	-0.0016
2	0	2	1	0	1	5804.2621	-0.0012
2	1	2	1	1	1	5625.3059	-0.0015
3	0	3	2	0	2	8673.6171	0.0000
3	2	2	2	2	1	8726.1889	-0.0017
3	2	1	2	2	0	8778.7600	-0.0013
3	1	2	2	1	1	9005.8910	0.0006
3	1	3	2	0	2	10243.3239	0.0057
3	1	2	2	0	2	11395.9482	0.0067
3	2	2	2	1	1	14703.3765	0.0023
3	2	2	2	1	2	15279.9955	-0.0005
3	2	1	2	1	2	15345.8135	0.0002
3	1	3	2	1	2	8429.8819	0.0006
4	0	4	3	1	3	9936.2461	0.0004
4	1	4	3	1	3	11225.5528	-0.0003
4	0	4	3	0	3	11505.9577	0.0013
4	2	3	3	2	2	11624.4535	0.0006
4	3	2	3	3	1	11659.6435	0.0002
4	3	1	3	3	0	11663.0682	-0.0013
4	2	2	3	2	1	11753.2539	0.0013
4	1	4	3	0	3	12795.2651	-0.0001
4	1	3	3	0	3	14713.1842	0.0043
4	1	3	3	1	2	11990.8565	-0.0058
5	2	4	5	1	5	7752.2436	-0.0016
5	0	5	4	1	4	13006.1789	0.0008

229

5	1	5	4	1	4	14010.5759	0.0002
5	0	5	4	0	4	14295.4859	-0.0002
5	2	4	4	2	3	14513.8041	-0.0001
5	3	3	4	3	2	14583.0534	0.0006
5	3	2	4	3	1	14594.9537	0.0009
5	2	3	4	2	2	14761.4102	-0.0007
5	1	4	4	1	3	14959.4918	-0.0021
5	1	5	4	0	4	15299.8808	0.0013
6	1	6	5	1	5	16784.1118	-0.0028
6	0	6	5	0	5	17044.5191	0.0004
6	2	5	5	2	4	17392.1300	-0.0002
6	2	4	5	2	3	17798.4594	-0.0011
6	1	5	5	1	4	17905.6045	0.0021

[a] $\Delta \nu = \nu_{CALC.} - \nu_{EXP}$.

Table 8. S3. Observed transition frequencies of the *i g* TFE··DOH conformer.

J'	Ka'	Kc'	J"	Ka"	Kc"	ν_{EXP} / MHz	$\Delta\nu^{a}$ / MHz
2	2	1	1	1	0	11802.8104	-0.0080
2	2	0	1	1	1	12010.9629	0.0024
2	1	2	1	0	1	7494.2446	0.0007
2	1	1	1	1	0	5923.0894	0.0018
2	0	2	1	0	1	5714.9510	-0.0007
2	1	2	1	1	1	5534.3237	-0.0006
3	1	3	2	1	2	8293.1106	-0.0019
3	0	3	2	0	2	8538.4238	0.0003
3	1	2	2	1	1	8875.6143	-0.0040
3	2	2	2	2	1	8592.9850	0.0013
3	2	1	2	2	0	8647.5490	0.0028
3	1	3	2	0	2	10072.4103	0.0056
3	2	2	2	1	1	14472.7200	0.0056
4	2	3	3	2	2	11446.4517	-0.0022
4	0	4	3	1	3	9789.6345	0.0010
4	1	4	3	1	3	11042.6837	0.0002
4	0	4	3	0	3	11323.6132	-0.0014
4	3	2	3	3	1	11482.9486	0.0020
4	3	1	3	3	0	11486.5945	-0.0011
4	2	2	3	2	1	11579.9951	0.0008
4	1	3	3	1	2	11816.4660	-0.0027
4	1	4	3	0	3	12576.6605	-0.0042
5	1	5	4	1	4	13781.2750	0.0015
5	0	5	4	0	4	14064.8475	0.0011
5	2	4	4	2	3	14290.6751	0.0023
5	3	3	4	3	2	14362.4202	-0.0016

5	3	2	4	3	1	14375.1014	-0.0016
5	2	3	4	2	2	14546.9001	0.0016
5	1	4	4	1	3	14740.2974	-0.0001
5	1	5	4	0	4	15034.3225	-0.0011

[a] $\Delta v = v_{CALC.} - v_{EXP.}$

Table 8. S4. Observed transition frequencies of the *i g* TFE··D_2O conformer.

J'	Ka'	Kc'	J"	Ka"	Kc"	v_{EXP} / MHz	Δv^a / MHz
2	0	2	1	0	1	5502.2762	0.0002
2	1	2	1	1	1	5332.3840	-0.0048
2	2	1	1	1	0	11716.7669	0.0006
2	2	0	1	1	1	11910.2256	-0.0008
3	1	2	2	1	1	8535.8904	-0.0019
3	2	2	2	2	1	8271.0032	-0.0120
3	0	3	2	0	2	8224.2198	0.0029
3	1	3	2	1	2	7991.3852	-0.0024
3	2	1	2	2	0	8317.8239	-0.0004
3	1	3	2	0	2	9828.5313	0.0041
4	2	3	3	2	2	11018.7109	-0.0023
4	0	4	3	1	3	9308.6507	0.0016
4	1	4	3	1	3	10642.4093	0.0025
4	3	1	3	3	0	11052.9566	0.0042
4	3	2	3	3	1	11050.0914	0.0054
4	2	2	3	2	1	11133.6524	0.0013
4	1	3	3	1	2	11366.1392	0.0034
4	0	4	3	0	3	10912.9642	0.0049
4	1	4	3	0	3	12246.7144	-0.0027
5	1	5	4	1	4	13283.8235	0.0001
5	0	5	4	0	4	13562.7008	-0.0004
5	2	4	4	2	3	13758.4763	0.0024
5	3	3	4	3	2	13820.3461	-0.0039
5	3	2	4	3	1	13830.3171	-0.0056
5	2	3	4	2	2	13980.3395	-0.0009
5	1	4	4	1	3	14182.0161	0.0012

[a] $\Delta v = v_{CALC.} - v_{EXP.}$

Table 8. S5. Observed transition frequencies of the *i g* TFEOD··DOH conformer.

J'	Ka'	Kc'	J"	Ka"	Kc"	ν_{EXP} / MHz	$\Delta\nu^a$ / MHz
2	1	2	1	1	1	5483.1881	-0.0079
2	0	2	1	0	1	5663.3595	-0.0008
2	1	1	1	1	0	5870.9689	0.0023
2	1	2	1	0	1	7437.8585	0.0076
3	1	3	2	1	2	8216.4433	-0.0012
3	1	2	2	1	1	8797.4654	0.0002
3	2	1	2	2	0	8569.9800	-0.0026
3	2	2	2	2	1	8515.5553	0.0021
3	1	3	2	0	2	9990.9354	0.0002
3	3	1	3	2	2	10266.2425	-0.0056
3	3	0	3	2	1	10198.7141	0.0077
3	0	3	2	0	2	8461.1278	0.0035
3	1	2	2	0	2	11153.6139	-0.0030
4	1	4	3	1	3	10940.5064	0.0034
4	2	3	3	2	2	11343.2460	-0.0039
4	2	2	3	2	1	11476.4664	0.0014
4	3	1	3	3	0	11383.2989	0.0037
4	3	2	4	2	3	10302.6506	-0.0023
4	0	4	3	1	3	9690.8930	-0.0024
4	1	3	3	1	2	11712.3203	0.0010
4	1	4	3	0	3	12470.3104	-0.0035
5	3	3	5	2	4	10374.2290	0.0003
5	1	5	4	1	4	13653.6166	0.0033
5	0	5	4	0	4	13936.4474	0.0035
5	2	4	4	2	3	14161.7256	-0.0007
5	2	3	4	2	2	14417.3296	0.0014
5	1	4	4	1	3	14610.1998	-0.0030
5	1	5	4	0	4	14903.2166	-0.0043

^{a} $\Delta\nu = \nu_{CALC.} - \nu_{EXP.}$

Table 8. S6. Observed transition frequencies of the *i g* TFEOD··HOD conformer.

J'	Ka'	Kc'	J"	Ka"	Kc"	ν_{EXP} / MHz	$\Delta\nu^a$ / MHz
2	1	2	1	1	1	5367.8220	0.0042
2	0	2	1	0	1	5536.0539	-0.0010
2	1	2	1	0	1	7399.7047	-0.0035
3	1	3	2	1	2	8044.7628	0.0015
3	0	3	2	0	2	8275.8436	0.0013

3	2	2	2	2	1	8321.1008	0.0038
3	1	2	2	1	1	8583.1742	-0.0011
3	1	3	2	0	2	9908.4149	0.0003
4	1	3	3	1	2	11429.7118	-0.0023
4	0	4	3	1	3	9350.8744	0.0053
4	1	4	3	1	3	10713.9642	-0.0008
4	0	4	3	0	3	10983.4352	-0.0062
4	2	3	3	2	2	11085.8044	0.0062
4	3	2	3	3	1	11116.1510	-0.0059
4	2	2	3	2	1	11197.0422	0.0048
4	1	3	3	1	2	11429.7104	-0.0037
4	1	4	3	0	3	12346.5325	-0.0048
5	1	5	4	1	4	13373.8285	-0.0018
5	0	5	4	0	4	13653.0062	-0.0134
5	2	4	4	2	3	13842.8318	0.0088
5	3	3	4	3	2	13902.7493	0.0031
5	3	2	4	3	1	13912.1789	0.0023
5	2	3	4	2	2	14057.8761	0.0096
5	1	4	4	1	3	14262.4170	-0.0070
5	1	5	4	0	4	14736.9354	0.0091
5	0	5	4	1	4	12289.9155	-0.0082

[a] $\Delta v = v_{CALC.} - v_{EXP}$.

Table 8. S7. Observed transition frequencies of the *i g* TFEOD··D_2O conformer.

J'	Ka'	Kc'	J"	Ka"	Kc"	v_{EXP} / MHz	Δv^a / MHz
2	1	2	1	1	1	5286.4302	0.0058
2	0	2	1	0	1	5456.1827	-0.0030
2	1	2	1	0	1	7285.7343	0.0027
2	2	1	1	1	0	11647.4731	0.0016
2	2	0	1	1	1	11840.8563	-0.0100
3	1	3	2	1	2	7922.4195	-0.0022
3	1	2	2	1	1	8466.6439	-0.0023
3	1	3	2	0	2	9751.9749	0.0073
3	0	3	2	0	2	8155.0034	-0.0043
3	2	2	2	2	1	8201.9363	0.0061
3	2	1	2	2	0	8248.8604	0.0007
3	2	2	2	1	1	14199.8300	0.0037
3	2	1	2	1	2	14803.3054	0.0038
4	0	4	3	1	3	9223.5959	-0.0001
4	1	4	3	1	3	10550.4128	-0.0062
4	0	4	3	0	3	10820.5533	-0.0027
4	2	3	3	2	2	10926.5905	0.0095
4	2	2	3	2	1	11041.7990	-0.0057

4	1	3	3	1	2	11273.7735	-0.0006
4	1	4	3	0	3	12147.3710	-0.0079
5	1	5	4	1	4	13168.7963	0.0048
5	0	5	4	0	4	13447.0397	-0.0027
5	2	4	4	2	3	13643.2768	-0.0009
5	3	3	4	3	2	13705.3022	0.0002
5	3	2	4	3	1	13715.3327	0.0015
5	2	3	4	2	2	13865.6642	0.0073
5	1	4	4	1	3	14066.4921	-0.0068
5	1	5	4	0	4	14495.6158	0.0013

[a] $\Delta\nu = \nu_{CALC.} - \nu_{EXP.}$